Formulation of Slurry for the Process of Interconnect Metal (Cu)-Barrier Metal (Ru/Co) Chemical Mechanical Planarization

A THESIS

Submitted in Partial Fulfilment of the Requirements

for the Degree of

DOCTOR OF PHILOSOPHY

Jenasree Hazarika

DEPARTMENT OF CHEMICAL ENGINEERING

INDIAN INSTITUTE OF TECHNOLOGY GUWAHATI,

GUWAHATI – 781039, ASSAM, INDIA

March, 2023

DEDICATION

To Papa, Bitupan Hazarika; Mumma, Ava Hazarika and brother, Ansu.

It would not have been possible without your endless love, support, encouragement.

Thank you for always believing in me.

To my Guru, Dr. R. Prasanna Venkatesh

For your patience, support and faith

Thank you for always showing me the right path.

And

To the Almighty.

For giving me the power and strength to go through the right way.

STATEMENT ON ACADEMIC INTEGRITY

I hereby declare that the work contained herein is exclusively the result of investigations accomplished by me in the Department of Chemical Engineering, Indian Institute of Technology Guwahati, Guwahati, Assam, India under the supervision of **Dr. Prasanna Venkatesh Rajaraman**.

In keeping with the general practice of reporting scientific observations, the thesis has been prepared without resorting to plagiarism and due acknowledgement and citation has been made wherever the work described is based on the findings of other investigations.

Place: IIT Guwahati, India **Jenasree Hazarika**

March 2023 166107118

Dr. Prasanna Venkatesh Rajaraman
Assistant Professor
Department of Chemical Engineering
Indian Institute of Technology Guwahati
Guwahati-781039, Assam, India

CERTIFICATE

It is certified that the work contained in the thesis entitled, **Formulation of Slurry for the process of interconnect metal (Cu)-barrier metal (Ru/Co) Chemical Mechanical Planarization**, by Jenasree Hazarika (166107118), has been carried out by her in the Department of Chemical Engineering, Indian Institute of Technology Guwahati, Guwahati, Assam, India under my supervision and that this work has not been submitted elsewhere for a degree.

Date:

Dr. Prasanna Venkatesh Rajaraman

(Supervisor)

ACKNOWLEDGEMENT

This wonderful Ph.D. journey of mine has become a reality due to the support and presence of many individuals. At this moment of accomplishment, I would like to thank everyone and expresses my deepest gratitude for helping me in making this thesis possible and accomplishing this dream of mine.

First and foremost, I would like to express my sincere gratitude and warmest regards to my supervisor ***Dr. Prasanna Venkatesh Rajaraman,*** for imparting the knowledge and guiding me in every possible way. His kindness, politeness, patience, professionalism, cooperativeness and enthusiasm have motivated me towards the completion of my research work and making this thesis possible. I could not have imagined having a better mentor and supervisor for my Ph.D. journey. It was a great honour to work under him and I will be forever indebted to him for his immense support. I would also to express my gratefulness to my Doctoral Committee members, ***Prof. G. Pugazhenthi*** (Department of Chemical Engineering), ***Prof. Mahuya De*** (Department of Chemical Engineering) and ***Dr. Akshai Kumar A.S*** (Department of Chemistry) for their priceless time, valuable suggestions and relevant insights throughout my research period.

I express my gratitude to ***Prof. Kaustubha Mohanty***, Head of the Department of Chemical Engineering for his benevolent support. I am also thankful to the faculty members of the Department of Chemical Engineering along with other departments of Indian Institute of Technology Guwahati, for their generousness and assistance. I am also grateful to all the technical staff members of Department of Chemical Engineering along with other departments for helping me in using the analytical research facilities. I am also thankful to the non-teaching staff of all the departments for their immense help.

I take this opportunity to acknowledge to ***Council of Scientific and Industrial Research (Scheme number: 22(0710)/16/EMR-II), MHRD*** India for supporting my Ph.D. work. I

sincerely acknowledge Central Workshop, Analytical Lab-Department of Chemical Engineering, Department of Nano Technology and Central Instruments Facility, IIT Guwahati for providing me with the fabrication and analytical facilities required for my research work. I would also like to thank the Council of Scientific and Industrial Research- North East Institute of Science and Technology (CSIR-NEIST) Jorhat, Assam, India for providing me with X-Ray Photoelectron facility. I would like to extend my sincere grateful to ***Prof. Ramanathan Srinivasan***, Department of Chemical Engineering, Indian Institute of Technology Madras, Chennai, Tamil Nadu, India for several valuable advices and providing the KKT Transform software for my research analysis.

An immense thank you to my "pre-doc supervisors" ***Dr. Mriganka Shekar Manna*** in National Institute of Technology, Agartala and ***Dr. Leela Manohar Aeshala*** in National Institute of Technology, Hamipur for being such a huge influence and enlightening me while I enter my PhD journey. I am also sincerely grateful to my first primary school teacher ***Late. Teresa Basumatary;*** junior high school teachers ***Mr. Roshit Basumatary***, ***Mr. Bhim Pradhan*** and ***Mr. Jitu Sharma*** and senior high school teacher ***Mr. Hari Deka*** from whom I have learned so much. I thank them from the core of my heart, for always believing in me and inspiring me in the early stages of my life.

My heartful thanks and respect to my research family ***Dr. Apeksha Gupta***, ***Dr. Prince Baranwal***, ***Dr. Shravan Kumar, Nikhil Dhondge, Rushabh Kale, Chetana S. Patil***, ***Shaimpu Babu***, ***Vinay Kumar***, ***Rohan Kumar, Mansi Singh*** and in particular ***Dr. Anusuya Talukdar*** and ***Sayani Adhikari*** for the continuous affection and love. My deepest gratitude to ***Dr. Barnali Bhui, Dr. Pradeep Sahu, Shekhar Jyoti Pathak, Roni Mallick, Koushik Jena, Uttkarsh Goyal and Gaurav Sharma*** for all the care and support***.*** The joyful, friendly and supportive nature that you all showered in the lab has always helped me in carrying out my research work smoothly and made my stay worth memorable.

A very special thanks to ***Udayan Banik*** for the endless support in the correction, suggestions in my work and all ways possible. My love to my friends ***Shilpi Kumari, Dr. Vibhuti Nougain, Purnima Singhal, Ashima Chandra, Diksha Barnwal, Aniruddha Das, Dr. Shivani Gupta, Sutapa Das, Dr. Surabhi Patel, Dr. Nihaal Gujre, Dr. Kushagra Agrawal, Bhaskar Kalita, Saptarshi Gupta,*** and ***Sudhansu Rauniyar*** for their unwavering and unending care, love and support.

I believe in the saying that "Life's greatest achievement is the love of one's family". And I consider myself very lucky to have one such. My papa ***Mr. Bitupan Hazarika***, Rtd. District Agricultural Officer and Deputy Director, Agriculture department, Chirang Assam, India and my mumma ***Mrs. Ava Buragohain Hazarika,*** Child Development Project Officer (CDPO), Dhubri, Assam, India are my pillars of strength and my everything. They stood by me in all odds of my life. Their efforts, sacrifices and struggles are the reason behind my courage to reveal every mystery and challenges in my life. I thank you both from the core of my heart for believing in me always. And I will forever be grateful to you for all the support, freedom and encouragement that you have always bestowed on me. I owe everything to you. I also consider myself lucky to have ***Debasish Hazarika (Ansu)*** as my brother, who was always there beside me, loving me and supporting me in all my ups and downs. Thank you for being there for me always.

Being the first child of our generation in my whole family, I was always showered in unending love. Hence, I am always thankful to everyone in my family for all the lavish affections and care. A special thanks to my maternal grandparents ***Lt. Dr. Chandra Buragohain*** and ***Mrs. Padma Buragohain*** and my aunt ***Rani Buragohain Rajkumari*** for the ethical principles and values that they gave me which helped me shape my life beautifully. And my deepest gratitude and respect to my paternal grandparents ***Lt. Sukheswar Hazarika*** and ***Lt. Maikon Hazarika*** for their blessings, their unending love and their advices that helped in moulding a better me.

And lastly, I convey my utmost respect and thanks to all the persons in my life whose names have been missed out and who have directly or indirectly made remarkable impacts in my life.

And above all to the Almighty God, for showering with invisible support and unending blessings in the form of wisdom, strength, courage, endurance capacity and patience in every stages of life.

Thank You.

Jenasree Hazarika

ABSTRACT

Failure of Integrated Circuits (IC) due to maintenance of diffusion barrier property is a major concern in the semiconductor industry. Hence, cobalt (Co) and ruthenium (Ru) are introduced as new promising barrier metals. After deposition of the metals, better surface uniformity is required for further level metallization for which Chemical Mechanical Planarization (CMP) is opted. The main rational behind using CMP process is the removal of interconnect and barrier metal without excessive thinning. This demands a slurry which gives a removal selectivity of 1:1. In the present work, slurries giving desire removal selectivity for Ru/Cu and Co/Cu CMP are proposed.

In the initial part of the study, an optimized formulation of slurry for CMP of Copper (Cu) as interconnect material and Ruthenium (Ru) as barrier line with removal selectivity is investigated. Thermogravimetric analysis (TGA), effect of abrasives concentrations, pH and solution temperature on etch rate are also examined. The results revealed that a Ru-Cu selectivity of ~1.003: 1 is obtained using 2 wt. % fumed silica, 0.2 M potassium iodate (KIO_3) and 5 mM 1,2,3 Benzotriazole (BTA) based slurry. The activation energy (E_a) of Cu and Ru dissolution in the solution is determined to be 27.3 KJ/mol for Cu and 25.2 KJ/mol for Ru respectively. The thermodynamic process was found to be endothermic in nature and the dissolution followed an associative mechanism. The proposed slurry follows a non-Prestonian behavior.

CMP of interconnect metal copper and barrier metal cobalt using NaOCl based slurry is investigated as the second objective in this study. The slurry consists of 2 wt. % silica, 0.5 wt. % NaOCl and 5 mM BTA as inhibitor. It is seen that the formulated slurry gives a combination of low etch rates and comparatively fair removal rates along with selectivity of ~1:1.006 at pH 9, which are desired to be used in semiconductor industry. A decrease in

removal rates for both Cu and Co is observed as the pH regime changes from acidic to alkaline. At acidic pH, the passive layer if any formed on the surface becomes very unstable resulting in higher polish rates. However, at neutral and alkaline medium, the passivation layer comprising of Co (II) oxide/hydroxides is formed which subsequently decreases the polish rate. A highly stable and dense passivation layer of Co (III) oxides comprising of mostly Co_3O_4 and CoOOH is formed at the highly alkaline region explaining the reason behind lower removal rates. The variation in turntable speed and down force pressure does not have any significant impact on selectivity obtained at optimum conditions. XRD analysis reveals the formation of oxide on Co surface after etching at pH 9.

The third objective focuses on the reduction of galvanic corrosion associated with Co and Cu along with investigation of Co/Cu removal rate (RR) selectivity by using oxalic acid (weak acid) as the complexing agent and imidazole as an inhibitor in hydrogen peroxide (H_2O_2) and fumed silica-based slurry. The results obtained from dissolution study, polishing experiments and potentiodynamic polarization measurements revealed that the proposed chemistry can achieve a desirable Co/Cu RR selectivity and a significant decrease in corrosion potential of Co and Cu (pH 9) to be used in the semiconductor industry. The corrosion potential difference ($Cu_{Ecorr} - Co_{Ecorr}$) is reduced to 12 mV by using 0.1 wt.% H_2O_2 + 0.02 M oxalic acid + 5 ppm imidazole solution at pH 9. Meanwhile, a removal rate of ~147 nm/min for Co and ~140 nm/min for Cu was achieved using the same composition in a fumed silica slurry which resulted in Co/Cu selectivity ratio of 1.05:1, which is acceptable for cobalt barrier and copper interconnect CMP. Based on FTIR and UV spectra, the dissolution mechanism in the proposed chemistry is also discussed.

In the fourth part of the study, the anodic dissolution of Co in H_2O_2 solution is investigated both in the presence and absence of complexing agent, oxalic acid by using various techniques including electrochemical impedance spectroscopy (EIS). Anodic polarization

measurements of both the solutions show that active dissolution occurs in the potential range of 0 to 600 mV w.r.t open circuit potential (OCP) and the addition of oxalic acid enhances the dissolution rate significantly. EIS measurements at OCP confirm the same trend while the kinetics of dissolution is investigated by performing EIS measurements at various overpotentials under anodic conditions. EIS spectra exhibit two loops; capacitance (higher frequency) followed by inductance (lower frequency) at all the overpotentials and it is modelled by a multi- step mechanism with 3 intermediate adsorbed species. The dissolution via both chemical and electrochemical steps is considered in the proposed model. From the parameters obtained, dominance of Co (III) compound formation is observed for both the systems. The oxides formed on the Co surface on addition of oxalic acid to H_2O_2 are higher than using only H_2O_2 thus properly justifying the role of a complexing agent in a CMP slurry. Products formed on exposure of Co to H_2O_2 and H_2O_2+oxalic acid solution at pH 9 are analyzed using Contact angle analysis and FESEM and XPS analysis. The results confirm the formation and dominance of Co-oxalate complexes for H_2O_2+oxalic acid system.

We believe that these results obtained can significantly improve the polishing efficiency and providing desired selectivity without excessive thinning of the interconnect barrier interface and thereby reducing failure in IC production.

KEYWORDS: Chemical Mechanical Polishing (CMP); Ruthenium; Cobalt; Copper; Selectivity; Galvanic Corrosion; Electrochemical Studies; Potentiodynamic Polarization; Electrochemical Impedance Spectroscopy (EIS); Electrical Equivalent Circuit (EEC); Reaction Mechanism Analysis (RMA); Thermodynamic Analysis; XPS; FESEM; Contact Angle; UV Spectroscopy; FTIR; XRD; TGA

NOMENCLATURE

English Symbols

A	Area
C	Capacitance
C_{dl}	Double Layer Capacitance
d	Density
E	Potential
E^0/E_{oc}	Equilibrium Potential
E_{corr}	Corrosion Potential
F	Faraday Constant
f	Frequency
Co_{ad}^{n+}	Charged Species of Iron Adsorbed onto the Electrode Surface
Co_{sol}^{n+}	Charged Species of Iron in Solution
I	Current
I	Current or Current Density
I^0	Reaction Dependent Constant (Exchange Current)
I_{corr}	Corrosion Current or Corrosion Current Density
I_0	Amplitude of Current
I_{ox}	Oxidation Current
I_{red}	Reduction Current
$I_{summation}$	Net Current
J	Unsteady State Current Density

J_{ss}	Steady State Current Density
j	Imaginary Component (Square Root of -1)
k_i	Kinetic Rate Constant
k_{i0}	Kinetic Rate Constant Coefficient
L	Inductance
n	Number of Electrons
n_1	Exponent of Constant Phase Element
P	Pressure
Q	Constant Phase Element
R	Resistance
R_{ct}	Charge Transfer Resistance
R	Ideal Gas Constant
R_p	Polarization Resistance
R_{sol}	Solution Resistance
T	Temperature
t	Time
V	Overpotential
Y_0	Constant Phase Element Parameter
Z	Impedance
Z_0	Magnitude of Impedance
Z_F	Faradic Impedance
Z_{Re}	Real Component of Impedance
Z_{Im}	Imaginary Component of Impedance
Z_{total}	Total Impedance z

Greek Symbols

α	Transfer Coefficient
β	Tafel Constant
β_a	Anodic Tafel Constant
β_c	Cathodic Tafel Constant
Ω	Ohm (Unit of Resistance)
π	Pi
τ	Number of Surface Sites
ω	Angular Frequency
θ_i	Surface Coverage
θ_{iss}	Steady State Surface Coverage
ϕ	Phase Shift
ω_{Re}	Weighing Function for Calculating Residue in Real Component
ω_{Im}	Weighing Function for Calculating Residue in Imaginary Component

ABBREVIATION

Al	Aluminium
A	Ampere
ac	Alternating Current
AR	Analytical Reagent
CA	Chronoamperometry
CPE	Constant Phase Element
CMP	Chemical Mechanical Polishing
CNLS	Complex Nonlinear Least Squares
Cu	Copper
Co	Cobalt
Conc.	Concentration
dc	Direct Current
EDL	Electrical Double Layer
EEC	Electrical Equivalent Circuit
EIS	Electrochemical Impedance Spectroscopy
FESEM	Field Emission Scanning Electron Microscopy
FTIR	Fourier Transform Infrared Spectroscopy
g	Gram
IC	Integrated Circuit
ILD	Interlayer dielectrics
KKT	Kramers Kronig Transform
M	Molar
mM	Milli Molar
max	Maximum
MOC	Materials of Construction

MRR	Material removal rate
OCP	Open Circuit Potential
PMD	Pre-metal dielectrics
PP	Potentiodynamic Polarization
RIE EB	Reactive ion etching and etch back
RMA	Reaction Mechanism Analysis
RR	Removal Rate
Ru	Ruthenium
s	Second
SOD	Spin on deposition
SEP	Spin etch planarization
SER	Static Etch Rate
SQP	Sequential Quadratic Programming
TGA	Thermogravimetric Analysis
T	Time
UV Vis	Ultra Violet Visible Spectrophotometer
V	Volt
wt	Weight
XPS	X-ray photoelectron spectroscopy
XRD	X-ray Diffraction

Table of Contents

List of Table

List of Figures

THIS PAGE IS LEFT BLANK INTENTIONALLY

CHAPTER 1

1. INTRODUCTION

1.1 Overview

With the passage of time, technologies have permeated into every aspects of our day-to-day life starting from mobile phones, GPS facilities to entertainment gadgets etc. These technology wonders are the results of the advancement of semiconductor manufacturing processes. The semiconductor enterprises have been experiencing the steady change for more than six decades. However, in the most recent decade, the advancement in semiconductor industries has been fast, especially in manufacturing of integrated circuits (IC). With the advancement of semiconductor manufacturing techniques, the power of electronic goods and circuit complexity at the wafer level are increasing whereas the size is comparatively decreasing day by day. Without the continuous decrease in size of the semiconductors, it is difficult to build the advance microelectronic devices.

The successful fabrication of the smaller features on a wafer is mainly dependent on the lithographic step. The lithographic tool should have the capability to focus all points on the wafer to create the required minute structures on features. However, while reducing these sizes; the depth of focus is also compromised and a minuscule mistake in the surface might lead to performance degradation of the devices. To prevent this challenge the polishing process such as Chemical Mechanical Planarization (CMP) was first brought into existence in early 1980's by Klaus D. Beyer(Beyer, 1999).

1.2 Importance of CMP

A single chip consists of many active (transistors, diodes etc) and passive elements (capacitors, resistors etc) which are connected with a conductive wire in order to complete a circuit (Li, 2007).With the decrease in size of the chips, both complexity increases and demand for a

precise and efficient interconnect system. Employing a multilevel interconnect system across the elements is one of the signification solutions to it. This reduces the signal processing delays as well as improves the chip performance. However, with the incorporation of multilevel interconnect system, surface roughness has become a major issue. This surface roughness effects negatively on the efficiency and accuracy of pattern transfer in photolithography resulting in failure of the multilevel interconnect network. Thus, to achieve an effective planarization, the CMP process was implemented. The other yield related issues that CMP eliminates are missing contacts, undesired leaks, electro migrations etc.

Devising of interlayer dielectrics (ILD) and planar pre-metal dielectrics (PMD) on the wafers are two of the most implemented steps of CMP. CMP of PMD is conducted to planarize between the back-end devices and front-end active devices. Whereas CMP of ILD is done to planarize the metal layers in the back end.

1.3 Advantages and Disadvantages of CMP

The different methods that can be implemented to obtain global and local planarization are spin etch planarization (SEP), reactive ion etching and etch back (RIE EB), spin on deposition (SOD), reflow of boron phosphorus silicate glass (BPSG), CMP etc. However, amongst all these techniques, CMP is preferable as it offers both excellent local and global planerites along with surface smoothing at the same time unlike the other methods which deliver only one of them at a time. Some of the advantages and disadvantages of CMP are listed herewith:

1.3.1 Advantages

- Achieves both global and local planarization.
- Multiple materials can be planarized at the same polish step.
- Easier to etch metals and alloys, thus providing an alternative means to eliminate the use of plasma etch.

- Increases IC reliability, speed and yield (low defects) of the 0.5 μm and lower sized devices.
- Eliminates the use of any hazardous gas (dry etch process).
- Eliminates sidewall thinning of the planarized surface caused as a result of poor PVD deposition process.

1.3.2 Disadvantages

- CMP being a new technology used to planarize wafer, control over process variables is relatively low.
- Could be critical for the yield of sub 0.25 μm sized devices.
- Requirement of proper maintenance and restoration of the CMP parts at a frequent basis.

1.4 Applications

CMP was initially implemented to planarize the interlayer dielectric (SiO_2) in a multi-layered metallization scheme (Zantye, Kumar and Sikder, 2004). After its successful implementation, the use of CMP has been inflated to:

- Different metal polishing such as Al, Cu, Ta, Ti, Pt, Au, etc.
- Polishing of doped/undoped oxides of Si, low-k dielectrics, insulators such as Si_3N_4 etc.

1.5 Basics and principle of CMP

By definition, CMP is a process where the collaborative effect of the chemical and mechanical actions improvises the material removal rate (MRR) to give a near perfect planar surface on which layers of integrated circuitry are to be assembled. The unwanted materials on the wafer are removed by using a chemical slurry in complement with the mechanical impacts.

The three salient elements in the CMP process are: a) entity to be polished b) polishing pad and c) polishing slurry. The sample/metal/dielectric coated wafer is mounted on the holder and the

surface to be polished is pressed upon a polymer-based pad. Slurry containing abrasives and chemical reagents are allowed to flow between the sample surface and the pad. The simultaneous rotation of the sample holder and the polishing pad (usually circular) on its own axis causes removal of the material. The polishing pad is attached on the platen and a membrane like object is mounted on the sample holder to apply appropriate downforce on the sample. The applied force usually lies in the range of 1-10 psi (Oliver, 2004). The planarization ability of the CMP process is measured by calculating the removal rate by weight loss method given by

$$\text{Removal rate (RR)}\left(\frac{\text{nm}}{min}\right) = \frac{\text{Weight loss (gm)} \times 10^7}{\text{Density}\left(\frac{gm}{cm^3}\right) \times \text{Time}\,(min) \times \text{Surface area}(\text{cm}^2)} \quad [1.1]$$

The typical CMP equipment that are commercially available in the industries can be segregated into four section (a) rotary-type polisher where the sample carrier and the platen move in reciprocation; (b) rotary-type polisher with an oscillating carrier; (c) orbital-type polisher with orbital rotating platen; and (d) linear-type polisher where the polishing pad is a linear motion belt. It is to be noted that the table diameter for most of the commercial CMP machines are in the range of 20-26"(Oliver, 2004). Such CMP machines which are commercially used, usually polish one wafer at a time.

A typical CMP process is displayed in Figure1.1. As shown, the slurry comprising of abrasives and different chemical reagents are allowed to dispense from a tube to the pad and the surface of the sample to be polished. As the platen and the sample rotates, the slurry envelops into the groves of the polishing pad and comes in proximity with the surface of the sample to be polished. The relative motion between the sample and pad with adequate of downforce applied

on the sample will cause the required removal of material. The sample moves relatively to the pad and the material removal rate is governed by Preston's law (Qin, Moudgil and Park, 2004):

$$\text{Removal Rate (RR)} = K_p \times P \times v \qquad [1.2]$$

Here, K_p stands for Preston's coefficient (constant), P stands for pressure applied on the sample surface and v for relative velocity between the sample holder and pad respectively.

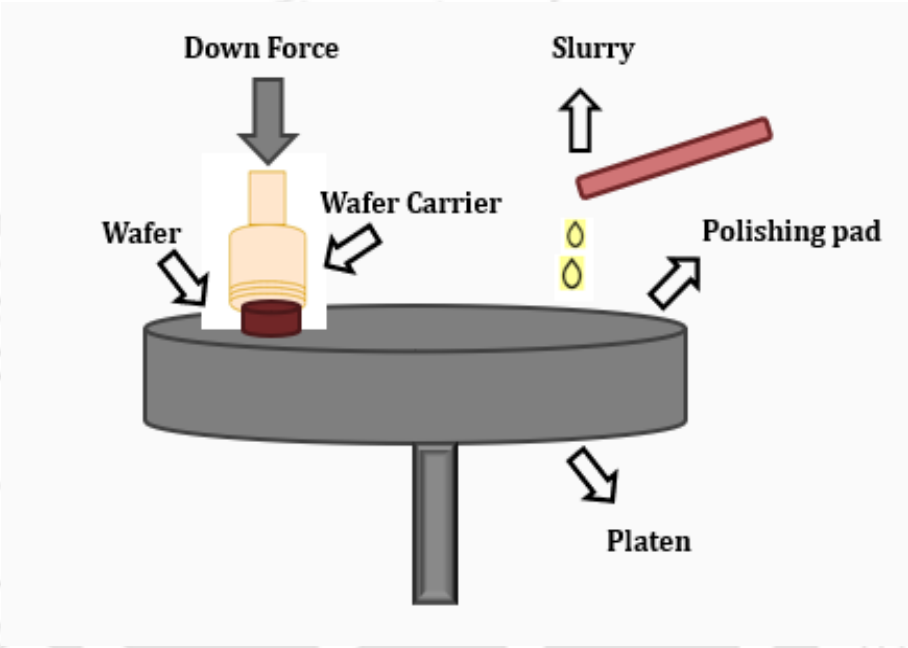

Figure 1. 1 A Schematic diagram of Chemical Mechanical Polishing Process

1.6 Factors/Variables/Parameters Governing the CMP

The output variables such surface smoothness, the uniformity, the material removal rate etc determine the efficiency of a CMP process/machine. However, the factors or input variables relating to sample-pad interaction play a very prominent role in achieving this efficiency. The ultimate polishing rates obtained is the synergetic action of the input variables. Some of the input variables and output variables (Li, 2007; Baklanov, Ho and Zschech, 2012) for the CMP process are as follows:

1.6.1 **Input Variables** (Li, 2007)

- **Process parameters:** Down force, linear velocity, flow rate of the slurry.
- **Slurry chemistry:** Abrasives, oxidizers, complexing agents, inhibitors, surfactants, pH tuners, pH.
- **Pad properties:** Pad uniformity, conditioning, mechanical strength.
- Substrate properties: Wafer size, wafer layer and its strength, size to density ratio.

1.6.2 **Output Variables**(Li, 2007)

- Polishing rate
- Polishing efficiency
- Surface texture
- Selectivity between metals
- Uniformity amongst multiple wafer
- Surface Uniformity
- Dishing and erosion

A brief illustration on the major parameters such as slurry chemistry, machine parameter, and material removal rate are as follows:

- **Slurry chemistry:** The slurry comprising of abrasives and other chemical reagents such as oxidizer, complexing agent, inhibitor, surfactant etc. in DI water is the most complex component consumed in a CMP process (Zhao and Lu, 2013). The pH value of the chemical slurry along with the particle size, concentration of the chemicals and abrasives used play an important role in providing excellent local and global planarization in a CMP process. An ideal CMP slurry should have the capability to provide uniformity with good surface quality, desired removal rate, desired selectivity, less failure along with reduced corrosion. The slurry being the most complex consumable in a CMP process, mechanism related to it and its interaction with the pad

and the wafer/samples are the most unexplored part in a semiconductor fabrication process.

- **Machine parameters:** As mentioned above, the CMP process involves both chemical and mechanical actions. This collaboration has been the concern of numerous investigations; however, focus was mainly on the mechanical impacts as understanding the chemical mechanism was complicated. However, mechanical impacts can't alone affect the global planarity and diminish the micro scale roughness of IC fabrication as the contribution of the chemical reagents also has a prime role on it. The variations in different machine parameters are the initial adjustments made in the CMP process to acquire desirable results (Zantye, Kumar and Sikder, 2004).
- **Removal rate:** Removal rate of a particular metal to be polished is highly dependent on the slurry chemistry used in the CMP process. Different components used in a slurry have different impact on the removal rate. The oxidizer accelerates passivation on the metal surface (due to anodic shift of corrosion potential) (Ein-Eli and Starosvetsky, 2007). Complexing agents are added to form soluble compounds and to get an enhanced etch rate and a desired removal rate (Ein-Eli and Starosvetsky, 2007). Inhibitors plays an key role in controlling the corrosion damage on the metal caused due to exposure of various chemicals during CMP process (Ein-Eli and Starosvetsky, 2007). The slurry pH has a significant role as the oxidation state of the metal along with the compounds formed on its interaction with the chemical reagents are highly reliant on the pH value of the system.
- **Selectivity:** The selectivity is one of the most important criteria in formulating a CMP slurry. The ratio of removal rate of a given material as compared to the other material on using the same slurry gives the selectivity. Selectivity is important when a slurry

need to remove the materials at a time, example: the interconnect and the barrier metal or the underlying dielectric materials.

1.7 Challenges in CMP

CMP involves a balanced requirement of both chemical and mechanical processes to obtain the required removal rates. For a CMP process that is inclined more towards the mechanical nature, the removed material from the surface will mainly be insoluble byproducts which might cause redeposition onto the material surface (Steigerwald *et al.*, 1995). Also, the final surface will be too rough in nature. This roughness/scratches might affect the electrical performance of the interconnects. Similarly, if the CMP process is too inclined towards the chemical process, achieving as well as maintaining the surface planarity would be a challenge (Steigerwald *et al.*, 1995). This would increase the surface roughness and thereby resulting in decrease of electro migration resistance. Hence, a balance of both chemical and mechanical activity is required in order to achieve planar surfaces of higher quality. Some of the other common challenges faced during a CMP process due to the various CMP parameters are discussed below:

- **Challenges due to polishing pad:**

MRR and surface uniformity of the material polished is strongly dependant on the hardness of the polishing pad. Porous polyurethane having a filler substance for modifying the hardness is usually used as polishing pad. The type of pad (hard pad or soft pad) required in a CMP process is strongly influenced by the material being used and the different steps it undergoes. The physical properties of a pad such as surface roughness, hardness, compressibility, elastic modulus etc varies due to mechanical stress and the chemical reaction occurring on the surface of the pad. This effects the overall CMP process. In order to avoid the mentioned issues and maintain the pad performance, a pad conditioning process is introduced. Another important factor that decides the pad performance is the groove design of the pad. A well-designed groove

is mandate for proper flow of the slurry and removal of the polishing residues. To procure a uniform planarity, it is necessary to ensure that there is symmetrical contact between the pad and the surface to be polished (Steigerwald *et al.*, 1995). A smoother rigid pad usually serves this purpose as it avoids any sort of bending.

- **Slurry complexity:**

Understanding the complexity of a slurry and how it reacts with the material to be polished is one of the most principal challenges in a CMP process. The primary requirement of a well formulated slurry is that it should properly dissolve the mechanically abraded debris from the polished surface. Failure in dissolution would result in lower polish rates as the debris settled on the metal surface as oxides could not be mechanically abraded alone and efficiently. The second requirement of the slurry is that it should planarize the surface uniformly.

- **Passivation of metals:**

Based on the solution pH and high metal surface energy, the metals tend to passivate. Passivation or development of a protective stable film on the surface is essential to prevent or diminish unwanted metal reactions with the surrounding environment. Passivation, which is one of the important steps of semiconductor fabrication is required to prevent oxidation and damage of the metals (specially interconnects/barrier) during processing, storing or removal of contamination during post CMP process (Park, Paluvai and Venkatesh, 2018). In order to get a proper passivation film, understanding the surface chemistry along with proper screening of the passivating agent is required.

1.8 Evolution of CMP

1.8.1 Interconnect Materials

The urge of producing higher performance products, weensy structures at lower unit costs is the prime driving force for instigating new materials or technologies or innovations in the

semiconductor industry(Hazarika, Patil and Rajaraman, 2020). Fabrication of transistor device is known as the front end of the line (FEOL) whereas back end of the line (BEOL) is the interconnect part (both local and global wiring) affixing different elements in a circuit (Krishnan, Nalaskowski and Cook, 2010).

With the miniaturization of feature size of the semiconductor devices to less than 0.5 μm, a delay in the signal process comes into existence which hinders the improvement of device performances. The two types of delays are intrinsic gate delay and interconnect delay. The time required in switching the transistor from on to off or vice-versa is the intrinsic gate delay whereas time taken in a circuit for a voltage/signal to pass from the source to the end of the line is known as the interconnect delay. With the reduction of device size below 0.5 μm, interconnect delay overrules. Intrinsic resistance (R) of the metal lines and capacitance (C) of the dielectric material are the two prime components of interconnect delay (also known as RC delay). To reduce this interconnect delay that comes with miniaturization of chips, aluminium (Al), the customary interconnect material is replaced with a finer conductor copper (Cu) and SiO_2 is been substituted with low-k dielectric materials.

Aluminium (Al) with a resistivity of 2.66 μΩ cm was the first-generation interconnect material(Li, 2007). However, it was found that the resistance and signal delays can be reduced by opting for a lower electrical resistivity metal. A wide variety of metal was suggested for that in the 1990s. Gold and silver are amongst the few to be named. Silver has lower resistivity as compared to Al, but is easily susceptible to corrosion and electro mitigation. Unlike silver, gold had better corrosion resistance and electro mitigation but the conductivity of it is equivalent to that of Al. Hence, taking all the necessary factor into consideration, copper (Cu) having a resistivity of 1.67 μΩ cm and exceptional resistance to electro migration as compared to Al was selected as the interconnect material. Copper interconnects which are still in use was introduced in 1997. It is to be mentioned that in the BEOL part of the semiconductor device, a

dielectric based material is used to isolate the copper lines. Typical silicon-based material is usually used as the dielectric materials however studies are going on currently to replace it with ultra-low- k materials, e.g.; SiCOH.

Although Cu is considered as the most promising interconnect materials, it adheres poorly to the dielectric materials, i.e. it is highly mobile and liable to diffuse into dielectric material. This would deteriorate the device performance. Therefore, to address these matters, a barrier metal is introduced between the Cu and the dielectric. The deposition of the barrier metal is done prior to Cu deposition in order to isolate it from the dielectric material. Some of the barrier materials are Ta, TaN, Mn, Co, CoMn, TaC, Ru, Mo etc. The major requirements for a material to act as suitable barrier metal:

- The barrier metal should not affect the conductivity of the system and should have a lower resistivity to both the Cu and the dielectric. However, an acceptable conductivity of the barrier metal is necessary for depositing the interconnect on it.
- It should obstruct Cu diffusion to the dielectric even at high temperatures.
- The barrier metals should properly adhere to both the dielectric and Cu and should be capable enough to avert any sort of external stresses.
- There should be negligence galvanic corrosion between the Cu and the barrier metal.
- The barrier layer should be inert to both Cu and the dielectric.
- Most importantly, selective removal with adequate process parameters should be fulfilled to attain a global planarization.

1.8.2 Introduction of Ruthenium (Ru) and Cobalt (Co) as barrier for Cu diffusion

It is not possible for a material to have all the properties as per mentioned above to act as a barrier metal. Therefore, a material is chosen based on some important properties compromising with the others. Tantalum (Ta) being nonreactive with Cu and having ability to

withheld its diffusion to 600 ºC was considered as the first-generation barrier metal for Cu (Tan *et al.*, 2022). However, beyond 600 ºC, Cu diffuses through it forming Ta silicides(Abu-Zeid, Yousef and Kordia, 1992; Halloway *et al.*, 1992).To improve barrier properties of Ta by blocking the Cu diffusion, impurities (such as nitrogen) were added to the Ta film(Min, Chun and Kim Ki-Bum, 1996). However, the Ta/TaN resists direct deposition of Cu on it, as a result of which Cu-seed layer deposition became a necessary step prior to every physical vapor deposition (PVD) of Cu (Sverdlov, 2011).

However, with the shrinkage of the technology node to less than, maintaining the thickness, integrity and diffusive barrier property of Ta/TaN film has become a major challenge(Hazarika, Patil and Rajaraman, 2020). Therefore, to overcome these challenges several other barrier materials namely Co, CoMn, Mn, CuMn, TiZrN, TaC, WSiN, BN, Ru, Mo etc were investigated(Qu *et al.*, 2004; Tiruchirapalli N Arunagiri *et al.*, 2005; Shima, Fukunaga and Tsujimura, 2007).

Barrier metal, Ruthenium (Ru): Ru being a low electrical resistivity (7.6 μΩ cm) metal with high melting point (2334 ºC) and no reactivity with Cu was considered as a good contender for the existing barrier metal(M Damayanti *et al.*, 2006; Amanapu *et al.*, 2013). Unlike Ta/TaN, direct electroplating of Cu on Ru was feasible thereby putting an end to the need of Cu seed layer deposition(Josell et al., 2003; Seo et al., 2011; Amanapu et al., 2013). Because of these many characteristics, Ru is proposed to be one of the encouraging candidates as diffusion barrier of Cu(Lee and Park, 2004; Ranaweera *et al.*, 2019; Zhang, Wang and Lu, 2020).

Barrier metal, Cobalt (Co): Qualities like low hardness (5.0 Mohs), low resistivity (~6.2 μΩ cm), good stability and economical, make Co as one of the most potent barrier metals for Cu diffusion(Sagi and Babu, 2016). In addition to that, Co adheres well with Cu and thus eliminating the need of any seed layer deposition.The next challenge, after depositing the

barrier metal and Cu interconnect, is planarizing the surface with uniformity for the next level metallization(Cheng *et al.*, 2015).

Just like the dual damascene process, CMP of a metals is a two-step mechanism. The initial step comprises of bulk removal of interconnect Cu with an effective CMP slurry under controlled process parameters. The initial step is stopped at the slight unveiling of the barrier metal. The secondary step comprises controlled removal of the remaining Cu along with the barrier metal without excessing thinning throughout(Krishnan, Nalaskowski and Cook, 2010). This demand the requirement of a slurry that can selectively (near to 1) polish the barrier metal and Cu. Post CMP and prior to the next level metallization, the surfaces are rinsed chemically to remove the debris or oxides. A typical CMP process is illustrated in Figure 1.2.

It is to be noted that as compared to Ru, dissolution and removal rates of Co is higher. Therefore, the formulated CMP should be able to control the metal dissolution as well as give a selectivity of 1.

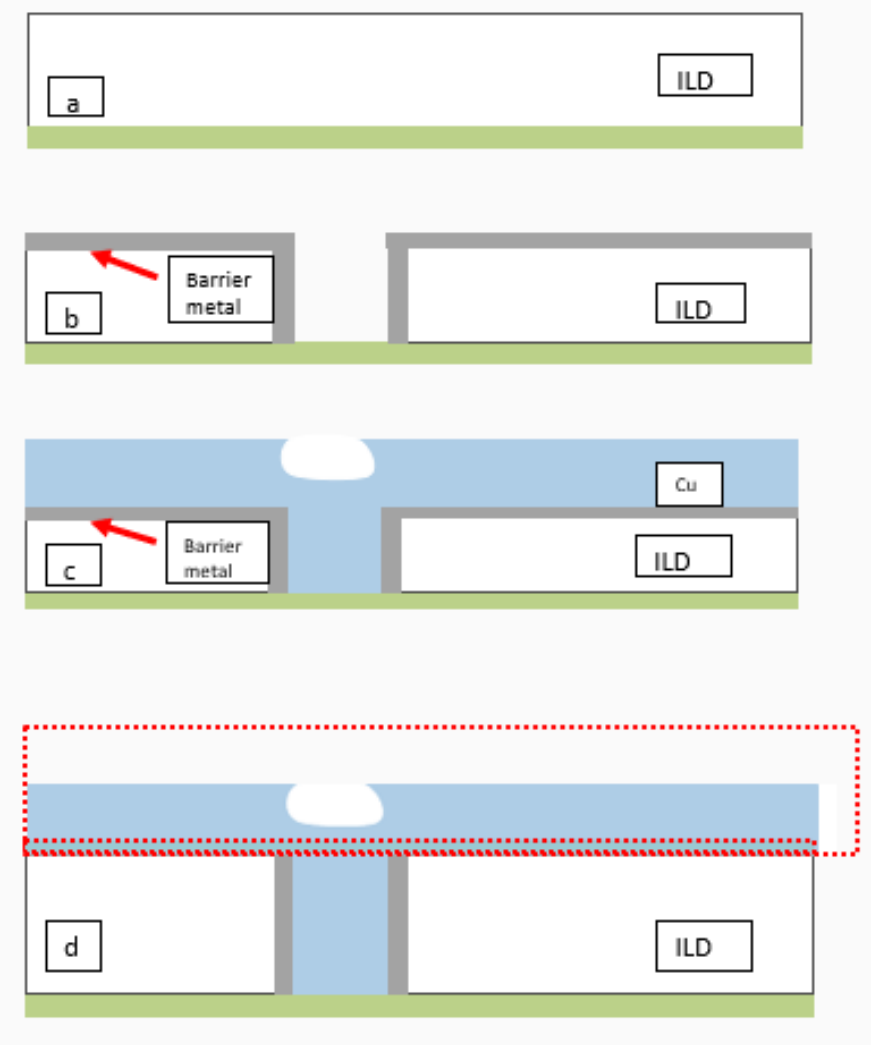

Figure 1. 2 Process flow in interconnect Cu CMP, (a) patterning inter layer dielectric (ILD), (b) conformal deposition of Ru, (c) copper Electrodeposition, (d) After Cu CMP steps 1 & 2.

1.8.3 Galvanic Corrosion

By definition, galvanic corrosion is the damage that occurs due to corrosion when two electrically different metals are exposed to one another in the presence of an electrolyte. Here, corrosion observed is more on the active metal rather than the noble one. The active metal corrodes faster than normal, whereas the noble one corrodes slowly or might not corrode at all.

In the same environment, the more active metal usually acts as the anode while the more noble metal acts as the cathode. The electrolyte acts as a medium for ion transfer from the anode to the cathode. Difference in potential between the metals is the prime instigator for galvanic corrosion. The other factors influencing galvanic corrosion rates are ratio of area of contacts between the metals, cathode efficiency, electrical resistance between metals and the environment etc.

Cu/Ru galvanic corrosion: In a typical galvanic couple**,** Ru usually acts as the cathode whereas Cu as the anode giving rise to differences in open circuit potentials (E_{oc}) between the two metals(Ã *et al.*, 2009; Peethala, Roy and Babu, 2011a; Cheng, Wang and Lu, 2017). The E_{oc} difference is solely dependent on the electrolyte (slurry in case of CMP process)(Cheng, 2017). Therefore, in order to minimize galvanic corrosion, the formulated slurry should have the capability to deduce E_{oc} difference between the two metal (Cu/Ru). The slurry should contain additives which suppresses cathodic reactions of Ru and anodic reaction of Cu.

Cu/Co galvanic corrosion: Unlike Cu/Ru galvanic couple, Cu act as the cathode and whereas Co acts as the anode in a Cu/Co galvanic couple(Bian *et al.*, 2020). Co being the more active metal with lower standard potential undergoes faster dissolution than normal when in contact with Cu in a reactive environment (CMP slurry)(Bilouk *et al.*, 2009a). Therefore, in order to diminish galvanic corrosion, the formulated slurry should contain chemical reagents which would either lower the E_{oc} of Cu or escalate the E_{oc} of Co respectively(Cheng, 2017).

1.9 Electrochemistry

Electrochemical methods are employed to monitor and understand the electrochemistry and corrosion process of the metal in a solution. A metal in contact with a solution undergoes electrochemical reaction as show in the following equations 1.3 and 1.4. To get a detailed view of the reactions occurring on the barrier metal and Cu in the formulated slurry, electrochemical studies are being performed.

$$M \rightarrow M^{+} + e^{-} \quad [1.3]$$

$$2H_2O + O_2 + 4e^{-} \rightarrow 4OH^{-} \quad [1.4]$$

Some advantages of using electrochemical technique to study corrosion are its speed, non-destructiveness, high resolution and detailed mechanistic information. The three main sources of analytical signal are potential, current and charge. The different electrochemical techniques employed in electrochemistry to understand the metal corrosion in detailed are as follows:

1.9.1 Open circuit potential (OCP)

Open circuit potential (OCP)/corrosion potential/ equilibrium potential /rest potential, is the initial step for most of the electrochemical experiments. OCP is the steady state potential developed at the working electrode surface with respect to the reference electrode in a corrosive environment. OCP occurs when the cathodic reactions are in equilibrium with the anodic reaction rates without any applied current or potential i.e. the electron flow rate in the system is zero. If the OCP is stable, it signifies that the working material has reached its equilibrium with the electrolyte and further experiments can be carried out on the particular system. A typical OCP curve vs time is illustrated in Figure 1.3.

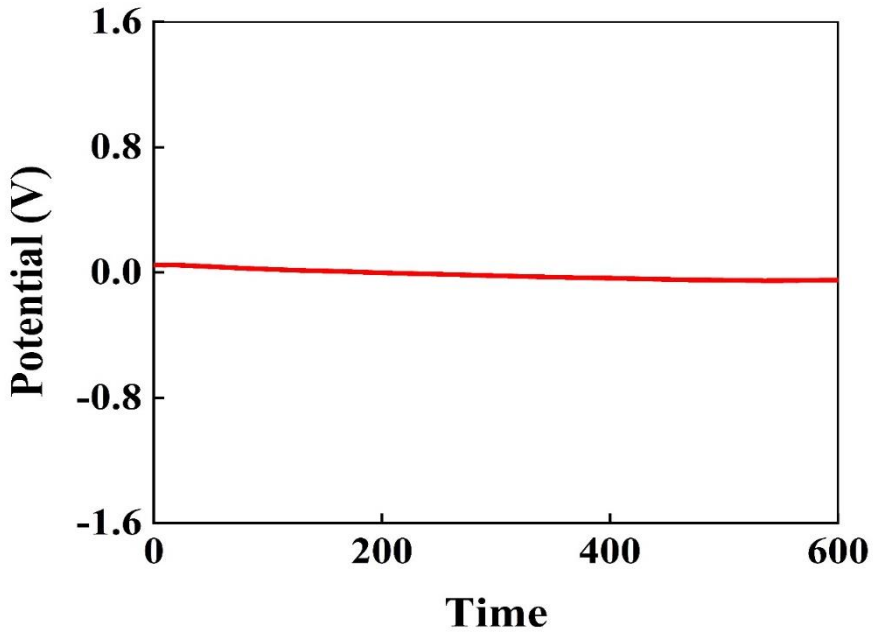

Figure 1. 3 An OCP vs time representative curve

The two most important parameters to understand the corrosion behavior of the metals in a solution are the corrosion potential (E_{corr}) and corrosion current (I_{corr}). E_{corr} gives us an idea about corrosion condition of the metal whereas I_{corr} enlightens us with the real time corrosion rate data(Orazem and Tribollet, 2008). However, as the I_{corr} , the summation of (I_{ox} +I_{red}) (equations 1.5) equals to zero at OCP, it is not possible to measure the I_{corr} value directly at this condition. Therefore, to get clear idea about the corrosion rate, the I_{corr} value is measured using potentiodynamic polarization.

$$I_{summation} = I_{corr} = I_{ox} + I_{red} = 0 \qquad [1.5]$$

1.9.2 Potentiodynamic polarization (PP)

The Potentiodynamic polarization (PP) is useful to estimate the corrosion rate and investigate the inclination of materials toward corrosion. PP technique involves sweeping the potential (either in positive or negative direction w.r.t. OCP) of metal sample (working electrode) toward a final potential which is away from the OCP. Change in potential is the driving force in PP

method. The current in PP which is measured by a potentiostat is monitored as a function of time or potential.

Polarization curve displayed in Figure 1.4 is the plot of potential (volts,V) vs logarithm of the absolute current (ampere w.r.t to exposed surface area of electrode A/cm^2) under steady state conditions. As the current density magnitudes are different, for easier demonstration logarithmic values of the absolute current are taken into consideration during plotting. The curved line observed in Figure 1.4 is the summation of the currents (cathodic and anodic) at different potentials of the working electrode. The point marked 'A' in the figure is corrosion potential or OCP. The lower part of the curve w.r.t. to OCP is cathodic polarization curve (cathodic current is dominant) whereas the upper part of the curve w.r.t. to OCP is the anodic polarization curve (anodic current is dominant). The point of intersection of the extrapolation of the linear section of the cathodic and anodic curve as shown in Figure 1.4 gives the E_{corr} and I_{corr} values of the system. Higher I_{corr} values signifies more corrosion rate (Orazem and Tribollet, 2008). It is to be noted that current is measured if PP is conducted through potentiostatic polarization and voltage is measured is PP is performed through galvanostatic polarization.

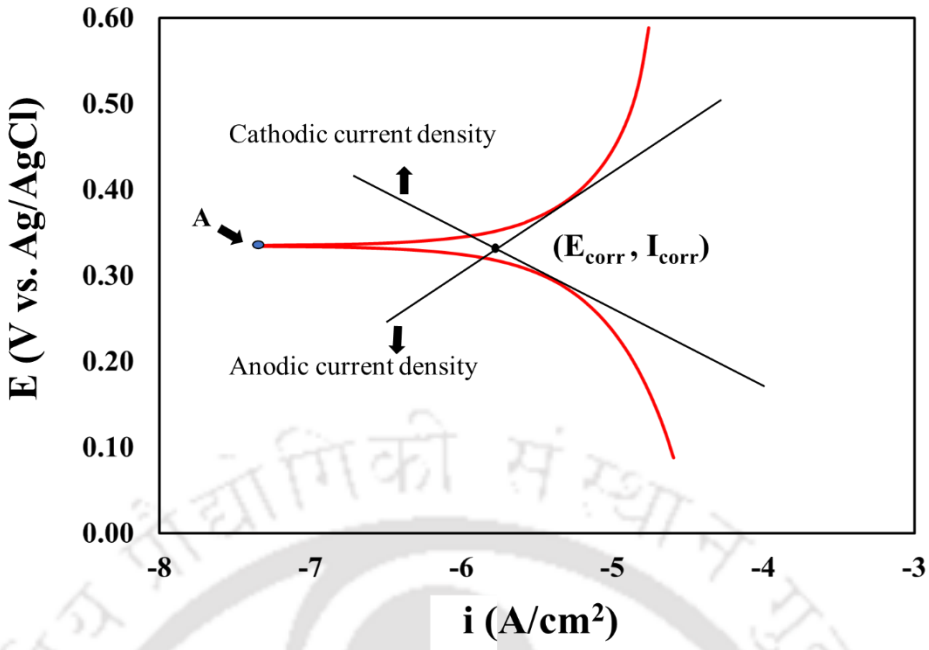

Figure 1. 4 A polarization curve obtained from potentiodynamic polarization measurements

When the working electrode acts as an anode, anodic polarization (equations 1.6) occurs by releasing electrons and the potential moves more on the positive direction. Here, the anodic current is considered to be positive. On the other hand, cathodic polarization occurs when electrons cohere to the surface of the working electrode (equations 1.7). Addition of excess electrons to the surface, in some cases causes electrodeposition. Overvoltage (η) which is the difference between the final potential and equilibrium potential is negative in this case. Here, formation of metal ions is lower than the deposition rate.

$$\text{Metal} - ne^- \rightarrow \text{Metal}^{n+} \qquad [1.6]$$

$$\text{Metal}^{n+} + ne^- \rightarrow \text{Metal} \qquad [1.7]$$

To get a better understanding of the oxidation and reduction processes with the assumption that that the anodic and cathodic reactions are controlled by the kinetics of electron transfer at the surface of the metal, the following two models were proposed: Butler-Volmer equation and *Stern-Geary equation.*

Butler-Volmer equation:

This basic model estimates the corrosion rate of the system by respectively calculating the corrosion current (I_{corr}). To find the Icorr values both the cathodic and anodic reactions of the tafel equation (equations 1.8) are taken into consideration which is displayed in equations 1.9 (Faulkner, 2000)

$$I = I^0 \left(e^{\frac{2.303(E-E^0)}{\beta}} \right) \qquad [1.8]$$

Here, I (A) and I^0 (A) are the reaction current and reaction dependent constant (exchange current) respectively. E (V) signifies the applied electrode potential whereas E^0 (V) the equilibrium potential. The Tafel constant (constant for particular reaction) of the reaction is given by β (V/decade). Log of 10 is represented by 2.303.

The Butler-Volmer equation[14] is given by

$$I = I_{corr} \left(e^{\frac{2.303(E-E_{corr})}{\beta_a}} - e^{\frac{-2.303(E-E_{corr})}{\beta_c}} \right) \qquad [1.9]$$

I (A), I_{corr} (A), E (V) and E_{corr} (V) signifies the measured cell current, the corrosion current, the applied electrode potential and the corrosion potential. β_a (V/decade of current) and β_c (V/decade of current) are the respective anodic and cathodic Tafel constant. At high cathodic

overpotentials, the cathodic compound $\left(e^{\frac{-2.303(E-E_{corr})}{\beta_c}} \right)$ equals to 0 whereas at higher anodic overpotentials, the anodic compound $\left(e^{\frac{2.303(E-E_{corr})}{\beta_a}} \right)$ equals thereby reducing the Butler-Volmer equations to respective Tafel equations.

$$I = I^0 \left(e \frac{2.303(E - E^0)}{\beta_a} \right) \quad [1.10]$$

$$I = I^0 \left(e \frac{2.303(E - E^0)}{\beta_c} \right) \quad [1.11]$$

Stern-Geary equation:

Some of the approximations of Butler-Volmer equations are as follows: (a) potential deviates ± 10-25 mV w.r.t. E_{corr} or OCP, with the resulting curve being a straight line whose slope has a unit of resistance; (b) $\left(e^{\frac{2.303(E-E^0)}{\beta}} \right)$ of the Taylor equation is expanded neglecting second and higher order terms. Simplifying and rearranging the Butler-Volmer equations[15], the Stern-Geary equation (equations 1.9) is obtained.

$$I_{corr} = \frac{1}{R_p} \left(\frac{\beta_a \beta_c}{2.303(\beta_a + \beta_c)} \right) \quad [1.12]$$

Here,

$$R_p = \left(\frac{\Delta E}{\Delta I} \right)_{\Delta E \to 0} \quad [1.13]$$

Here, Polarization resistance, R_p (Ω) signifies the resistance against oxidation of the corroding species when a potential is applied. Lowers the corrosion rate, higher will be the R_p values and vice versa. I_{corr} (A) stands for corrosion current and β_a (V/decade of current) and β_c (V/decade of current) are the respective anodic and cathodic Tafel constant. ΔE which almost nears to E_{corr} is the applied potential difference whereas ΔI is its associated polarization current.

1.9.3 Electrochemical Impedance Spectroscopy (EIS):

Different types of reactions such as electrochemical, diffusion, adsorption-desorption etc occurs at the working electrode-electrolyte interface and in the bulk solution. Electrochemical impedance spectroscopy which has capability to measure the impedance precisely even at very low frequencies (1 mHz) is useful to investigate such mechanisms. The information that can be obtained from EIS are adsorption/desorption/diffusion of compounds, passive layer formation, faradic/non-faradic reaction, electrical double layer formation etc. Impedance spectroscopy employs a small amplitude, alternating voltage signal perturbation to record the response of the electrochemical system in terms of AC current. Small amplitude AC signal perturbation is employed to get a linear or pseudo linear output response of the system.

Ohm's Law (E=IR) states that the capacity of an element to endure the flow of electric current is known as resistance. However, impedance implies for circuit elements which are much more complex and tougher to understand as compared to resistance. Therefore, in simpler words it can be said that, impedance is the frequency dependent resistance (opposition of any form) to current flow of a complex circuit element that consists of not only resistors but also capacitors, inductor etc. It is to be noted that unlike resistor, inductor and capacitor has an imaginary component and is dependent on frequency.(Brett, Brett and Electrochemistry, 1993; Faulkner, 2000).The impedance of resistor, inductor and capacitor are as follows:

Table 1.1: Electrical components vs. impedance

Component	Current vs. Voltage	Impedance
Resistor	$E = IR$	$Z = R$
Inductor	$E = L\frac{dI}{dt}$	$Z = j\omega L$
Capacitor	$I = C\frac{dE}{dt}$	$Z = \frac{1}{j\omega C}$

Here, E stands for applied voltage, I, R, L and C are the current, resistance, inductance and capacitance respectively. ω and t are the angular frequency and time whereas j stands for √-1which is an imaginary component.

As already mentioned, a small amplitude, alternating voltage signal perturbation is employed to obtain the impedance data. The perturbation and the measured output response signal in sinusoidal form is given by the following expression (equation 1.14 and 1.15 respectively):

$$E_t = E_0 \sin(\omega t) \quad [1.14]$$

$$I_t = I_0 \sin(\omega t + \phi) \quad [1.15]$$

Here,

$$\omega = 2\pi f \quad [1.16]$$

E_t (V) and E_0 (V) signifies the potential {at time(t)} and amplitude of the applied signal. I_t (A) and I_0 (A) are the *ac* current response {time *t* (s)}and the amplitude current respectively. ω stands for angular frequency (rad s^{-1}) and *f* (Hz) for frequency. ϕ is the phase shift with respect to the input voltage signal.

Therefore, combining equation 1.14 and 1.15, impedance (Z) can be represented as:

$$Z = \frac{E_t}{I_t} = \frac{E_0 \sin(\omega t)}{I_0 \sin(\omega t + \phi)} = Z_0 \frac{\sin(\omega t)}{\sin(\omega t + \phi)} \quad [1.17]$$

Here, Z_0 (Ω) signifies the magnitude of impedance.

Expressing the impedance data (in complex form) using Euler's relationship

($e^{j\phi} = \cos\phi + j\sin\phi$) is as follows

$$Z(\omega) = \frac{E_t}{I_t} = Z_0 e^{j\phi} = e^{j\phi} = Z_0(\cos\phi + j\sin\phi) = |Z|(\cos\phi + j\sin\phi) = \left[(\mathrm{Re}(Z))^2 + (\mathrm{Im}(Z))^2\right]^{1/2}(\cos\phi + j\sin\phi) \quad [1.18]$$

Here,

$$\phi = (\arg Z) = \tan^{-1}\left(\frac{\mathrm{Im}(Z)}{\mathrm{Re}(Z)}\right) \quad [1.19]$$

The EIS data is represented either by Nyquist plot (real part of impedance data vs imaginary part of impedance data) or Bode plot {Bode modulus (impedance vs log of frequency) and bode phase plot (phase shift vs log of frequency). It is to be noted that, although both plots give similar information, unlike Bode plot, Nyquist plot don't display the frequency at which the impedance data are being noted. Typical EIS plots {(a) Nyquist (b) Bode modulus (c) Bode phase plot} are illustrated in Figure 1.5.

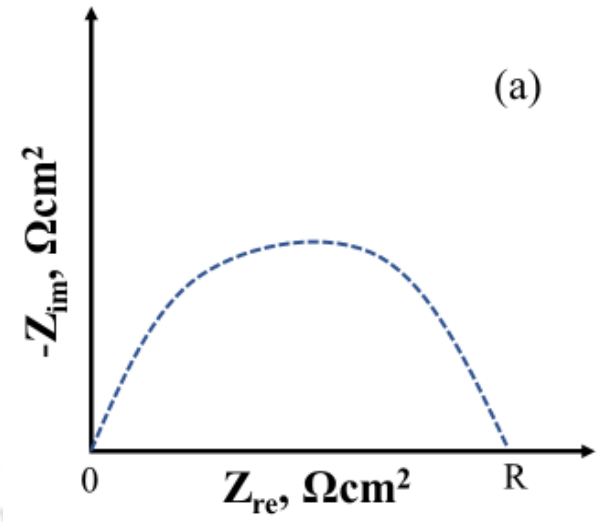

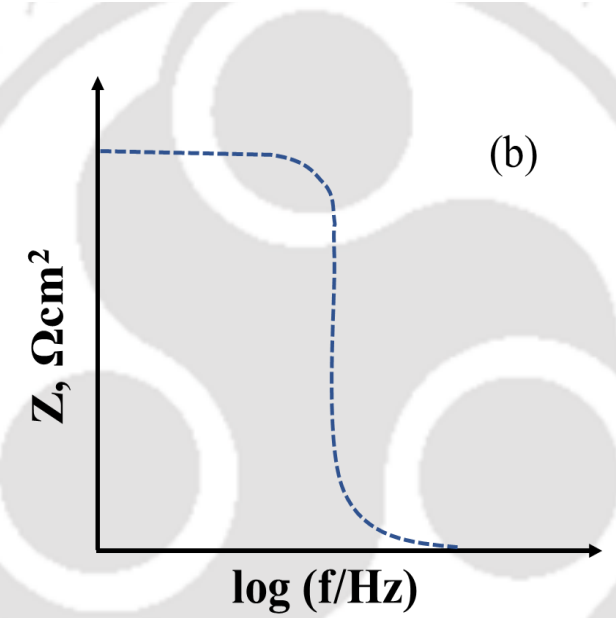

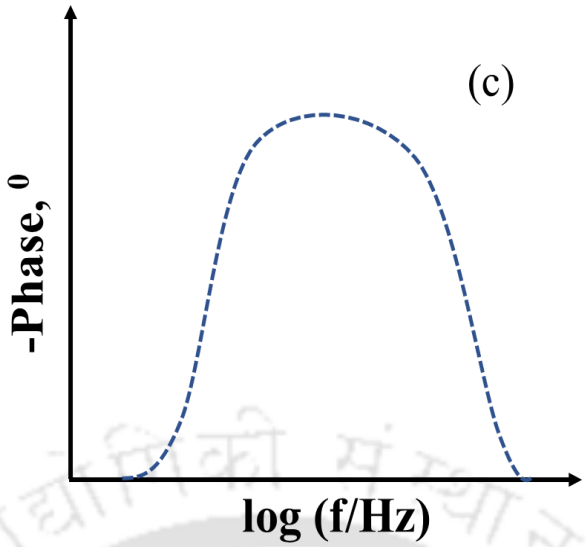

Figure 1. 5 A standard EIS plot (a) Nyquist (b) Bode modulus (c) Bode phase

The impedance data obtained can be modelled through two different approached: Electrical Equivalent Circuit (EEC) model and reaction mechanism analysis (RMA).

1.10 Electrical Equivalent Circuit Model (EEC)

The physio chemical process occurring at the bulk solution and solution metal interface are evaluated using the Electrical Equivalent Circuit (EEC) model. The experimental data is fitted with the best fit EEC or Voight circuit. A typical circuit known as Randles circuit is displayed in Figure 1.6.(Orazem and Tribollet, 2008).

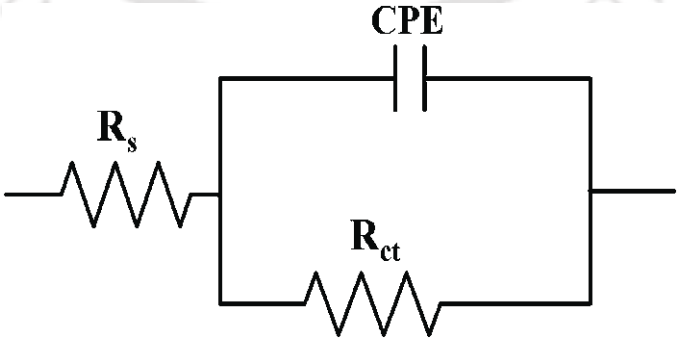

Figure 1. 6 The Randles circuit

Here, (R_{sol}) signifies solution resistance, R_{ct} is the charge transfer resistance, C_{dl} signifies double layer capacitance and *W* stands for Warburg impedance. For a given impedance data, the circuit elements of fitted EEC circuit could be in both series and parallel connection. Elements in series signifies, that similar current passes through all the elements whereas elements in parallel signifies that the current through each element sums up to the total current. Representation of the EEC elements and its relation with impedance is displayed in Table 1.1

Table 1. 1 EEC elements and its relation with impedance.

Elements	**representation**	**Impedance (Unit)**
Capacitance (C)		$\frac{1}{j\omega C}$ (F)
Resistance(R)		R (Ω)
Inductance (L)		jωL (H)
Constant phase element (Q /CPE)		$\frac{1}{Y_{0i}(j\omega)^{n_i}}$ ($\Omega^{-1}s^n$)

1.11 Reaction Mechanism Analysis (RMA)

Reaction Mechanism Analysis (RMA), which is a modeling approach gives a detailed understanding about the reactions/electrochemistry/corrosion occurring on the metal solution interface. Based on the impedance data, different reaction mechanisms are proposed for a

particular system. However, the simulated data obtained from a particular mechanism which fits best with the experimental data are taken into consideration.

Thus, the intention of this study is to formulate suitable slurries for Cu-Ru and Cu-Co CMP with desired removal rate selectivity. In addition to that, the study also focuses on tailoring a slurry that would give reduced potential gap between Cu-Co galvanic couple. Also, the dissolution behavior of Co in the solution of interest is investigated using previously mentioned electrochemical and it supporting techniques. In Chapter 2, a substantial literature study is given.

CHAPTER 2

2. LITERATURE REVIEW

Chemical mechanical polishing (CMP) which was first employed for BEOL metallization in the early 1990s, has emerged out as an enabling technology for planarizing materials in the semiconductor industry. CMP is extensively used in microelectronic chip fabrication industries to polish the surfaces of various materials such as copper, ruthenium, tantalum, tungsten, dielectric materials such as silicon dioxide and so on.

The investigations done on CMP, along with corrosion related studies by different researchers till date mainly on Cu, Co and Ru are presented in this section. Studies related to CMP on the first-generation interconnect, Al and first-generation barrier metal Ta/TaN are also reported in brief. This section is categorized into 5 sections, i.e. study on Al, Cu, Ta/TaN, Co and Ru.

2.1 Aluminum (Al), the first-generation interconnect

As mentioned earlier Al, a polycrystalline material having low cost, good conductivity, easier to etch and deposit, better adherence to both silicon and silicon dioxide has emerged as an interconnect in the earlier times.(Künzelmann *et al.*, 2012) Various studies were carried out to study the CMP of Al.(Chen *et al.*, 2018) Easily removable aluminum hydroxide layer forms on the metal surface when treated in alkaline solutions.(Zhang *et al.*, 2016) Alumina nanoparticles combined with H_2O_2 were effective in removing the steady passive layer formed on Al surface, however a deformed surface was observed.(Ng *et al.*, 2007) A chemical free CMP slurry containing only inorganic resin abrasives gave a scratch free Al surface with high removal rates.(Yano *et al.*, 2001) Ahn et. al. (Ahn *et al.*, 2004) observed a similar result comprising of reduced scratches and higher removal using colloidal silica as abrasives in the CMP slurry. The formation of scratches can also be reduced by using a chemical wafer buff process along with a soft pad at lower downforce.(Hsien *et al.*, 2012) Use of novel chelating agents, FA/O I and

FA/O II surfactants in a H_2O_2 based slurry also gave similar results.(Feng *et al.*, 2016) It was seen that the formation and dissolution of the passive layer is highly influenced by the pH value of the system and optimized selections of chemicals. Wang et.al (Wang *et al.*, 1998) reported that dissolution of Al compounds is directly proportional to the concentration of glycine and pH of the slurry.

However, the Al CMP process is overshadowed by the corrosion nature of Al. Al has the tendency to corrode on the slightest exposure of solution containing such as chloride (Cl^-), sulphate (SO_4^{2-}), nitrate (NO_3^-), or fluoride (F^-) ions.(Stupian and Fleischauer, 1981) The reason behind the higher corrosion rate observed is due to occurrence of the following series of equations (in terms of chlorine)(Park, Paluvai and Venkatesh, 2018):

$$Cl^- + H_2O \rightarrow HCl + OH^- \quad [2.1]$$

$$2HCl + 2Al \rightarrow 2AlCl_3 + 3H_2 \quad [2.2]$$

$$2AlCl_3 + 3H_2O \rightarrow Al(OH)_3 + 3HCl \quad [2.3]$$

No additional Cl^- is required once HCl is formed from the reactions to corrode the Al surface. The small amount of Cl^- recycles the formation of HCl thereby severing the corrosion of the Al lines.

2.2 Study on Chemical Mechanical Polishing and Galvanic Corrosion of Copper

With the upgradation of the devices, Cu (1.67 μΩ) is introduced as an interconnect in place of Al (2.66 μΩ) due to its comparatively low resistivity, high immunity to electro migration and lower IC failure rates.(Gutmann *et al.*, 1995; Hu *et al.*, 1995; Paul *et al.*, 2005) The initial step in fabrication is deposition of copper in vias and trenches using electrochemical deposition technique or copper electroplating. The excess copper after deposition is being removed by the CMP technique, in order to obtain global planarization or a more uniform surface. The

efficiency of CMP processes depends on many factors such as type of slurry composition, pH, abrasives, polishing pad, pressure velocity, reduced erosion etc.(Zantye, Kumar and Sikder, 2004) The removal of Cu is dependent on the deposited texture as well as the impurity content.(Feng *et al.*, 2008) Based on SEM analysis, it is said that a lower polish rate for Cu <100> texture is observed as compared to <200> texture. (Feng *et al.*, 2008) Minimum strain energy occurring from mechanical stresses for Cu <200> texture causes the higher polish rates observed.

In a proposed slurry, the oxidizer accelerates the passive layer formation at the copper surface. Inhibitors prevent the corrosion damages and buffering agents maintains the pH value of the CMP slurry. Formation and deposition of insoluble compounds are lowered on the addition of complexing agents. Different slurries for Cu CMP application are proposed till date, with ammonium hydroxide, nitric acid and peroxide based solutions being the most prominent ones. (Ein-Eli and Starosvetsky, 2007) Ammonium hydroxide-based slurry is strongly alkaline in nature with pH ranging between 11 and 12 for desired polish rates. Nitric acid-based slurry is acidic in nature with pH being around ≤2. (Koutec W et.al; 1990). And the pH range of peroxide-based slurry varies from 3.5 to 4. However, Pourbaix diagram(Pourbaix, 1974) predicts that dissolution of Cu is vigorous in the acidic range. Hence, the use of acidic solutions is predicatively not favourable as it cannot provide copper passivity. The passive layer formed protects the underlying bulk metal from unwanted diffusion and also hinders chemical reaction. A thin oxide film is observed on the Cu surface when treated in aqueous solution or when exposed to the atmosphere oxygen. Different factors such as electrochemical potential developed at metal-solution interface and pH affect the protective properties of the oxide film. The two-step mechanism of thin oxide layer formation is illustrated in equation 2.4-2.6.(Griffin, 1984; Sato, 1990)

Cu metal (M) in a reacting environment oxide form metal hydroxide ion (X^{n+}), which adsorbs (ads) onto the metal surface.

$$M(s) \rightarrow M^{n+}(ads) + ne^{-} \quad [2.4]$$

The adsorbed ion then condenses to form a metal oxide.

$$M^{n+}(ads) \rightarrow M^{n+}(oxide) \quad [2.5]$$

The parallel reaction, occurring in the aqueous solution, facilities corrosion.

$$M^{n+}(ads) \rightarrow M^{n+}(aq) \quad [2.6]$$

The oxide layer comprises of cuprous oxide (Cu_2O) as inner layer and cupric oxide, (CuO) and copper hydroxide $Cu(OH)_2$ as the outer layer. Based on porosity, the protectiveness of the oxide layer is determined. The anodic reactions of the oxides/hydroxides formation are(Luan *et al.*, 2016):

$$2Cu + H_2O \leftrightarrow Cu_2O + 2H^{+} + 2e^{-} \quad [2.7]$$

$$Cu_2O + H_2O \leftrightarrow 2CuO + 2H^{+} + 2e^{-} \quad [2.8]$$

$$Cu_2O + 3\,H_2O \leftrightarrow 2Cu(OH)_2 + 2H^{+} + 2e^{-} \quad [2.9]$$

2.2.1 Ammonium hydroxide (NH_4OH) based slurry

The first slurry that was formulated and practically used for copper CMP was ammonium hydroxide.(Maugis and Pollock, 1984) The other ammonia-based slurry that were used for CMP are ammonium nitride(Jindal and Babu, 2004) and ammonium chloride(Starosvetsky and Ein-Eli, 2009). Presence of passive layer is usually observed in the neutral or basic pH range.

Hence, development of ammonia containing slurry was highly preferred for Cu CMP.(Prasanna Venkatesh and Ramanathan, 2010) Another advantage of using ammonia based slurries are that, ammonia enhances dissolution by forming Cu complexes such as $Cu(NH_3)^{2+}$ and $Cu(NH_3)_4^{2+}$ which are soluble in this pH range, thereby preventing and deposition of unwanted oxides on the metal surface.(Pourbaix, 1974) It is to be noted that the dissolution depends on the concentration of ammonia.(Ein-Eli *et al.*, 2003) The possibilities of formation of $Cu(NH_3)^{2+}$ decreases at lower ammonium concentration. This results in presence of insoluble oxides and hydroxides in abundance on the Cu surface.

In a NH_4OH based slurry, addition of a defined quantity of hydrogen peroxide enhances the removal rate of Cu. (Prasanna Venkatesh and Ramanathan, 2010) The dissolution rate accelerated due to shifting of the corrosion potential anodically. Self-passivation is not observed on Cu in the presence of ammonium hydroxide. This explains the similar dissolution rate observed from both abraded Cu (0.92 nm/min) and non-abraded Cu (0.91 nm/min) coupons.(Ein-Eli and Starosvetsky, 2007)

A high polish rate with a lower etch rate is observed in ammonia based slurries, clearly indicating that the polishing is done is purely by mechanical abrasion.(Oliver, 2004) The addition of various oxidizing agents such as, $Cu(NO_3)_2$ (Steigerwald *et al.*, 1995), NH_4NO_3(Steigerwald *et al.*, 1995) and $NaClO_3$ (Luo, Mackay and Babu, 1997) to the ammonic based slurries also lead to active dissolution without passivation on the surface.

Copper surface morphology studied by SEM analysis shows the occurrence of corrosion in an uneven pattern with extreme localized corrosion.(Oliver, 2004) A damage in the Cu layer could occur resulting in breakage of the Cu interconnect. Hence, the usage of ammonium hydroxide-based solutions in CMP slurries is not preferable.

2.2.2 Nitric Acid based CMP Slurry

Nitric Acid (acidic slurry) which is considered to be a strong oxidizer favours the formation of Cu^{2+} ions thereby causing actively high dissolution of the metal in the form of Cu (II)$^{-}$ ions. The potentiodynamic studies done by Eli et.al(Ein-Eli *et al.*, 2003) confirm active dissolution at different concentration of nitric acid. Hence, nitric acid-based slurry is considered inappropriate for conventional CMP of Cu. To prevent this, inclusion of inhibitors such as benzotriazole (BTA) was suggested.(Carpio, Farkas and Jairath, 1995) BTA forms a Cu-BTA layer on the surface thereby blocking dissolution.(Ryu *et al.*, 2019) Repetitive formation and dissolution of passive layer results in controlled surface polishing. A reduction in corrosion rate with an increase in BTA concentration is observed. However, it was seen that the inhibiting effect of BTA saturates beyond 0.01 M concentration.(Wang *et al.*, 1997) Nevertheless, as required, BTA does not immediately protects the metal from dissolution. This demands the requirements of a different chemical that would give a better protection as compared to BTA. Thus, different inhibitors were suggested such as Bis-aminazoles(El-Naggar, 2000), Imidazole(Lee, 2003), Citric acid(Kim *et al.*, 2003), Hydrazine (Sekhar and Ramanathan, 2006)

However, usage of nitric acid has a drawback. Its low pH corrodes the polishing instrument, pipelines which carry the slurry and the slurry mixing tanks. Therefore, nitric acid-based slurries are not suggested for CMP applications.

2.2.3 Peroxide based CMP slurries

Hydrogen peroxide (H_2O_2) being a strong and clean oxidizer can be used in different solutions at different pH ranges.(Shima, Fukunaga and Tsujimura, 2007). The dissociation of H_2O_2 causes evolution of mainly hydrogen, oxygen, hydroxide-ions and water and thus, major post CMP complication are not observed on its usage.(Ein-Eli and Starosvetsky, 2007) Oxygen was also proposed as an oxidizer in CMP slurry but it revealed that it had lower efficiency as

compared to peroxide(DeNardis *et al.*, 2005). An increase in Cu dissolution due to increase in cathodic process rate as H_2O_2 concentration (1 to 3 vol. %) increases is observed.(Kolodny, 2009) However, for concentration higher than 3 vol.%, the dissolution rate decreases due to formation of Cu passive layer.(Kondo *et al.*, 2000; Nguyen *et al.*, 2001) The combination of hydrogen peroxide, uric acid, and arginine gives a more robust polish rate and desired Cu/SiO_2 selectivity as compared to hydrogen peroxide, glycine and BTA based slurries.(Prasad and Ramanathan, 2007) Uric acid optimizes the dissolution rate of the metal by forming an passivation film. As compared to uric acid and potassium sorbate, higher inhibition efficiency of BTA for Cu corrosion in an alkaline media is observed.(Prasad and Ramanathan, 2007)

Low anodic current values obtained in H_2O_2–H_2O solution seconds the copper passivity.(Carpio, Farkas and Jairath, 1995). It is to be noted that metals with corrosion rate higher than 0.1 mm/year are contemplated highly corrosive materials. Hence Cu dissolution at 15 vol. % H_2O_2 (gives 10nm/min which equals to 5 mm/yr) cannot be considered.(Nguyen *et al.*, 2001)

Incorporation of inhibitors, such as ammonium dodecyl sulphate or BTA (Hong *et al.*, 2005) to peroxide solutions encourages a rapid copper passivity. An electrochemical study at various concentration of H_2O_2 concludes that complexing agents are necessary for H_2O_2 solution for dissolution of abraded Cu species. Addition of glycine as complexing agent was also suggested to restrict the formation of oxides and hydroxides.(Hegde, Patri and Babu, 2005) (The other complexing agents suggested were arginine(Prasad and Ramanathan, 2007), acetic acid(V R K Gorantla *et al.*, 2005), ethylenediamine (V R K Gorantla *et al.*, 2005), glycolic acid(Tsai, Wu and Yen, 2005), Phthalic acid salt(Tsai, Wu and Yen, 2005), Citric acid(V R K Gorantla *et al.*, 2005), Oxalic acid(Hazarika, Gupta and Rajaraman, 2022). It is to be noted that aging time plays a key role in slurry composition and removal rate of the metal.(Kim *et al.*, 2022)

2.2.4 Other Slurries

Molybdenum oxide abrasives in a potassium iodate (KIO_3) based slurry gave a relatively high removal rate at highly acidic medium.(Zantye, Kumar and Sikder, 2004) Generation of I_2 due to reaction between MoO_2 and KIO_3 gave an enhanced removal rate. Various other oxidizers suggested for Cu CMP applications are $KMnO_4$ (K. V. Sagi *et al.*, 2016); KIO_3(Hegde, Patri and Babu, 2005); Carbonate and Sorbate based solutions(Ein-Eli and Starosvetsky, 2007), etc. It is observed that addition of small amount of 5-methyl-benzotriazole (MBTA) in place of BTA served the purpose of an effective inhibitor.(Ryu *et al.*, 2019) Also, polyvinyl pyrrolidone (PVP) proved to be a better inhibitor as compared to BTA.(G. Yang *et al.*, 2019) PVA protects the metal surface by adsorbing physically on the exposed layer.

2.3 Study on Chemical Mechanical Polishing of Tantalum and its Nitride (Ta/Ta_2N/TaN)

Due to the poor adhesive properties of Cu with the dielectric material, it diffuses into it thereby depreciating the circuit performance. Hence, in order to avoid this issue, barrier material was introduced in between the interconnect and the dielectric. Tantalum (Ta) is the first generation of barrier material used in the semiconductor industry.(Min, 1996) Tantalum (Ta) with ability to avert Cu diffusion up to 600 ºC as well as being non-reactive with Cu was considered as one of the elementary metals for Cu barrier metal (~50 nm thick deposited on Si).(Edelstein *et al.*, 2002) However, beyond this temperature, Cu diffusion through Ta and formation of Ta silicide was observed.(Min, 1996) Thus, to enhance the barrier properties of Ta and to prevent Cu diffusion, impurities such as nitrogen was added to the Ta film resulting in formation of Ta/TaN/ Ta_2N. In a semiconductor industry, a selectivity of 1:1 of removal rates for the Cu and the barrier metal is required. Shukla et al(Shukla, Selvam and Ramachandran, 2022) reported that addition of uric acid to Na_2CO_3 and alumina particles slurry gave the desired selectivity.

With increase in pH towards alkalinity, Uric acid enhances the dissolution of Ta and suppresses the dissolution of Cu. Ta undergoes oxidation and forms a tantalum pentoxide (Ta_2O_5) layer at all pH ranges. Ta_2O_5 is highly stable layer, and hence, difficulty in removal arises.

$$2Ta + 5H_2O \rightarrow Ta_2O_5 + 10H^+ + 10e^- \quad [2.10]$$

Ta_2O_5 reacts with NaOH formed from Na_2CO_3 and results in formation of highly soluble and less stable $Na_8Ta_6O_{19}$.(Chen, Tsai and Yen, 2010)

$$3Ta_2O_5 + 8NaOH \rightarrow Na_8Ta_6O_{19} + 4H_2O \quad [2.11]$$

Different combination of chemistries used for Cu/Ta polishing are: colloidal silica,H_2O_2, tartaric acid(Janjam *et al.*, 2008); alumina, H_2O_2, tartaric acid; silica, caesium carbonate(Kaufman, C. Kistler and Wang, 2000), silica, H_2O_2, glycine.(Jindal and Babu, 2004). It is be noted that Ta or its nitrides shows a repelling behavior towards receiving Cu plating. This demands the need of Cu-seed layer before the electroplating of Cu. With the shrinkage of the technology node to 10 nm and below, various technological problems such as maintaining the diffusion barrier property and the desired thickness at the same time would appear. Hence, various other barrier metals namely Co, Ru were studied in order to substitute the Ta/TaN.

2.4 Study on Chemical Mechanical Polishing of Ruthenium

Ruthenium (Ru), a noble metal can be used as a barrier metal for lower node devices due its various properties such as low resistivity (~7 μΩ cm), high melting point (2334 °C) and negligible solid solubility with copper.(M. Damayanti *et al.*, 2006; K. V Sagi *et al.*, 2016) However, the planarization of Ru is very challenging because of its high chemical resistance and mechanical hardness. Hence, it was suggested that modification of the chemical composition might enhance the removal rate of Ru. Ru is soluble in an aqueous solution in the

form of RuO_4. Hence, the slurry formulated should be such that the Ru surface should be oxidized to RuO_4 or $RuO_2.2H_2O$ on the Ru surface.(Zeng, J.-X. Wang, *et al.*, 2012; Cheng *et al.*, 2016) Addition of only abrasives in the slurry such as silica, alumina and ceria gave negligible polish rate (< 1nm/min).(Peethala, Roy and Babu, 2011a; Victoria *et al.*, 2012; Yadav, Jitendra C. Bisen, *et al.*, 2017) Therefore, addition of several oxidizing agents and additives were suggested for Ru CMP. Some of the suggested oxidizers are ceric ammonium nitrate (CAN)(Lee and Park, 2004), hydrogen peroxide (H_2O_2)(Cui, Park and Park, 2013; Duan *et al.*, 2015), percarbonate based slurries(Turk *et al.*, 2013), potassium bromate(Victoria *et al.*, 2010a), Oxone(Victoria *et al.*, 2012), sodium hypochlorite(Yadav, Jitendra C. Bisen, *et al.*, 2017) and sodium periodate ($NaIO_4$)(Cheng *et al.*, 2015) etc.

Ceric ammonium nitrate (CAN) used as oxidizer for Ru polishing in highly acidic (pH =1) region leads to formation of Ru_2O_3 and RuO_2 (Lee and Park, 2004). At acidic medium, Ru oxidizes to form ruthenium dioxide (RuO_2) which further converts to ruthenium tetraoxide (RuO_4).(Wei *et al.*, 2007a)

$$RuO_4 + 2H_2O \leftrightarrow H_2RuO_5 \qquad [2.12]$$

However, use of CAN causes undesirable high etching. The soluble products are unstable in nature hence not preferred. H_2O_2 based slurries also gave very low removal rates. Addition of guanidine carbonate (GC) along with to H_2O_2 forms soluble Ru complexes, thereby enhancing the removal rates.(Amanapu *et al.*, 2013). Also, optimized GC concentration along with 1,2,4 triazole in H_2O_2 based slurry can give a desired Cu-Ru selectivity.(Wang *et al.*, 2018). The RR of Ru can also be enhanced in the presence of potassium ions.(Jiang, He, Yuzhuo Li, *et al.*, 2014) However, the performance of GC ions on enhancing removal rates is comparatively better than that of potassium ions.(Du *et al.*, 2017) However, GC in $KMNO_4$ suppresses the removal rate to unacceptably low values.(K. V. Sagi *et al.*, 2016) It was observed that sodium periodate in an alumina-based slurry gave comparatively good removal rates, however the

dissolution obtained was high (20 nm/min). Also, contamination of sodium is observed. The high dissolution is attributed to formation of soluble RuO_4 in abundance. The reaction occurring are Ru surface are as follows.

$$4RuO_4^- + 4H^+ \leftrightarrow RuO_2.2H_2O + 3RuO_4 \quad [2.12]$$

$$IO_4^- + 2(RuO_2.2H_2O) \leftrightarrow 4H_2O + RuO_4 + I^- \quad [2.13]$$

$$RuO_4 + H_2O \leftrightarrow H_2RuO_5 \quad [2.14]$$

At acidic pH, Ru dissociates into perruthenate (RuO_4^-) oxidizes to form ruthenium dioxide (RuO_2) and RuO_4. At alkaline pH, perruthenate (RuO_4^-) and RuO_2 (insoluble species) were formed and very low etch rates were observed. The RR doesn't follow Preston equation with respect to pressure and velocity.(Victoria *et al.*, 2012; Yadav, Jitendra C. Bisen, *et al.*, 2017) A slurry comprising of potassium periodate (KIO_4) as oxidizer and glycine was studied. Effect of glycine at pH 9 for Ru-Cu selectivity was studied.(Zeng, J.-X. Wang, *et al.*, 2012) It revealed that glycine suppresses etching of Ru while it accelerates dissolution of Cu thereby giving a selectivity of 1:1.

Potentiodynamic polarization studies with potassium bromate as oxidizing agent reveals that current density is increased at the anodic part and the removal is mainly due to mechanical abrasion.(Victoria *et al.*, 2010a) Ammonium ion enhances the surface corrosion rate of Ru by forming water soluble complexes. Hence, with an increase in concentration of the ions, the removal rate increases.(Ziyan Wang *et al.*, 2019) Also, an optimized concentration could give a relatively smoother surface. Wang et.al reported that UV activated potassium persulfate loosen the Ru surface, hence enhancing the RR to 26.36%. (Wang *et al.*, 2021)

2.4.1 Galvanic corrosion of Ruthenium and Copper

In a Ru polishing slurry, Cu being an active metal acts as anode whereas Ru being more noble in nature acts as anode. This difference in current corrosion potential leads to galvanic

corrosion between Cu and Ru. Hence to minimize the galvanic corrosion and excessive dissolution of Cu, different additives are proposed.(Patlolla *et al.*, 2018) 2,2'-[[(methyl-1H-benzotriazol-1-yl)methyl]imino]diethanol (TT) added as an inhibitor to ammonium sulfate and H_2O_2 slurry suppresses the dissolution of Cu by forming adsorbed passivation on its surface.(Patlolla *et al.*, 2018) However, such effect was not seen on Ru surface but a reduced dishing and erosion defects were observed in both the metals. Addition of ascorbic acid and BTA as cathodic and anodic inhibitors to KIO_4 based solution reduced the galvanic corrosion of Cu-Ru to 20 mV.(Peethala, Roy and Babu, 2011a) It was seen that potassium molybdate ions modifies the Cu and Ru surface in a BTA+ KIO_4 based slurry. The ions adsorbed facilitates the BTA absorbed-passive layer thereby suppressing the galvanic corrosion between them.(Cheng *et al.*, 2014) Insoluble $Cu(IO_3)_2 \cdot nH_2O$ compounds on the surface also suppresses the dissolution rate of Cu.(Cheng *et al.*, 2018) Similar inhibition properties as BTA can be observed using 1,2,4 triazole.(Cheng, Wang and Lu, 2020) BTA usually inhibits by forming a 3-dimensional adsorbed structure on the Cu surface. However, the adsorption of the 1,2,4 triazole is 2 dimensional, and an excess of it can destabilize the passivation film, and reduce its inhibition efficiency on Cu. Tian et.al (Tian *et al.*, 2022) suggested that potassium Tolyltriazole (TTAK) as inhibitor in a H_2O_2-glycine based slurry effectively reduces the corrosion rates of both Cu and Ru by forming a passive film on its surface. A reduced erosion and dishing are also observed in its presence.

2.5 Study on Chemical Mechanical Polishing of Cobalt (Co)

In the recent times, Co has evolved as a leading replacement metal for both the barrier as well as interconnect (Cu) because of its exclusively unique properties such as accurate deposition, cheaper adhesion techniques, high resistivity to diffusion of Cu into the dielectric, easily available and lower cost.(Ranaweera *et al.*, 2019; Ryu *et al.*, 2020) However, some major

drawbacks such as corrosion and defectivity post CMP are mainly observed for Co (CVD/PVD) films.(Hu, Pan, Li, *et al.*, 2019) The corrosion could be general corrosion or pitting or galvanic corrosion. It is to be noted that, Co can only be commercialized for the next generation semiconductors if the mentioned issues are eliminated. The dissolution of Co via Co^{2+} ions is illustrated below.(Peethala *et al.*, 2012)

$$Co + 2H^+ \rightarrow Co^{2+} + H_2 \quad [2.14]$$

To eliminate such corrosion via dissolution, formation of passive layer is the utmost priority. The passive layer could either be in the form of Co (II) or/and Co (III) oxide/hydroxides. Lower potential Co (II) oxide/hydroxide are usually formed at acidic pH and at lower potentials. At higher potentials and at neutral and alkaline pH, Co (II) oxide/hydroxide oxidizes to form Co(III) oxides/hydroxides.(Park, Paluvai and Venkatesh, 2018) The passive layer formed at highly alkaline region is more stable in nature.(S. Yang *et al.*, 2019)

$$Co + H_2O \rightarrow Co(H_2O)(ads) \quad [2.15]$$

$$Co(H_2O)(ads) \rightarrow Co(OH)^+ + H^+ + 2e^- \quad [2.16]$$

$$Co(OH)^+ + H_2O \rightarrow Co(OH)_2 + H^+ \quad [2.17]$$

$$Co(OH)_2 \rightarrow CoO + H_2O \quad [2.18]$$

$$Co(OH)_2 + OH^- \rightarrow CoOOH + H_2O + 2e^- \quad [2.19]$$

$$3CoO + 2OH^- \rightarrow Co_3O_4 + H_2O + 2e^- \quad [2.20]$$

The issues can be controlled by proper tuning of the slurry chemistry. Different oxidizers such as ammonium per sulphate,(Ranaweera *et al.*, 2019), H_2O_2(Hu, Pan, Xu, *et al.*, 2020a), potassium per sulphate(Zhang, Wang and Lu, 2020) ; complexing agents such as:, cystine(Zhi Wang *et al.*, 2019), citric acid(R Popuri, Sagi, Alety, Peethala, Amanapu and Patlolla, 2017), glycine(Paul and Srinivasan, 2020), hydroxyethylidene diphosphonic acid (HEDP)(Hu, Pan,

Xu, *et al.*, 2020a), potassium tartrate(Hu, Pan, Li, *et al.*, 2019), ethylenediaminetetraacetic acid (EDTA)(Kwon *et al.*, 2020) and inhibitors such as: 1,2,4 triazole(Zhong *et al.*, 2014), BTA(Ryu *et al.*, 2020), diethanolamine (DEA)(Xu *et al.*, 2021), potassium oleate(Ranaweera *et al.*, 2019) etc. are suggested in literature to attain a planar Co surface with reduced defects and corrosion. Alkaline solutions are usually preferred over acidic solution due to controlled occurrence of dissolution at this region. Although BTA was the most preferable inhibitor in most of the studies done till date, it was seen that it forms easily soluble Co-BTA passive layer.(Ryu *et al.*, 2020) This gives rise to unwanted residue generation post CMP. Ji et.al (Ji *et al.*, 2017) reported that presence of ethylene diamine tetra acetic acid (EDTA) derivative, in an oxidizer absent slurry can also give and enhanced removal rate for Co.

2.5.1 Galvanic Corrosion of Cobalt and Copper

Co, being more fragile chemically as compared to Cu is highly inclined towards corrosion and oxidation.(S. Yang *et al.*, 2019) Also, the difference in reduction potential makes them more prone to galvanic corrosion.(Peethala, Roy and Babu, 2011a) In addition to that that Co (Mohs hardness 5) is mechanically harder than Cu (Mohs hardness 3).(Peethala *et al.*, 2012) Hence, maintaining desired removal selectivity along with reduced galvanic corrosion is a big challenge. Difference in open circuit potential (OCP) between Cu and Co acts as the main driving force behind galvanic corrosion. Hence the slurry formulated should be capable enough to reduce the difference between them.(Peethala *et al.*, 2012)Slurry solutions containing BTA and glycolic acid at pH 2 were investigated and it was observed that Co corrosion can be minimized in the presence of BTA and glycolic acid.(Bilouk *et al.*, 2009a) Literature proved that pH of a slurry has a major role in attaining selectivity between Co/Cu.(Nishizawa, Nojo and Isobe, 2010b) Nishizawa et.al(Nishizawa, Nojo and Isobe, 2010b) also proposed a slurry comprising of H_2O_2, citric acid and BTA, however the slurry lead to high current densities with increase corrosion defects. For devices less than 14 nm, an abrasives slurry comprising of

mainly potassium acetate, hydrogen peroxide, and benzotriazole gave a controlled corrosion for Co/Cu system.(Johnson, Wei and Roy, 2018) Hu et.al reported that, novel inhibitor, TT-Lyk adsorbs on the Cu surface forming Cu-TT-Lyk passivating film, thereby reducing the potential difference between the two metal.(Hu, Pan, Zhang, *et al.*, 2019) A higher galvanic corrosion at static condition is observed as compared to dynamic condition. Zhang et.al proposed a green inhibitor, sarcosine that inhibited the corrosion in two different ways: forming passive layer and hindering further oxidation, reducing the glycine-metal complexes on the metal surface.(Zhang *et al.*, 2022) It was reported that potassium hydrogen phthalate (KHP) and 1, 2, 4-triazole (TAZ) as chelating agent and inhibitor in a H_2O_2 based slurry gave a reduced Cu/Co potential gap better surface quality.(Yang, Zhang and Yang, 2022)

2.6 Dissolution Mechanism of Co by EIS

EIS, a highly potent electrochemical technique is used to study the reaction mechanistic detail of the metal dissolution or passivation of films forming on the metal surface.(Barsoukov and Macdonald, 2005) The anodic metal dissolution in detailed via the impedance data was understood by employing reaction mechanism approach (RMA).(Keddam, Mottos and Takenouti, 1981) The reaction mechanism analysis procedure is explained elaborately in the next chapter.

Reaction mechanism analysis of Co dissolution based on polarization and EIS studies in different media are summarized herewith. The mechanism proposed for Co dissolution were mainly in carbonate and bicarbonate solution. (Calderón, Barcia and Mattos, 2008; Real, Ribotta and Arvia, 2008) Davies et.al.(Davies and Burstein, 1980) and Burstein et.al.(Burstein and Davies, 1980) proposed Co dissolution in the form of formation of CoO film in a carbonate/bicarbonate solution.

$$Co(s) + HCO_{3(aq)}^{-} \xrightarrow{k_1} (CoCO_3)_s + H_{(aq)}^{+} + e^{-} \quad [2.21]$$

$$Co + H_2O \xrightarrow{k_2} CoO_{(s)} + 2H_{(aq)}^{+} + e^{-} \quad [2.22]$$

$$CoO_{(s)} + HCO_{3(aq)}^{-} \xrightarrow{k_3} CoCO_{3(s)} + OH_{aq}^{-} \quad [2.23]$$

$$CoCO_{3(s)} + HCO_3^{-} \underset{k_{-4}}{\overset{k_4}{\rightleftharpoons}} Co(CO_3)_{2(aq)}^{2-} + H_{(aq)}^{+} \quad [2.24]$$

Gervasi et.al(Gervasi *et al.*, 1991; Gervasi, Vilche and Alvarez, 1996) proposed a similar mechanism with dissolution occurring in the form of Co_3O_4 instead of CoO.

Paul et.al(Paul and Srinivasan, 2020) suggested mechanism comprising of four adsorbed intermediates {two of each Co(II) and Co(III)} in a glycine system.

$$Co \underset{k_{-A}}{\overset{k_A}{\rightleftharpoons}} Co_{ads}^{2+} + 2e^{-} \quad [2.25]$$

$$Co_{ads}^{2+} \underset{k_{-B}}{\overset{k_B}{\rightleftharpoons}} Co_{ads}^{3+} + e^{-} \quad [2.26]$$

$$Co_{ads}^{3+} \xrightarrow{k_c} Co_{sol}^{3+} \quad [2.27]$$

$$Co_{ads}^{2+} \xrightarrow{k_D} Co_{sol}^{3+} + e^{-} \quad [2.28]$$

$$Co_{ads}^{3+} + Co \xrightarrow{k_E} Co_{ads}^{3+} + Co_{sol}^{3+} + 3e^{-} \quad [2.29]$$

2.7 Lacunae

The formulation of slurry for planarizing Cu interconnects with Ru or Co as barrier material is of greatest interest among microelectronics fabrication industries as other proposed slurry possess various issue such as selectivity, galvanic corrosion, post-CMP cleaning issue and so on. With the miniaturization of devices, usage of Cobalt and Ruthenium diffusion barrier alternatives to the Ta/TaN bilayer was suggested due to the desired properties they possess as mentioned earlier. Cobalt (Co) has evolved as a leading replacement metal for both the barrier

layer (TaN/Ta) as well as the conductive layer (Cu) because of its many unique properties such as conformal deposition (especially in high aspect ratio areas), low resistivity, inexpensive adhesion techniques, high resistivity to act as a barrier (Ta/TaN replacement) and large scale and inexpensive commercial availability.

Although many types of slurry have been proposed for Cu CMP most of them were oriented towards higher selectivity between Cu and Ta. Only limited studies are available for Cu-Ru CMP and Cu-Co CMP. Especially, the CMP studies on Cu as interconnect material and Ru/Co as barrier material with the aim of achieving desired selectivity, minimum galvanic corrosion is limited. Besides, the dissolution mechanism of Co in solution containing oxidizer and complexing agents are not reported yet.

2.8 Objectives

Based on the lacunae obtained from extensive literature review, the objectives of the work are as follows:

- To tailor a suitable slurry by optimizing the process parameters and slurry components (abrasive and chemicals) that would yield desired polishing characteristics and desired selectivity between Ru-Cu substrates and Co-Cu substrates.
- To find the effect of various pH and additives on the polishing performance and selectivity of Ru-Cu and Co-Cu substrates.
- To understand the galvanic corrosion between Co-Cu using electrochemical techniques in the proposed slurry.
- To suggest a suitable mechanism to understand the anodic dissolution behavior of Co in the solution of interest.

THIS PAGE IS LEFT BLANK INTENTIONALLY

CHAPTER 3

3. EXPERIMENTAL MATERIALS AND METHODOLOGY

The different materials and methodologies employed in this research is elaborated here.

3.1 Materials

3.1.1 Chemical Mechanical Polishing Experiments

Cu coupon (99.98% pure) of 25.4 mm diameter, Co coupon (99.95% pure) of 25 mm diameter and Ru coupon (99.9% pure) of 25.4 mm diameter procured from Tecnisco Advance Materials Private Limited, Singapore were used to perform the polishing experiments. Non-woven Buehler Texmet C PSA pads of dia. 203 mm (8') were used as the polishing pads. Cab-o-sil, M-5, fumed silica abrasives (Cabot Sanmar Limited, India) was used as the prime abrasives. The other abrasives that were also part of the experiments were alumina (Beuhler, India) and titania (TTP, India) abrasives.

3.1.2 Static Etch Experiments

Cu coupon (99.98 % purity) of 7 mm diameter and 2 mm thickness, Co coupon (99.95% pure) of 9 mm diameter and 1 mm thickness and Ru coupon (99.9 % purity) of 15 mm diameter and 1 mm thickness were used to perform the static etch experiment. Water-resistant emery paper of 600 grit size was used to polish the coupons before every set of experiment.

3.1.3 Electrochemical Experiments

Cu (99.98% pure, 7 mm diameter), Co (99.95% pure, 9 mm diameter) and Ru (99.9% pure, 15 mm diameter) embedded in Teflon rod and connected with Cu wire were used as working electrodes for performing the electrochemical experiments. Prior to every run, the electrode was polished with the following emery sheet of grit size 180, 320,600 and 1000. 1µm micro polish alumina paste (Buehler, USA) and 0.3µm micro polish alumina paste (Buehler, USA) were used to further smoothen the surface of the electrode.

The different chemical reagents used in the polishing/etching and electrochemical experiments are displayed in Table 3.1. It is to be noted that all the chemical purchased were of AR grade.

Table 3. 1 Chemicals reagents used in different experiments

	Chemical	**Manufacturing Company**
Oxidizer	Sodium hypochlorite	Finar, India
	H_2O_2	Loba Chemicals, India
	Potassium iodate	Merck, India
Complexing agents	Oxalic acid	Himedia, India
Inhibitors	BTA	Loba Chemicals, India
	L-ascorbic acid	Himedia, India
	Uric acid	Sigma Aldrich, India
	Imidazole	Himedia, India
pH tuners	Potassium Hydroxide	Himedia, India
	Nitric acid	Loba Chemicals, India
	Nitric acid (for the H_2O_2 system)	Himedia, India
Supporting electrolyte	sodium sulphate	Himedia, India
Sonication	Ethanol	Changshu Yangyuan, China

3.2 Methodology

3.2.1 Chemical Mechanical Polishing Experiments

All the polishing experiments were rendered on a benchtop Labopol-20/Laboforce- 50 polisher (Struers, USA). Unless otherwise mentioned, the sample rotational speed was set at 150 rpm, turntable with pad speed was set at 100 rpm and the applied downforce was 5.72 psi. The slurry was pumped to the CMP through a peristaltic pump, PP-ex 20 (Miclins, India) with a controlled flow rate of 100 ml/min. Blank runs with only fumed silica slurry was performed to obtain a stable and reproducible results for every new pad used. The pads were changed regularly after every similar set of experiments. To eliminate any sort of debris and obtain coherent results, prior to every run, conditioning of the polishing was performed. The pad was conditioned using a traditional method of manual conditioning using emery sheet of a fixed grit size (600). (Li and Babu, 2001; Manivannan and Ramanathan, 2009) The metal after polishing was cleaned by sonicating with Millipore water followed by ethanol for 2 min. The sample was dried and then weight loss was measured gravimetrically using weighing balance with readability 0.0001 g (Sartorius, USA). A minimum of 3 runs (polishing time per experiment =3 min) were performed for each set of condition and the average removal rate in nm/min with standard deviation is reported. The formula used for measuring the RR is displayed in equation 3.1 whereas Prestonian behavior of RR was investigated using equation 3.2 (Qin, Moudgil and Park, 2004). The schematic representation of the CMP experiments is displayed in Figure 3.1.

$$\text{Removal rate (RR)}\left(\frac{\text{nm}}{min}\right) = \frac{\text{Weight loss (gm)} \times 10^7}{\text{Density}\left(\frac{gm}{cm^3}\right) \times \text{Time}\,(min) \times \text{Surface area}(\text{cm}^2)} \quad [3.1]$$

Removal Rate (RR) [3.2]

$$= \text{Prestons coeficient } (K_p) \times \text{Down pressure } (P) \times \text{Turntabelespeed}(V)$$

Figure 3. 1 Experimental Setup for CMP experiments

3.2.2 Static etch rate experiment

To get an insight of the chemical dissolution of the metal (Cu, Co and Ru) in the presence of different chemical reagents, etch rate experiments were performed. For the Cu/Co system and Cu/Ru system the etchant time was set to 30 min and 60 min respectively. As per ASTM E 3 (Standard Guide for Preparation of Metallographic Specimens) and ASTM E407 (Standard Practice for Micro etching Metals and Alloys) methodology, prior to every experiment the coupons were polishing and smoothed using 600 grit size emery sheets. The tared coupons

after completion of etching was washed properly with Millipore water and ethanol. The metal is then dried and weighed gravimetrically using weighing balance with ±0.0001g precision (Sartorius, USA). To ensure repeatability, a minimum of three runs were conducted for every system and the average etch rate with the standard deviation is reported. The formula for measuring the etch rate is similar to equation 3.1. The schematic representation of the etch experiments is displayed in Figure 3.2

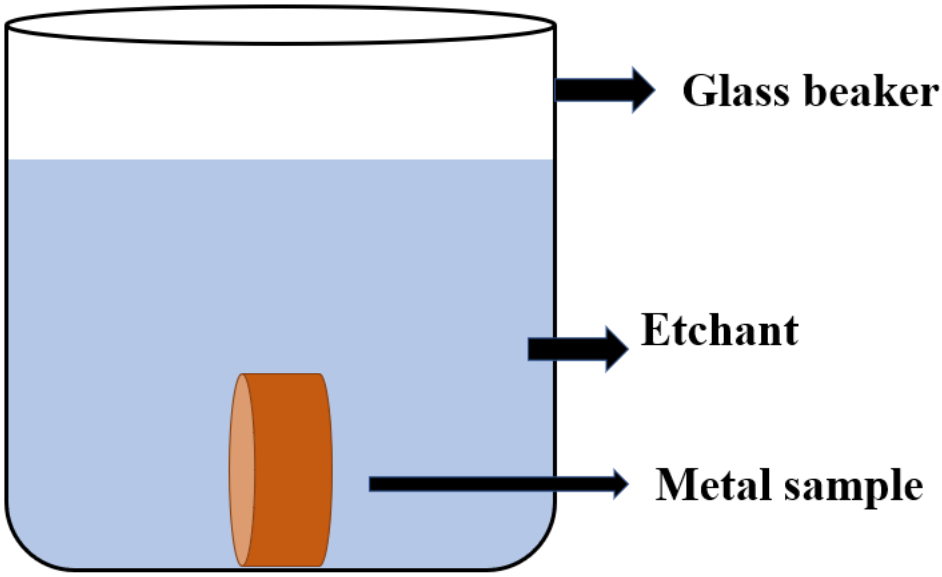

Figure 3. 2 Schematic representation of static etch experiments

3.2.3 Electrochemical experiments

Electrochemical experiments on Cu/Co for H_2O_2+ oxalic acid + imidazole system was performed on a Gamry-1010 electrochemical workstation. Whereas experiments on Cu/Co and Cu/Ru for H_2O_2+ oxalic acid system and KIO_3+BTA system respectively were conducted on Metrohm Autolab potentiostat, (PGSTAT 204, Switzerland). A three-electrode (working, reference and counter) glass cell (500 ml volume) was employed to perform all the experiments. Cu/Co/Ru embedded in Teflon tube is used as the working electrode. Platinum

wire and Ag/AgCl (3 M KCl) are the counter electrode and the reference electrode (RE) respectively. RE detects and controls the potential of electrode whereas CE prevents passing of current between the working electrode and RE in order to jot down the exact potential of the working electrode. Prior to every experiment, the working electrode surface was smoothed using emery sheets in the following order: 180, 320,600 and 1000 grit size followed by micro polish alumina paste (Buehlar, USA) (1 µm, 0.3µm). Before proceeding with the experiments, the polished electrode was cleaned and sonicated with Millipore water and ethanol and then dried. All the electrochemical experiments were conducted at room temperature and inside faraday cage to reduce perturbation from the surrounding environment. The electrochemical experimental setup is displayed in Figure 2.3.

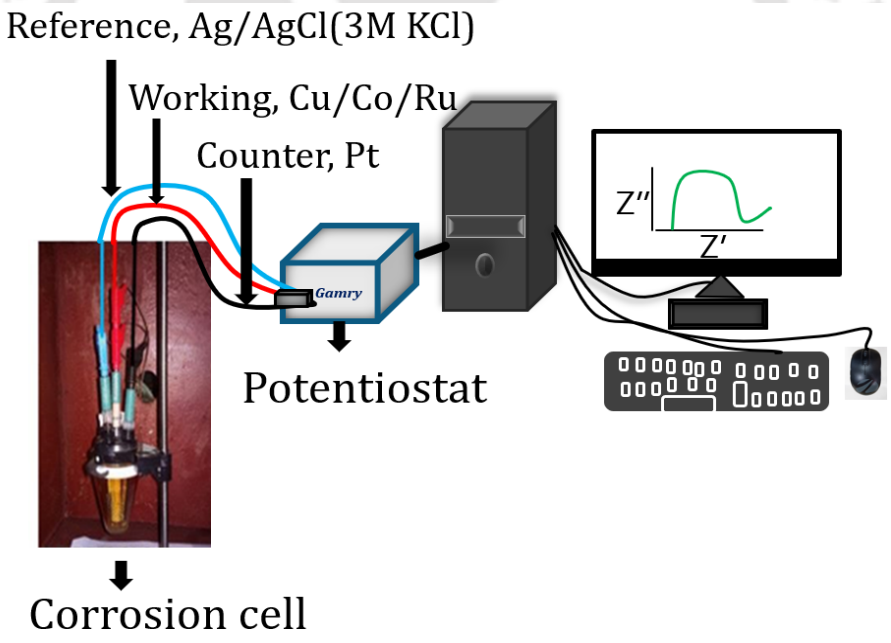

Figure 3. 3 Experimental setup for electrochemical experiments

It is to be noted that the electrochemical experiments in our case are performed without any abrasive particles in the electrolyte solution. To ensure repeatability, a minimum of three experiments for the similar system were performed. The various electrochemical experiments performed are:

3.2.3.1 Open Circuit Potential (OCP)

Open circuit potential (OCP/Eoc) is the electrical potential or potential difference of a working electrode measured w.r.t reference electrode when there is no net current enforced to an electrochemical cell. The change in the Eoc value indicates the conversion in the nature of the metal surface. The OCP is measured before starting every other electrochemical experiment to ensure the stability of the system when immersed in the electrolyte. The potential vs Ag/AgCl (3M KCl) in the electrolyte is measured for a given time (varies with system) and the final stable value is considered as the OCP.

3.2.3.2 Potentiodynamic Polarization (PP)

Potentiodynamic polarization experiments were performed by scanning the potential from -1 V to 1 V w.r.t OCP at a rate of 1 mV/s. The corrosion current density (I_{corr}) and corrosion potential (E_{corr}) were calculated from the intersection points by extrapolating the anodic and cathodic branches by using the inbuilt software, Gamry Echem Analyst of Gamry-1010 electrochemical workstation.

3.2.3.3 Electrochemical Impedance Spectroscopy (EIS)

Electrochemical impedance spectroscopy (EIS) were conducted by sweeping at 20000 Hz to 10 Hz frequency range with 7 frequencies per decade interval. In order to ensure linearity, 10 mV (rms) amplitude AC voltage signal was applied to perform all the EIS measurements. EIS experiments were performed at OCP and also at various overpotentials. While plotting, the lower frequency noisy data was not considered. Hence, in order to validate the remaining data, Kramers Kroing transform (KKT) in Nova 1.10, Metrohm was performed.

Kramers-Kronig Transform (KKT)

KKT ensures that the EIS experimental data obtained is linear, doesn't irrelevantly change during the measurements and respond accordingly to the applied input sinusoidal impulse.

(Boukamp, 1993; Pachimatla and Srinivasan, 2018; Ranjith *et al.*, 2018). The real and the imaginary components of the impedance data are correlated in KKT. If within a frequency range of zero to infinity, the real component of the experimental impedance is known, the imaginary component can directly be obtained from KKT and vice versa. The corresponding equations (Barsoukov and Macdonald, 2005) of it are as follows:

$$Z_{\mathrm{Re}}(\omega) - Z_{\mathrm{Re}}(\infty) = \left(\frac{2}{\pi}\right)\int_0^{\infty} \frac{xZ_{\mathrm{Im}}(x) - \omega Z_{\mathrm{Im}}(\omega)}{x^2 - \omega^2} dx \qquad [3.3]$$

$$Z_{\mathrm{Re}}(\omega) - Z_{\mathrm{Re}}(0) = \left(\frac{2\omega}{\pi}\right)\int_0^{\infty} \frac{(\frac{\omega}{x})Z_{\mathrm{Im}}(x) - \omega Z_{\mathrm{Im}}(\omega)}{x^2 - \omega^2} dx \qquad [3.4]$$

$$Z_{\mathrm{Im}}(\omega) = \left(\frac{2\omega}{\pi}\right)\int_0^{\infty} \frac{Z_{\mathrm{Re}}(x) - \omega Z_{\mathrm{Re}}(\omega)}{x^2 - \omega^2} dx \qquad [3.5]$$

Here, Z_{Re} and Z_{Im} are the real and the imaginary components of impedance where the angular frequencies are ω and x.

3.3 Modelling methods

After validation using KKT, the impedance data were modelled and analyzed using electrical equivalent circuit (EEC) model and reaction mechanism analysis (RMA).

3.3.1 Electrical Equivalent Circuit (EEC) model

Electrical equivalent circuit (EEC) model gives an insight about different physiochemical reactions such as solution, polarization and charge transfer resistances; electro static double layer capacitance and many more processes occurring on the working electrode-solution interface as well as on the bulk part of the solution (Barsoukov and Macdonald, 2005; Orazem and Tribollet, 2008). EEC modelling was done using commercial software Zsimpwin (Version 3.6). To obtain a near perfect fit, Zsimpsin uses complex non-linear least squares (CNLS) fitting technique. The modelling is done using a Voight or EEC circuit. Here, the experimental impedance data is fitted with the best fit EEC circuit comprising of different electrical components such as capacitor, resistor, inductor etc and the best fit with least error and chi square (χ^2) values are considered. An example of EEC circuit is illustrated in Figure 3.4.

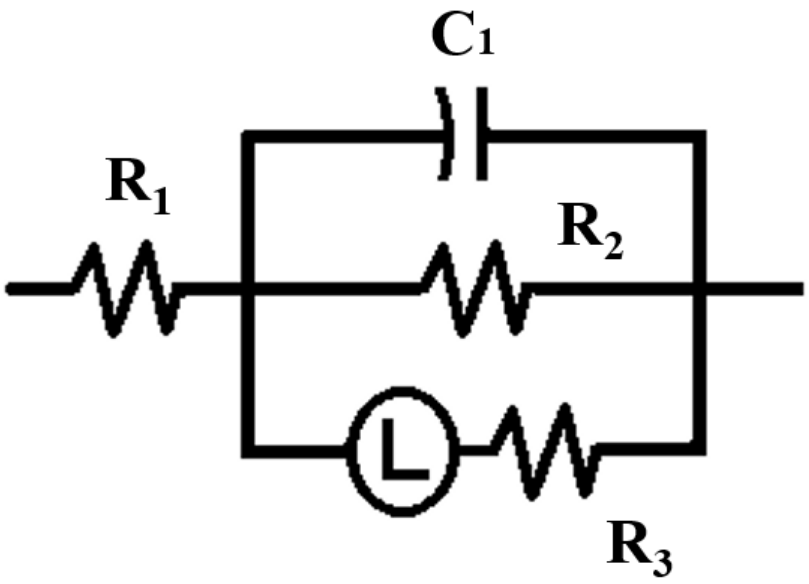

Figure 3. 4 A general representation of a simple EEC circuit

Here, in the circuit shown above, capacitor (C_1), resistor 2 (R_2) and resistor 3 or polarization resistance (R_3/R_p) are in parallel. Resistor 3 (R_3) is connected to inductance in series. All these elements are in series with resistor 1 (R_1) which is also commonly known as solution resistance (R_{sol}). For an depressed capacitance loop, capacitor (C_1) is replaced by constant phase element (CPE) which signifies the metal-electrolyte interface electrostatic double layer. The two-prime parameters of CPE are Y_0 and n. The value of n lies within 0 and 1. A CPE where n equals to 0,0.5,1 and -1 signifies pure resistor, Warburg impedance element (result of diffusion), ideal capacitor and an inductor respectively(Barsoukov and Macdonald, 2005; Orazem and Tribollet, 2008).

$$\text{CPE} = \frac{1}{Y_0(j\omega)^n} \qquad [3.6]$$

As per Kirchhoff's law, the impedance (Z_t) of RC (Resistance-Capacitance) element for series and parallel conncetions can be calculated using equation 3.7 and 3.8 respectively.

$$Z = R + \frac{1}{j\omega C} \qquad [3.7]$$

$$Z = \frac{1}{\left(R + \frac{1}{j\omega C}\right)} \qquad [3.8]$$

Therefore, the total impedance for the circuit shown in Figure 3.4, can be written as

$$Z_t = R_1 + \left\{\frac{1}{R_2} + j\omega C_1 + \left(\frac{1}{j\omega L + R_3}\right)\right\}^{-1} \qquad [3.9]$$

In the presence of CPE element (Y_0, n_i) equation 3.9 is expressed as

$$Z_t = R_1 + \left\{ \frac{1}{R_2} + Y_0 (j\omega)^{n_i} + \left(\frac{1}{j\omega L + R_3} \right) \right\}^{-1} \qquad [3.10]$$

Here, Y_0 and n_1 are the CPE parameters. $j = \sqrt{-1}$ and ω is the angular frequency ($\omega = 2\pi f$).

3.3.2 Reaction Mechanism Analysis (RMA)

Unlike EEC, Reaction Mechanism Analysis (RMA) gives more a detailed information about the processes a metal undergoes when in contact with a reacting environment. Here, depending on the experimental data, a reaction mechanism is proposed. Using the proposed mechanism, impedance data is then simulated via sequential quadratic programming through MATLAB code. The mechanism which gives best fit to experimental data along with low error values and least number of parameters is considered (Keddam, Mottos and Takenouti, 1981; Barsoukov and Macdonald, 2005; Maddala *et al.*, 2010; Venkatesh and Ramanathan, 2010). Some of the assumptions considered while proposing a mechanism are as follows (Maddala *et al.*, 2010)

- A constant double layer capacitance is assumed all through the simulated voltage range.
- Surface coverage is considered unity as per Langmuir isotherm.
- Perturbation is considered linear and higher order expressions are omitted.
- The exponents of forward reactions are positive while that of backward is negative.
- Just like the Tafel constant, it is assumed that the kinetic parameters are related exponentially to voltage.

The steps involved in the following mechanism for metal, M are shown below:

$$M \underset{k_{-1}}{\overset{k_1}{\rightleftharpoons}} M_{ad}^{+} + e^{-} \xrightarrow{k_2} M_{sol}^{+} \quad [3.11]$$

M^{+}_{ads} = adsorbed species with +1 oxidation state (could be chloride/oxide/hydroxide)

M^{+}_{sol} = dissolved metal ion solution.

k_1, k_{-1} and k_2 = kinetic rate constant.

Here, M to M^{+}_{ads} is the electrochemical step whereas M^{+}_{ads} to M^{+}_{sol} is the dissolution step.

The unsteady state mass balance equation for reaction 3.11 is:

$$\tau \frac{d\theta_1}{dt} = k_1(1-\theta_1) - k_{-1}\theta_1 - k_2\theta_1 \quad [3.12]$$

τ = total site existing per unit area

θ_1 and $(1-\theta_1)$ = surface coverage of the adsorbed metal species and vacant site respectively.

Kinetic rate constant, k_i is given by

$$k_i = k_{i0} e^{b_i V} \quad [3.13]$$

Here,

$$b_i = \pm \frac{\alpha n F}{RT} \quad [3.14]$$

Here,

$i = 1,2$ (forward reaction) and (-1) backward reaction.

V = over-potential (dc)

α = transfer coefficient, (lies between 0 to 1),

n = number of electrons taking part in the rate determining step.

F, R, T= Faraday's constant, gas constant and temperature respectively

b = for forward reaction (oxidation) it is positive whereas for backward reaction (reduction) it is negative.

At steady state condition, Equation 3.12 is represented as:

$$k_1(1-\theta_{1ss}) = k_{-1}\theta_{1ss} + k_2\theta_{1ss} \quad [3.15]$$

Rearranging it, fractional steady state surface coverage (θ_{1ss}) can be obtained as

$$\theta_{1ss} = \frac{k_1}{k_1 + k_{-1} + k_2} \quad [3.16]$$

The unsteady state current density (J) obtained due to faradaic reaction is expressed as

$$J = nF\left[k_1(1-\theta_1) - k_{-1}\theta_1)\right] \quad [3.17]$$

To determine the faradic impedance equation at the metal solution interface ($Z_{F,m/s}$) Equation 3.17 is differentiated w.r.t voltage.

$$\frac{dJ}{dV} = \left(Z_{F,m/s}\right)^{-1} = nF\left[\frac{dk_1}{dV}(1-\theta_{1ss}) - k_1(\frac{d\theta_1}{dV}) - \frac{dk_{-1}}{dV}\theta_{1ss} - k_{-1}\frac{d\theta_1}{dV}\right] \quad [3.18]$$

$$\left(Z_{F,m/s}\right)^{-1} = R_{ct}^{-1} - nF\left[\frac{d\theta_1}{dV}(k_1 + k_{-1})\right] \quad [3.19]$$

Therefore, charge transfer resistance (R_{ct}) equals to

$$R_{ct}^{-1} = nF\left[(k_1 b_1(1-\theta_{1ss}) - k_{-1} b_{-1}\theta_{1ss}\right] \quad [3.20]$$

The steady state current density is expressed as

$$J_{ss} = nF\left[k_2\theta_{1ss}\right] \quad [3.21]$$

Using Taylor series, the rate constant and surface coverage are expanded. It is to be noted that the higher order terms are being neglected n the expansion. On further expanding the mass balance equation $\frac{d\theta_1}{dV}$ is determined.

$$k_i = k_{i0}e^{b_i(V_{dc}+V_{dac})} \approx k_{i0}e^{b_i V_{dc}}(1 + b_i V_{ac}) = k_{i0}(1 + b_i V_{ac}) \quad [3.22]$$

$$\theta_i = \theta_{iss} + \frac{d\theta_i}{dV}V_{ac} \quad [3.23]$$

$$\frac{d\theta_1}{dV} = \frac{A_1}{B_1} \quad [3.24]$$

Where, $n = 1$

$$A_1 = k_1 b_1 (1 - \theta_{1ss}) - (k_2 b_2 + k_{-1} b_{-1}) \theta_{1ss} \quad [3.25]$$

$$B_1 = k_1 + k_{-1} + k_2 + j\omega\tau \quad [3.26]$$

Therefore, total impedance of the system is represented by

$$Z_{total} = R_{sol} + \frac{1}{(Z_{F,m/s})^{-1} + Y_0 (j\omega)^{n_i}} \quad [3.27]$$

R_{sol} =solution resistance

Y_0, n_i =CPE parameters

$j = \sqrt{-1}$

ω ($\omega = 2\pi f$) = angular frequency

The minimum value of the optimal RMA parameters (determined by sequential quadratic programming (SQP)) residue form is given by

$$Residue = \sum \left[\omega_{\mathrm{Re}} \left(Z_{\mathrm{Re}_{experimental}} - Z_{\mathrm{Re}_{bestfit}} \right)^2 + \omega_{\mathrm{Im}} \left(Z_{\mathrm{Im}_{experimental}} - Z_{\mathrm{Im}_{bestfit}} \right)^2 \right] \quad [3.28]$$

Here, ω_{Re}, ω_{Im} =weighing functions. It equals to unity or transpose of real value and the imaginary value. It could also be the inverse of the square of the real and imaginary part of the experimental impedance. For very high magnitude impedance values, weighing functions may vary with the optimized parameter set values(Venkatesh and Ramanathan, 2010).

3.4 Characterization studies

To get a clear picture of the surface morphology of the metal treated at different slurries along with the compounds formed, characterization studies were being performed. The different studies done along with the sample preparation are as follows:

3.4.1 X-ray Diffraction (XRD) Measurements

To characterize the changes occurring on the Co surface post etching XRD analysis was performed. The measurements were conducted with SmartLab9KW diffractometer (Rigaku Corporation, Japan) that emits Cu radiation of 1.5406 Å wavelength. For analysis, Co sample was polished using emery sheets and dipped in the etchant solution for 30 min. The sample was dried properly using N_2 gas before placing it in the diffractometer. For reference purpose, XRD analysis of Co prior to etching was conducted.

3.4.2 Fourier Transform Infrared Spectroscopy (FTIR)

Fourier Transform Infrared Spectroscopy (FTIR) was performed by scanning the Cu and Co coupons in the wavenumber range of 4000-400 cm^{-1} on Spectrum series (Perkin Elmer, USA) unit. ATR accessory with a diamond crystal was used to analyze the treated metal coupons. The compounds of Co and Cu formed at the mentioned chemical treatments were confirmed by detecting the functional groups from the peaks.

3.4.3 Ultra Violet Visible Spectrophotometer (UV Vis)

To second the FTIR analysis and confirm the Cu and Co compounds formed, UV VIS spectroscopy was performed. UV -Vis analysis was conducted on Ultra Violet Visible Spectrophotometer (UV Vis) (Perkin Elmer, USA). An inbuilt software named UV WinLab was used to identify the peaks and the valleys of the UV adsorption spectra. The specimens are prepared as mentioned in Section 3.4.2.

3.4.4 Field Emission Scanning Electron Microscopy (FESEM)

FESEM analysis of Co was conducted on field emission scanning electron microscope (FESEM) (Zeiss, Sigma). Before every analysis the Co samples were polished using emery sheets and cleaned properly to removes the impurities or oxides. The samples are cleaned thoroughly and dipped in the solutions (H_2O_2 and H_2O_2+ oxalic acid) for 2 hrs. The samples are then washed again, dried and taken for analysis. The surface morphology and corrosion type of Co on treatment with the mentioned chemicals was analyzed and compared from the images.

3.4.5 Contact angle analysis

The traditional sessile drop technique was employed to determine contact angle between the droplet and treated Co sample surface. The liquid droplet comprises of water, methylene iodide (MI), and corrosive solution of two µL. The contact angle of the settled droplet was measured with the help of the camera present along with the inbuilt Holmarc software. The analysis was evaluated in a Goniometer (Holmarc opto-mechatronics). Contact angle analysis sample preparation is similar to that of FESEM analysis. It is to be mentioned that a minimum of 4 droplets were deposited separately and angle was measured to ensure repeatability. A contact angle difference of less than 2^0 was observed on the both the sides of the droplet ensuring reproducibility.

3.4.6 X-ray photoelectron spectroscopy (XPS)

To determine the different states of Co and identify the Co compounds formed when treated with H_2O_2 and H_2O_2+ oxalic acid at pH 9, XPS was conducted using ESCALAB Xi+ spectrometer (Thermo fisher Scientific Pvt. Ltd., UK) rigged with monochromatic Al Kα X-ray source radiation 1486.6 eV. The analysis was performed at room temperature and a base pressure of 5×10^{-10} mbar. Prior to XPS analysis Co metal was polished and the metal sample

was held in the solution of interest at +0.25 V w.r.t OCP for a duration of 3 hrs. This was done in order to obtain ample amount of product for analysis. The sample was then rinsed and dried using Nitrogen in a vacuum desiccator and then eventually taken for analysis.

3.4.7 Thermogravimetric Analysis (TGA)

Interaction between fumed silica, KIO_3 and BTA were studied using TGA. After proper mixing of the components (different combinations) in DI water, the dispersion was centrifuged, strained and dried using a vacuum pump. The sample was then kept in a hot air oven for drying, subsequently crumbled to fine powder for analysis. Thermogravimetric analyzer (STA449F3A00) (Netzch, India) was used for performing the TGA analysis. The analysis was done in a nitrogen environment while rising the temperature from 20℃ to 650℃ at a rate of 10℃/min.

CHAPTER 4

4. RESULTS AND DISCUSSION

4.1 Investigation of Polishing Characteristics of Interconnect (Cu) – Barrier Metal (Ru) in Potassium Iodate-Based Slurry

4.1.1 Motivation

The never-ending pursuit to fabricate technology node to <14 nm demands barrier metals that would provide a good diffusion barrier property along with desired thickness. A suitable barrier metal can decrease the resistance-capacitance delay of copper (Cu) and can encourage the process of size reduction of the devices (Krishnan, Nalaskowski and Cook, 2010). Compared to the already prevalent Ta/TaN barrier used in industry, Ruthenium (Ru) as a barrier metal layer has demonstrated many promising properties in previous studies that would make it a better alternative (T. N. Arunagiri *et al.*, 2005; Wei *et al.*, 2007b; Ding *et al.*, 2010; K. V. Sagi *et al.*, 2016). Although other barrier metals such as Cobalt (Co), Manganese (Mn) and its alloys(Aledresse and Alfantazi, 2004; Matsumoto *et al.*, 2009; Wang *et al.*, 2014a; Hazarika and Rajaraman, 2020) have been investigated, high resistivity and difficulty in controlling galvanic corrosion in between Co/Mn interface has proven to be extremely challenging (Bernhard, Pfandzelter and Winter, 2003).

Ru however, is a stable transition metal and is preferred because of its many exigent dynamics such as lower electrical resistivity (7.6 μΩ cm) as compared to Ta/ TaN, better adhesion ability with Cu and possibility of direct electrodeposition of Cu on Ru eliminating the need of Cu seed layer (Josell *et al.*, 2003; Seo *et al.*, 2011; Amanapu *et al.*, 2013). An additional advantage of using Ru is that at high temperatures, Ru shows almost negligible diffusivity with Cu(Massalski and Okamoto, 1990).

Precise metal layer removal and a polished top surface is required for fabrication of integrated circuits. Chemical Mechanical Planarization (CMP) is an efficient and industrially applied alternative process used to remove the initial surplus Cu followed by removal of the remaining Ru-Cu (in a ratio ~1:1). Ru is a hard metal and thus polishing it and obtaining a reasonable removal rate has proven to be a very challenging task. However, previous studies have revealed that by adjusting the components in the polishing slurry, a considerable removal rate (RR) can be attained. Peethala et.al.(Peethala, Roy and Babu, 2011b) reported a desirable selectivity of ~1:1 could be attained using silica particles and insoluble KIO_4 along with KOH at pH 9 and thereby preventing the formation of toxic RuO_4. Yadav et.al(Yadav, Jitendra C Bisen, *et al.*, 2017) used silica, sodium hypochlorite along with BTA to achieve a near desired selectivity ~1:1 while reducing the formation of toxic Ru compounds. They suggested that RuO_4^- and RuO_4^{2-}formed in the alkaline range assisted the formation of porous RuO_3/RuO_2 and the formed oxide help maintain the RR of Ru. Zeng et.al(Zeng, J.-X. Wang, *et al.*, 2012) identified that the addition of glycine to KIO_4 slurry improves the Cu-RR selectivity as Glycine reduces the etching of Ru and increases the Cu dissolution thereby affecting the RR of the metals. Amanapu et.al.(Amanapu *et al.*, 2013) analyzed the consequences of using guanidine carbonate and H_2O_2 on Ru. They found that unlike when individually used; a combination of both the components gave an enhanced RR. It was found difficult to achieve 1:1 Ru-Cu selectivity at alkaline region with a fair removal rate and lower etching value as Ru is a metal with higher chemical inertness as compared to Cu. Although multiple studies has been conducted using KIO_4(Peethala, Roy and Babu, 2011b), extra additives like KOH and higher abrasive concentration were used in the slurry to achieve desired selectivity. This can cause post CMP challenges like cross contamination and damaged surface layer(Steigerwald, Murarka and Gutmann, 2008). These physical damages (scratches/cavities) on the surface affects the surface property of the metal leading to internal stress and thus decreasing the life span.

Hence, we formulated a suitable slurry by optimizing the process parameters and slurry components that would yield desired polishing characteristics and selectivity between Cu-Ru substrates without the release of toxic RuO_4. We studied the role of oxidizer, abrasives and inhibitor on RR along with the change of etch rate at different alkaline regions on the polishing performance of the metals. Through TGA analysis, we examined the effect on RR with the reactivity of the components. We performed polarization experiments to investigate the performance of 1,2,3 Benzotriazole (BTA) as a barrier metal inhibitor. We also investigated the effect of process parameters on selectivity and determined the thermodynamic nature of the Cu –Ru dissolution. Temperature plays a very important role in CMP and dissolution of metal and is often neglected in most of the studies. We investigated effect of temperature on the etching performance and found that the dissolution process follows an endothermic nature.

Potassium iodate (KIO_3) as oxidizer was used instead of potassium periodate (KIO_4) due to its higher stability in the presence of salt impurities and humidity. Also, as compared to KIO_4, KIO_3 is less hazardous to human body.(Identification and Identification, 2008) Moreover, unlike KIO_4 or other periodates and iodates, KIO_3 also acts as a good corrosion inhibitor and an effective passivator for Cu (Shibli and Saji, 2005) . A slurry demonstrating good selectivity achieved with lower concentration (reduced by 60%) of abrasives and lesser chemicals has not been previously demonstrated. We achieved a selectivity of 1:1 with the optimized slurry formulation. A low etch rate with fair RR (60.7 nm/min for Ru and 58.7 nm/min for Cu respectively) and desired Ru: Cu selectivity of ~1.03 :1 using 2 wt. % silica, 0.2 M potassium iodate (KIO_3) and 5 mM BTA was attained at pH 9. We show the relevant polishing properties of the slurry in the following sections.

4.1.2 Experimental Conditions

Chemical Mechanical Polishing Experiments

All the polishing experiments were carried out on 25.4 mm diameter Cu and Ru disk with 99.9% purity (Tecniso Advance Pvt. Ltd, Singapore). Nonwoven polishing pads, Texmet C PSA (Buehler, India) of 203 mm diameter, fixed on a benchtop Labopol-20/Laboforce-50 polisher (Struers, Denmark) were used to polish the coupons. This polisher has an inbuilt carrier speed of 100 rpm. A peristaltic pump, PP-ex 20 (Miclins, India) was used to transport the slurry into the polisher. The flowrate of the slurry was maintained at 100 ml/min. The turntable speed and the applied pressure was fixed at 100 rpm and 5.72 psi respectively, unless explicitly mentioned. After each run the Cu/Ru metal was ultrasonically washed (in deionized water (DI)), dried and weighed in a microbalance (Sartorius Private Limited, India). The weight loss measured was used to calculate the average removal rates (RR, nm/min). To achieve consistent removal, rate the polishing pads were conditioned with DI water. Prestonian behaviour of RR of the metals was calculated using the formula

$$\mathrm{RR}\left(\frac{\mathrm{nm}}{\mathrm{min}}\right) = \mathrm{KPv} \qquad [4.1.1]$$

where P stands for down pressure, v for table speed, K for Preston coefficient and RR for removal rate (Zhao and Lu, 2013). All the slurries were prepared in deionized water and potassium iodate (Merck, India) was used as oxidizer. Cab-o-sil, M-5, fumed silica abrasives (Cabot Sanmar Limited) was used as the prime abrasives. Alumina (Beuhler, India) and titania (TTP, India) abrasives were also tried as part of the experiment. BTA (Loba chemicals Private Limited, India), Uric acid (Sigma Aldrich, India) and L-Ascorbic acid (Himedia, India) were investigated as inhibitors. For tuning the pH diluted Nitric acid (Loba chemicals Private Limited, India) and Potassium hydroxide (Himedia, India) were used.

Static Etch Experiments (SER)

SER were carried out at different alkaline pH range and at different temperature variations. KIO_3 dissolved in DI water was used as etchant for conducting the static experiments on Cu and Ru. Each coupon was dipped into the etchant for a time duration of 60 min. The metal coupons were then sonicated in DI water, dried and weighed. For each system a minimum of three repetitions were performed and the average was reported as the final etch rate (nm/min).

Electrochemical Experiments

The electrochemical experiments were performed on a potentiostat (PGSTAT 204, Switzerland). Ag/AgCl electrodes and Platinum wires were used as reference and counter electrode respectively. A 15 mm diameter Ru disc (99.9% purity) embedded in Teflon rod was used as the working electrode. Prior to every run, the electrode was polished with emery sheets in the following order (180, 320,600 and 1000 grit size). This was followed by polishing the electrode with 0.3µm and 1µm micro polish alumina powder (Buehlar, USA). The electrode was then sonicated in ethanol and was washed thoroughly in DI water. Open circuit potentials were performed for a duration of 600 secs before every potentiodynamic runs and the scanning rate used for anodic polarization was 1 mV/sec.

Thermogravimetric Analysis (TGA)

The TGA of KIO_3 was analyzed in pure salt form. The abrasives, oxidizers and inhibitors were analyzed by dissolving in DI water. After proper mixing of the components, the dispersion was centrifuged, strained and dried using a vacuum pump. The sample was then kept in a hot air oven for purging, subsequently crumbled to fine powder. Thermogravimetric analyzer (STA449F3A00) (Netzch, India) was used for performing the TGA analysis. The analysis was done in a nitrogen environment while rising the temperature from 20°C to 650°C at a rate of 10°C/min.

4.1.3 Results and Discussions

Etch experiments using varying KIO_3 concentration

As per the pourbaix diagram, formation of RuO_4 is usually observed in the acidic regime.(Han, 2016) RuO_4 formed is soluble in water and further converts to ruthenic acid which is toxic in nature(Peethala, Roy and Babu, 2011b; Yadav, Jitendra C Bisen, *et al.*, 2017). It was also reported that dissolution of metals and occurrence of corrosion of the polishing equipment is usually high at acidic pH (Luo, Campbell and Babu, 1997) and therefore, alkaline region over acidic region is preferred. Thus, in this study static etch experiments (SER) were carried out at a specified pH 9 for initial screening and to study the outcome of oxidizer (KIO_3) concentration on Cu and Ru coupons. The etching experiments were performed with oxidizer concentration ranging 0.1 M - 0.3 M with an interval of 0.05 M. The results are shown in Figure 4.1.1. For Cu coupons, a linear increase in etch rates with increase in KIO_3 concentration is observed. This is due to the emergence of double passivation film (copper oxide(s)/$Cu(IO_3)_2$) on the Cu metal surface using KIO_3 based slurries(Li and Babu, 2001). With the increase in KIO_3 concentration, formed copper oxides reacts with the more available IO_3^- ions forming abundance of insoluble $Cu(IO_3)_2$ compounds. These insoluble compounds accumulate on the metal surface and is likely the reason behind SER increase with increase in oxidizer concentration at pH 9. A similar Cu SER increase was also observed in reported literature(Steigerwald *et al.*, 1995). However, for Ru coupon with more than 0.2 M oxidizer concentration, the etch rate was found to be almost static. Less exposure of the surface of the Ru coupon to the etchant solution for oxidation could possibly be the reason behind the saturated result(Yadav, Jitendra C Bisen, *et al.*, 2017). As seen from Figure 4.1.1, for concentration above 0.2 M KIO_3 an undesirably higher dissolution of Cu was observed. At 0.2 M KIO_3 the SER was observed to be almost same and had the lowest standard deviation and therefore this oxidizer concentration was used for further experiments and analysis.

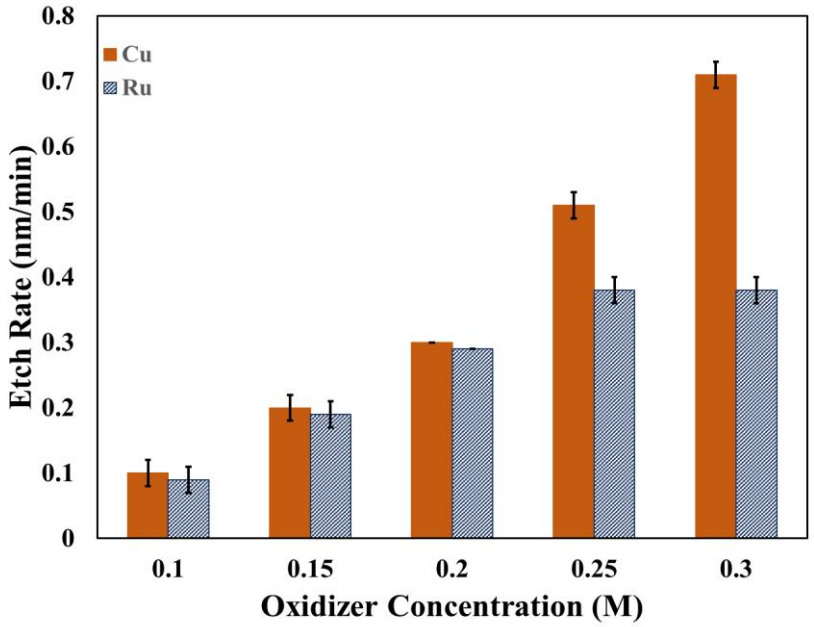

Figure 4.1. 1 Effect of oxidizer concentration (KIO_3) on SER at pH 9

Polishing and static etch experiments using only 0.2 M KIO_3 concentration

RR and SER experiments of the Cu and Ru coupons using 0.2 M KIO_3 concentration slurry without any other additives were carried out to study the outcome of change in pH. The results are displayed in Figure 4.1.2(a) and Figure 4.1.2(b). The polish rates were estimated at different alkaline pH values (8, 9, 10, and 11). From the results displayed in Figure 4.1.2(a), it can be seen that both the metal coupons show a decreasing trend in RR as the pH decreases from 8 to 11 (~58.7 nm/min to ~26.4 nm/min for Cu, ~51.2 nm/min to ~24.3 nm/min for Ru). KIO_3 in aqueous solution dissociates to form IO_3^- and K^+ ions. However, the formation of IO_3^- above pH 7 decreases, thus resulting in less oxidation of Cu and Ru metal surface. This reduction in IO_3^- formation explains the decreasing pattern of Cu and Ru RR.

$$KIO_3 \rightarrow IO_3^- + K^+ \qquad [4.1.2]$$

To substantiate the decrease in formation of IO_3^-, etch experiments at a similar environment was performed, the results of which are displayed in Figure 2(b). As anticipated, a decrease in

SER of both Cu (~0.4 nm/min to ~0.2 nm/min) and Ru (~0.4 nm/min to ~0.2 nm/min) was observed owing to less dissolution of the metal as the pH increases from 8 to 11. A similar decreasing SER trend of Cu and Ru was also observed in literature(Zeng, J.-X. Wang, *et al.*, 2012; Yadav, Jitendra C Bisen, *et al.*, 2017). From figure 4.1.2 it can be seen that the SERs were much lower than the RRs confirming that the direct dissolution of the metal have a very small role in the overall metal removal.

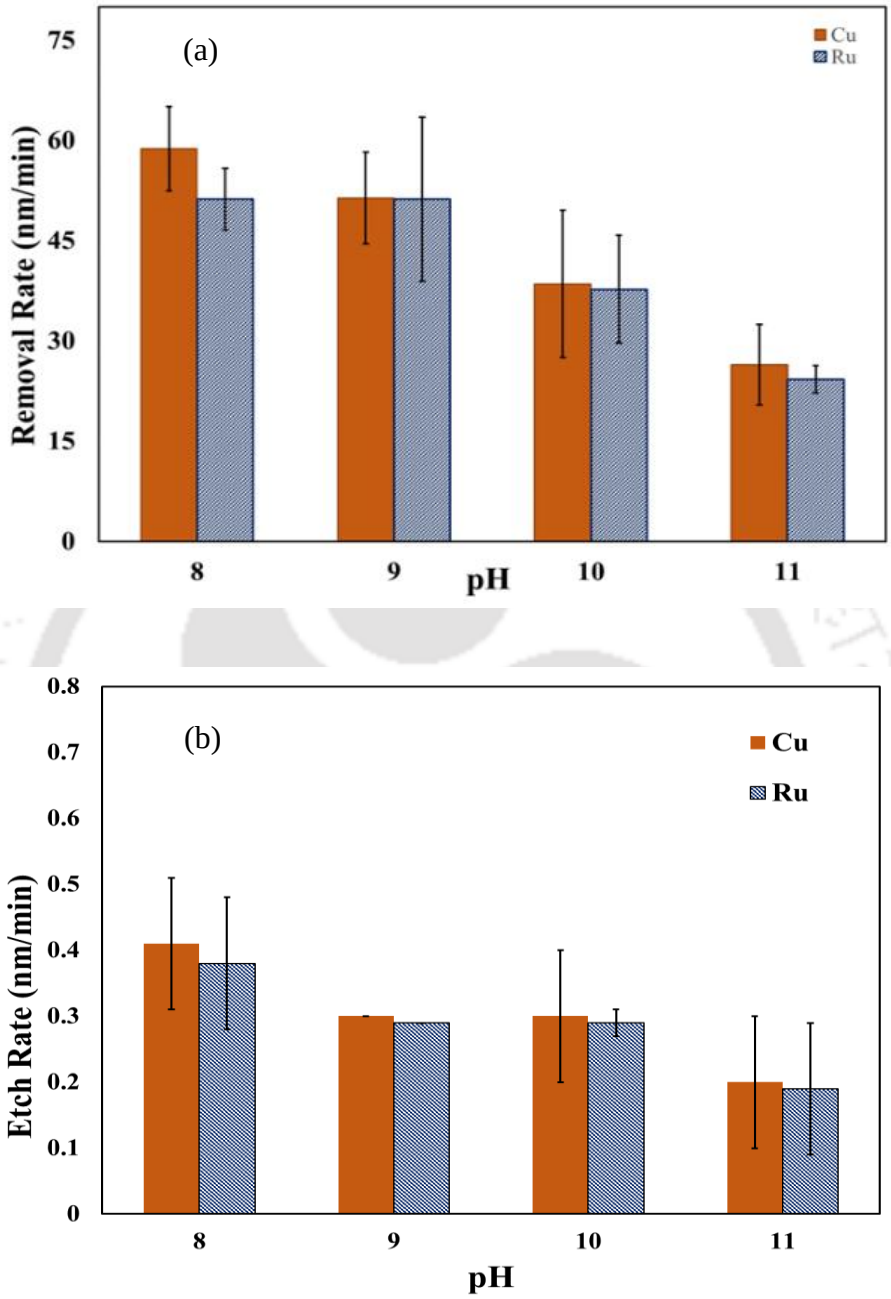

*Figure 4.1. 2**(a)** Effect of pH on RR using only 0.2 M KIO_3 **(b)** Effect of pH on SER using only 0.2 M KIO_3*

Etch experiments at different temperature range (0.2 M KIO_3)

Figure 4.1.3(a) illustrates the effect of temperature on etch rate of Cu and Ru coupons using 0.2 M KIO_3 as oxidizer. The temperatures at which the experiments were performed ranged between 25 to 85 ℃. The pH of the etchant was tuned to 9 for all temperature variation. From Figure 4.1.3(a), it is seen that with an increase in temperature, the SER drastically increases from ~0.3 nm/min to ~1.6 nm/min for Cu and ~0.3 nm/min to ~1.5 nm/min for Ru. With increasing temperature, there is a high probability of increase in occurrence of chemical reaction between KIO_3 and the metal surface (Yadav, Jitendra C Bisen, *et al.*, 2017), which could explain the rapid increase in SER. From the results obtained, it is seen that temperature plays a very vital role in metal-solution reaction. Since our aim is to obtain a lower but acceptable etch rate without high dissolution we opted to perform the experiments at a temperature of 25℃.

Activation energy (E_a) of Cu and Ru dissolution of the proposed solution (0.2 M KIO_3) were calculated using the Arrhenius Equation(Yadav, Jitendra C Bisen, *et al.*, 2017; Gupta, Manivannan and Noyel Victoria, 2019)

$$log(\mathrm{ER}) = \log\mathrm{A} - \frac{\mathrm{E_A}}{2.303\mathrm{RT}} \qquad [4.1.3]$$

Where, A stands for Arrhenius pre-exponential factor, T stands for absolute temperature and R stands for universal gas constant (8.314 J/mol.K). A semi-logarithmic graph of ER vs 1/T was plotted using the Arrhenius equation, which is demonstrated in Figure 4.1.3(b). A straight line is interpolated whose intercept and slope is log A and $\frac{-E_A}{2.303R}$ respectively. The activation energy for Cu and Ru dissolution process was 27.3 KJ/mol and 25.20KJ/mol respectively.

To determine the thermodynamic nature of Cu and Ru dissolution and to calculate the enthalpy and entropy, transition state equation was taken into consideration(Gupta, Manivannan and Noyel Victoria, 2019).

$$log\left(\frac{\mathrm{ER}}{\mathrm{T}}\right) = [log\left(\frac{\mathrm{R}}{\mathrm{Nh}}\right) + \frac{\Delta \mathrm{S_{act}}}{2.303\mathrm{R}}] - \frac{\Delta \mathrm{H_{act}}}{2.303\mathrm{RT}} \qquad [4.1.4]$$

Where, N is Avogadro's number (6.02252×10^{23} mol^{-1}), h stands for Plank's constant (6.626176×10^{-34} Js), ΔH_{act} is enthalpy of activation and ΔS_{act} stands for entropy of activation. Enthalpy and entropy were calculated by equating the intercept $[\log\left(\frac{R}{Nh}\right) + \frac{\Delta S_{act}}{2.303R}]$ and slope $[-\frac{\Delta H_{act}}{2.303R}]$ of the straight line as demonstrated in Figure 4.1.3(c). The calculated values of ΔH_{act} for Cu and Ru is as +27.2 KJ/mol and +29.9 KJ/mol respectively. From the values, it can be clearly seen that the dissolution process is endothermic in nature. The measured values of ΔS_{act} for Cu and Ru is -160.5 J/mol.K and -150.1 J/mol.K. The calculated values of ΔS_{act} is negative, indicating that the process of dissolution is more inclined towards associative mechanism thus forming an activated complex(Kuijer, Giling and Bloem, 1974; Yadav, Jitendra C Bisen, *et al.*, 2017; Gupta, Manivannan and Noyel Victoria, 2019). This explains the reason behind lower etch rates of the metals in the KIO_3 solution.

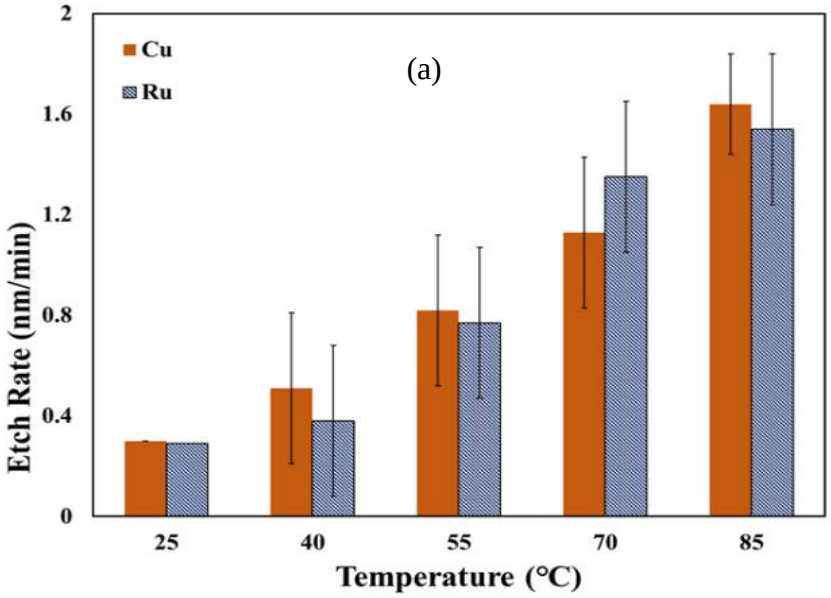

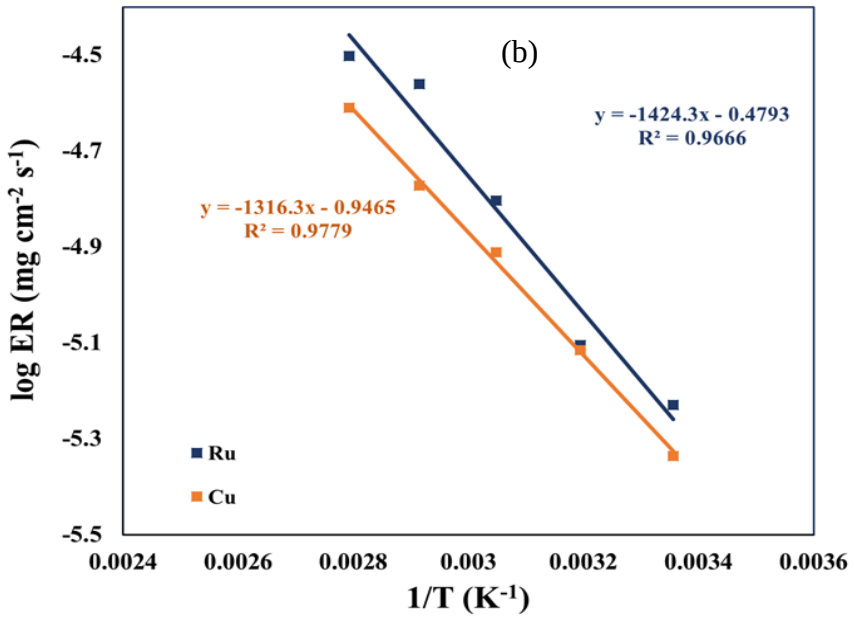

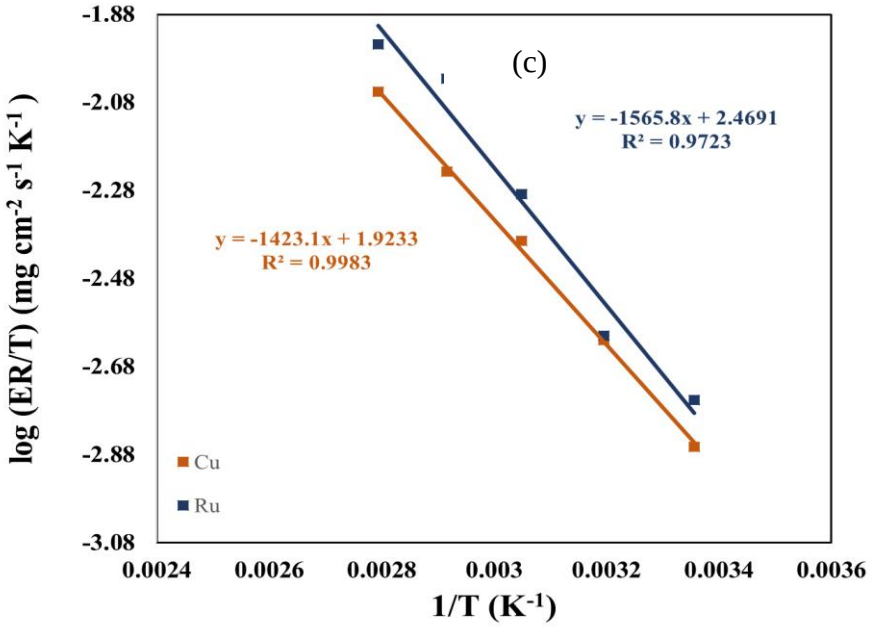

Figure 4.1. 3 ***(a)*** *Effect of temperature on SER using 0.2 M KIO_3* ***(b)*** *Arrhenius plot for Cu and Ru dissolution at pH 9 using only 0.2 M KIO_3* ***(c)*** *Log (ER/T) vs 1/T for Cu and Ru dissolution at pH 9 using only 0.2 M KIO_3*

Polishing experiments using 2 wt. % silica abrasives along with 0.2 M KIO_3

Chemical reaction between metal and abrasives and at times oxidizers and abrasives are often observed leading to the enhanced surface oxidization and higher RR(Li, 2007). The RR of Cu and Ru on addition of silica abrasives along with 0.2 M KIO_3 at pH range 8-11 were studied and the results are illustrated in Figure 4.1.4. In the absence of abrasive, RR ranged from ~58.7 nm/min to ~26.4 nm/min for Cu and ~51.2 nm/min to ~24.3 nm/min for Ru (for pH range 8-11). Whereas, adding the silica abrasives increased the RRs for both Cu and Ru. Polishing using only 2 wt% silica revealed almost negligible removal rate. This enhanced RR observed for Cu and Ru is due to the dual effect of mechanical exertion along with chemical interaction of the silica particles with the ruthenium and copper oxides(Victoria *et al.*, 2010b; Peddeti *et al.*, 2011). This combined effect of fumed silica particles and KIO_3 have more impact on Ru as

compared to Cu (Yadav, Jitendra C Bisen, *et al.*, 2017). Therefore, a higher Ru RR rate is obtained as can be seen confirmed from Figure 4.1.4.

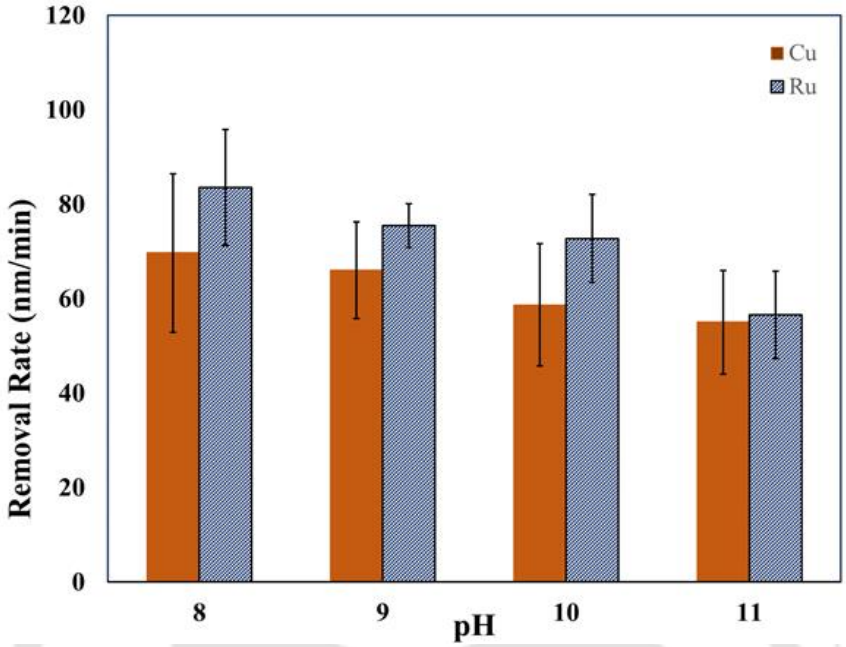

Figure 4.1. 4 Effect of pH on RR using 2 wt. % of silica abrasives along with 0.2 M KIO_3

Moreover, as per literature it was seen that, IO_3^- reduces to I^- to form less soluble CuI on the metal surface and on polishing pad. This CuI layer formed causes lower efficiency of the polishing properties of the pad thus resulting in lower RRs(Du *et al.*, 2004). Although this precipitation layer formation is more prominent in the lower pH, and its effect reduces as it moves towards alkalinity, this could be the reason behind the lower Cu RRs obtained as displayed in the Figure 4.1.4. It is to be mentioned that polishing experiments on both the metals were performed using 2%, 3%, 4% and 5% fumed silica. The results obtained showed very low and negligible change in the removal rates (~1-2 nm/min). So, keeping the post CMP issues in priority the optimized 2 wt% silica was selected as the abrasive concentration.

Polishing and static etch experiments using silica abrasives, KIO_3 and inhibitor BTA

The role of inhibitor BTA (Bilouk *et al.*, 2009b; Peethala, Roy and Babu, 2011b; Peethala *et al.*, 2012) in controlling corrosion for Cu and Ru along with attaining global planarization is notable. The effect of BTA on RR was studied and the results of it is demonstrated in Figure 4.1.5(a). BTA is a compound containing 3 nitrogen atoms on its surface. The slurry comprising of 5mM corrosion inhibitor BTA along with 2 wt% silica and 0.2 M KIO_3.was used in our case. As per requirement, BTA accepts or releases proton to one of the nitrogen atoms and acts as a weak acid or base. These electrons then form a bond with the metal forming an insoluble metal-BTA complex. This adsorbed metal-BTA complex on the metal surface protects the metal from corrosion. This formed complex prevents the formation of passivation layer on the metal surface(Venkatesh *et al.*, 2013). This is the reason behind why comparatively lower RR is observed in presence of inhibitor for both Cu and Ru as compared to RRs without using it.

The metal BTA complex formation mechanism is as follows(Allam, Nazeer and Ashour, 2009)

$$\mathrm{M(s) + BTA^-\ (aq) = M{:}\ BTA^-\ (ads)} \qquad [4.1.5]$$

$$\mathrm{nM{:}\ BTA^-(ads) = [M(BTA)]_n + \ nH^+ + ne^-} \qquad [4.1.6]$$

where M(s) stands for metal, BTA^- (aq) for BTA in aqueous solution, $M{:}\ BTA^-\ (ads)$ for BTA adsorbed on metal surface and $nM{:}\ BTA^-(ads)$ for number of stabilized films of the complex compound.

The static etch experiments on both the metal coupons were performed in pH range 8-11 using 0.2 M KIO_3 and 5mM BTA to study metal dissolution when in contact with the etchant. The results are displayed in Figure 4.1.5(b). Just like the previous cases, a decrease in SER occurs as the etchant proceeds towards more alkalinity. Also, compared to SER obtained previously,

a decrease in SER is observed on adding BTA to the slurry. This confirms the formation of metal- BTA complex on the metal surface, thus preventing the dissolution of it. A desired Ru-Cu selectivity of ~1.03:1 using BTA is attained at pH 9. Owing to this desired selectivity along with low etch rates at pH 9, a slurry consisting of 2 wt. % silica, 0.2 M potassium iodate (KIO_3) and 5 mM BTA is considered most effective for planarization of Cu and Ru.

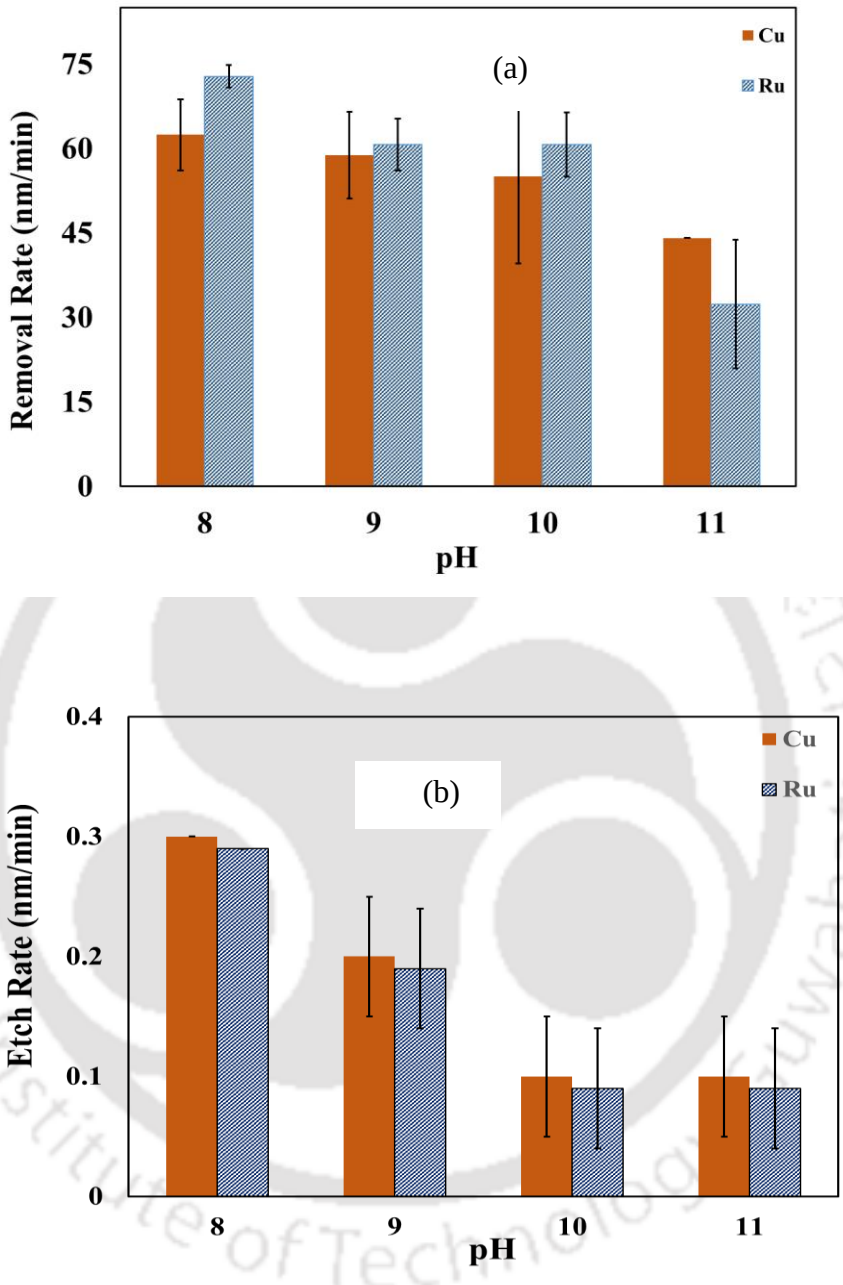

Figure 4.1. 5 Effect of pH on RR using 0.2 M KIO_3, 2 wt. % silica and 5 Mm BTA ***(b)*** *Effect of pH on SER using 0.2 M KIO_3, 2 wt. % silica and 5 Mm BTA*

Thermogravimetric Analysis (TGA)

Although the solubility of KIO_3 is low, the adsorption of additives on silica plays an important role in determining the removal rate and selectivity. To prove this, TGA analysis was performed and is displayed in Figure 4.1.6. As shown, the TGA graph for pure KIO_3 decomposes at ~550℃to KI, oxygen gas and small amount of iodine vapor (Boyd and Larson, 1969). Whereas for silica exposed to KIO_3, two decompositions are observed. The initial stage change observed is due to moisture evaporation and the second stage change observed at ~550℃ is due to decomposition of KIO_3 adsorbed on silica surface. Comparing it with the TGA curve of pure KIO_3, we can say that the weight loss is almost negligible.

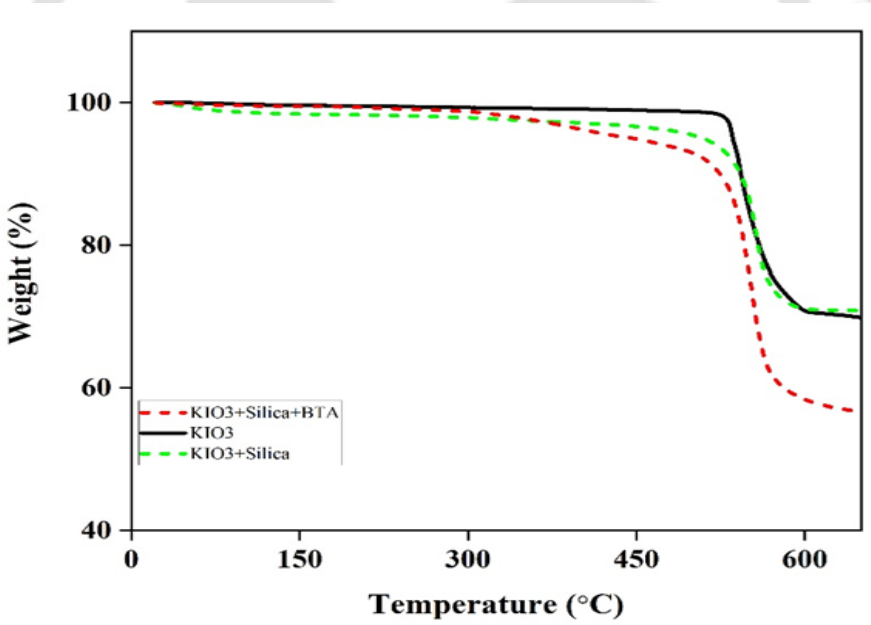

Figure 4.1. 6 TGA graph of pure KIO_3; TGA graph of centrifuged, filtered and dried slurry comprising of (i) 2 wt % silica and 0.2 M KIO_3; (ii) 2 wt % silica, 0.2 M KIO_3 and 5 mM BTA

The slightly dented curve obtained at ~300℃ confirms, although not to a higher extent, there is a chemical interaction between the silica particles and KIO_3 in the solution. This validates

that high RR observed in Figure 4.1.4 as compared to Figure 4.1.2(a) is due to dual role of the silica abrasives in the silica- KIO_3 system. The fumed silica acts as a competent abrasive and generates a chemically active silica-KIO_3 complex which reacts with the metal oxides resulting in high RRs. The formation of silica- KIO_3 complex eliminates the need of an extra additive to enhance the solubility factor of KIO_3 and its oxidizing power. For KIO_3 exposed to silica and BTA, decomposition around ~300℃ and ~550℃ is observed. The initial weight loss is due to decomposition of BTA adhered with KIO_3 and silica, whereas the weight loss at ~550℃ is due to decomposition of KIO_3 adsorbed on silica surface. The initial weight loss is probably due to the interaction of the BTA with KIO_3 and silica. The BTA complex formed, adsorbs on the metal surface forming metal-BTA complex and thus reduces the dissolution and RR of the metal coupons, thus acting as a good inhibitor. It is to be mentioned that the weight loss of the curves are not the same, since different additives were exposed to silica abrasive surface(Oh *et al.*, 2011; Peethala and Babu, 2011).

Proposed reaction mechanism

Based on the results obtained the mechanism of Ru is put forward henceforth. As per literature, KIO_3 is a crystalline powdered oxidizer that usually reduces to iodide (I^-) and oxygen (O_2) at an alkaline region (Boyd and Larson, 1969; Shibli and Saji, 2005). The further reduction of the dissociated O_2 to OH^- plays the major role in oxidation of the metal surface. The cathodic reactions involved in the process are presented in equation 7-9.

$$KIO_3 \rightarrow IO_3^- + K^+ \qquad [4.1.7]$$

$$IO_3^- + H_2O + 2e^- \rightarrow I^- + 2OH^- + O_2 \qquad [4.1.8]$$

$$O_2 + H_2O + 4e^- \rightarrow 4OH^- \quad [4.1.9]$$

As per the Pourbaix diagram for at $pH \geq 7$, $Ru(OH)_3$, $RuO_2.2H_2O$, RuO_4^- or RuO_4^{2-} is usually formed (Zeng, J. Wang, *et al.*, 2012). RuO_4^- (Perruthenate) is unstable and gets easily decomposed to O_2 and $RuO_2.2H_2O$(Peethala and Babu, 2011). The series of equations involved at this pH range are illustrated in equations 10-13.

$$Ru + 8OH^- \rightarrow RuO_4^- + 4H_2O + 7e^- \quad [4.1.10]$$

$$Ru + 3OH^- \rightarrow Ru(OH)_3 + 3e^- \quad [4.1.11]$$

$$Ru + 4OH^- \rightarrow RuO_2.2H_2O + 4e^- \quad [4.1.12]$$

$$2(RuO_4^-) + 2OH^- \rightarrow 2(RuO_4^{2-}) + H_2O + \frac{1}{2}O_2 \quad [4.1.13]$$

It is to be mentioned that Ru and Cu in typical slurries acts as a galvanic couple attributing to dishing of the metal (Peethala, Roy and Babu, 2011b). Although galvanic corrosion study is not included in this work, BTA is added to the formulated slurry with the purpose of acting as corrosion inhibitor. As already mentioned, BTA prevents dissolution of the metal by forming a metal-BTA complex on the surface of the metal.(Ryu *et al.*, 2019) This adsorption of the Ru-BTA complex is shown in equation 14.

$$4Ru + 4BTA^-_{(ads)} + O_2 \rightarrow 4Ru - BTA + 2H_2O + 4e^- \quad [4.1.14]$$

A graphical representation of the oxide formation mechanism is also illustrated in Figure 4.1.7.

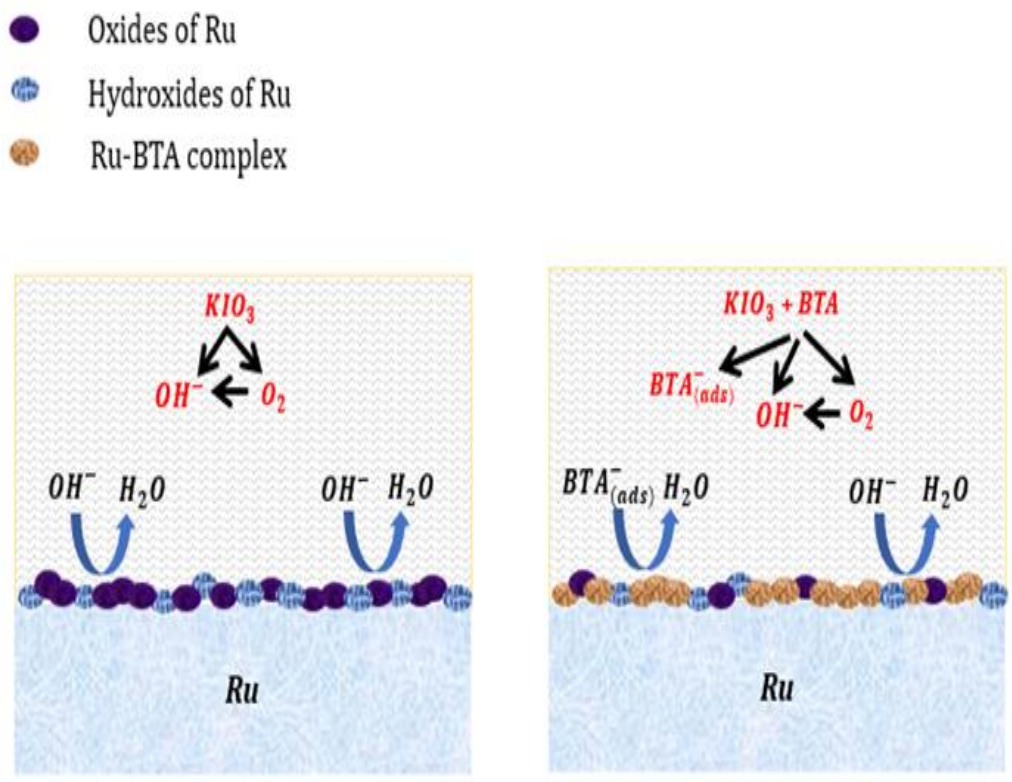

Figure 4.1. 7 Schematic diagram of Ru surface oxidation in presence KIO_3 and KIO_3 + BTA

The potentiodynamic curve of Ru in 0.2 M KIO_3 and 0.2M KIO_3 + 5 mM BTA at pH 9 is displayed in Figure 4.1.8. As seen in the Tafel plot (for KIO_3) the current on the anodic section is almost continually above 0.15 V suggesting the formation of Ru hydroxide and oxides, as displayed in equations 10, 11, 12, 13. The formation of the Ru hydroxides and oxides in the alkaline region can be supported by the Ru Pourbaix diagram (Han, 2016). In the presence of the inhibitor BTA, the anodic current decreases indicating BTA adsorption on the metal surface. The formation of BTA-metal film diminishes the possibility of any metal dissolution. The corrosion current density (I_{corr}) and current potential (E_{corr}) with and without inhibitor were calculated by extrapolating the tafel plot and is displayed in Table 4.1.1. On addition of inhibitor, the E_{corr} value decreases from 142.2 mV to 128.1 mV whereas I_{corr} value decreases

from 207.8 nA/cm^2 to 12.5 nA/cm^2. This reduction in I_{corr} approves the role of BTA as a good inhibitor in deaccelerating the corrosion process.

Table 4.1. 1 Corrosion potential (E_{corr}) and corrosion current density (I_{corr}) extrapolated from Tafel plot

Ru	E_{corr} (mV)	I_{corr} (nA/cm^2)
0.2 M KIO_3	142.2	207.8
0.2 M KIO_3 + 5 mM BTA	128.1	12.5

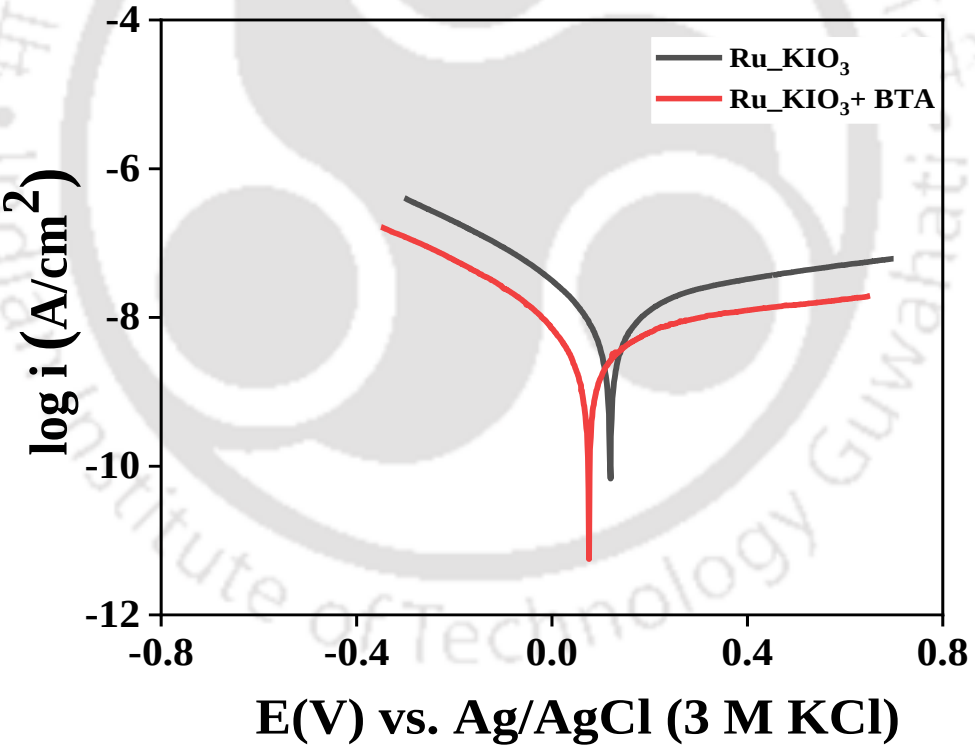

Figure 4.1. 8 Tafel curves for Ru using 0.2 M KIO_3 and 0.2 M KIO_3 + 5 mM BTA

Effect of different inhibitors and abrasives on selectivity at tailored conditions

Cu-Ru selectivity using different inhibitors is displayed in Figure 4.1.9. The inhibitors studied were ascorbic acid(Peethala and Babu, 2011), uric acid(Jeong *et al.*, 2019) and BTA in a concentration of 5mM. From the RRs obtained, it was seen that BTA gave the coveted selectivity of 1:1.03 unlike ascorbic acid and uric acid. The selectivity obtained using uric Acid and L-Ascorbic acid is 1.66: 1 and 2.04: 1 respectively.

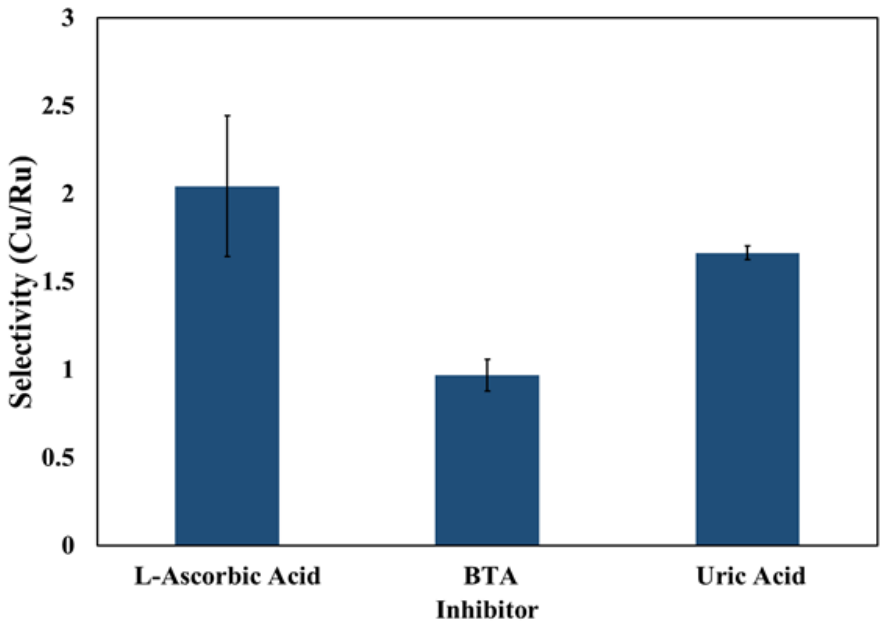

Figure 4.1. 9 Effect of different inhibitors on selectivity using Silica (2 wt.%), KIO_3 (0.2 M) and inhibitor (5mM) at 100 rpm table speed and pH 9

Table 4.1. 2 Removal rate on using Silica (2 wt.%), KIO_3 (0.2 M) and inhibitor (5mM) at pH 9 and 100 rpm table speed

	Alumina	**Silica**	**Titania**
Cu RR (nm/min)	132.1	58.7	113.8
Ru RR (nm/min)	99.7	60.7	105.1

The removal rates of the metals on using different abrasives at pH 9 are displayed in Table 4.1.2. It was seen that alumina and titania resulted in a high RR as compared to silica. To corroborate these RR results, TGA analysis of the three systems containing alumina, silica and titania along with 0.2 M KIO_3 were conducted and displayed in Figure 4.1.10a. For comparison TGA analysis of pure KIO_3 was also performed. The initial weight loss just under 100°C can be considered due to moisture evaporation. For pure KIO_3, decomposition is observed at ~550 °C and for KIO_3 adsorbed on abrasives (silica, alumina, titania) surface, decomposition is observed between ~500-550°C. However, the weight loss percentage of KIO_3 adsorbed on titania and alumina surface is comparatively lower than KIO_3 absorbed silica. This decreased weight loss percentage or decomposition, attributes to lower interaction of the IO_3^- ion with abrasives as compared to the ones with higher weight loss percentage. Thus, the available IO_3^- ions rather than reacting with the abrasive particles, reacts with the metal coupon forming a passivation layer over it. The abrasives efficiently play its role by abrading the passivated layer on the metal surface and at times chemically reacting with it(Li, 2007). This explains the reason behind high RR for Ru in the following order, silica (~60.7 nm/min) < alumina (~99.7 nm/min) < titania (~105.1 nm/min).

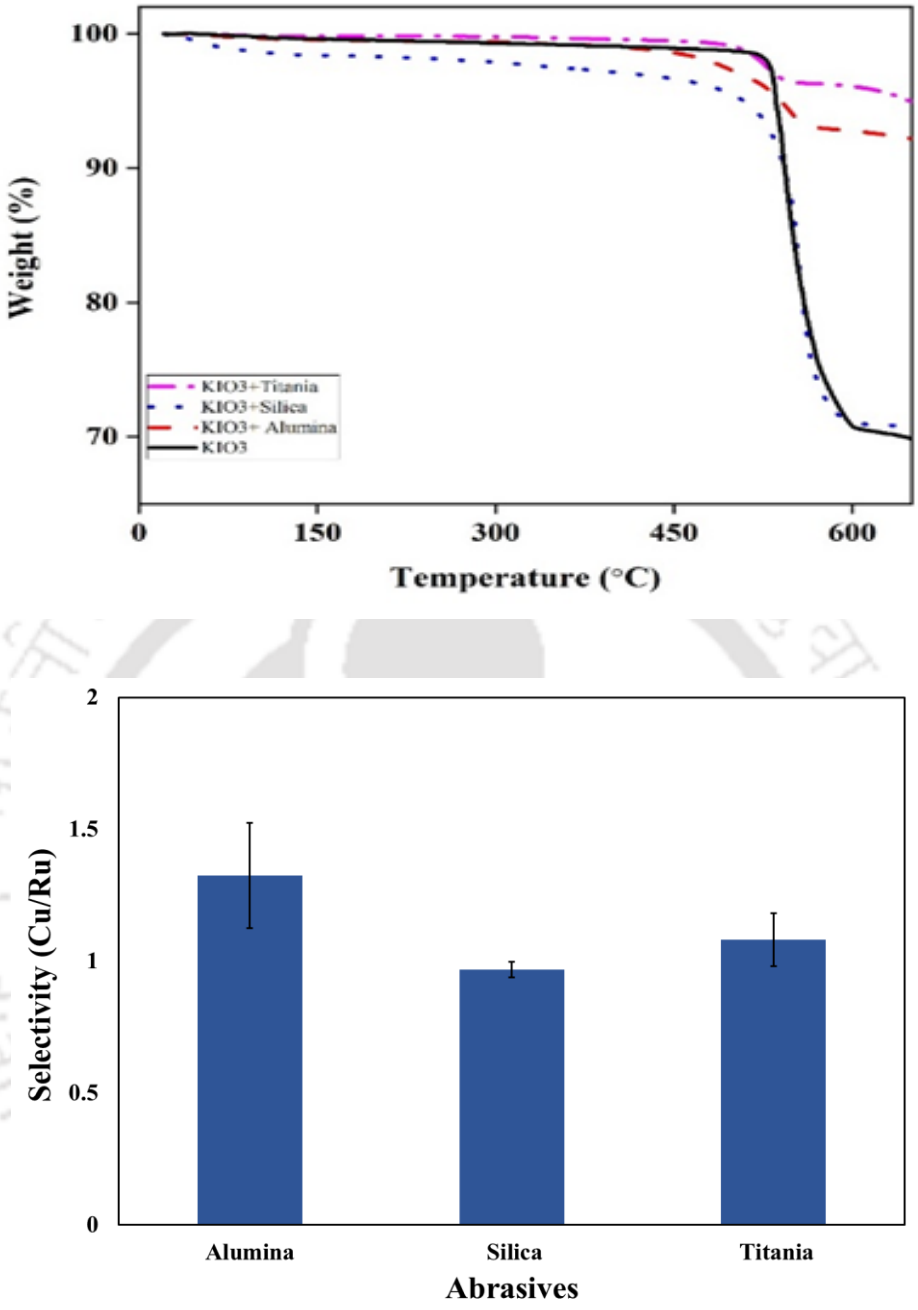

Figure 4.1. 10 ***(a)*** *TGA graph of pure KIO_3; TGA graph of centrifuged, filtered and dried slurry comprising of (i) 2 wt % silica and 0.2 M KIO_3; (ii) 2 wt % titania, 0.2 M KIO_3 and; (iii) 2 wt % alumina, 0.2 M KIO_3* ***(b)*** *Effect of different abrasives on selectivity using abrasives (2 wt %), KIO_3 (0.2 M) and BTA (5mM) at 100 rpm table speed and pH 9*

Cu being a soft metal, hardness of the abrasives particles (along with chemical interaction) plays a key role in determining the RRs of metal(Peddeti *et al.*, 2011). Since, hardness of alumina is more as compared to others, a high Cu RR rate (~132.1 nm/min) was obtained. The Cu removal rate using silica and titania abrasives are ~58.7 nm/min and ~113.8 nm/min respectively. Although the RR using alumina and titania based slurries are high, it is observed from Figure 4.1.10b that slurry comprising of silica, KIO_3 and BTA gives a desired selectivity of 1:1.03.

Importance of process parameters on Cu-Ru removal rates and selectivity at optimized slurry conditions

To understand the role of process parameters on Cu and Ru RR, CMP experiments using the tailored slurry {fumed silica (2 wt. %), KIO_3 (0.2 M) and BTA (5 mM) at pH 9} was performed. Figure 4.1.11a illustrates the RR procured at varying applied pressure (1.41, 2.86, 5.72 and 8.91 psi) and at constant a turntable speed of 100 rpm. From the graph it can be seen that with increase in pressure, the surface contact points between the metal surface and plate increases(Carpio, Farkas and Jairath, 1995). This attributes to the higher RRs obtained with increase in pressure. It should be mentioned the RR obtained for both the metals at zero pressure does not have a zero intercept. Emergence of a passive layer on the metal surface could be a probable reason behind this(Victoria *et al.*, 2012). As the graph is nonlinear in nature, the system disobeys Preston empirical equation. Thus, the slurry follows a Non-Prestonian behavior with increase pressure. A similar case of non-prestonian behavior was also reported in literature(Cheng *et al.*, 2015).

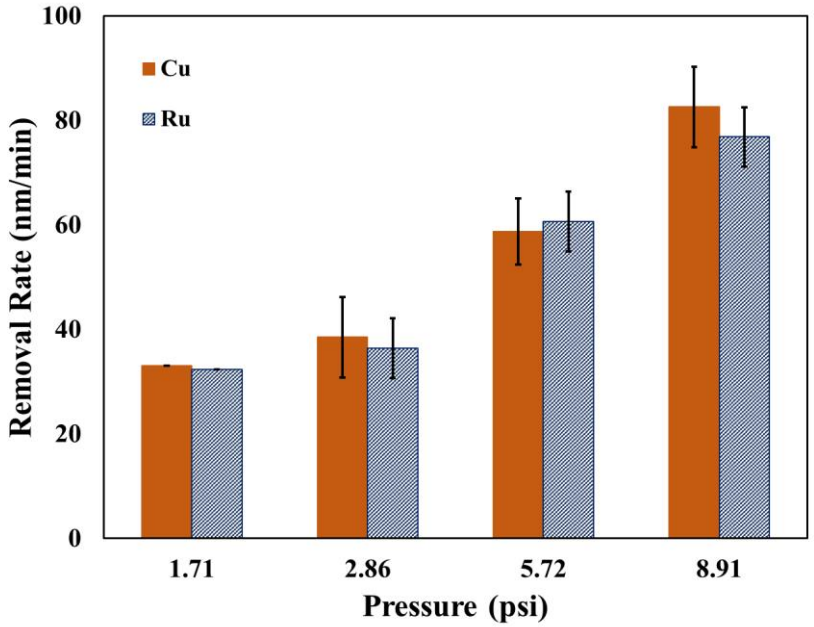

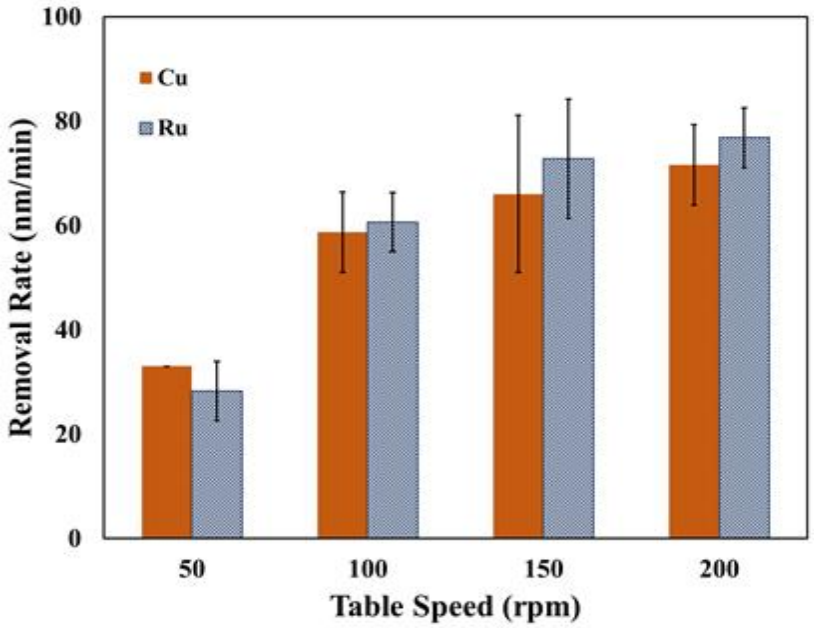

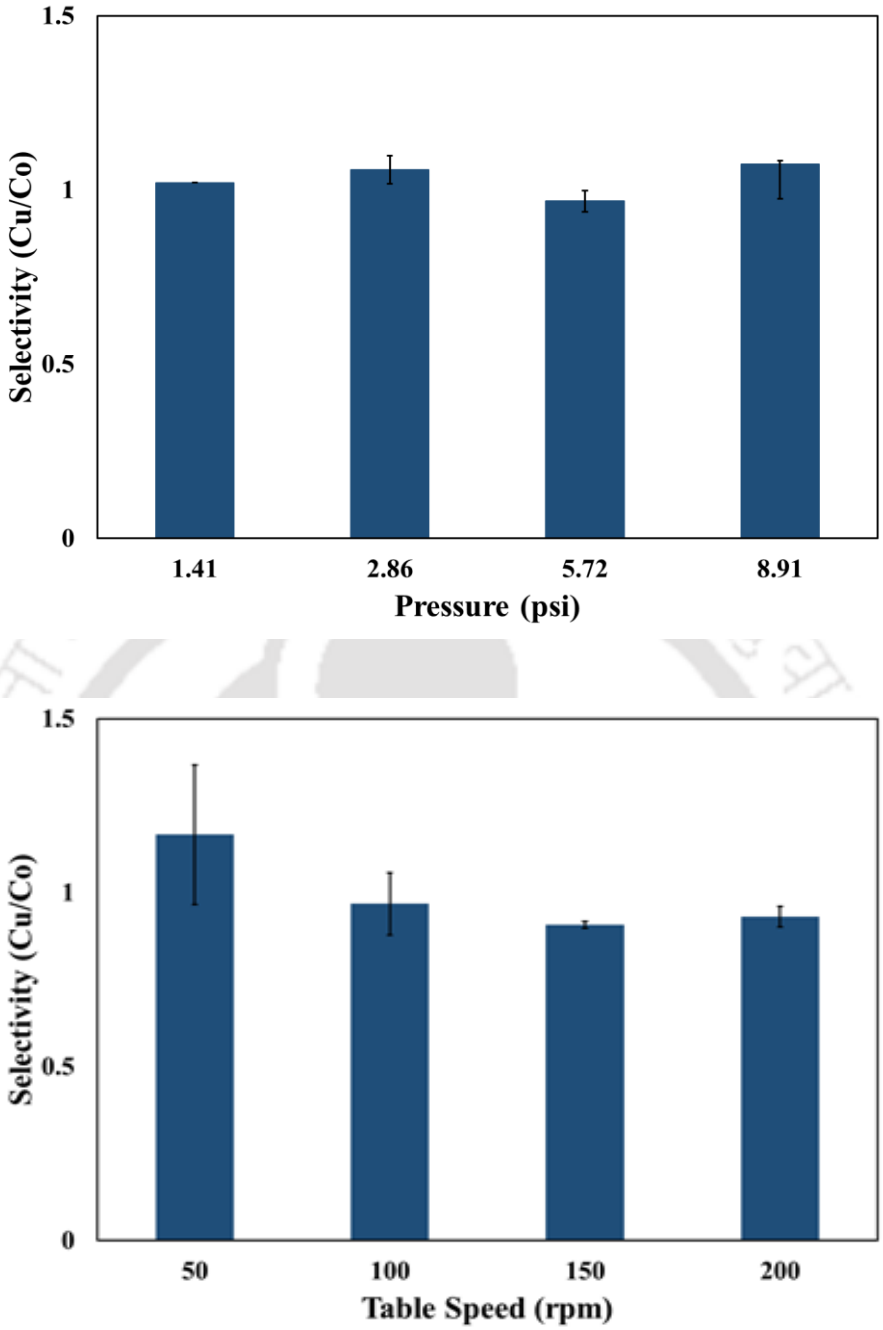

Figure 4.1. 11 At optimized pH 9 ***(a)*** *Effect of pressure on RR using silica (2 wt. %), KIO_3 (0.2 M), BTA (5 mM)* ***(b)*** *Effect of turntable speed on RR using silica (2 wt. %), KIO_3 (0.2 M) BTA (5 mM)* ***(c)*** *Effect of pressure on selectivity using silica (2 wt. %), KIO_3 (0.2 M), BTA (5 mM)* ***(d)*** *Effect of turntable speed on selectivity using silica (2 wt. %), KIO_3 (0.2 M) BTA (5 mM)*

CMP experiments of Cu and Ru coupons at varying turntables speeds (50, 100, 150 and 200 rpm) and constant applied pressure of 5.71 psi were performed, the results of which are displayed in Figure 4.1.11b. From the figure it is observed that with the escalation of the turntable speed, the RR rises for both the cases. The rapid increase in friction between the abrasives, polishing pad and oxide layer formed at the metal surface could be reason behind this RR increase(Cheng *et al.*, 2015). The selectivity of Cu-Ru at variable pressure and turntable speed is calculated and the results are displayed in Figure 4.1.11c and Figure 4.1.11d. Although the RR increase is significant with change in process parameters, change in selectivity is almost negligible. This construes that change in process parameters has negligible effect on selectivity at the suggested slurry composition.

4.1.4 Conclusion

The role of KIO_3 as oxidizer in CMP of Cu- Ru was studied in this work. The study was conducted in the alkaline region, to prevent the occurrence of RuO_4, which is toxic in nature. A decreasing trend in removal rate was observed for both the metals at all conditions. This occurs due to lesser availability of IO_3^- ions to oxidize the metal surface beyond pH 7. Etch experiments at increasing temperature and at optimized pH was performed. A rapid increase in ER with temperature was observed. This is due to the occurrence of chemical reaction on the metal surface at a high temperature. The dissolution of the metals in the etchant follows an endothermic nature and activation energy E_a measured was 27.3 KJ/mol for Cu and 25.2 KJ/mol for Ru. BTA behaves as a good inhibitor by forming at BTA-complex on the metal surface. This slightly reduces the RR as compared to RR while using silica and KIO_3. However, a desired Cu-Ru selectivity of ~1:1.03 was obtained at pH 9 which suggest that the solution comprising of fumed silica (2 wt. %), KIO_3 (0.2 M) and BTA (5 mM) is suggestively appropriate for effective polishing of barrier metal and interconnect which can be applied in semiconductor industry. TGA analysis were performed to verify the effect of abrasives and

different component of slurry on RR. It was found that the system disobeys Preston empirical equation with pressure and table speed. It was also observed that the process parameters play a negligible role on selectivity at the given optimized slurry.

4.2 Formulation of sodium hypochlorite-based slurry for copper - cobalt chemical mechanical planarization process

4.2.1 Motivation

With the advancement of microelectronic devices in the passing time, in terms of circuit complexity and size reduction, the new generation devices demand for more competency and more speed. However, as the size decreases, the process in manufacturing the precise structures becomes an important challenge in preventing lower yield of the product. Usually during fabrication of the circuit, Cu is used as an interconnect since it is a good conductor of electricity and Ta/TaN was used as a barrier material to prevent the diffusion of Cu in to dielectric material.(Min *et al.*, 1996) However, with the shrinkage of technology node to 10 nm and below, various technological problems appears such as maintaining the diffusion barrier property and the desired thickness at the same time. Therefore, various other barrier metals such as Ru, Co, CoMn, Mn, CuMn, TiZrN, TaC, WSiN and BN were studied in order to substitute the existing Ta/TaN .(Aledresse, 2004; Kuo *et al.*, 2004; Qu *et al.*, 2004)

Recently Co and Ru are considered as two of the most potency metals to act as barrier metal. However, as per some of the works reported, Co seems to have better properties as compared to Ru.(Bilouk *et al.*, 2009b; Nishizawa, Nojo and Isobe, 2010b; Peethala *et al.*, 2012; Yin, Yang, Niu, *et al.*, 2020) It does not emit any toxic gases unlike Ru, which releases toxic RuO_4 gas in acidic medium. Moreover, Ru being a hard metal in nature (hardness of 6.5 Mohs), it is hard to find chemicals that provide higher polish rates. However, Co, possess various advantages such as relatively lower hardness (5.0 Mohs), lower resistivity (~6.2 μΩ cm), good stability, economical, and better adhesion properties with Cu, and most important of all, direct electrodeposition of Cu is possible as Co itself acts as a seed layer during Cu deposition.(Ma *et al.*, 2009; Rights, 2017) After the deposition of Cu and barrier metal, the structures demand for a planar topography for the following level metallization.

Typically, Cu CMP is a 2-step process. The first step involved is removal of bulk Cu that stops on the barrier layer or slightly before the exposure of the barrier layer. The second step involved is removal of the residual Cu along with barrier metal without excessive thinning. This demands the CMP slurry to achieve a selectivity (the ratio of Cu removal rate to Co removal rate) of ~1:1. It is to be noted that Cu and barrier metal, Co CMP have been mainly incorporated in the ULSI devices comprising of CMOS, FET (PMOS and NMOS transistors) etc. for attaining global planarization.(Tanwar, 2014)

Different components in a slurry namely, oxidizers, abrasives, complexing agents, inhibitors, pH tuners play a very important role in polishing as well as maintaining desired selectivity between barrier metal and interconnect. Nishizawa et al.(Nishizawa, Nojo and Isobe, 2010b) found out that using hydrogen peroxide as oxidizer, citric acid as complexing agent, and benzotrizaole (BTA) as inhibitor in an alkaline pH gave a Cu/Co RR selectivity of ~0.5:1. The influence of pH on polishing was also studied. Insignificant increase in RR rates of Cu was observed when the slurry pH increases. Whereas a drastic decrease in RRs of Co was seen, as the pH of slurry was changed from acidic to alkaline. This is due to the formation of denser passivation layer with the increase in pH.(Nishizawa, Nojo and Isobe, 2010b) In another case, Peethala et.al (Peethala *et al.*, 2012)und that polishing using colloidal silica slurry consisting of hydrogen peroxide as oxidizer, arginine as complexing agent and BTA as inhibitor gave a selectivity of 0.8:1 at measured pH 10. Arginine was added to enhance the Co RRs whereas BTA was added to inhibit Cu dissolution rates. This formulated slurry at pH 10 gave a good post-polish surface quality without any excessive high dissolution rate of Co. *Although many types of slurry for Cu CMP are suggested until date, they mainly focused on achieving desired selectivity between Cu and Ta. Only limited studies are available on Cu - Co CMP process. Thus, this study mainly focuses on the slurry formulation for finding the desired selectivity of Cu and Co in the ratio ~1:1 using sodium hypochlorite as oxidizer, fumed silica as abrasives*

and BTA as inhibitor. Besides, the impact of change in pressure, table speed and inhibitors on selectivity of Cu and Co at optimum pH was also investigated.

4.2.2 Experimental Conditions

Chemical Mechanical Polishing Experiments

The polishing experiments were rendered on a benchtop Labopol-20/ Laboforce- 50 polisher (Struers) with a sample rotational speed of 150 rpm. Non-woven Buehler Texmet C PSA pads of dia. 203 mm (8") were used as the polishing pad. The metals used for polishing were Cu coupon (99.9% pure) of 25.4 mm diameter and Co coupon (99.9% pure) of 25 mm diameter. Both the metals were procured from Tecnisco Advance Materials Pvt. Ltd, Singapore. The formulated slurry was pumped to the CMP machine through a peristaltic pump (Miclins PP-ex 20) with a controlled flow rate of 100 ml/min. Unless otherwise mentioned, the turntable speed was set at 100 rpm while the applied down force was 5.72 psi.

Fumed silica (Cab-o- sil, M-5P) supplied by Cabot- Sanmar was used as abrasive particles. Sodium hypochlorite (Finar) was used as the oxidizer whereas BTA (Loba chemicals), L-Ascorbic acid (Himedia) and Uric acid (Sigma Aldrich) were investigated as inhibitors. The slurry was prepared with the following concentration: 2 wt. % of abrasives, 0.5 wt. % of oxidizer and 5 mM of inhibitor. Potassium hydroxide (Himedia) and Nitric acid (Loba chemicals) were used to modulate the pH value. Prior to actual runs, few dummy runs were conducted with slurry containing only fumed silica for every new pad in order to obtain stable and coherent results. After weighing the metal, the polishing of each run was conducted for two minutes and a minimum of three identical runs were carried out for each system. The pad was conditioned before each run. The metal after polishing with slurry was washed with millipore water followed by sonication for 2 minutes. The sample was rewashed thoroughly,

dried and then weighed. Thereafter, the average removal rate in nm/min is estimated from the measured weight loss and reported with standard deviation.

Static Etch Rate Experiments

Static etch rate experiments were performed with both Cu and Co metal samples at various pH values 3, 5, 7, 9 and 11. The etchant solution was prepared by using 0.5 wt. % NaOCl based solution in Millipore water. After weighing the sample, it was immersed in the etchant solution for 30 min. Then, the sample was washed in Millipore water, dried and weighed again. Triplicate runs were performed for each case and the average static etch rate in nm/min is reported.

X-ray Diffraction

The changes happening on the Co surface after etching using NaOCl and BTA at pH 5 and 9 were observed by using XRD analysis. It was carried out with SmartLab9KW diffractometer (Rigaku Corporation, Japan) that emits Cu radiation of 1.5406 Å wavelength. For analysis, Co sample was polished and kept in an etchant solution containing NaOCl and BTA (at pH 5 and pH 9) for a time span of 30 min. The sample was then dried and kept in the diffractometer for analysis of products formed on the surface. For reference purpose, XRD analysis of Co prior to etching was also performed.

4.2.3 Results and Discussion

Polish rate experiments in the presence of only NaOCl

Figure 4.2.1 demonstrates the outcome of removal rate with respect to pH value (3, 5, 7, 9 and 11) for both the metals Cu and Co in a slurry comprising of only 0.5 wt. % NaOCl as oxidizer without any abrasive particles. It is clearly seen from this plot that with an increase in pH value, the polish rate decreases from 532.30 nm/min to 33.03 nm/min for Cu and from 499.26 nm/min

to 44.05 nm/min for Co. The higher polish rate in acidic medium is attributed to the direct dissolution of metal ions in the slurry whereas in neutral to alkaline medium, the passivation layer forms on the metal surface, which subsequently decreases the polish rate. Although the overall trend is same for both the metals, the polish rate is higher for Cu as compared to that Co at pH 3 (532.30 nm/min vs. 499.26 nm/min) while the polish rate is higher for Co when compared to Cu at all the remaining pH values being investigated in this study (33.03 vs nm/min vs. 44.05 nm/min at pH 11). It could be attributed to the fact that Co metal (Reduction potential E_0 = -0.277) is a stronger reducing agent than Cu metal (E_0 = 0.3419).(Pourbaix, Zhang and Pourbaix, 1997)

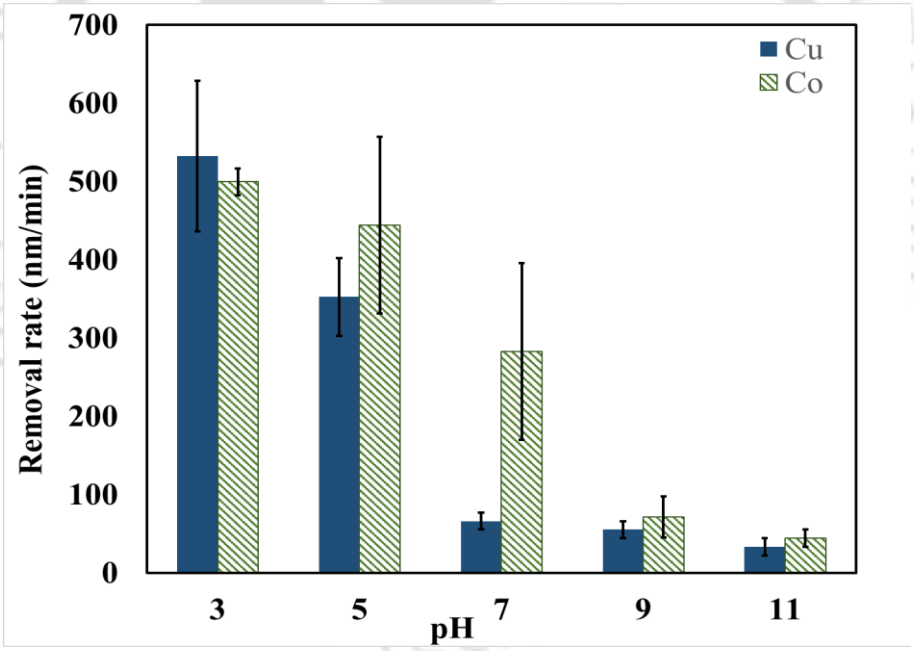

Figure 4.2. 1 Change in pH and its effect on removal rate of Cu and Co using only NaOCl (0.5 wt. %)

In order to verify this, the static etch experiments were also carried out for both the metals in the etchant solution containing only 0.5 wt.% NaOCl at various solution pH values (3,5,7,9 and

11) and the results are displayed in Figure 4.1.2. In few cases, the standard deviation obtained is negligible and hence error bars are not visible in the plot. As expected, the Co etch rate is higher compared to that of Cu at all the pH values. The static etch rate of Co decreases from 9.54 nm/min to ~ 2 nm/min when the solution pH shifted from acidic regime to alkaline regime as observed in the polishing experiments. Likewise, Cu too follows the decreasing trend i.e. the static etch rate decreases from 8.63 nm/min to 0.92 nm/min. This is clearly indicating the fact that the stable passive layer is formed on both the metal surfaces in an alkaline regime resulting in less dissolution of the metal. It is also to be noted from Pourbaix diagram for Cu and Co that the formation of Cu oxides is thermodynamically more feasible in the neutral regime as compared to that of formation of Co oxides at lower reduction potentials.(Pourbaix, Zhang and Pourbaix, 1997; Gerken *et al.*, 2011) This could be the potential reason for observing drastic reduction in the Cu polish rate (~352 nm/min to ~66 nm/min) comparing to Co (~444 nm/min to ~ 282 nm/min) when the solution pH changes from 5 to 7.

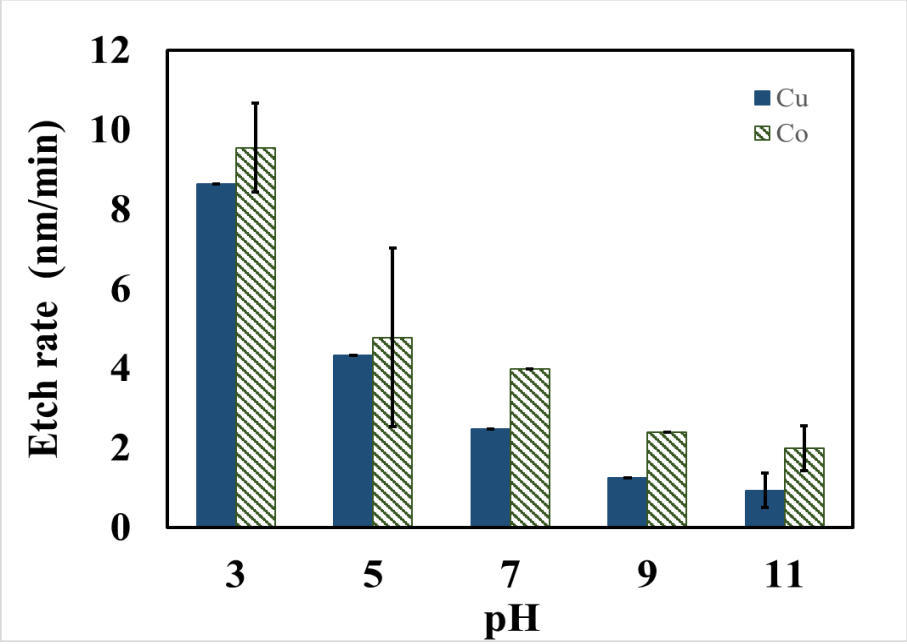

Figure 4.2. 2 Change in pH and its effect on etch rate using NaOCl (0.5 wt. %)

Polish rate experiments in the presence of both NaOCl and abrasives

The removal rates of Cu and Co using slurry containing 0.5 wt. % NaOCl and 2 wt. % silica at various pH values (3,5,7,9 and 11) is presented in Figure 4.1.3. The removal rates for Co varies from ~1095 nm/min to ~49 nm/min when the pH value increases from 3 to 11. In the same manner, the removal rates for Cu showing the decreasing trend (~792 nm/min to 66 nm/min) with respect to pH value. As expected, enhancement in the polish rate is observed due to the mechanical abrasion between substrate and abrasive particles. Although, the trend (polish rate decreases with an increase in pH value) remains the same, the polish rate of Cu is slightly higher compared to that of Co at pH value 11 as opposed to the previous case (slurry containing only oxidizer). Although, silica particles were added to the slurry with the intention of removing material via mechanical abrasion process, the chemical interaction of silica particles with the metal to be polished has also been observed and reported in the literature.(Li, 2007) Thus, the interaction of copper and cobalt oxides with the silica particles at pH 11 also plays an important role in determining the polish rate.

As the whole study is aimed to obtain 1:1 selectivity for Cu-Co, further tuning of the slurry is essential as the results showed that the achieved selectivity is far from 1:1. It is well known that the role of an oxidizer is to form a passivation layer, which is necessary for removing the metal in the CMP processes whereas inhibitor play a very important role in corrosion inhibition as well as in controlling the removal rate.(SASTRI, 1998; Cao, Gu and Tian, 2002). The use of benzotriazole as a corrosion inhibitor for Cu and Co is notable.(Kondo *et al.*, 2000; S. Yang *et al.*, 2019; Wang *et al.*, 2020; Yin, Yang, Ma, *et al.*, 2020) Therefore, the removal rates of Cu and Co polishing using slurry comprising of 2 wt. %, NaOCl, 2 wt. % silica and 5mM BTA as inhibitor are further studied.

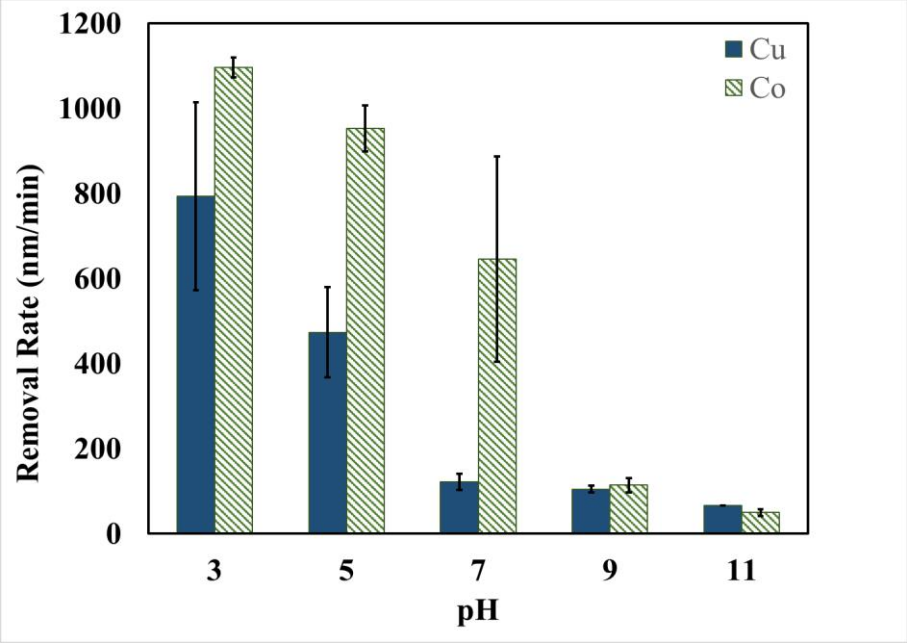

Figure 4.2. 3 Change in pH and its effect on Removal rate using NaOCl (0.5 wt. %) and fumed silica (2 wt. %)

Polish rate experiments in the presence of NaOCl, abrasives and corrosion inhibitor

The removal rates with respect to change in pH value (3,5,7,9 and 11) using 2 wt. % silica, 0.5 wt% NaOCl and 5 mM BTA is demonstrated in Figure 4.2.4. Only a slight decrease in the polish rate is observed with the addition of BTA for both the metals. The highest removal rate for Cu obtained is 787.4394 nm/min at pH 3 and the polish rate decreases with further increase in pH value. Similar trend is also observed for Co i.e. the removal rate decreases from 1042 nm/min to 44 nm/min when the pH value increases from 3 to 11. The desired selectivity of ~1:1.006 is achieved at pH 9. Similar results were obtained for Cu-Ru system as well.(Yadav, Jitendra C Bisen, *et al.*, 2017) However, for Ru, the polish rate increases and then decreases with an increase in pH value when NaOCl is used as an oxidizer.

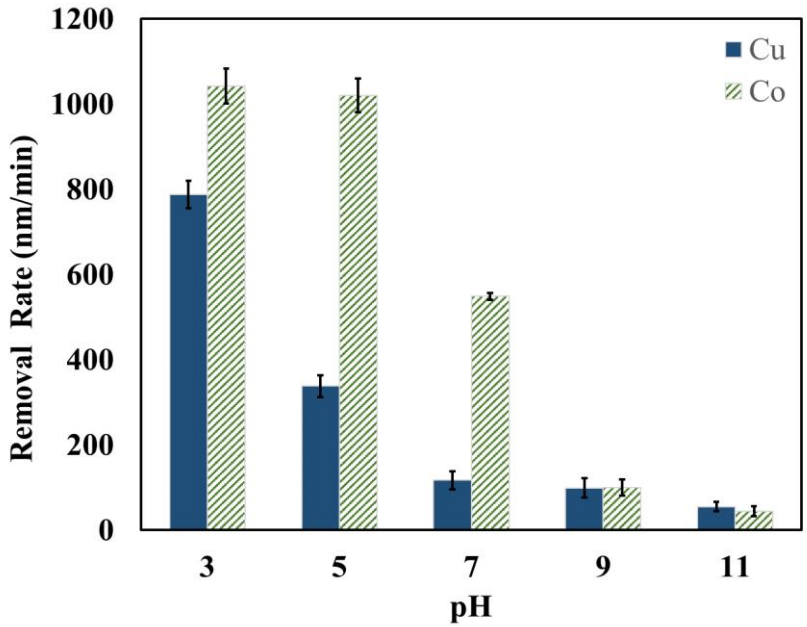

Figure 4.2. 4 Change in pH and its effect on removal rate of Cu and Co using silica (2 wt. %), NaOCl (0.5 wt. %) and BTA (5 mM)

The static etch rates of Cu and Co in the etchant solution containing 0.5 wt. % NaOCl along with 5mM BTA are presented in Figure 4.2.5. The etch rate of both the metals reduces with the addition of BTA. The combination of desired low etch rates (Cu ~ 0.9 nm/min, Co ~ 1.1 nm/min) and comparatively fair removal rates (Cu ~ 99.1 nm/min, Co ~ 99.7 nm/min) at pH 9 implies that the solution comprising of 2 wt. % fumed silica, 5 wt. % NaOCl and 5 mM BTA is apt for effective planarization. It is to be noted that all the polishing experiments were performed on Cu and Co coupons in the present study. However, in semiconductor industry, PVD Cu and CVD Co films are mainly employed as interconnect and barrier metals respectively. It was observed that metal film deposition technique on the given substrate strongly influences the polish rate of the metal. (Hsu *et al.*, 2014; R Popuri, Sagi, Alety, Peethala, Amanapu and Patlolla, 2017)Hence, further tuning of the slurry will be required to attain desired selectivity and to control the erosion and dishing issues, if PVD Cu and CVD Co films deposited on silicon /oxide substrate are used and the polish results obtained are quite different.

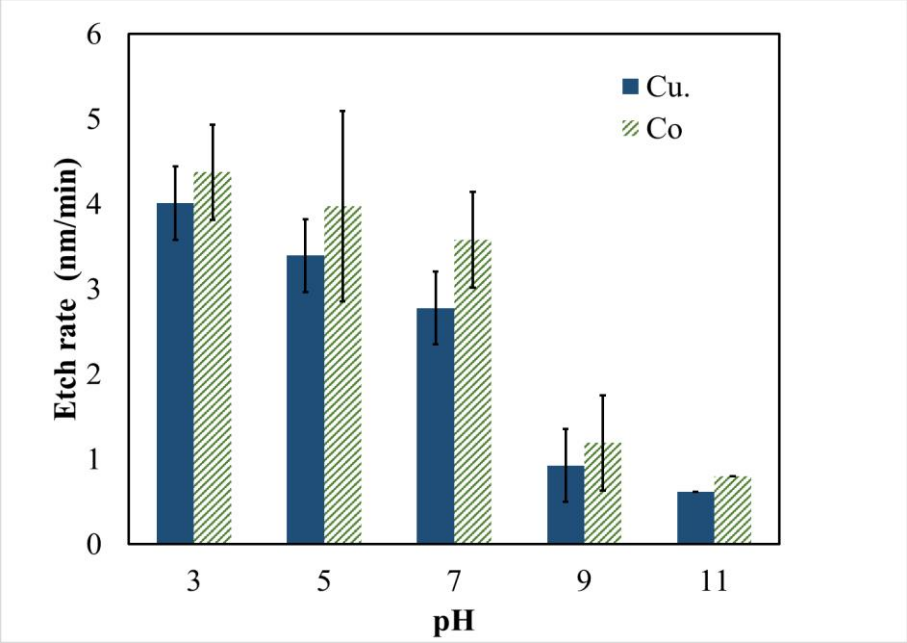

Figure 4.2. 5 Change in pH and its effect on etch rate using NaOCl (0.5 wt.%) along with inhibitor BTA (5mM)

The decreasing trend of Cu polish rate w.r.t pH is reported in literature when sodium hypochlorite, BTA and silica is used as oxidizer, inhibitor and abrasives respectively.(Yadav, Jitendra C Bisen, *et al.*, 2017) For Co as well, a similar decreasing trend of polish rate w.r.t pH is reported when H_2O_2, citric acid and silica is used as oxidizer, inhibitor and abrasives respectively.(R Popuri, Sagi, Alety, Peethala, Amanapu and Patlolla, 2017) The polishing behavior of Cu at various pH regimes is well documented in the literature(Nishizawa, Nojo and Isobe, 2010a; Peethala, Roy and Babu, 2011a; Yadav, Jitendra C Bisen, *et al.*, 2017) and hence not discussed here. Co in aqueous solution usually forms a native passive layer on its surface comprising of its oxide (CoO) or hydrated oxides (CoO. H_2O) which is an indigenous characteristic of most of the transition metals.(Badawy, F.M. Al-Kharafi and Al-Ajmi, 2000; Ismail and Badawy, 2000) When treated at acidic pH, this passivation layer of Co becomes very unstable and thus gets easily deliquesced which is illustrated in equation in equations 4.2.1 and 4.2.2.(Badawy, F.M. Al-Kharafi and Al-Ajmi, 2000; Ismail and Badawy, 2000; Aledresse, 2004; Jiang, He, Yan Li, *et al.*, 2014a)

$$Co + H_2O \rightarrow CoO + 2H^+ + 2e^- \rightarrow Co^{2+} + H_2O + 2e^- \quad [4.2.1]$$

$$Co + 2H_2O \rightarrow CoO.H_2O + 2H^+ + 2e^- \rightarrow Co^{2+} + 2H_2O + 2e^- \quad [4.2.2]$$

Besides, the bulk Co is exposed to the solution, which undergoes direct dissolution as shown in the following equation. This explains the reason for high removal rates of Co at acidic region pH 3 and 5.(Badawy, F.M. Al-Kharafi and Al-Ajmi, 2000)

$$Co + 2H^+ \rightarrow Co^{2+} + H_2 \quad [4.2.3]$$

The NaOCl exists as hypochlorous acid (HOCl) in the acidic regime. It accelerates the above oxidation reactions by undergoing the following reduction reaction.(Li *et al.*, 1999; Prasad and Ramanathan, 2007; Peethala, Roy and Babu, 2011a)

$$2HClO + 2H^+ + 2e^- \leftrightarrow Cl_2(g) + 2H_2O \quad [4.2.4]$$

Whereas at neutral and lower alkaline region Co(II) oxide/hydroxides are presume to form which is comparatively more stable than the passive layer formed at acidic pH. The series of equations involved at this pH range is illustrated from equations 4.2.5 to 4.2.7.(Gayer and Garrett, 1949; Badawy, F.M. Al-Kharafi and Al-Ajmi, 2000; Ismail and Badawy, 2000)

$$Co + H_2O \rightarrow Co(H_2O)(ads) \quad [4.2.5]$$

$$Co(H_2O)(ads) \rightarrow Co(OH)^+ + H^+ + 2e^- \quad [4.2.6]$$

$$Co(OH)^+ + H_2O \rightarrow Co(OH)_2 + H^+ \quad [4.2.7]$$

At higher alkaline region, a more stable and dense passivation layer seem to form, which explains the reason behind comparatively lower removal rates than acidic region. The compounds that are most likely assumed to form at this region are Co (II) hydroxides, which further oxidized to form Co (III) oxides comprising of mostly Co_3O_4 and CoOOH. The probablaction involved here are descr in the following equations 4.2.8 and 4.2.9.(Jiang, He,

Yan Li, *et al.*, 2014a; Park, Paluvai and Venkatesh, 2018)(Jiang, He, Yan Li, *et al.*, 2014a; Park, Paluvai and Venkatesh, 2018)

$$Co(OH)_2 + OH^- \rightarrow CoOOH + H_2O + 2e^- \quad [4.2.8]$$

$$3Co(OH)_2 + 2OH^- \rightarrow Co_3O_4 + 4H_2O + 2e^- \quad [4.2.9]$$

The corresponding reduction reaction in the alkaline region is given below(Li *et al.*, 1999; Prasad and Ramanathan, 2007; Peethala, Roy and Babu, 2011a)

$$ClO^- + H_2O + 2e^- \rightarrow Cl^- + 2OH^- \quad [4.2.10]$$

Co being a metal with lower equilibrium potential as compared to Cu undergoes galvanic corrosion when in contact with it. Owing to this fact, controlling the galvanic corrosion is a major concern for slurry formulation. Although, electrochemical experiments were performed on Cu and Co ingot metal using this optimized slurry, the results obtained are not promising. Since, the corrosion of Co is strongly influenced by the type of film used in experiments, further optimization of the slurry needs to be carried out with CVD Co metal film for addressing the galvanic corrosion issues.

Effect of process parameters on selectivity

Cu and Co CMP with a slurry comprising of 2 wt. % fumed silica, 0.5 wt. % sodium hypochlorite and 5 mM BTA at optimized pH 9 were performed at different turntable speeds and pressure. The impact of turntable speed (50, 100, 150 and 200 rpm) at applied pressure 5.72 psi on selectivity is shown in Figure 4.2.6. On the other side, Figure 4.2.7 displays the effect of pressure (1.41, 2.86, 5.72 and 8.91 psi) on selectivity at a turntable speed of 100 rpm. It is evident from the results that the lowest selectivity is observed at the turntable speed of 50 rpm and at a pressure of 1.41 psi while at other process parameter values, the selectivity does not change significantly and the value remains close to 1:1. Thus, the results are clearly

indicating a robust performance of slurry as insignificant perturbations in the process conditions do not seem to impact much on the selectivity of Cu and Co.

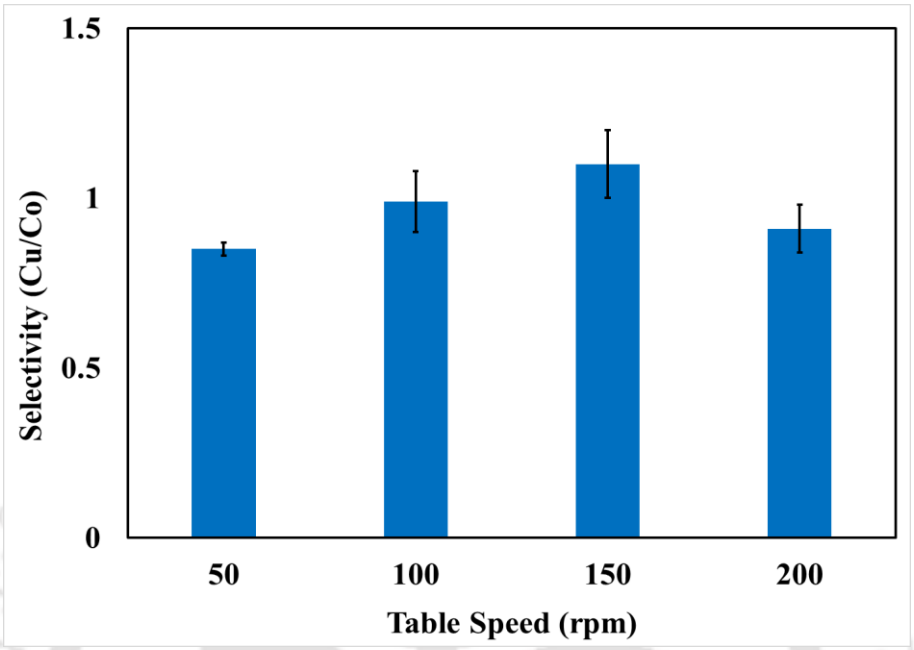

Figure 4.2. 6 Varying table speed and its effect on selectivity using silica (2 wt. %), NaOCl (0.5 wt. %,) BTA (5 mM) at pH 9

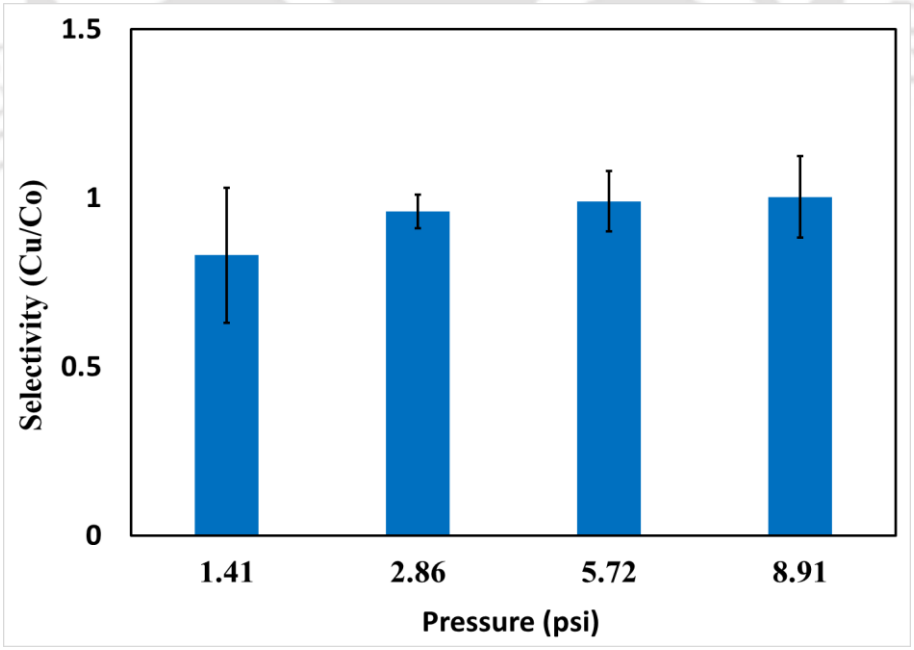

Figure 4.2. 7 Varying pressure and its effect on selectivity using silica (2 wt. %), NaOCl (0.5 wt. %), BTA (5 mM) at pH 9

Effect of various inhibitors on selectivity at optimized conditions

Besides BTA, various inhibitors such as uric acid(Prasad and Ramanathan, 2007) and ascorbic acid(Prasad and Ramanathan, 2007) has been suggested for chemical mechanical polishing. Thus, the effect of these inhibitors on selectivity was also investigated at optimized conditions: pH 9, 100 rpm turntable speed and 5.72 psi pressure and the outcomes are presented in Figure 4.2.8. The experiments were conducted with the slurry that comprises 2 wt. % silica, 0.5 wt. % NaOCl and 5 mM of inhibitor. Selectivity of Cu-Co using L-Ascorbic acid is 1: 1.16, whereas for Uric Acid is 1: 1.14 and that while using BTA is 1: 1.006. Although the polish rate of Co is higher as compared to Cu with all these inhibitors, still BTA gives the nearest desired selectivity of 1:1. Thus, BTA is the most preferable inhibitor for NaOCl based slurry.

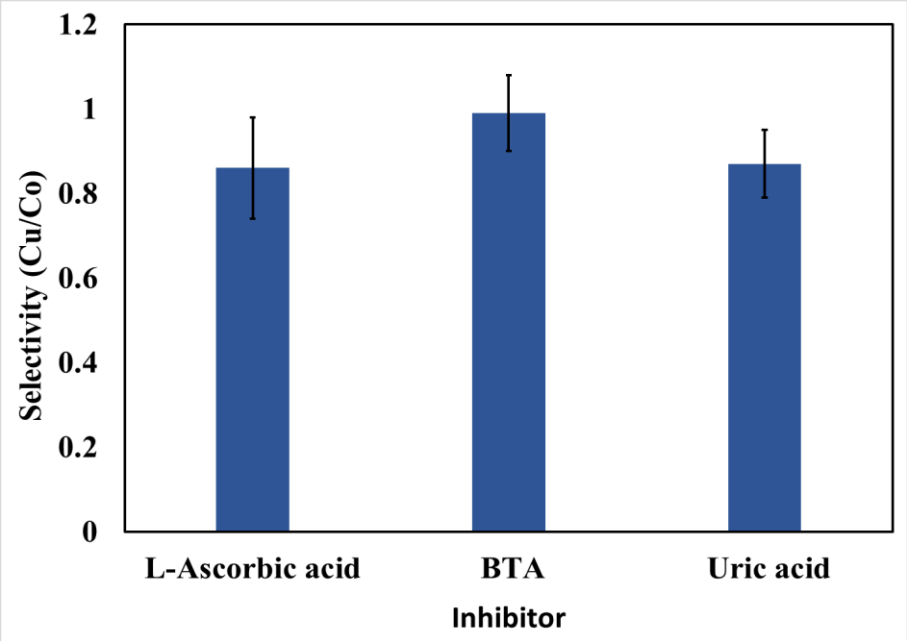

Figure 4.2. 8 The effect of different inhibitors on selectivity using NaOCl (0.5 wt. %), fumed silica (2 wt. %) and inhibitor (5mM) at 100 rpm table speed and pH 9

X-ray diffraction analysis

XRD analysis on Co surface prior to etching and post etching with 0.5 wt. % NaOCl and 5 mM BTA at pH 5 and pH 9 was performed and the results obtained are displayed in Figure 4.2.9.

XRD analysis (Bragg Brentano geometry) on Co surface prior to etching and post etching with 0.5 wt. % NaOCl and 5 mM BTA at pH 5 and pH 9 was performed and the results obtained are displayed in Figure 4.2.9. Here, Cu Kα (grit wavelength= 1.5406 Å) was selected as the X-ray source. Indexing of the peaks are done using JCPDS (Joint Committee for Powder Diffraction Standards) software. The diffraction peaks at 41.6º, 44.4º, 47.4º and 75.72º corresponding to miller indices of (100), (002), (101) and (101) were observed for Co surface prior to etching. No additional peaks were observed for the Co surface etched at pH 5. For Co coupon etched at pH 9, an extra peak at 62.8º that corresponds to $Co(OH)_2$ is observed. Ever, the intensity of the peak is not significant which indicates that the formation and removal of oxides are more dynamic in nature.

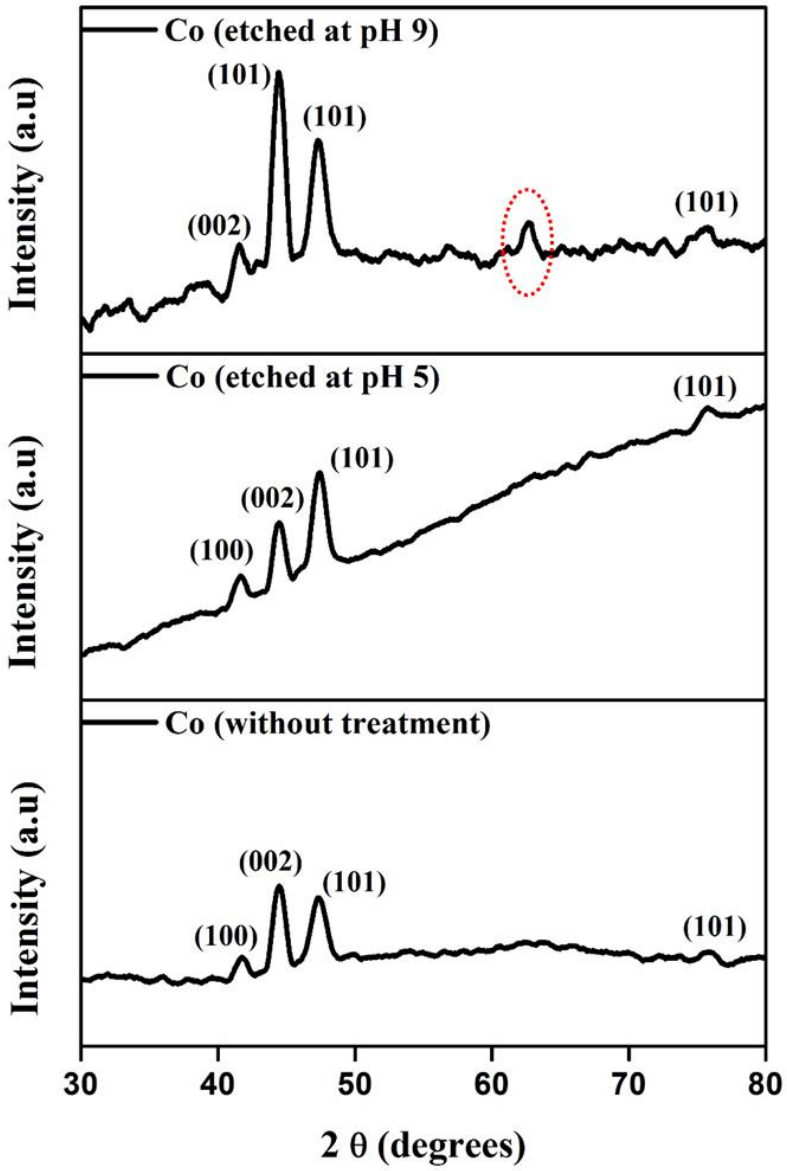

Figure 4.2. 9 XRD pattern of Co prior and post etching using NaOCl (0.5 wt.%) along with inhibitor BTA (5mM) at pH 5 and pH 9

4.2.4 CONCLUSION

Chemical Mechanical Planarization of Copper and Cobalt using NaOCl, fumed silica, and BTA is studied in the work. A slight decrease in polish rate is observed with an addition of BTA along with NaOCl and silica as compared to the slurry containing only silica and NaOCl. This

slurry gives a selectivity of ~1:1.006 at pH 9 which is desired for interconnect and barrier metals to be used in semiconductor industry. The decrease in removal and etch rates from neutral to highly alkaline regions is observed for all the experiments performed using NaOCl based slurries. This indicates a formation of stable passive layer on both the metal surfaces in the alkaline regime resulting in less dissolution of the metal as compared to that of acidic regime. Co(II) oxide/hydroxides ($Co(OH)_2$) are formed at neutral and lower alkaline region. The effect of varying turntable speed and down force pressure does not have any prominent impact on selectivity obtained with formulated slurry at optimized conditions.

4.3 Controlling Galvanic Corrosion with Oxalic acid and Imidazole for Chemical Mechanical Planarization of Cobalt-Copper Interface

4.3.1 Motivation

The shrinkage of ultra large scale integrated (ULSI) circuits to sub-10nm nodes result in numerous challenges during fabrication of Copper (Cu) damascene interconnects. These mainly consist of increasing resistivity, inadequate gap filling, thickness reduction, resistance-capacitance signal delay and pinched-off opening caused by Ta/TaN barrier structure.(Wang *et al.*, 2014b; Li *et al.*, 2016; R Popuri, Sagi, Alety, Peethala, Amanapu and Patlolla, 2017; Zhang *et al.*, 2017) Recently cobalt (Co) has come up as a promising barrier or capping material with the feasibility of direct deposition of Cu without the need of any seed layer.(Roule *et al.*, 2007; Kadam, Yerramilli and Bahadur, 2009; Lu, Wang, *et al.*, 2012; Jiang, He, Yan Li, *et al.*, 2014b; Zhong *et al.*, 2014) Even at smaller dimensions, cobalt has a lower resistivity of ~6.2 μΩ cm. It also provides a good step coverage, higher thermal stability, good Cu line adhesion and is chemically inert.(Peethala *et al.*, 2012; Jiang, He, Yan Li, *et al.*, 2014b; Li *et al.*, 2016; S. Yang *et al.*, 2019)

During fabrication of semiconductors, post electrodeposition of Cu interconnect and Co barrier, a planar surface is required for further level metallization for which the Chemical mechanical polishing (CMP) method is opted. However, for proper execution of Co/Cu CMP, a polishing slurry is required that would reduce Cu and Co galvanic corrosion along with providing a near ~ 1:1 Co/Cu removal rate (RR) selectivity. The standard equilibrium potential (E°) of Co/Co^{2+} (-0.28/SHE) is less than Cu/Cu^{2+}(+0.34V/SHE) and this difference of ~0.61 V results in galvanic corrosion(Peethala *et al.*, 2012; Li *et al.*, 2016; Fu *et al.*, 2018; S. Yang *et al.*, 2019), unless the potential gap is maintained to be less than 20 mV.(Peethala *et al.*, 2012; Li *et al.*, 2016; Fu *et al.*, 2018; S. Yang *et al.*, 2019) Else, during the CMP process voids are formed due to the dissolution of Co (acts as anode) which subsequently leads to Cu diffusion in dielectric

layer resulting in device failure.(Li *et al.*, 2016) According to literature, usually alkaline slurries are preferable for Co CMP as they form a passive oxide on the Co surface.(Nishizawa, Nojo and Isobe, 2010b; Yao *et al.*, 2018). It is to be mentioned that a formulated slurry should also be capable enough to provide lower dissolution and high removal rate (>100 nm/min) with Co/Cu selectivity ~1:1 to avoid copper dishing.(Shi, Schlueter and O'Neill, 2016; R Popuri, Sagi, Alety, Peethala, Amanapu and Patlolla, 2017) Along with the other components in a slurry, the polishing pad plays a crucial role in the CMP performance.(Bajaj *et al.*, 2019) Stavreva et.al(Stavreva *et al.*, 1997) suggested the use of IC 1000/SUBA IV pad over IC 1000 pad as the addition of SUBA IV layer to IC 1000 gave both good uniformity and higher removal rates.(Stavreva *et al.*, 1997) Besides, the removal rate and uniformity of the polished metal are also strongly influenced by conditioning of the pad.(Khanna, Kakireddy, *et al.*, 2020; Khanna, Yamamura, *et al.*, 2020)

There are various types of components present in a CMP slurry – abrasives, oxidizers, complexing agents, inhibitors etc.(Ein-eli and Starosvetsky, 2007) Among which the role of complexing agent to improve the removal rates of the metals is well known.(Venkata R K Gorantla *et al.*, 2005; Peethala *et al.*, 2012; R Popuri, Sagi, Alety, Peethala, Amanapu, Patlolla, *et al.*, 2017; Yao *et al.*, 2018) Using acetic acid as complexing agent, a good material removal rate along with reduced root mean square roughness is observed.(Zuo *et al.*, no date) Some other complexing agents which gave promising removal rates and lower dissolution rates are potassium tartrate(Hu *et al.*, 2021), Diethylenetriamine Pentaacetate Pentapotassium(Liu *et al.*, 2019),citric acid(Peethala *et al.*, 2012) etc.

The role of an inhibitor in a CMP slurry is noteworthy.(Nishizawa, Nojo and Isobe, 2010b; Peethala *et al.*, 2012; Ryu *et al.*, 2020; Xu *et al.*, 2021) Xu et.al(Xu *et al.*, 2021) reported that addition of diethanolamine as an inhibitor reduced the Co surface scratches in an ammonium sulfate and H_2O_2 based slurry.

Popuri et.al(R. Popuri *et al.*, 2017) studied the effect of potassium oleate (PO) as a corrosion inhibitor for Co CVD films at a neutral pH for both bulk removal (Step 1 of damascene process) and barrier removal/interconnect removal (step 2 of damascene process) processes in an H_2O_2 and citric acid based slurry. It was found that PO act as an effective inhibitor for Co-Ti/ Ti-TiN couple by reducing the galvanic corrosion current to very low values (0.1 $\mu A/cm^2$) and also giving better post CMP surface quality.(R. Popuri *et al.*, 2017) Also, it was seen that addition of PO further reduced the galvanic corrosion current to 0.04 $\mu A/cm^2$ (E_{corr} ~7 mV) for Co-TiN couple along with negligible dissolution and much better post CMP surface quality in an ammonium persulfate based slurry.(Ranaweera *et al.*, 2019) Hu et.al.(Hu, Pan, Xu, *et al.*, 2020b) found that inhibitor MBTA along with H_2O_2 and hydroxyethylidene diphosphonic acid in an alkaline based solution acted as a good candidate for Co/Cu planarization and gave a comparatively good selectivity. It was found that BTA gave better inhibition as compared to TAZ for Co surface.(Yin, Yang, Niu, *et al.*, 2020) BTA forms Co-BTA complex on both the metallic and oxide Co, thus enhancing the inhibition property of BTA.

With the aim to diminish the galvanic corrosion between Co and Cu, Yang et al.(S. Yang *et al.*, 2019) reported that solution of 0.1 wt.% H_2O_2 + 200 ppm benzotriazole + 100 ppm PMP (1-phenyl-3-methyl-5-pyrazolone) at pH 10 reduced the potential difference from ~250 to ~5 mV of Co and Cu disk. Fu et al.(Fu *et al.*, 2018) formulated a slurry consisting of 345 ppm 1,2,4-triazole and 0.05 wt.% FA/O chelating agent in 0.1 vol% H_2O_2 + 0.5 wt.% colloidal silica to reduce the corrosion potential to 1 mV and current density to 0.02 nA/cm^2 providing Co/Cu selectivity of 1.32:1. Li et al.(Li *et al.*, 2016) proposed that slurry consisting of 5 wt.% silica + 1ml/L H_2O_2 + 30 ml/L AEO (fatty alcohol polyoxyethylene) + 5 ml/L FA/O at pH < 8 decreases the potential difference from ~300 mV to 20 mV between Co and Cu coupons. Peethala et al.(Peethala *et al.*, 2012) proposed a slurry consisting of 3 wt.% colloidal silica + 1 wt.% H_2O_2 along with 0.5 wt.% arginine and 5 mM benzotriazole at pH 10 to reduce the open circuit

potential to ~10 mV and Cu/Co RR selectivity ratio to ~0.8:1. Hu et.al(Hu, Pan, Li, *et al.*, 2020) claimed that use of potassium tartrate as complexing agent and TT-LYK as inhibitor in an alkaline based H_2O_2 slurry gave a reduced galvanic corrosion and desired selectivity along with minimized post CMP issues for a Cu/Co/TaN system. From the studies done till date, it was observed that Co is more prone to corrosion owing to the fact of having lower reduction potential than Cu.(Wang *et al.*, 2014b; Park, Paluvai and Venkatesh, 2018) Hence, the selected slurry should be capable enough to passivate the surface as well as inhibit galvanic corrosion. Although a few slurry formulations have been proposed for Co / Cu system, most of them were either oriented towards selectivity or towards reducing galvanic corrosion. Studies referring to obtain desired selectivity of ~1:1 for Co/Cu along with reduced galvanic corrosion and high polish rate: static etch ratio are limited in the literature.

Therefore, in this objective, we have focused on formulating a silica-based polishing slurry to attain Co/Cu RR selectivity ratio of 1:1 (with good removal rates and lower etch rates) and to reduce the corrosion potential gap of a Co-Cu galvanic couple. The experiments were performed at different pH values. However, based on the polishing and the electrochemical results obtained during screening (using 0.1wt.% H_2O_2 solution), pH 9 was considered as the optimal pH for further investigation. Thus, we studied the role of different components of the slurry on removal of Cu and Co at pH 9. Oxalic acid as complexing agent along with hydrogen peroxide (H_2O_2), and imidazole (azole) are the different components used. The electrochemical measurements of the proposed solution were performed for investigating Co-Cu galvanic corrosion reduction at pH 9. It is to be noted that although various complexing agents (guanidine carbonate, L-arginine, glycine and oxalic acid) and inhibitors (uric acid, BTA, L-ascorbic and imidazole) have been tried (the results are not shown here), oxalic acid as complexing agent and imidazole as inhibitor were suggested amongst other combinations based on the polishing performance and corrosion potential gap (ΔE_{corr}) values.

4.3.2 Experimental Conditions

Electrochemical experiments

Electrochemical experiments were carried on a Gamry-1010 electrochemical workstation using a three-electrode glass cell (500 ml volume). Ag/AgCl (3M KCl) electrode and platinum wire were used as reference and counter electrode respectively. Cobalt (99.95% pure, 9 mm diameter) and copper (99.98% pure, 7 mm diameter) were used as working electrodes for performing the electrochemical experiments. As per ASTM E 3 (Standard Guide for Preparation of Metallographic Specimens) the working electrodes were wet polished initially with 1µm micro polish alumina paste followed by 0.3µm micro polish alumina paste (Buehler, USA) prior to each electrochemical run. The polishing was done in a specific pattern until visibly clear blazing surface is acquired. The electrodes were then cleaned thoroughly and sonicated for 1 min in DI water. The scanning range for open circuit potential versus time curves was set to -1 V to 1 V for 600 sec. For generating potentiodynamic polarization (Tafel) curves the scanning rate was 1 mV/s OCP in the range of E_{OC} ±250 mV. The pH of the solutions was tuned either using nitric acid or potassium hydroxide. The corrosion current density (I_{corr}) and corrosion potential (E_{corr}) were ascertained by using the system inbuilt software (Gamry Instrument). The pH of the solution was set at pH 9 for all experiments unless mentioned otherwise.

Static etch rate experiments

Static etch rate (SER) of Cu and Co were conducted using 99.95% pure cobalt (9 mm diameter and 1 mm thick) and 99.98% pure copper (7 mm diameter and 2 mm thick) bulk metal coupons. As per ASTM E 3 (Standard Guide for Preparation of Metallographic Specimens) and ASTM E407 (Standard Practice for Micro etching Metals and Alloys) methodology, a water-resistant emery paper of 600 grit size was used to polish Cu and Co coupons before every set of

experiment. Each pre-weighted coupon was immersed for 30 min of time in the etchant solution, followed by thorough washing with Millipore water and air dried before weighing again. The weight loss was determined using gravimetric analysis and the average value of three sets of experiments are taken as the reported results.

Polishing Experiments

CMP experiments were conducted on bench top Labopol-20/ Laboforce- 50 polisher (Struers, Denmark). All the polishing experiments were conducted at 100 rpm turntable speed and with a down pressure of 5.72 psi. For polishing experiments non-woven Texmet C, PSA pad (Buehler) with 8" diameter was used. Bulk Cobalt (25 mm dia.) and copper (25.4 mm dia.) metal coupons with 99.95% and 99.98% purity respectively were used for the polishing experiments. It is to be noted that all the metals discs were acquired from Tecnisco Advance Materials Pvt. Ltd, Singapore. Prior to each polishing run, conditioning of the polishing pad was done in order to eliminate the residue formation on the pad. For conditioning the polishing pad, a traditional method of manual conditioning using emery sheet of a fixed grit size (600) was opted. Similar conditioning of polishing pad using emery sheet of fixed grit size is reported in literature.(Li and Babu, 2001; Manivannan and Ramanathan, 2009) Cab-o- Sil, M-5P, fumed silica (Cabot- Sanmar, India) was used as abrasives. Imidazole (Himedia India), oxalic acid (Himedia, India) and H_2O_2 (Loba Chemie Private Limited, India) were used as inhibitor, complexing agent and oxidizer respectively. The pH of the slurry was tuned either by using potassium hydroxide (Himedia, India), or nitric acid (Himedia, India). The slurry was transported to the polishing machine through Miclins (Model PP- EX 20) peristaltic pump that had a maintained flowrate of 100 ml/min. Dummy runs comprising of 1 wt. % silica was performed prior to actual runs for every new pad used. There runs were carried out in order to get a stable and consistent result. The weight loss was studied gravimetrically using Sartorius balance with readability 0.0001 g and the removal rate was calculated. The coupons were

cleaned with Millipore water and air dried before weighing each time. Polishing experiments were repeated thrice and the average removal rate (RR) value is reported with standard deviation.

Material Characterization

For determining the compounds of Co and Cu formed at various chemical treatments, a Fourier Transform Infrared Spectroscopy (FTIR) was performed by scanning the metal coupons in the wavenumber range of 4000-400 cm^{-1} on Spectrum series (Perkin Elmer, USA) unit. The analysis of FTIR on these treated metal coupons were done using an ATR accessory with a diamond crystal. The compounds were confirmed by determining the functional groups of the same. Ultra Violet Visible Spectrophotometer (UV Vis) (Perkin Elmer, USA) was performed to second the formation of the compounds. The peaks and the valleys of UV absorption spectra reported in the manuscript are identified by the inbuilt software, UV WinLab. Prior to analysis the coupons were treated in various aqueous solutions at pH 9 : (i) DI water (ii) 0.1wt.% H_2O_2 (iii) 0.1wt.% H_2O_2 + 0.02 M oxalic acid and (iv) 0.1wt.% H_2O_2 + 0.02 M oxalic acid + 5 ppm imidazole. The metal treated in DI at pH 9 is taken as reference.

4.3.3 Results and discussion

In terms of reactivity, Cu is considered more noble than Co metal. Therefore, in a Co-Cu galvanic couple, Co will acts as an anode whereas Cu will act as a cathode.(Bilouk *et al.*, 2009b; Shimizu, Sakoda and Shimogaki, 2013) The schematic of the galvanic corrosion between Cu and Co is shown in Figure.4.3.1 whereas the potentiodynamic polarization plot of Co and Cu in the DI water at pH 9 is displayed in Fig.4.3.2. A potential difference of ~279 mV between Co and Cu at pH 9 ensures the occurrence of galvanic corrosion. Thus, it is required to minimize the potential difference (driving force) to control galvanic corrosion between Co and Cu.

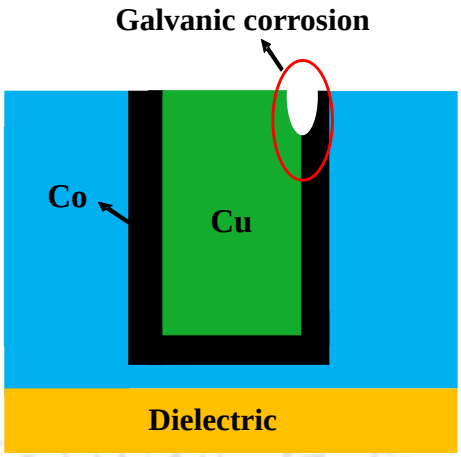

Figure 4.3. 1 Diagrammatic representation of galvanic corrosion between copper and cobalt.(Zhang et al., 2017)

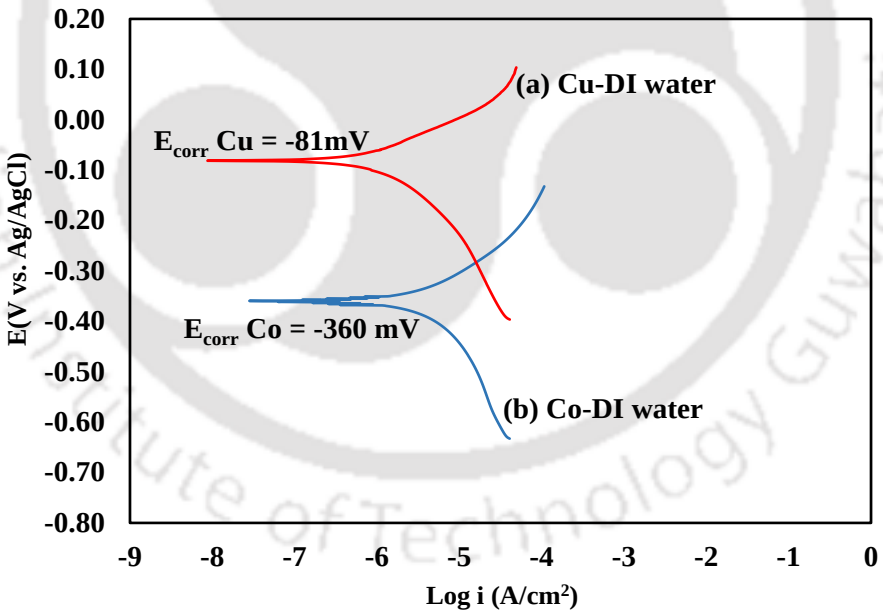

Figure 4.3. 2 The potentiodynamic polarization curves of DI water for Co and Cu at pH 9.

Effect of H_2O_2 on the SER, RR and electrochemical properties of Co and Cu:

Static etch rates (SER) of Co and Cu as a function of pH (3,5,7,9 and 11) in 0.1 wt.% H_2O_2 solution is displayed in Figure.4.3.3. A decreasing trend of SER with respect to pH is observed for both Co and Cu. For Co, SER of ~9 nm/min at pH 3 is decreased to ~1 nm/min at pH 11 whereas for Cu SER of ~14 nm/min at pH 3 is decreased to ~3 nm/min at pH 11. The reduced values of SER in alkaline region with respect to the low pH values is attributed to the generation of passivation film on the Co and Cu metal surfaces.(Peethala *et al.*, 2012) This film prevents the dissolution of metal in alkaline region.

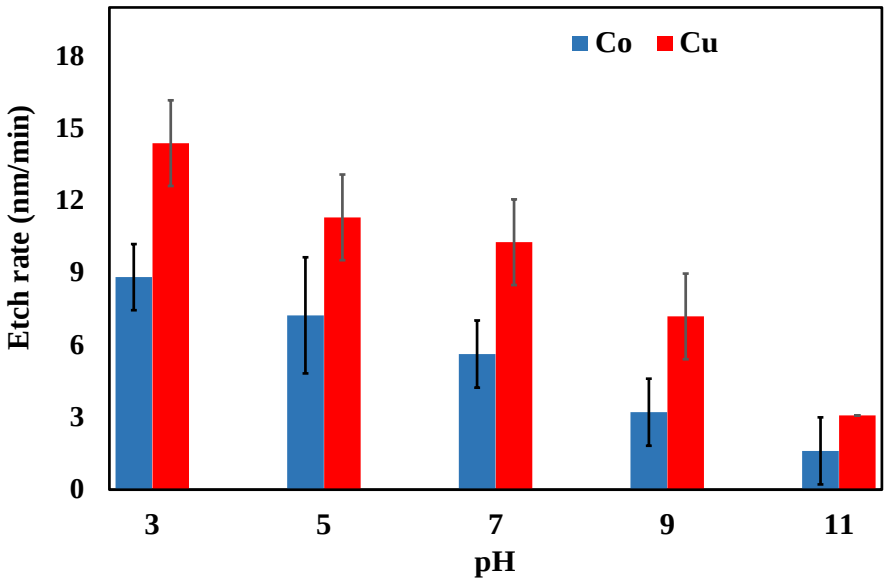

Figure 4.3. 3 Etch rate of Co and Cu in 0.1wt.% H_2O_2 at varying pH.

The passivation film formation is mainly based on the electrode potential and pH of the solution. The native passivating oxide formed on the surface of Co is CoO and $CoO.H_2O$.(Jiang, He, Yan Li, *et al.*, 2014b) However, in the acidic solution, the native passivating film becomes unstable and dissolves as shown in reaction (1). The etching of the unstable native passivating film at acidic medium results in exposure of the bulk Co and thus causing higher dissolution of the metal. Therefore, higher removal rate is observed at the acidic

medium which is illustrated in reaction (2). Also, Mohs' hardness of silica (6-7 Mohs') is more than Co (5.0 Mohs'). Therefore, while polishing in acidic medium, after subsequent dissolution of native passivating film, fumed silica (SiO_2) easily abrades the exposed bulk Co. In neutral (pH=7) and alkaline region (7 > pH < 10), a passivating stable film of $Co(OH)_2$ is formed on the Co surface as shown in reaction (3). Due to the presence of more dissolved oxygen, the passivation layer of Co (III) oxide (Co_3H_4 and $CoOOH$) is dominant in alkaline region on the Co surface which is illustrated in reactions (4.3.4-4.3.6).(Badawy, F M Al-Kharafi and Al-Ajmi, 2000; Lu, Wang, *et al.*, 2012; Lu, Zeng, *et al.*, 2012; Peethala *et al.*, 2012; Jiang, He, Yan Li, *et al.*, 2014b; Fu *et al.*, 2018; Hazarika and Rajaraman, 2020) For this reason, alkaline medium is usually preferred for Co polishing.

Likewise, Cu in alkaline solution forms passivating layers of CuO, Cu_2O or $Cu(OH)_2$, as shown in reactions (7-10).(Zhang *et al.*, 2017; Fu *et al.*, 2018) The presence of the mentioned passivating layers on Co and Cu surface in alkaline region can be seconded from the Pourbaix diagram.(Tamilmani *et al.*, 2002; Ichige *et al.*, 2015) H_2O_2 as an oxidizer assists in the generation of hydroxyl radicals (OH^-) as shown in equation (4.3.11) and accelerates the reactions (4.3.5-4.3.10).

The Co and Cu passivation observed at different pH regions are given by the following reactions:

Co reactions

At acidic medium

$$CoO(or CoO.H_2O) + 2H^+ \rightarrow Co^{2+} + H_2O(or 2H_2O) \quad [4.3.1]$$

$$Co + 2H^+ \rightarrow Co^{2+} + H_2 \quad [4.3.2]$$

At neutral/weakly alkaline medium

$$Co(OH)^{+} + OH^{-} \rightarrow Co(OH)_2 \quad [4.3.3]$$

At higher alkaline medium

$$O_2 + 2H_2O + 4e^{-} \leftrightarrow 4OH^{-} \quad [4.3.4]$$

$$3Co(OH)_2 + 2OH^{-} \leftrightarrow Co_3O_4 + 4H_2O + 2e^{-} \quad [4.3.5]$$

$$Co(OH)_2 + OH^{-} \leftrightarrow CoOOH + H_2O + e^{-} \quad [4.3.6]$$

Cu reactions

At alkaline medium

$$Cu + OH^{-} \rightarrow CuOH + e^{-} \quad [4.3.7]$$

$$CuOH + OH^{-} \rightarrow CuO + H_2O + 2e- \quad [4.3.8$$

$$Cu + 2OH^{-} \rightarrow Cu(OH)_2 + 2e- \quad [4.3.9]$$

$$Cu(OH)_2 \rightleftarrows Cu^{2+} + 2OH^{-} \quad [4.3.10]$$

Reduction reactions

$$H_2O_2 + 2e^{-} \leftrightarrow 2OH^{-} \quad [4.3.11]$$

$$4H^{+} + O_2 + 4e^{-} \rightarrow 2H_2O \quad [4.3.12]$$

The potentiodynamic polarization plot of Co and Cu in 0.1wt.% H_2O_2 is shown in Figure.4.3.4. It was observed that adding 0.1wt.% H_2O_2 in DI water reduces the corrosion potential gap (ΔE_{corr}) of Co and Cu to ~49 mV from ~279 mV at pH 9. According to literature,(Peethala *et al.*, 2012) small amount of H_2O_2 efficiently inhibits corrosion of Co-Cu couple. However, a high concentration of H_2O_2 at high pH is usually avoided as it affects the slurry stability.(Peethala *et al.*, 2012) The observed reduction in corrosion potential obtained from

Figure.4.3.4 after addition of H_2O_2 is attributed to the self-passivation of Co and Cu surfaces due to the generation of metal oxides by the hydroxyl radicals. The passivation film formed on Co and Cu surface in 0.1wt.% H_2O_2 solution at pH 9 are mainly insoluble Co_3H_4, CoOOH and CuO, $Cu(OH)_2$ metal oxides, respectively.(Lu, Wang, *et al.*, 2012; Peethala *et al.*, 2012; Jiang, He, Yan Li, *et al.*, 2014b; Zhang *et al.*, 2017; Fu *et al.*, 2018) A similar decrease in potential difference using hydrogen peroxide at pH 10 was reported earlier for Co and Cu.(Peethala *et al.*, 2012)

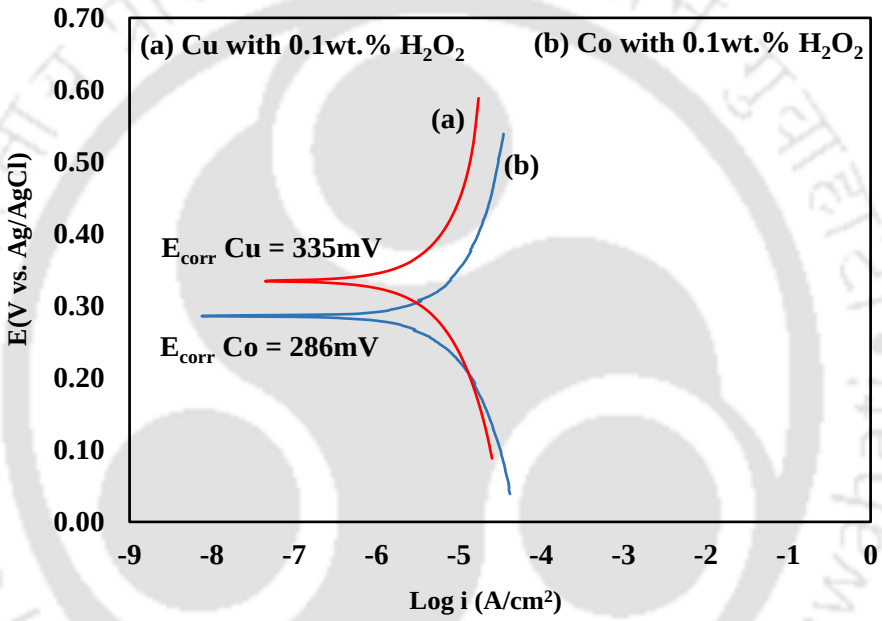

Figure 4.3. 4 The potentiodynamic polarization curves of Co and Cu at pH 9 in 0.1wt.% H_2O_2.

Further to get more insight on Co and Cu passivation, FTIR and UV spectra analysis for Co and Cu compounds were performed. The FTIR spectra were acquired in the range of 4000-400 cm^{-1} and are illustrated in Figure 4.3.5 (i) and (ii) respectively. The FTIR spectra of DI treated Co and Cu are taken as reference. For Co compounds formed on treatment of pure Co in H_2O_2, the peak observed at 3342 cm^{-1} correlates to the stretching of hydrogen bonded O-H group.(Xie

et al., 2010; Zhang *et al.*, 2012; Onwudiwe, Ravele and Elemike, 2020) Whereas, the band at 2924 cm^{-1} occurs anticipates to the O-OH bond that is in interaction with the atoms of Co.(Zhang *et al.*, 2012) The other peaks at 1615 cm^{-1} corresponds to the Co–O double bond in CoOOH compounds (Zhang *et al.*, 2012) and 2033 cm^{-1} and 1363 cm^{-1} bands corresponds to hydroxide (O-H) group stretching and bending of water molecules.(Xu and Zeng, 2003) The peaks ascribed at 1469 cm^{-1}, 1035 cm^{-1}, 839 cm^{-1} and 714 cm^{-1} are identified as vibrational stretching of $\upsilon(OCO_2)$, $\upsilon(C= O)$, $\delta(CO_3)$ and $\delta(OCO)$ respectively.(Xie *et al.*, 2010) Whereas the bond at 592 cm^{-1} are assigned to classic stretching of Co-O in Co_3O_4 compounds.(Guan *et al.*, 2003)

From FTIR spectra of Cu products on treatment with H_2O_2, it was seen that at 3796 cm^{-1} and 3644 cm^{-1}, free and hydrogen bonded O-H are observed.(Awwad and Albiss, 2015) The peak at 1356 cm^{-1} and 1140 cm^{-1} depict the stretching and vibrational Cu-OH in $Cu(OH)_2$.(Awwad and Albiss, 2015; Devamani, R Hepzi Pramila Alagar, 2017) Whereas, the bands at 614 cm^{-1} and 480 cm^{-1} attributes to presence of CuO compounds (Cu-O stretching and vibrational mode).(Jadhav *et al.*, 2011)

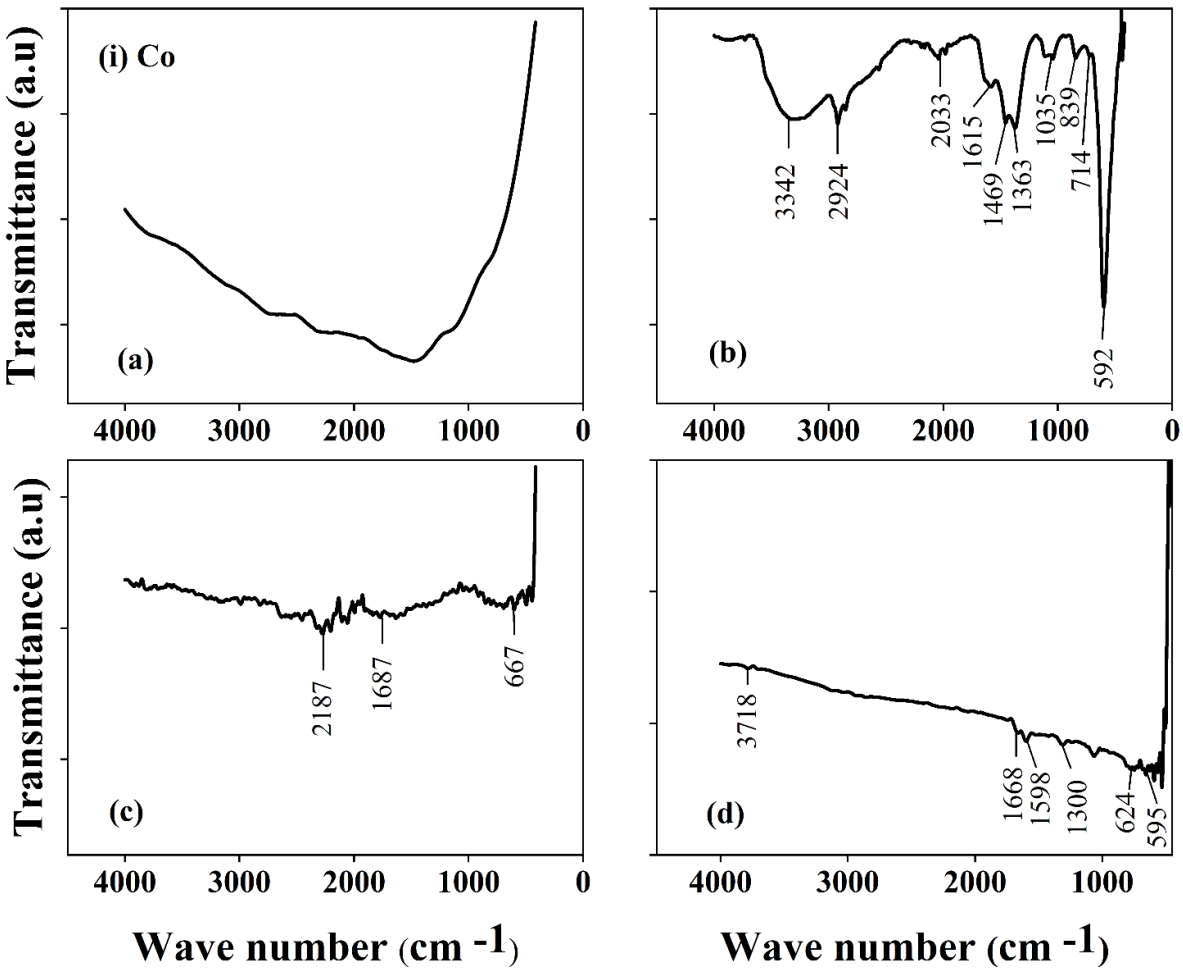

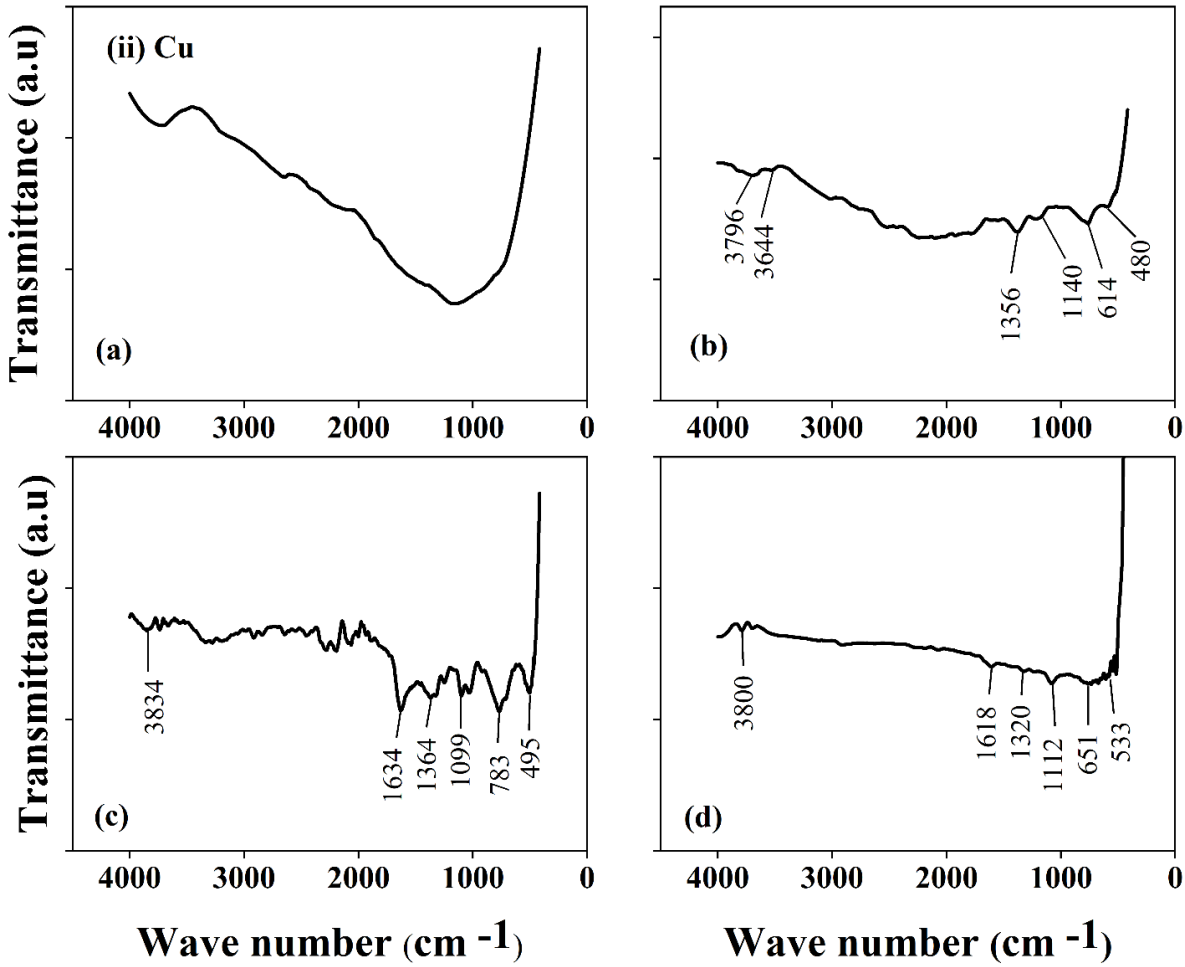

Figure 4.3. 5 FTIR spectra of (i) Co and (ii) Cu treated at pH 9 in (a) DI water (b) 0.1wt.% H_2O_2 (c) 0.1wt.% H_2O_2 + 0.02M oxalic acid and (d) 0.1wt.% H_2O_2 + 0.02M oxalic acid + 5ppm imidazole solution.

The UV spectrum were scanned in the range 200 to 800 nm and displayed in Figure 4.3.6 (i) and (ii). For H_2O_2 treated Co, an absorption valley and a peak band at 238 nm and 398 nm respectively are observed attributing the presence of CoOOH compounds.(Liu *et al.*, 2018) Also, typical absorption valleys and peaks at 215 nm, 568 nm and at 225 nm, 576 nm observed confirm the presence of Co_3O_4 compounds.(Dewi, Yulizar and Bagus Apriandanu, 2019) These peaks obtained stipulates the conversion of O^{2-} to Co^{2+} transition.(He *et al.*, 2005) For Cu

treated at H_2O_2, peak at 370 nm corresponds to $Cu(OH)_2$ adsorption band gap.(Li *et al.*, 2013) Also, a peak at 295 nm is observed in the absorption peak range which corresponds to CuO compounds.(Felix, Chakkravarthy and Grace, 2015)

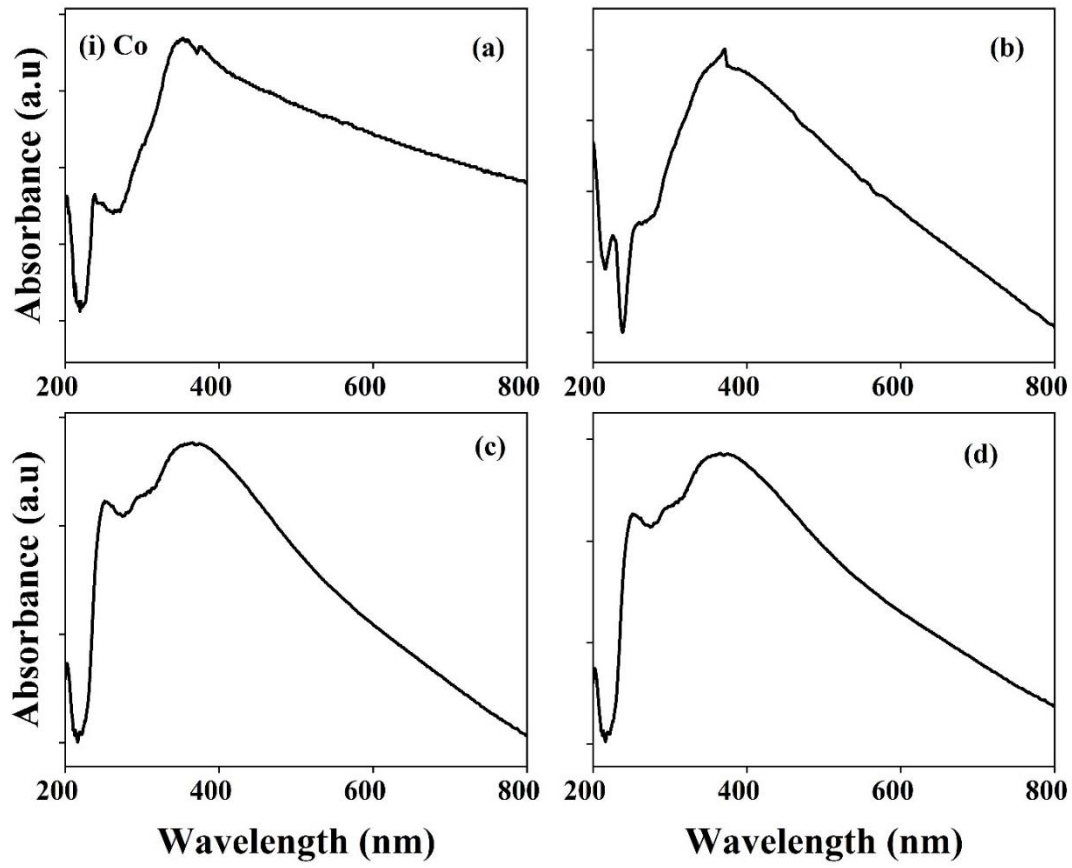

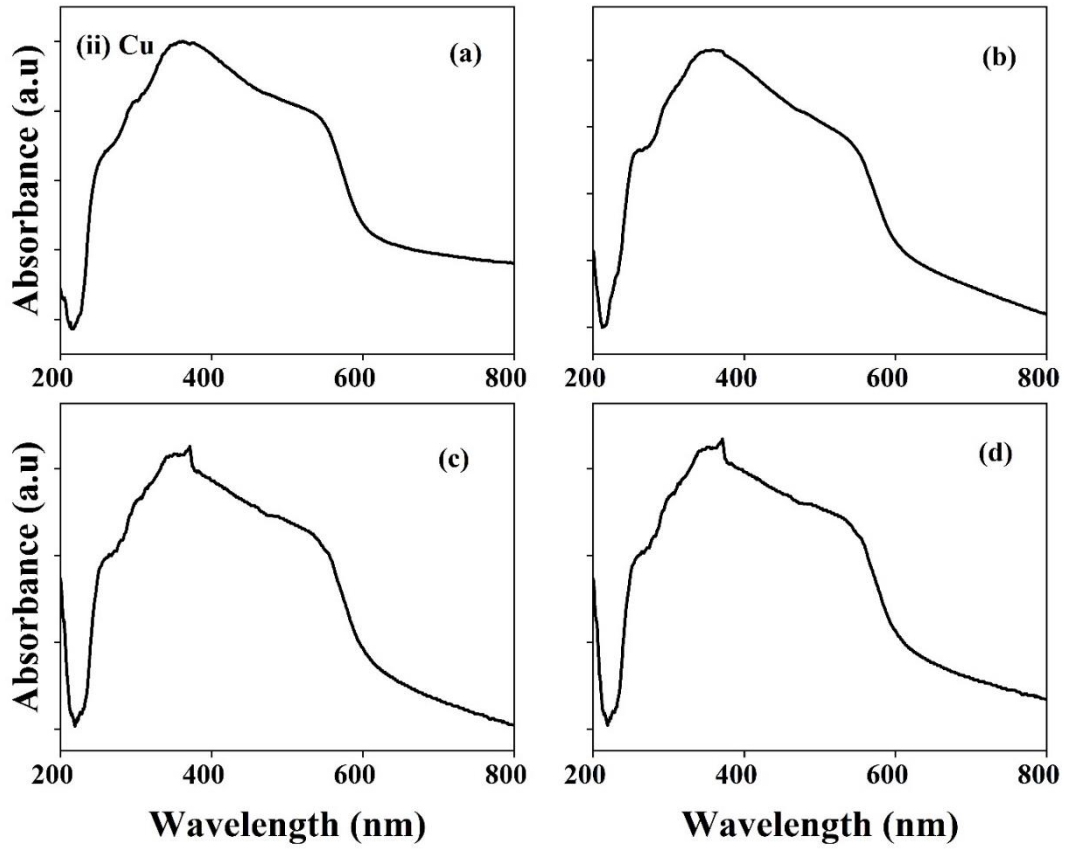

Figure 4.3. 6 UV spectra of (i) Co and (ii) Cu treated at pH 9 in (a) DI water (b) 0.1wt.% H_2O_2 (c) 0.1wt.% H_2O_2 + 0.02M oxalic acid and (d) 0.1wt.% H_2O_2 + 0.02M oxalic acid + 5ppm imidazole solution.

As mentioned earlier, apart from reducing galvanic corrosion, the barrier slurry should also be capable of polishing Co and Cu metals with a 1:1 removal rate selectivity ratio. Prior to the polishing experiments, the dissolution rates were investigated as shown in Figure. 4.3.7(i). The polishing experiments were performed using 1wt.% fumed silica along with 0.1wt.% H_2O_2 which is displayed in Figure 4.3.7(ii). From the figures it can been seen that the RR is higher as compared to the SER. The higher material RR in polishing experiments is attributed to the synergistic effect of fumed silica (abrasive) and H_2O_2 (oxidizer). The RR of Co and Cu was 29 nm/min and 76 nm/min at pH 9 resulting in a very low RR selectivity (Table I). The RR

selectivity of Co and Cu was found to be ~0.38, which in any case is not acceptable. Taken together the electrochemical and polishing results, 0.1wt.% H_2O_2 solution at pH 9 was considered for further investigation and chosen as reference solution.

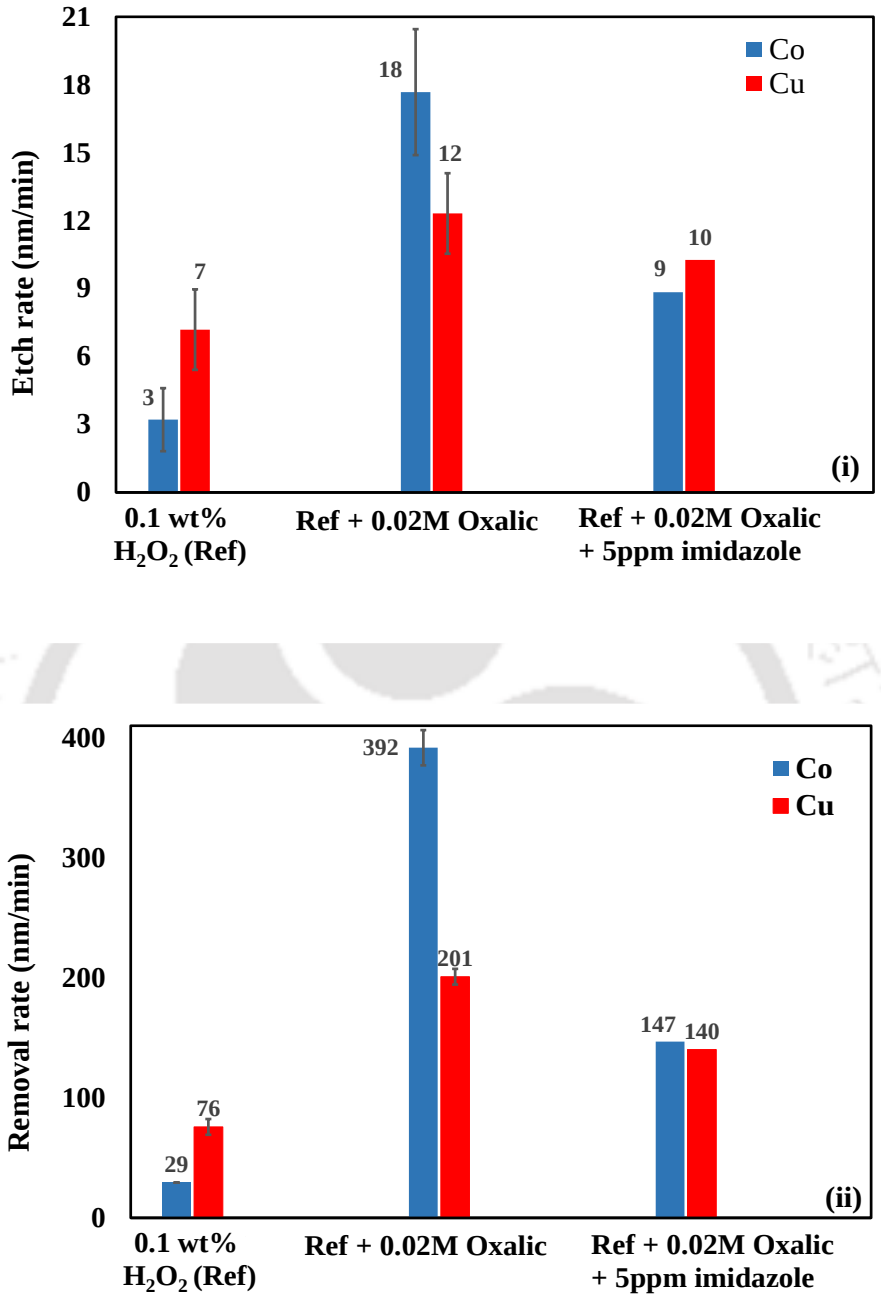

Figure 4.3. 7 (i) Etch rate and (ii) Removal rate of Co and Cu in various solutions (inclusive of 1 wt. % silica at all conditions).

Effect of oxalic acid on the ER, RR and electrochemical properties of Co and Cu:

Through a set of screening experiments which is not shown here, the concentration of complexing agent, oxalic acid was selected as 0.02 M. The polishing experiments shown in Figure.7(ii) were performed to evaluate the consequences of oxalic acid on RR of Co and Cu. It was observed that the Co RR and Cu RR showed a substantial rise after addition of 0.02 M oxalic acid. The rise of Co RR is more than the Cu RR. Oxalic acid acts as a potent complexing agent by forming complexes with the oxide layer on the metal (Co and Cu) surfaces, which is further removed by the abrasion of fumed silica, thus resulting in higher RR. On the inclusion of 0.02 M oxalic acid the RR, of Co increased from 29 nm/min (reference) to 392 nm/min and the RR of Cu increased from 76 nm/min to 201 nm/min respectively. The RR selectivity between Co and Cu also increased to ~1.95 from ~0.38 (reference), as shown in Table 4.3.1.

Table 4.3. 1 Calculated corrosion potential (E_{corr}), corrosion current density (I_{corr}) and galvanic corrosion current (I_{gc}) from potentiodynamic polarization plots

Solution system at pH9	Copper		Cobalt		Difference (Cu – Co)		Galvanic corrosion current	Co: Cu (RR Selectivity)
	E_{corr} (mV)	**I_{corr} (μA/cm²)**	**E_{corr} (mV)**	**I_{corr} (μA/cm²)**	**$\|\Delta E_{corr}\|$ (mV)**	**$\|\Delta I_{corr}\|$ (μA/cm²)**	**I_{gc} (μA/cm²)**	
DI water	-81	1.85	-360	3.76	279	1.91	1.65×10^{-5}	-
0.1wt.% H_2O_2	335	62.36	286	9.18	49	53.18	3.25×10^{-6}	29:76 (0.38)
0.1wt.% H_2O_2 + 0.02M Oxalic acid	136	137.10	76	56.06	60	81.04	2.50×10^{-5}	392:201 (1.95)
0.1wt.% H_2O_2+ 0.02M Oxalic acid + 5ppm Imidazole	177	57.63	189	36.31	12	21.32	5.52×10^{-6}	147:140 (1.05)

As per literature, carboxyl group are generally used to enhance the Co removal rate by forming complexes with the oxidized metal layer.(V R K Gorantla *et al.*, 2005; Venkata R K Gorantla *et al.*, 2005; Ramakrishnan *et al.*, 2007; Janjam *et al.*, 2008, 2009; Miller and Granstrom, 2017) Also, use of oxalic acid (dicarboxylic acid) as complexing agent in H_2O_2 based chemistry for Cu CMP is noteworthy.(Venkata R K Gorantla *et al.*, 2005; Lowalekar, 2006; Pandija, Roy and Babu, 2007; Wu and Tsai, 2007) In aqueous solution, oxalic acid dissociates in two steps as shown in reaction 4.3.13 and reaction 4.3.14 to form oxalate ions ($C_2O_4^{2-}$).(Qi, 2018) These oxalate ions ($Ox^{2-} \equiv C_2O_4^{2-}$) react with oxides of Co and Cu as shown in Equation 4.3.15-4.3.17 to form Co-oxalate [$Co(Ox)_2^{2-}$] and Cu-oxalate [$Cu(Ox)_2^{2-}$] complexes.(Meites, 1950; Barney, Argersinger and Reynolds, 1951; McAuley and Nancollas, 1960; Gašparac, Martin and Stupnišek-Lisac, 2000) These oxides have reasonable solubility in alkaline region.(Meites, 1950; Barney, Argersinger and Reynolds, 1951; McAuley and Nancollas, 1960) Thus, the observed higher material removal in the presence of oxalic acid might be attributed to the formation of Co-oxalate and Cu-oxalate complex, which is detached from the surface by the abrasive action of fumed silica. The molecular structure of oxalic acid(Abdel-Moemin, 2014) is displayed in Figure.4.3.8 (i).

$$C_2H_2O_4 \rightleftharpoons H^+ + HC_2O_4^- \quad [4.3.13]$$

$$HC_2O_4^- \rightleftharpoons H^+ + C_2O_4^{2-} \quad [4.3.14]$$

<u>At alkaline region</u>

$$Co(OH)_2 + 2Ox^{2-} \rightarrow Co(Ox)_2^{2-} + 2OH^- \quad [4.3.15]$$

$$CuO + H_2O + 2Ox^{2-} \rightarrow Cu(Ox)_2^{2-} + 2OH^- \quad [4.3.16]$$

$$Cu_2O + 4Ox^{2-} + H_2O \rightarrow 2Cu(Ox)_2^{2-} + 2OH^- + 2e^- \quad [4.3.17]$$

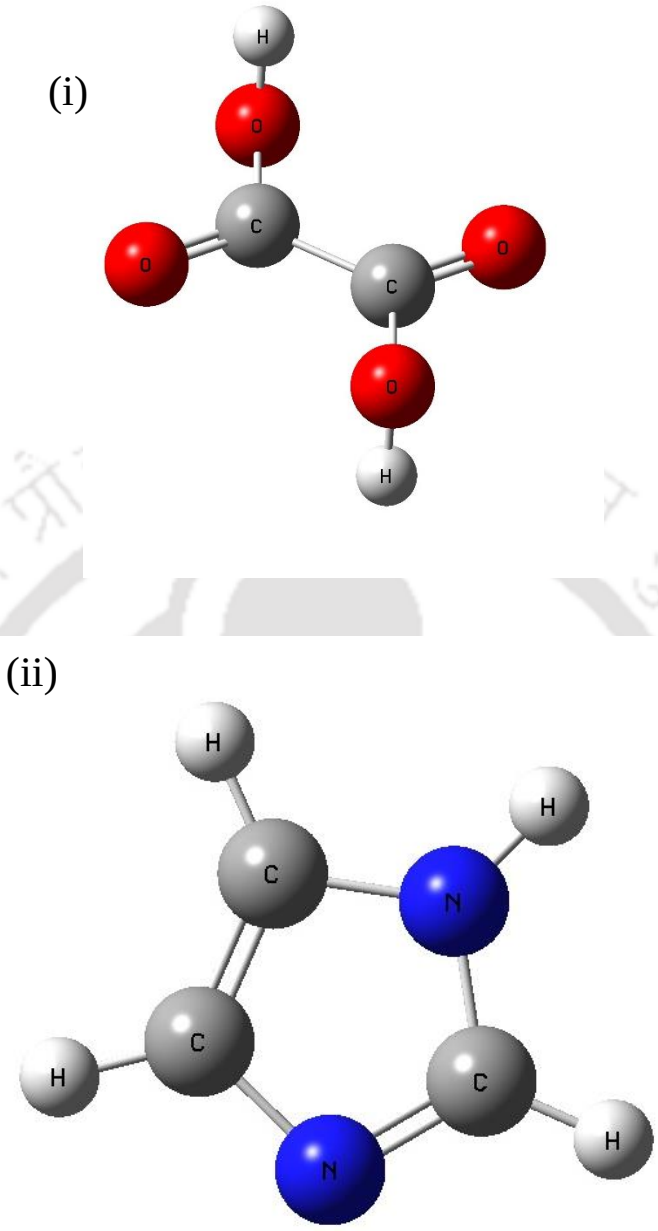

Figure 4.3. 8 Molecular structure of (i) oxalic acid (ii) imidazole

The Co and Cu potentiodynamic polarization curves in 0.02 M oxalic acid in the presence and absence of 0.1 wt.% H_2O_2 are shown in Figure.4.3.9(i) and (ii). These experiments were performed to study the effect of oxalic acid on potential difference of Co-Cu galvanic couple. A higher difference (ΔE_{corr}) of 352 mV is obtained in the presence of only 0.02 M oxalic acid at pH 9.

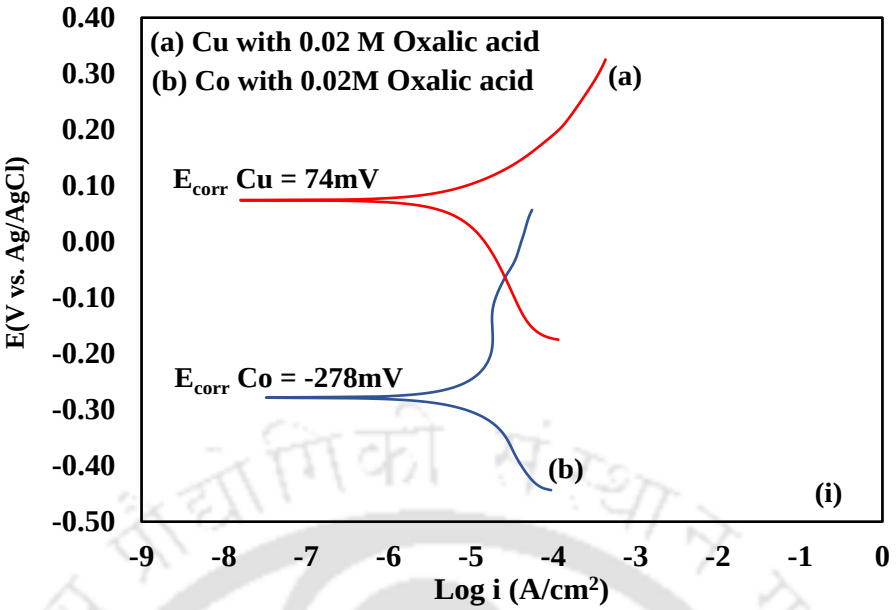

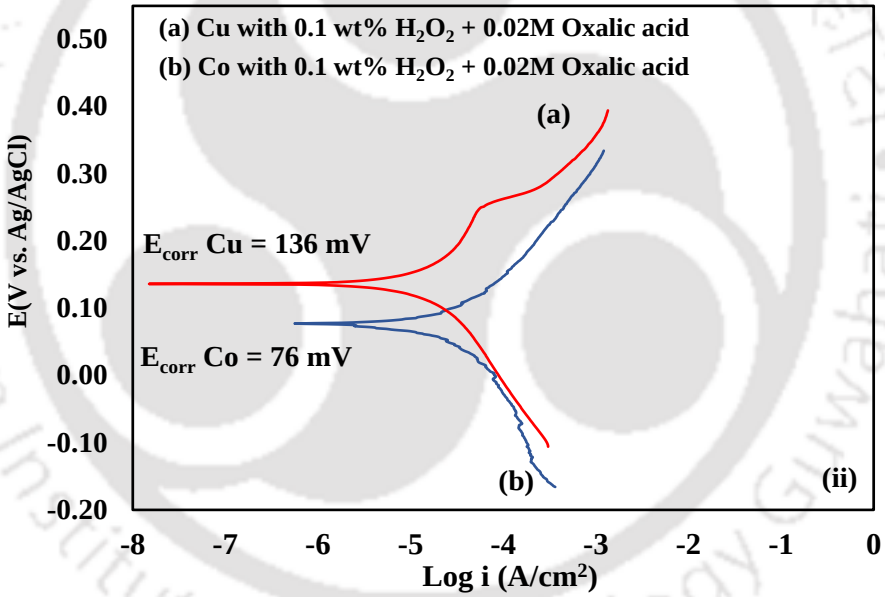

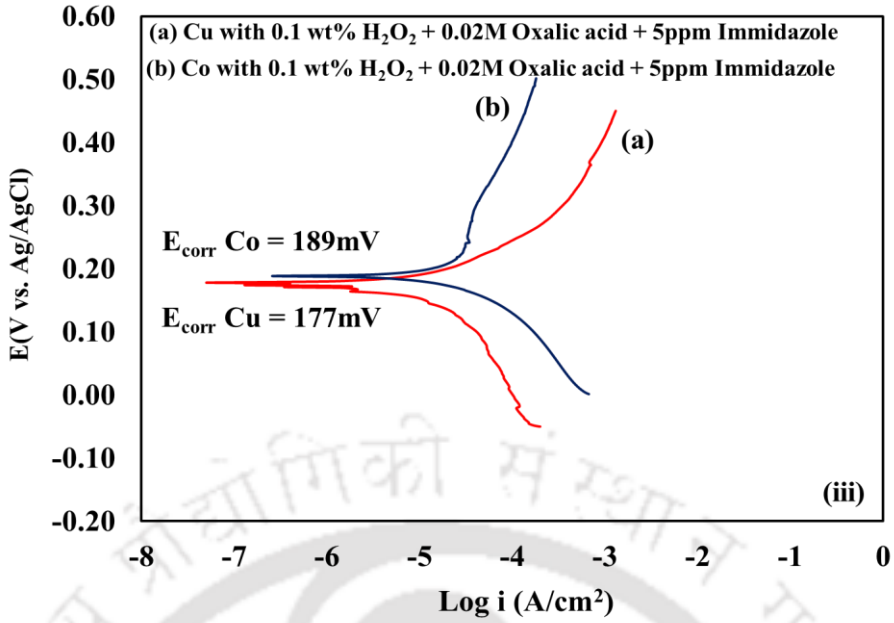

Figure 4.3. 9 The potentiodynamic polarization curves of Co and Cu with (i) 0.02M oxalic acid; (ii) 0.1wt.% H_2O_2 + 0.02M oxalic acid; (iii) 0.1wt.% H_2O_2 + 0.02M oxalic acid + 5ppm imidazole.

The addition of 0.02 M of oxalic acid to 0.1 wt.% H_2O_2 (Figure.4.3.9(ii)) solution varied the E_{corr} and I_{corr} for both Co and Cu as compared to the reference electrolyte (Figure.4.4.4). For Co, the E_{corr} value decreased from 286 mV to 76 mV and the I_{corr} value increased from 9.18 µA/cm^2 to 56.06 µA/cm^2. For Cu, the E_{corr} value decreased from 335 mV to 136 mV and the I_{corr} value increased from 62.36 µA/cm^2 to 137.10 µA/cm^2. The ΔE_{corr} showed an increase from 49 mV (reference) to 60 mV, whereas ΔI_{corr} increased to ~81 µA/cm^2 from ~53 µA/cm^2 (reference). Besides, the i_{gc} value increased from 3.25×10^{-6} µA/cm^2 (reference) to 2.50×10^{-5} µA/cm^2.The values are displayed in Table 4.3.1. It is to be mentioned that, the galvanic corrosion current (i_{gc}) is calculated from the (E, i) coordinates of the intersection of Co anodic Tafel branch and corresponding Cu cathodic Tafel branch.(Turk *et al.*, 2015) It is to be noted that galvanic current density highly depends on the potential gap of the two metals. Hence, in

this case, the point of intersection moves toward left with the reduced absolute value of potential gap between Cu and Co.(Ahmad, 2006)

The FTIR and UV spectra of Co and Cu compounds formed on treatment in H_2O_2 + oxalic acid are displayed in Figure 4.3.5 (i) and (ii) and, Figure 4.3.6 (i) and (ii) respectively. For FTIR spectra of Co compounds formed in oxalic acid added H_2O_2 solution, peak at 2187 cm^{-1} is attributed to C=O stretching (vibrational) of the carboxylic acid.(Muthuselvi, Arunkumar and Rajaperumal, 2017) Board adsorption peaks at 1687 cm^{-1} and 667 cm^{-1} correlates to the presence of Co-O double bond and Co-O stretching present in CoOOH and Co_3O_4 compounds.(Jagadale, Dubal and Lokhande, 2012; Zhang *et al.*, 2012) This confirms the formation of Cobalt-oxalate compound. Whereas for Cu compounds formed in H_2O_2-oxalate system, small bands belonging to oxalate structure are seen at 1634 cm^{-1}, 1364 cm^{-1}, 1099 cm^{-1} and 783 cm^{-1}.(Pandey, 2015; Minu Mary *et al.*, 2016) The peak at 3834 cm^{-1} hydrogen bonded 0-H.(Awwad and Albiss, 2015) Also, at 495 cm^{-1}, a band corresponding to Cu-O vibration is observed.(Jillani *et al.*, 2018) This confirms the formation of Copper oxalate compounds.(Hussain, Al-nuzal and Al-qazzaz, 2016)

From UV spectra of Co treated in H_2O_2 and oxalic acid solution, as expected absorption peaks at 255 nm, 274 nm and 382 nm are observed. This absorption region nearby at 250-450 nm range depicts the formation of Cobalt oxalate complexes on treatment with oxalic acid as complexing agent.(Pandey, 2015) Similarly, for Cu, peaks at 371 nm and 483 nm were identified as Cu compounds. The presence of a sharp peak at 392 nm confirms the formation of oxalic acid complexes.(bama, Kiruban and dran, 2017) Also, the decrease in absorbance intensity of the compounds formed on addition of oxalic acid to H_2O_2 seconds the formation of Cu-oxalate complexes.

Now, in order to improve selectivity and further reduce the corrosion potential and galvanic current density of Co -Cu galvanic couple, an addition of inhibitor imidazole as additive is taken into consideration. Although the role of imidazole and its derivatives as an inhibitor have been separately investigated for Co CMP(Shi, Schlueter and O'Neill, 2016; Shi *et al.*, 2019; Reichardt *et al.*, 2021) and Cu CMP(Gašparac, Martin and Stupnišek-Lisac, 2000; Lee, 2003; Ma *et al.*, 2020), to the best of our knowledge, the role of imidazole in reducing galvanic corrosion of Co/Cu couple along with obtaining desired selectivity has not been investigated yet.

Effect of imidazole on SER and Co/Cu RR selectivity and in reducing Co-Cu galvanic corrosion:

Imidazole being a nitrogenous heterocyclic compound of the azole –group, is reported as an effective corrosion inhibitor for various metals such as Cu, Ru, Al.(Gašparac, Martin and Stupnišek-Lisac, 2000; Stupnišek-Lisac, Gazivoda and Madžarac, 2002; Lee, 2003; Bui *et al.*, 2012; He *et al.*, 2014; Ko *et al.*, 2021) Thus, polishing experiments were performed to evaluate the combined effect of 1 wt.% fumed silica + 0.1 wt.% H_2O_2 + 0.02 M oxalic acid solution along with 5 ppm imidazole on removal rate selectivity of Co and Cu. Prior to polishing experiments, dissolution studies were conducted to investigate the dissolution rates of the metals in the solution. SER and RR (with fumed silica) of Co and Cu at pH 9 with reference solution + 0.02 M Oxalic acid + 5 ppm imidazole are illustrated in Figure. 4.3.7(i) and (ii). From these figures, it was seen that the addition of inhibitor decreases the SER from 18 nm/min to 9 nm/min and from 12 nm/min to 10 nm/min for Co and Cu respectively. The RR of Co and Cu in the presence of 1 wt.% fumed silica with reference solution + 0.02 M oxalic acid + 5 ppm imidazole solution was 147 nm/min and 140 nm/min respectively (Figure.4.3.7(ii)). The

use of 1 wt.% fumed silica + 0.1 wt.% H_2O_2 + 0.02 M oxalic acid + 5 ppm imidazole slurry gave a Co/Cu removal rate ratio (selectivity) of ~1.05:1.

The addition of 5 ppm imidazole directly into 0.1 wt.% H_2O_2 (without oxalic acid) solution showed reduction in potential gap between Co and Cu to a great extent but showed an inconsiderable RR selectivity.

For further investigation, Co and Cu potentiodynamic polarization plots with 5 ppm imidazole in 0.02 M oxalic acid and 0.1 wt. % H_2O_2 solution were acquired and are shown in Figure.4.3.9 (iii). The addition of 5 ppm imidazole to 0.02 M oxalic acid + 0.1 wt.% H_2O_2, reduced the ΔE_{corr} and ΔI_{corr} values. For Co, the E_{corr} and I_{corr} values were found to be 189 mV and 36.31 $\mu A/cm^2$ respectively (uncertainty on this value is higher due to passivation regime in anodic curve), whereas for Cu, the E_{corr} and I_{corr} values are 177 mV and 57.63 $\mu A/cm^2$ respectively. Thus, from the E_{corr} values, it is seen that presence of 5 ppm imidazole reduced the potential gap to 12 mV from 60 mV. This indicates that a small amount of imidazole in 0.02 M oxalic acid and 0.1 wt. % H_2O_2 solution can prevent Co and Cu galvanic corrosion significantly. With Co and Cu, the I_{corr} value was found to be 36.31 $\mu A/cm^2$ and 57.63 $\mu A/cm^2$, respectively, reducing the ΔI_{corr} to 21.32 $\mu A/cm^2$ from 81.04 $\mu A/cm^2$ (in the absence of imidazole). The galvanic current density (i_{gc}) decreased from 2.50×10^{-5} $\mu A/cm^2$ (in the absence of imidazole) to 5.52×10^{-6} $\mu A/cm^2$. The calculated values of E_{corr}, I_{corr}, ΔE_{corr}, ΔI_{corr} and I_{gc} obtained from Figure. 4.3.2, Figure. 4.3.4 and Figure. 4.3.9 are summarized in Table 4.3.1. It is to be mentioned that the metal converts to its ions at anodic potentials to release electrons forming insoluble products like oxides/hydroxides on the metal surface. Whereas, at cathodic potentials, the electrons released take part in the oxygen reduction reaction as shown in reactions (4.3.4) and (4.3.12).(Zhong *et al.*, 2014) In the present study, the addition of imidazole enhances E_{corr} values of both Cu (136 mV to 177 mV) and Co (76 mV to 189 mV) with Co being comparatively higher. It is to be noted that the formation of passive film on metal surface

enhances the E_{corr} value. Besides, the slope of the anodic polarization curve increases with imidazole addition for both the metals but again to a higher extent for Co. Thus, imidazole adsorbs on these metal/metal oxide surfaces via -C=NC and -C-NH-C interactions(Ko *et al.*, 2021) , forms a protective film and suppresses the anodic reaction rate for both the metals by blocking the active corrosive sites. However, the effect is more pronounced on Co compared to Cu as observed from polarization curves. Etch rate and polish rate results also mimic the same trend. The adsorption of imidazole on these metal surfaces could be physisorption or chemisorption or a combination of both. Further investigation is necessary to understand the nature of adsorption on these metal surfaces. The molecular structure of imidazole(Atanasova-Stamova, Georgieva and Georgieva, 2018) is displayed in Figure 4.3.8(ii).

For compounds formed in imidazole added oxalic acid + H_2O_2 solution, from FTIR spectra displayed in Figure 4.3.5 (i) and (ii), the peaks observed at (a) Co-624 cm^{-1} and 1300 cm^{-1} ,(b) Cu- 651 cm^{-1} and 1112 cm^{-1} corresponds to imidazole C-H stretching.(Rajkumar and Ranga Rao, 2008) Whereas, the smaller peak obtained at 1598 cm^{-1} for Co is attributed to the C=N bond stretching of imidazole.(Recovery *et al.*, 2016) Also, the peaks ascribed at 3718 cm^{-1}, 1668 cm^{-1} and 595 cm^{-1} for the Cobalt compound correspond to N-H stretching, N-H bending and Co-O stretching vibrations respectively.(Sipaut *et al.*, 2005; Zhang *et al.*, 2012) For Cu, the peak at 3800 cm^{-1} depicts hydrogen bonded OH group(Awwad and Albiss, 2015) whereas the ones ascribed at 1618 cm^{-1}, 1320 cm^{-1}, and 533 cm^{-1} depict C=N of imidazole stretching, Cu-OH stretching nodes and Cu-O vibrational modes respectively.(Devamani, R Hepzi Pramila Alagar, 2017; Jillani *et al.*, 2018) However, the peaks are not that prominent (flat orientation) for the oxidized compounds like the previous cases, this marks the possible involvement of imidazole adsorption on Co and Cu compounds. A similar case where use of inhibitors suppresses or flattens the peak is observed in literature.(Idouhli *et al.*, 2019)

For UV spectrum (Figure 4.3.6 (i) and (ii)) of Co and Cu treated in H_2O_2 and oxalic acid along with imidazole, for both the metal compounds a slight shift in the bands were seen as compared to the Co-complexes and Cu-complexes formed. A similar almost negligible shift in UV spectrum is observed on imidazole treatment with different components.(Bui *et al.*, 2012)

The experiments were conducted using bulk Co and Cu metal disc with 99.98% and 99.95% purity. In general, the physical and chemical properties of the metal will vary between thin metal film deposited on a substrate and bulk metal disc. Thus, the experiments need to be conducted with thin film wafers and the various parameters such as pressure, rotational speed, composition of the slurry needs to be tuned further to use this system in the semiconductor industry.

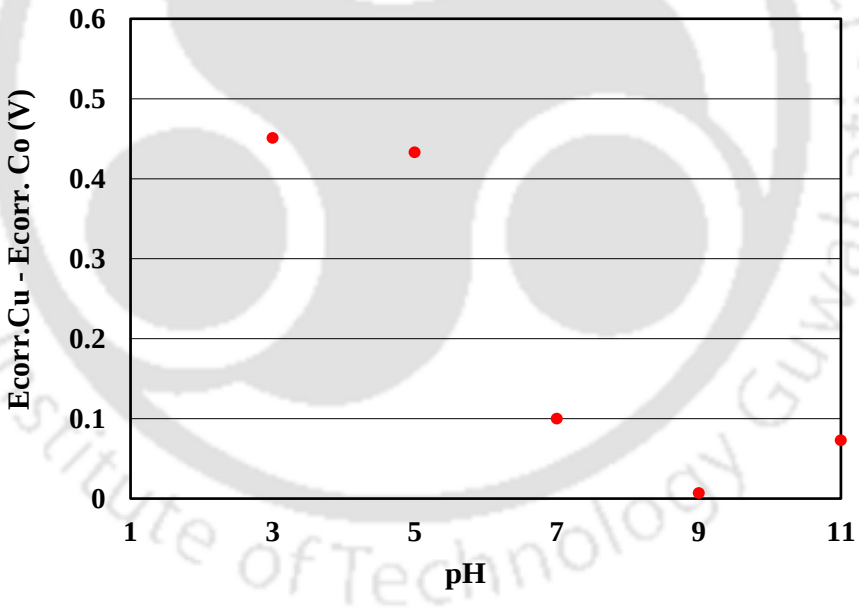

Figure 4.3. 10 Corrosion potential difference of Co and Cu in 0.1wt.% H_2O_2 + 0.02M oxalic acid + 5ppm imidazole solution at varying pH.

Figure. 4.3.10 shows the absolute value of Co and Cu corrosion potential difference by using the proposed solution (0.1 wt.% H_2O_2 + 0.02 M oxalic acid + 5 ppm imidazole) at different pH

values. However, a minimum value of ΔE_{corr} was observed at only pH 9. This is due to the fact that both (Co and Cu) show passivation mainly in the alkaline region.

In summary, the polishing and electrochemical results indicate that the proposed solution (0.1 wt.% H_2O_2 + 0.02 M oxalic acid + 5 ppm imidazole) at pH 9 can reduce the corrosion potential difference to 12 mV and give a desired Co/Cu RR selectivity of ~1.05:1.

4.3.4 Conclusion

The combined effect of oxalic acid and imidazole in a H_2O_2 solution on reducing Co-Cu galvanic corrosion and achieving desired Co/Cu removal rate selectivity was studied. It was found that both Co and Cu have a low dissolution rate (desired) in 0.1 wt.% H_2O_2 chemistry. The RR of Co and Cu in the presence of 1 wt.% fumed silica with 0.1 wt.% H_2O_2 was also very low with a Co/Cu RR selectivity of ~0.38 (not desired). However, the potential difference was found to be ~49 mV at pH 9. Addition of oxalic acid (complexing agent) increased the RR of Co significantly by forming Co-oxalate and Cu-oxalate complexes. It was observed that a small amount of imidazole exhibited desired results in reducing galvanic corrosion and to achieve desired selectivity. The addition of 5 ppm imidazole to 0.1 wt.% H_2O_2 + 0.02 M oxalic acid reduced the corrosion potential difference to ~12 mV at pH 9. Polishing experiments performed using 1wt.% fumed silica in proposed solution (0.1 wt.% H_2O_2 + 0.02 M oxalic acid + 5 ppm imidazole) showed an acceptable Co/Cu RR selectivity of ~1.05:1. The formation of Cu and Co complexes with oxalic acid and the inhibition effect of imidazole are observed by FTIR and UV spectroscopy measurements.

4.4 Anodic dissolution of Cobalt in hydrogen peroxide solutions with and without complexing agent: Kinetic analysis by electrochemical impedance spectroscopy.

4.4.1 Motivation

Cobalt (Co) has emerged as one of the most potent barrier metals in the semiconductor devices owing to its lower resistivity (~6.2 Ωm), non-requirement of seed layer deposition, improvement in electro-mitigation of interconnect etc.(Li *et al.*, 2005; Wu *et al.*, 2017) Hence, understanding the chemical and physical changes occurring on cobalt surface upon exposure to various solutions during fabrication of microelectronic chips is vital.(Lu, Zeng, *et al.*, 2012; Peethala *et al.*, 2012; Li *et al.*, 2016; R Popuri, Sagi, Alety, Peethala, Amanapu, Patlolla, *et al.*, 2017)

Co usually forms a passivating film of Co (II) or Co (III) compounds on its surface when in contact with a reacting environment.(Ismail and Badawy, 2000) At neutral and lower alkaline region a passivating film of $Co(OH)_2$ {Co(II) compounds} is predominant on the metal surface.(Badawy, F M Al-Kharafi and Al-Ajmi, 2000)

$$Co(OH)^+ + OH^- \rightarrow Co(OH)_2 \qquad [4.4.1]$$

At higher alkaline region, Co_3O_4 and $CoOOH$ {Co (III) compounds} are dominant as the passivating film. (Badawy, F M Al-Kharafi and Al-Ajmi, 2000; Lu, Wang, *et al.*, 2012; Lu, Zeng, *et al.*, 2012; Peethala *et al.*, 2012; Jiang, He, Yan Li, *et al.*, 2014b; Fu *et al.*, 2018; Hazarika and Rajaraman, 2020)

$$3Co(OH)_2 + 2OH^- \leftrightarrow Co_3O_4 + 4H_2O + 2e^- \qquad [4.4.2]$$

$$Co(OH)_2 + OH^- \leftrightarrow CoOOH + H_2O + e^- \qquad [4.4.3]$$

The formation of these compounds are dependent on pH value, oxidative environment or electrode potential of the exposed solution.[16,17] Thus, to get a more inclusive confirmation of

the products formed is obligatory to study both the oxidation and the dissolution of the Co metal in the solution of interest.

The studies on reaction mechanism of Co anodic dissolution in different media are modestly low as reported in literature. Most of the suggested models are mainly based on bicarbonate/carbonate solutions(Calderón, Barcia and Mattos, 2008; Real, Ribotta and Arvia, 2008) which are discussed herewith. Davies et.al.(Davies and Burstein, 1980) and Burstein et.al.(Burstein and Davies, 1980) investigated the Co behavior in a carbonate/bicarbonate solution. They suggested the formation of CoO film in the dissolution and also claimed the presence of { $Co(CO_3)_2^{2-}$ } intermediate complex ion.

$$Co(s) + HCO_{3(aq)}^{-} \xrightarrow{k_1} (CoCO_3)_s + H_{(aq)}^{+} + e^{-} \quad [4.4.4]$$

$$Co + H_2O \xrightarrow{k_2} CoO_{(s)} + 2H_{(aq)}^{+} + e^{-} \quad [4.4.5]$$

$$CoO_{(s)} + HCO_{3(aq)}^{-} \xrightarrow{k_3} CoCO_{3(s)} + OH_{aq}^{-} \quad [4.4.6]$$

$$CoCO_{3(s)} + HCO_3^{-} \underset{k_{-4}}{\overset{k_4}{\rightleftharpoons}} Co(CO_3)_{2(aq)}^{2-} + H_{(aq)}^{+} \quad [4.4.7]$$

Gervasi et.al(Gervasi *et al.*, 1991; Gervasi, Vilche and Alvarez, 1996) suggested a similar dissolution mechanism as Davies and Burstein(Burstein and Davies, 1980; Davies and Burstein, 1980), however he proposed that Co_3O_4 is formed instead of CoO since CoO film is sensitive to HCO_3^- ion. Real et.al.(Real, Ribotta and Arvia, 2008) suggested a model comprising of formation of Co(I)($Co(OH)_{ad}$) as intermediate species followed by soluble Co(II)(mass transfer contributions)($Co(CO_3)_2^{2-}$) ions as the final products in an alkaline carbonate–bicarbonate based solution.(Real, Ribotta and Arvia, 2008)

$$Co(s) + (H_2O)_i \underset{k_1}{\overset{k_{-1}}{\rightleftharpoons}} Co(OH)_{ad} + (H^+)_i + e^- \quad [4.4.8]$$

$$Co(OH)_{ad} \underset{k_2}{\overset{k_{-2}}{\rightleftharpoons}} Co(OH)^{+} + e^{-} \quad [4.4.9]$$

$$Co(OH)^{+} + CO_3^{2-} \underset{k_3}{\overset{k_{-3}}{\rightleftharpoons}} CoCO_3 + OH^{-} \quad [4.4.10]$$

$$CoCO_3 + HCO_3^{-} \underset{k_4}{\overset{k_{-4}}{\rightleftharpoons}} [Co(CO_3)_2^{2-}] + H^{+} \quad [4.4.11]$$

A two electro dissolution paths initiating with formation of $(CoHCO_3)_{ad}$ followed by formation of $Co(CO_3)_2^{2-}$ (mass transfer phenomenon) and CoO film respectively was observed by Calderon et.al(Calderón, Barcia and Mattos, 2008) in a carbonate/bicarbonate solution. Formation of CoO film is favored at higher anodic potentials (autocatalytic reactions) whereas formation of $(CoHCO_3)_{ad}$ is favored at lower anodic potentials.(Calderón, Barcia and Mattos, 2008)

$$Co(s) + HCO_3^{-} \xrightarrow{k_1} (CoHCO_3)_{ad} + e^{-} \quad [4.4.12]$$

$$(CoHCO_3)_{ad} + HCO_3^{-} + 2OH^{-} \underset{k_{-2}}{\overset{k_2}{\rightleftharpoons}} Co(CO_3)_2^{2-} + H_2O + e^{-} \quad [4.4.13]$$

$$(CoHCO_3)_{ad} + 2OH^{-} \underset{k_{-3}}{\overset{k_3}{\rightleftharpoons}} CoO + HCO_3^{-} + H_2O + e^{-} \quad [4.4.14]$$

$$Co + CoO \xrightarrow{k_4} Co^{2+} + CoO + 2e^{-} \quad [4.4.15]$$

Other than the dissolution studies in carbonate/bicarbonate solution, mechanistic analysis of Co anodic dissolution in glycine solution at alkaline conditions are reported in literature.(Paul and Srinivasan, 2020) Paul et.al(Paul and Srinivasan, 2020) proposed a catalytic mechanism comprising of four adsorbed intermediates {two of each Co(II) and Co(III)} in a glycine system at pH 10. They suggested that the chemical dissolution rate increases with anodic potential while electrochemical dissolution is maximum at intermediary potential. However, the chemical dissolution is found to be saturated at larger anodic potential. The corresponding reactions in the suggested mechanism are as follows

$$Co \underset{k_{-A}}{\overset{k_A}{\rightleftarrows}} Co_{ads}^{2+} + 2e^- \quad [4.4.16]$$

$$Co_{ads}^{2+} \underset{k_{-B}}{\overset{k_B}{\rightleftarrows}} Co_{ads}^{3+} + e^- \quad [4.4.17]$$

$$Co_{ads}^{3+} \xrightarrow{k_c} Co_{sol}^{3+} \quad [4.4.18]$$

$$Co_{ads}^{2+} \xrightarrow{k_D} Co_{sol}^{3+} + e^- \quad [4.4.19]$$

$$Co_{ads}^{3+} + Co \xrightarrow{k_E} Co_{ads}^{3+} + Co_{sol}^{3+} + 3e^- \quad [4.4.20]$$

In semiconductor industry, a polishing slurry is being used in chemical mechanical polishing (CMP) process to remove the excess Co. The slurry mainly consists of oxidizer along with complexing agent [13,17,18] such as Glycine(Lu, Zeng, *et al.*, 2012; Kwon *et al.*, 2020; Paul and Srinivasan, 2020), arginine(Peethala *et al.*, 2012), acetic acid(Zuo *et al.*, no date), EDTA(Kwon *et al.*, 2020), citric acid(Peethala *et al.*, 2012), oxalic acid(Oxide *et al.*, 2002; Lowalekar, 2006; Peethala, 2011; Raj *et al.*, 2012) etc.

One such potent component known to form complexes with Co barrier metal is oxalic acid. [17,50] The carboxyl group in an oxalic acid forms complexes with the oxidized Co layer and intensifies the removal rates.(V R K Gorantla *et al.*, 2005; Venkata R K Gorantla *et al.*, 2005; Ramakrishnan *et al.*, 2007; Janjam *et al.*, 2008, 2009; Miller and Granstrom, 2017) These complexes have an enhanced solubility in the alkaline region.(Meites, 1950; Barney, Argersinger and Reynolds, 1951; McAuley and Nancollas, 1960)

Similarly, hydrogen peroxide is commonly preferred oxidizer for the planarization of various metals such as Cu, Ru, Mo etc.(Amanapu *et al.*, 2013; Jiang, He, Yan Li, *et al.*, 2014b; Hu, Pan, Xu, *et al.*, 2020b; Zhang, Wang and Lu, 2020; Poddar *et al.*, 2021) Although the kinetics and mechanistic reaction pathway of Co in carbonate/bicarbonate, glycine etc. are investigated and reported in literature, the Co anodic dissolution mechanism in H_2O_2 (oxidizer) solution is yet to be studied. Reaction mechanistic analysis of Co in H_2O_2 solution in the presence of

complexing agent (oxalic acid) is also not reported in any literature to the best of our knowledge.

Thus, this work presented here focus on comparing the physio-chemical characteristics of Co metal upon exposure to only H_2O_2 solution and to H_2O_2 + oxalic acid solution. Various electrochemical experiments such as anodic polarization, electrochemical impedance spectroscopy (EIS) were performed to understand the anodic dissolution behavior. Both electrical equivalent circuit (EEC) and reaction mechanism analysis (RMA) were performed on EIS data to retrieve the kinetics of Co anodic dissolution. Field emission scanning electron microscopy (FESEM) and contact angle analysis were conducted to characterize the Co surface and X-ray photoelectron spectroscopy (XPS) measurements were performed to identify the surface products.

4.4.2 Experimental Conditions

Electrochemical experiments

A standard three-electrode cell connected to Metrohm Autolab potentiostat, (PGSTAT 204), was used to execute the electrochemical experiments. electrode and platinum wire were the reference and counter electrode respectively whereas Co (99.95% pure, 9mm diameter) metal embedded in Teflon rod and connected with a Cu wire was used as the working electrode. All the potentials mentioned in this manuscript are w.r.t Ag/AgCl (3 M KCl solution). Prior to each experiment, the working electrode surface was polished using emery sheets and then with micro polish alumina paste (Buehlar, USA) (initial 1µm followed by 0.3µm) in order to get a mirror like electrode surface. (Li and Babu, 2001; Manivannan and Ramanathan, 2009) The polished electrode is cleaned with Millipore water, sonicated in acetone and dried before using it to perform the measurements. 0.1 wt. % H_2O_2 (Loba Chemie Private Limited, India) and 0.02 M oxalic acid (Himedia, India) were used to prepare the electrolyte solutions. Whereas, sodium sulphate (Himedia, India) was used as the supporting electrolyte. Potassium hydroxide

(Himedia, India) was used to regulate the pH values. All the experiments were conducted at room temperature and at pH 9. Besides, open circuit potential (OCP**)** experiments were performed prior to every electrochemical experiment for a duration of 600 sec. All the experiments were repeated thrice to ensure repeatability. The electrochemical experiments performed are:

Anodic polarization studies

Anodic polarization measurements were performed in two different environments (0.1 wt.% H_2O_2 and 0.1 wt. % H_2O_2+ 0.02 M oxalic acid). Here, the working electrode was scanned at a rate of 1 mV/s from OCP to +600mV w.r.t OCP.

Electrochemical impedance spectroscopy (EIS)

Electrochemical impedance spectroscopy (EIS) were performed by sweeping at a frequency range of 20000 Hz to 0.1 Hz with 7 frequencies per decade interval. An AC voltage signal of 10 mV (rms) amplitude was employed to perform the EIS measurements to ensure linearity. The EIS measurements were also conducted at different DC potentials (+0.10, +0.30 and +0.50) w.r.t OCP. While plotting the lower frequency noisy data was not considered. Kramers Kronig Transform (KKT) (Nova, Metrohm) was performed on EIS data to ensure the linearity, stability and causality of the electrochemical system (not shown here). Electrical equivalent circuit (EEC) modelling was done using commercial purchased software named Zsimpwin (Version 3.6). Reaction Mechanism Analysis (RMA) was performed to get a detailed information about the processes a metal undergoes when in contact with a reacting environment. Code written in MATLAB was used for Reaction Mechanism Analysis (RMA).

Characterization of the products and surface analysis

To get an insight of the products formed when treated with two different solutions, the following characterization techniques were employed

Field emission scanning electron microscopy (FESEM) measurements

FESEM analysis of Co was conducted on field emission scanning electron microscope (FESEM) (Zeiss, Sigma). Before every analysis the Co samples were polished using emery sheets and cleaned properly to removes the impurities or oxides. The samples are cleaned thoroughly and dipped in the solutions (H_2O_2 and H_2O_2+ oxalic acid) for 2 hrs. The samples are then washed again, dried properly and taken for analysis. The surface morphology and corrosion type of Co on treatment with the mentioned chemicals was analyzed and compared from the images.

Contact Angle Analyzer

The traditional sessile drop technique was employed to determine contact angle between the droplet and treated Co sample surface. The liquid droplet comprises of water, methylene iodide (MI), and corrosive solution of two µL. The analysis was evaluated in Goniometer (Holmarc software). Contact angle analysis sample preparation is similar to that of FESEM analysis. It is to be mentioned that a minimum of 4 droplets were deposited separately and angle was measured to ensure repeatability. A contact angle difference of less than 2^0 was observed on the both the sides of the droplet ensuring reproducibility.

X-ray photoelectron spectroscopy (XPS)

To determine the different states of Co and identify the Co compounds formed when treated with H_2O_2 and H_2O_2+ oxalic acid at pH 9, XPS was performed using ESCALAB Xi+ spectrometer (Thermo fisher Scientific Pvt. Ltd., UK) rigged with monochromatic Al Kα X-ray source radiation of 1486.6 eV. The analysis was conducted at room temperature and a base pressure of 5×10^{-10} mbar.

4.4.3 Results and Discussion

Anodic polarization studies

OCP measurements revealed that the OCP stabilizes within 600 sec as displayed in Figure 4.4.1a. The OCP values of 0.250 V and 0.045 V were obtained at pH 9 for 0.1 wt.% H_2O_2 and 0.1 wt.% H_2O_2+ oxalic acid systems respectively. The decrease in OCP value clearly shows that the oxide/hydroxide layer formed on the Co surface in H_2O_2 solution dissolves with the addition of oxalic acid. Similar behavior is reported for other systems in the literature. The anodic polarizations graphs are displayed in Figure 4.4.1b. The current density increases with overpotential for both the systems in the potential range of 0 to +600 mV w.r.t OCP. There is no sign of passivation/constant current density regime/decrease in current density with increase in potential for both the systems within the measured potential range. However, as shown in Figure 4.4.1b, the anodic current density is higher for H_2O_2+ oxalic acid solution compared to that of H_2O_2 solution at any given overpotential. Also, the rate at which current density increases with overpotential is higher for H_2O_2+ oxalic acid solution when compared to solution containing only H_2O_2. Thus, it is clearly evident that the Co anodic dissolution rate is higher in H_2O_2 +oxalic acid solution than in H_2O_2 solution. This explains the reason behind increase in removal rate of metal on addition of complexing agent (oxalic acid) in a CMP process.(Prasanna Venkatesh and Ramanathan, 2010; Kwon *et al.*, 2020)

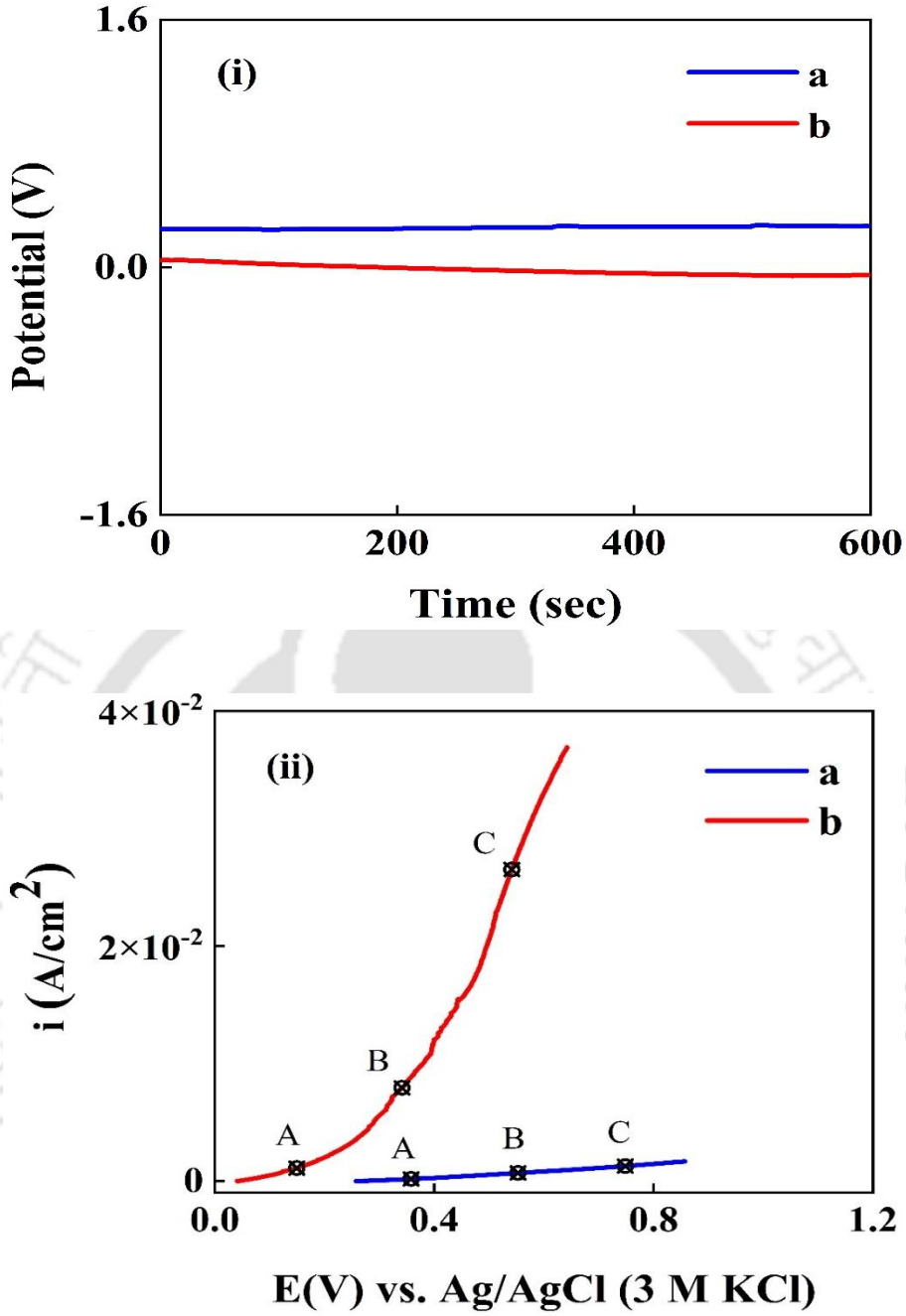

Figure 4.4. 1(i) OCP and (ii) Anodic polarization in (a) 1 wt.% H_2O_2 and (b) 1 wt.% H_2O_2 + 0.02M oxalic acid system (pH 9). Here marks A, B and C represent 0.10 V, 0.30 V and 0.50 V w.r.t OCP respectively for both the systems.

Table 4.4. 1 Current densities at different potentials w.r.t. OCP potentiodynamic polarization plots

Solution system at pH 9	Potential (V)	Anodic current density (A/cm^2)
(a) 0.1wt.% H_2O_2	0.1	1.79E-04
	0.3	7.04E-04
	0.5	1.31E-03
(b) 0.1wt.% H_2O_2 + 0.02M Oxalic acid	0.1	1.01E-03
	0.3	*7.94E-03*
	0.5	*2.65E-02*

Characterization studies

FESEM analysis

To study the surface morphology of Co metal specimen treated in 1 wt. % H_2O_2 and 1 wt. % H_2O_2+0.02 M oxalic acid solution at pH 9, FESEM analysis was conducted. The FESEM images (at 2 different magnifications) are displayed in Figure 4.4.2i – 4.4.2iv. The surface of Co treated in H_2O_2+oxalic acid solution as observed comprises of mainly small yet uniformly spread tubes/grains/flakes. The Co film comprising of tubes/grains/flakes with interconnected messy structure (as observed at higher magnification) are likely the Co-oxalate complexes.(Salavati-Niasari, Mir and Davar, 2009; Abu-Zied *et al.*, 2015) Similarly, for Co treated in H_2O_2 solution, widely spaced coarse tubes were observed. At higher magnification, unlike Co treated in H_2O_2+oxalic acid, the tubes are without any messy or flake like structures. This is to an extent can be identified as Co(III) oxides (mainly Co_3O_4, CoOOH) as reported in the literature.(Chen *et al.*, 2017; Niveditha *et al.*, 2018) It is to be noted that pitting corrosion

is not observed on any of the treated surfaces. The corrosion occurring is identified as general corrosion.

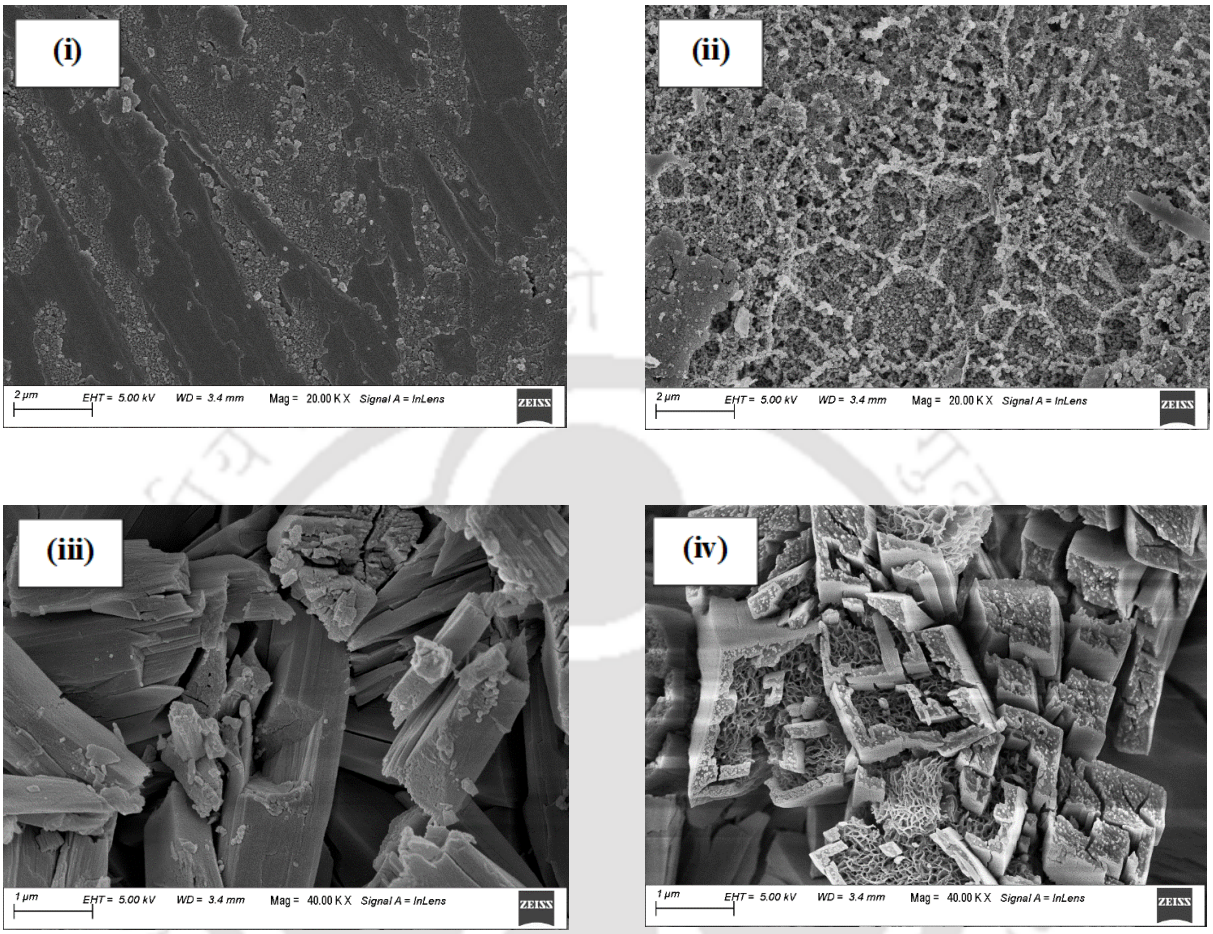

Figure 4.4. 2 FESEM images of Co treated in (i, iii) 0.1wt.% H_2O_2 (ii, iv) 0.1wt.% H_2O_2 + 0.02 M oxalic acid at pH 9. (i, ii) are images taken at 20.00 KX magnification and (iii, iv) are taken at 40.00 KX magnification

Contact angle analysis

The formation of Co oxides and Co-oxalate complexes on treating the metal specimen in the two mentioned solutions was characterized by contact angle measurements. Figure 4.4.3a and 4.4.3b illustrate the contact angle images of Co treated in (a) H_2O_2 and (b) H_2O_2+oxalic acid solution at pH 9. From the data obtained, it was seen that addition of oxalic acid to H_2O_2

solution decreased the contact angle between the droplet and Co to 23˚from 61˚. The decrease in contact angle on addition of oxalic acid indicates the formation of complexes with Co oxides/hydroxides. The complexes get dissolved in the solution to a greater extent. As a consequence, increase in hydrophilicity between the Co metal and the droplet is observed.(Sun *et al.*, 2021) This justifies the SEM results obtained in Figure 4.4.3a and 4.4.3b and eventually explains the increase in removal rate on addition of complexing agents to an oxidizer based CMP solution.(Venkata R K Gorantla *et al.*, 2005; R Popuri, Sagi, Alety, Peethala, Amanapu and Patlolla, 2017)

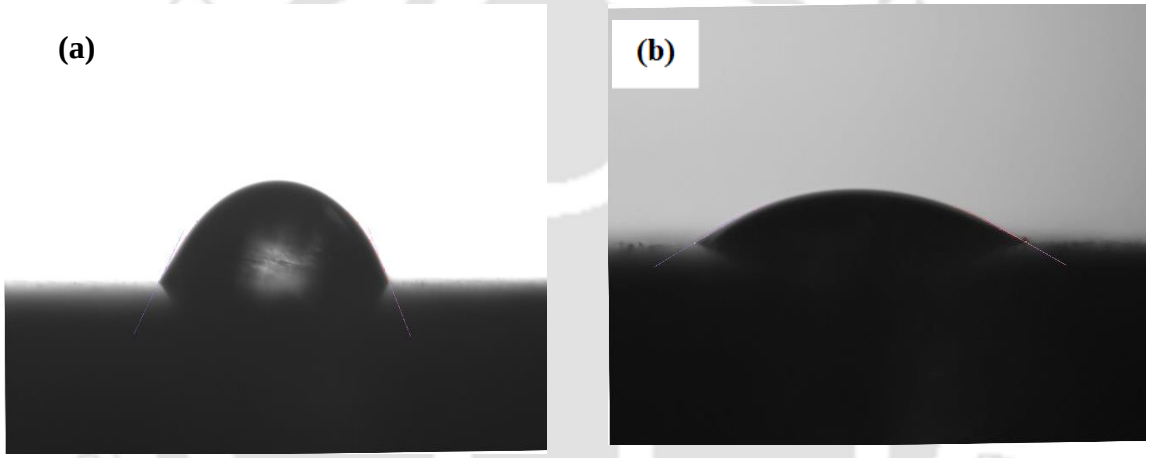

Figure 4.4. 3 Contact angle image of Co treated in (a) 0.1wt.% H_2O_2 (b) 0.1wt.% H_2O_2 + 0.02 M oxalic acid at pH 9

X-ray photoelectron spectroscopy (XPS) analysis

In order to investigate the elemental compositions and confirm the products formed on the Co surface on treatment with the solutions (H_2O_2, H_2O_2—oxalic acid at pH 9), XPS spectrum analysis method was opted. The XPS spectra are illustrated in Figure 4.4.4 a(i, iii) and 4.4.4 b(ii,iv,v). The peaks were fitted using Gaussian model.

The deconvoluted spectrum of Co treated in H_2O_2 solution Figure 4.4.4 a(i) contains 2 major peaks at 779.8 eV and 796.1 eV corresponding to $Co2p_{1/2}$. These observed peaks are attributed

to the presence of Co_3O_4 [1,2] whereas the deconvoluted peak at 781.7 eV corresponds to $Co2p_{3/2}$ of CoOOH[3] respectively. For H_2O_2—oxalic acid solution, the deconvoluted peaks Figure 4.4.4 b(ii) with binding energies 780.4 eV, 782 eV, 785.2 eV, 796.5 eV, and 802.48 eV were observed. Peaks observed at binding energy of 780.4 eV and 796.5 eV are coincident with $Co2p_{3/2}$ of CoOOH[3] and $Co2p_{1/2}$ of Co_3O_4[2] respectively. Whereas peak at 782 eV binding energy is identical with $Co2p_{3/2}$ band of oxalate[4], confirming the presence of Co-oxalates complexes. The satellite peaks appearing at 785.1 eV (for H_2O_2 treated Co) and at 785.2 eV (for H_2O_2-oxalic acid treated Co) depict the presence of Co_3O_4.[5] The peaks obtained at a binding energy value of 802.3 eV (for H_2O_2 treated Co) and 802.48 eV (for H_2O_2—oxalic acid treated Co) could be of Co_3O_4 or $Co(OH)_2$.[3,6] A slight shift in the binding energies and broadening of the peaks of CoOOH, Co_3O_4 and $Co(OH)_2$ are observed for Co treated in H_2O_2—oxalic acid. This indicates the possibility of presence of combination of Co-oxalate complexes along with the CoOOH /Co_3O_4 or the presence of individual complexes or oxides when treated in H_2O_2—oxalic acid solution. A similar case of overlaps of peaks due to lower differences in binding energies is reported in literature.[7]

The O1s spectrum for Co Figure 4.4.4 a(iii) treated in H_2O_2 shows 2 peaks at 530.2 eV and 532.8 eV. Spin orbit peak at 530.2 eV corresponds to lattice oxygen of Co_3O_4 whereas 532.8 eV corresponds to that of CoOOH. O1s peak of Co_3O_4 at 530.2 eV and O 1s peak of CoOOH at 532.8 eV is also reported by Feng et.al.[8] and Ismail et.al[3] respectively. For Co treated in H_2O_2—oxalic acid, 2 deconvoluted peaks at 531.1 eV and 532.6 eV are observed as shown in Figure 4.4.4 b(iv). An exact spin orbit peak at 532.6 eV attributes to the presence of Co-oxalate complexes. Sergey et.al.[9] reported the presence of O1 of oxalate ions $C_2O_4^{2-}$ (or –O–C–O– groups) at 532.6 eV whereas Feng et.al.[8] reported presence of O1s of CoOOH at 531.4 eV. Due to overlaps of peaks, 531.1 eV could depict Co_3O_4/CoOOH or both.

The C1s spectrum for Co treated in H_2O_2—oxalic acid is displayed in Figure 4.4.4 b(v). Spin orbit peak at 284.7 eV could be due to unpremeditated contamination of adventitious carbon. A similar case of contamination is reported in literature.[9,10] C1s deconvoluted peak at 288 eV attributes to O−C═O from COOH group of the oxalates.[11]

A reduction in peak intensities is observed for all the compounds formed from Co treated in H_2O_2—oxalic acid system. This reduced intensity signifies higher dissolution of the products when oxalic acid was added to H_2O_2 system.[12] From the XPS analysis done, it can be concluded that on treatment with H_2O_2, Co_3O_4(prime product)/ CoOOH/ $Co(OH)_2$ (likely) compounds are formed where H_2O_2—oxalic acid results in formation of Co-oxalate complexes along with these oxides.

The XPS survey spectra of Cobalt held in - (a) 1 wt.% H_2O_2 and (b) 1 wt.% H_2O_2—0.02 M oxalic acid system in active dissolution region is displayed in Figure 4.4.4 a(vi) and Figure 4.4.4 b(vii).

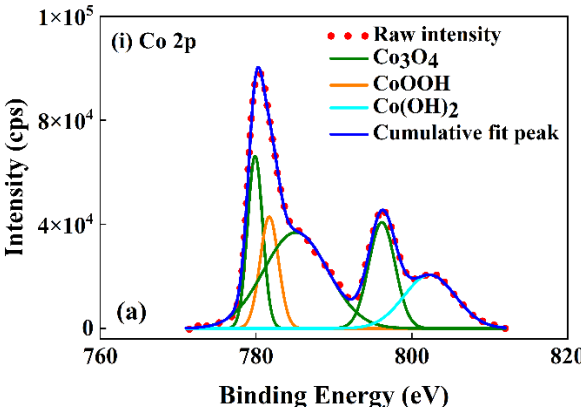

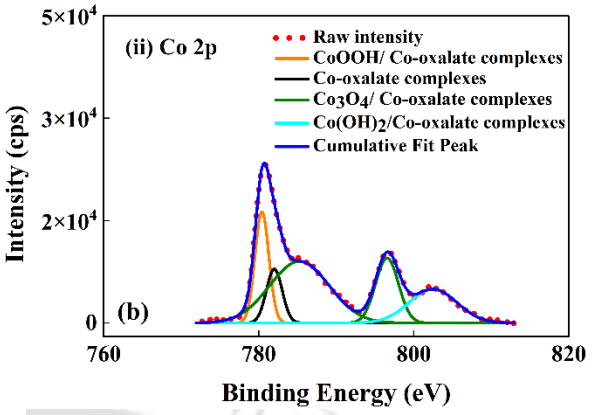

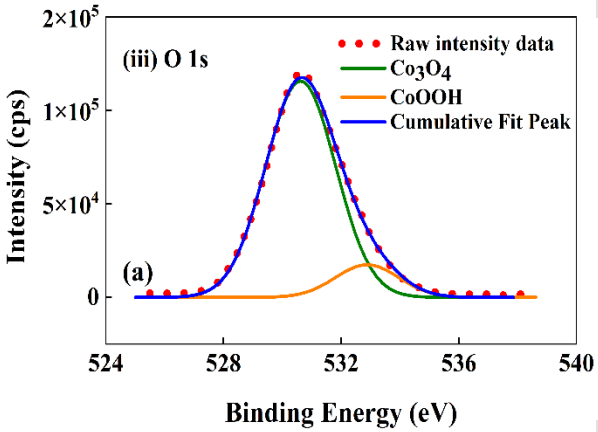

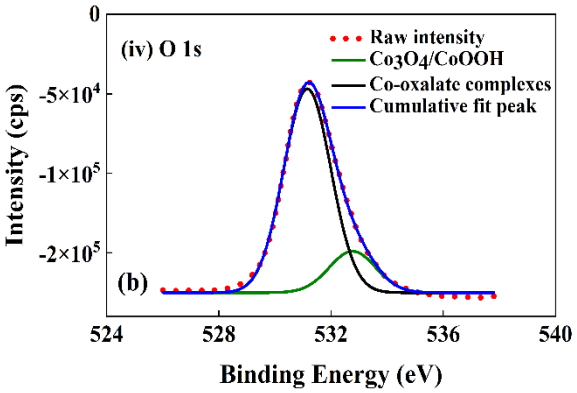

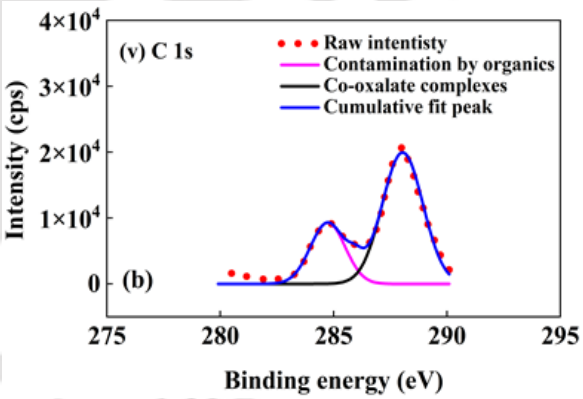

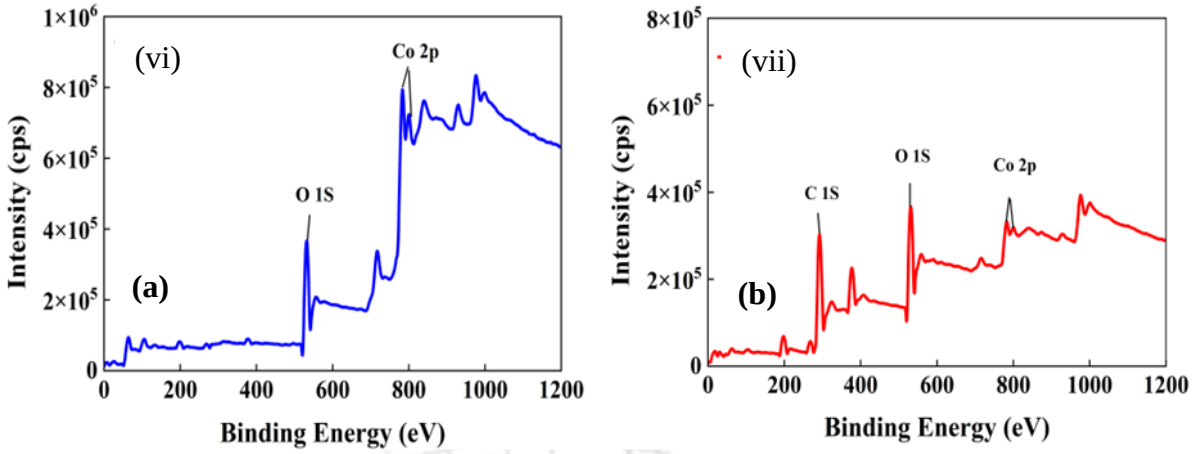

Figure 4.4. 4 XPS spectra of Co treated in (a) 0.1wt.% H_2O_2 (b) 0.1wt.% H_2O_2 + 0.02 M oxalic acid at pH 9 in active dissolution region: (i, ii) represents Co 2p (iii, iv) represents O1s and (v) represents C 1s deconvoluted peaks; XPS survey spectra of Cobalt held in - (vi) 1 wt.% H_2O_2 and (vii) 1 wt.% H_2O_2—0.02 M oxalic acid system in active dissolution region.

Electrochemical Impedance Spectroscopy

Electrochemical impedance spectroscopy is a precise technique used to investigate the electrochemical (dissolution) occurrence in a particular system. To compare and explicate the mechanism of Co anodic dissolution in 1wt. % H_2O_2 and 1 wt. % H_2O_2 + 0.02M oxalic acid system at pH 9, the experiments were performed at 3 different over potentials +0.10 V, +0.30 V and +0.50 V w.r.t. OCP as marked A, B and C in Figure 4.4.2. From the EIS plots illustrated in Figure 4.4.5, it can be seen that two loops i.e. a capacitance loop at higher frequency and an inductance loop at lower frequency were observed for both the systems at all the overpotentials being investigated. The capacitance loop is associated with the charge transfer resistance and electrical double layer. Whereas, the faradic and non-faradic reactions processes occurring between the interface of the metal and the bulk solution give rise to inductance loop at lower frequency. The curtailment in the total impedance w.r.t to the increase in DC potentials for

both the systems depicts that the passivation layer is not formed on the Co surface. Besides, the total impedance is lower in the presence of oxalic acid at any given overpotential which indicates the higher dissolution of metal with the addition of oxalic acid. Further, the impedance data is analyzed using various approaches as described herewith.

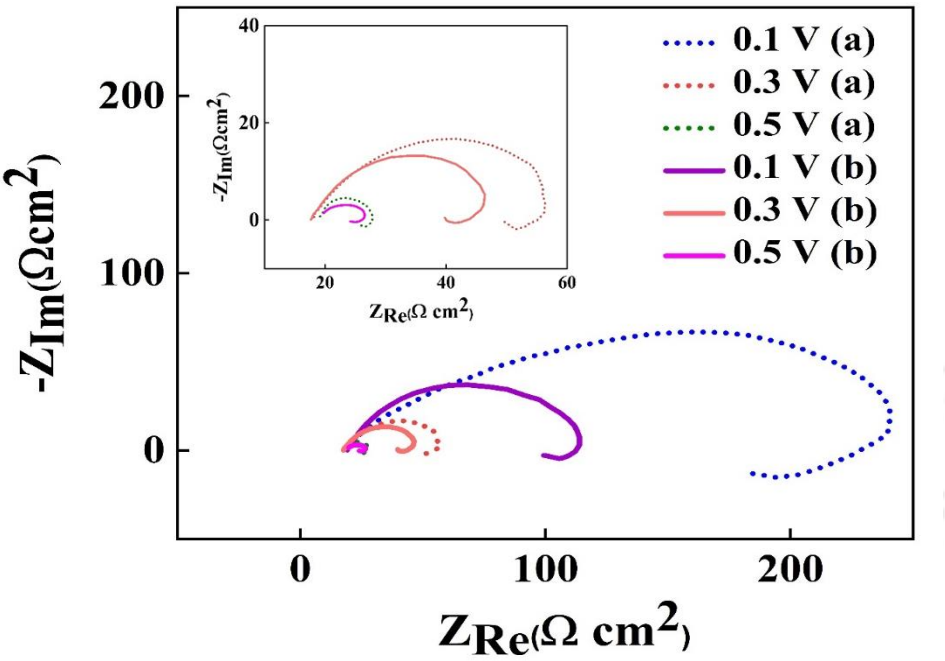

Figure 4.4. 5. EIS data of Co treated in (a) 0.1wt.% H_2O_2 and (b) 0.1wt.% H_2O_2 + 0.02 M oxalic acid at pH 9

Electrical Equivalent Circuit Analysis

The validation of linearity and stability of the EIS data obtained were done with Kramers Kroing transform (KKT) using Nova software. It was observed that the KKT maps fits well with the experimental impedance data (results not displayed here). The impedance data obtained were than analyzed using electrical equivalent circuit model fitting(EEC).(Maddala *et al.*, 2010; Baranwal and Rajaraman, 2019a; Paul and Srinivasan, 2020; Talukdar and

Rajaraman, 2020) . The equivalent circuit proposed for the systems is illustrated in Figure 4.4.6(a) The EEC simulated and experimental EIS curve is displayed in Figure 4.4.6(b) and Figure 4.4.6(c) whereas the best fitted EEC parameters with percentage error of less than 5% between experimental and simulated data are displayed in Table 4.4.2. The parameters in the EEC model includes R_{sol} (solution resistance), R_1 (resistance associated with charge transfer reactions occurring at the metal-solution interface), CPE (constant phase element associated with electrical double layer) and Maxwell pair L and R_2 (inductance and resistance associated with relaxation of intermediate adsorbates). The CPE is defined by two parameters Y_{01} and n $_{as}$ shown in equation 4.4.21 and the "n" value lies between 0 (for pure resistor) and 1 (ideal capacitor). If the impedance spectrum shows depressed semicircle, the data could be modeled better by CPE instead of ideal capacitor.

$$CPE = \frac{1}{Y_{01}(j\omega)^{n_i}} \qquad [4.4.21]$$

Braggs equation expressed in equation 4.4.22 is employed to calculate the electrical double layer capacitance from the CPE element.

$$C_{dl} = \left[Y_0 \left(\frac{1}{R_S} + \frac{1}{R_{ct}} \right)^{n-1} \right]^{\frac{1}{n}} \qquad [4.4.22]$$

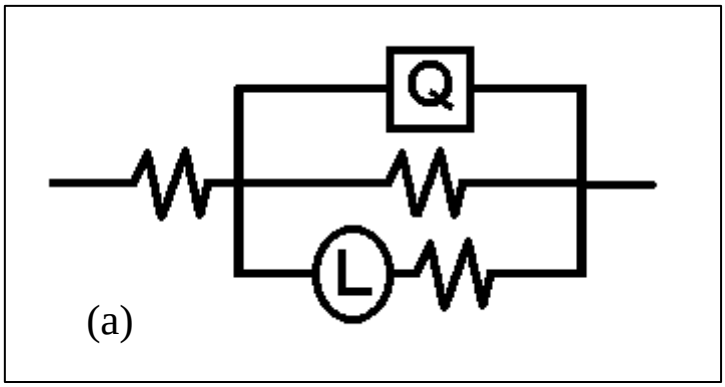

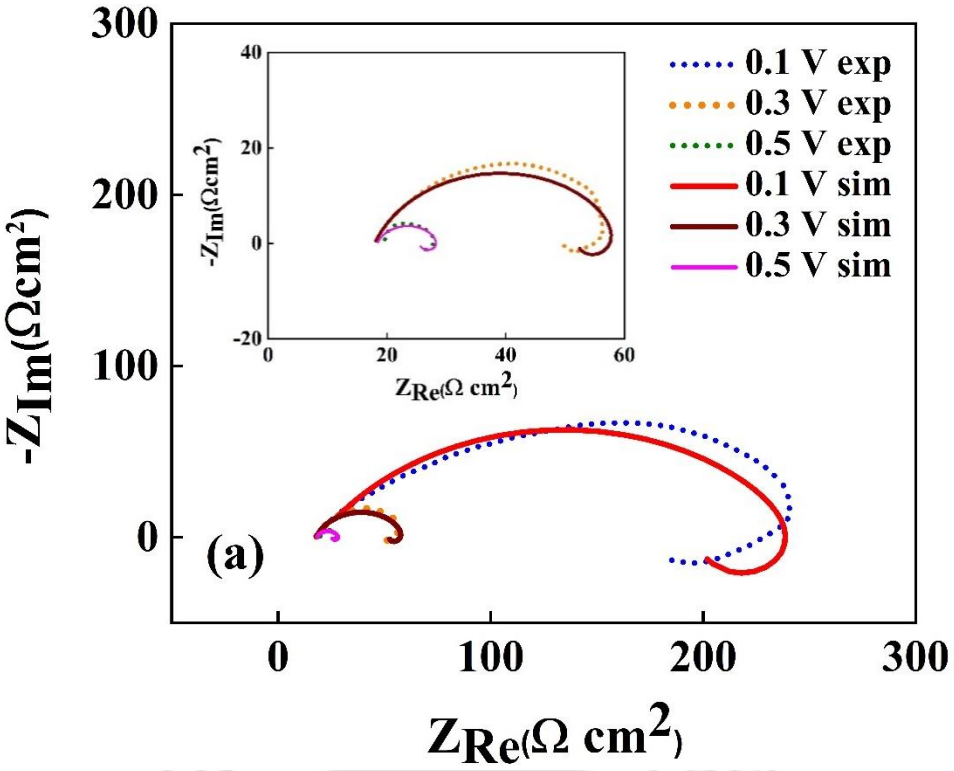

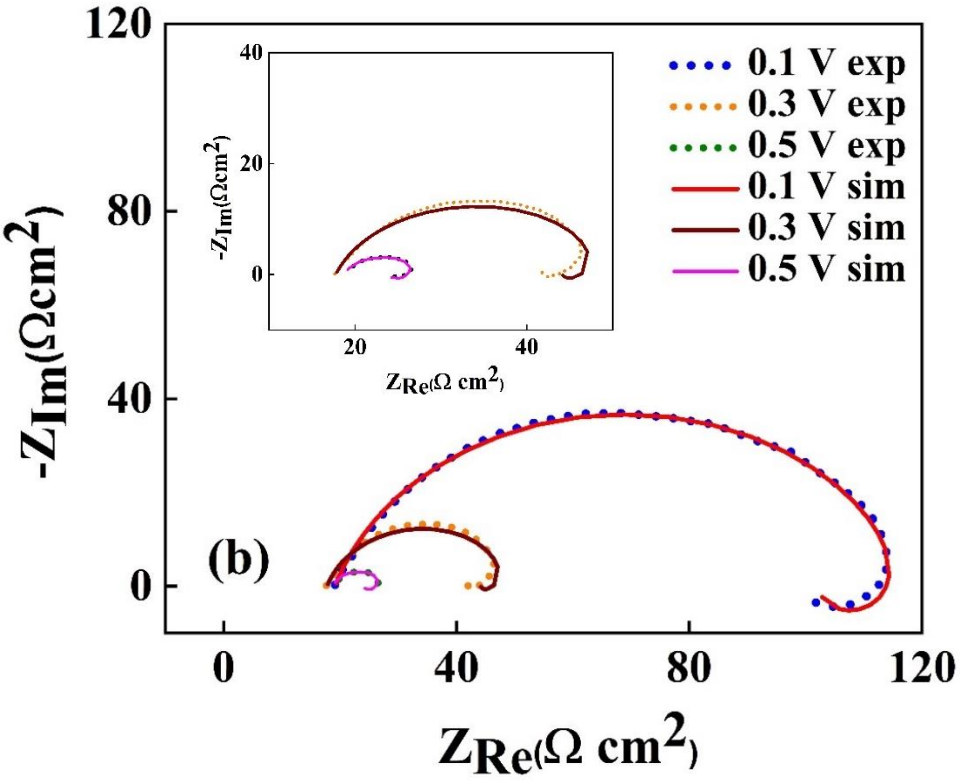

Figure 4.4. 6 (a) Proposed equivalent electrical circuit employed to simulate EIS data at different overpotentials w.r.t. OCP for both the systems. (b) Experimental and simulated EEC impedance plots in 1wt. % H_2O_2 (c) Experimental and simulated EEC impedance plots in 1wt. % H_2O_2 + 0.02M oxalic acid system (pH 9) at different DC potential applied over OCP.

Table 4.4. 2 EEC kinetic parameters obtained for Co dissolution in (a) 0.1wt.% H_2O_2 (b) 0.1wt.% H_2O_2 + 0.02 M oxalic acid at pH 9 at different overpotentials (0.1 V, 0.30 V, 0.50 V).

Parameters	**0.1 wt.% H_2O_2**			**0.1 wt.% H_2O_2 + oxalic acid**			**units**
	0.1 V	**0.3 V**	**0.5 V**	**0.1 V**	**0.3 V**	**0.5 V**	
R_{sol}	19.2	18.5	18.3	19.1	17.8	18.9	Ω cm^2
Y_{o1}	1.1 E-4	1.9 E-4	4.0E-4	1.2 E-4	1.7 E-4	1.9 E-4	Ω^{-1} cm^{-2}s^n
n_i	0.65	0.77	0.78	0.81	0.80	0.79	
R_1	234.3	42.6	10.3	99.8	33.6	6.0	Ω cm^2
L	157.6	15.7	2.9	116.3	2.3	0.01	H cm^2
R_2	796.2	176.3	23.2	502.5	124.60	1.9	Ω cm^2
R_p	179.6	34.3	7.1	83.3	26.5	1.5	Ω cm^2

From Table 4.4.2, it is evident that R_1 values decreasing with overpotential for both the systems. Thus, both the systems are in the active dissolution regime within the potential range investigated as observed in polarization measurements. Also, R_1 values for Co treated in H_2O_2 solution are higher compared to that of Co treated in H_2O_2+oxalic acid for all the three overpotentials being studied. This validates the higher dissolution rate with the addition of oxalic acid in to H_2O_2 solution. The "n" values are less than one at all conditions indicating an irregular surface post chemical treatment with these solutions. The active dissolution of Co via the formation of intermediate adsorbates and Co-oxalate complexes in H_2O_2 and H_2O_2 + oxalic acid solutions at pH 9 justifies the irregularity observed. The values of Maxwell pair L and R_2 decreases with overpotential for both the systems. Polarization resistance (R_p), which can be

estimated from the Maxwell circuit by calculating the faradaic impedance value at zero frequency limit, is also given in Table 4.4.2. Higher R_p values of the H_2O_2 system signifies more adsorbed species present on the Co surface. Besides, positive R_p values for both the systems confirm the absence of passive layer on the metal surface. Again, these trends confirm the enhancement of dissolution in the presence of oxalic acid. Although EEC model fitting gives an insight idea about the dissolution process; detailed anodic dissolution along with total surface coverage of the adsorbed species cannot be explained using it. Hence, in order to get better understanding on reaction pathway, RMA was performed as discussed below.

Reaction Mechanism Analysis

Reaction mechanism analysis (RMA) method was carried out to get a clear picture of the reaction pathway (Keddam, Mottos and Takenouti, 1981; Maddala *et al.*, 2010; Lee *et al.*, 2016). Recently, Paul et.al(Paul and Srinivasan, 2020) studied the dissolution of Co in an alkaline glycine solution. They proposed a mechanism with catalytic step comprising of 4 adsorbed species i.e. 2 Co(II) and two Co (III) intermediates. However, in this work, the focus is on to investigate the impact of addition of complexing agent in the presence of strong oxidizer H_2O_2. Moreover, the impedance patterns observed in this work are different from their system.

Thus, the following mechanism {Refer equation (4.4.23 and 4.4.24)} is suggested to explain the impedance patterns observed for both H_2O_2 and H_2O_2 + oxalic acid solutions.

$$Co \underset{k_{-1}}{\overset{k_1}{\rightleftharpoons}} Co_{ad}^{+} \underset{k_{-2}}{\overset{k_2}{\rightleftharpoons}} Co_{ad}^{2+} \underset{k_{-3}}{\overset{k_3}{\rightleftharpoons}} Co_{ad}^{3+} \xrightarrow{k_4} Co_{sol}^{3+} \qquad [4.4.23]$$

$$Co_{ad}^{2+} \xrightarrow{k_5} Co_{sol}^{3+} \qquad [4.4.24]$$

In this multistep mechanism, three adsorbed intermediate species Co_{ad}^{+}, Co_{ad}^{2+} and Co_{ad}^{3+} with oxidation states +1, +2 and +3 respectively were considered for Co dissolution in these two

solutions. Based on Pourbaix diagram,(Pourbaix, 1974) Co^{3+} is considered as the dissolution species instead of $Co^{+}$and Co^{2+} at pH 9 and the applied potential. Paul et. al(Paul and Srinivasan, 2020) also proposed the mechanism with Co^{3+} as the dissolution species in alkaline condition.

Here, Co_{sol}^{3+} represents the dissolved metal ions. Co_{ad}^{2+} and Co_{ad}^{3+} corresponds to hydroxides, oxides and oxalates of Co (II) and Co (III) respectively. Here, kinetic rate constant, k_4 depicts the dissolution through chemical reaction whereas k_5 represents dissolution rate through electrochemical reaction. Unlike that of chemical reactions (k_4 step), it is assumed that the kinetic rate constant/parameters $(k_i, i = +1, -1, +2, -2, +3, -3, +5)$ of electrochemical reactions are related to voltage in an exponential manner.(Maddala *et al.*, 2010; Baranwal and Prasanna Venkatesh, 2017) The relation of the rate constants (electrochemical reactions) with voltage is given by the following equation:

$$k_i = k_{i0} e^{b_i V} \qquad [4.4.25]$$

where,

$$b_i = \pm \frac{\alpha n F}{RT} \qquad [4.4.26]$$

Here, for oxidation reaction (forward), b_i value is positive while for reduction reaction (reverse), it is is negative. k_{i0} (pre-exponential factor) and b_i are independent of applied DC potential. α stands for transfer coefficient (0≤ α ≤1), n for the number of electrons transferred in the rate determining step, F for faraday constant and, R and T for molar gas constant and temperature respectively.

While developing the equations using the proposed mechanism, the exponents of forward (i= +1 to +5) and backward reactions (i= -1 to -3) are taken as positive and negative respectively.(Maddala *et al.*, 2010) Only linear terms are taken into consideration as small

amplitude ac voltage signal is applied to enforce linear perturbations.(Gregori *et al.*, 2006; Maddala *et al.*, 2010; Baranwal and Prasanna Venkatesh, 2017; Baranwal and Rajaraman, 2019b)

Unsteady state mass balance of adsorbed species Co_{ad}^{+}, Co_{ad}^{2+} and Co_{ad}^{3+} for the proposed mechanism are given by the following expressions:

$$\tau \frac{d\theta_1}{dt} = k_1(1-\theta_1-\theta_2-\theta_3) - k_2\theta_1 - k_{-1}\theta_1 + k_{-2}\theta_2 \quad [4.4.27]$$

$$\tau \frac{d\theta_2}{dt} = k_2\theta_1 - k_3\theta_2 - k_5\theta_2 - k_{-2}\theta_2 + k_{-3}\theta_3 \quad [4.4.28]$$

$$\tau \frac{d\theta_3}{dt} = k_3\theta_2 - k_4\theta_3 - k_{-3}\theta_3 \quad [4.4.29]$$

The current density (J) for the unsteady state is given by

$$J = nF\left[k_1\left(1-\theta_1-\theta_2-\theta_3\right) - k_{-1}\theta_1 + k_2\theta_1 - k_{-2}\theta_2 + k_3\theta_2 - k_{-3}\theta_3 + k_5\theta_2\right] \quad [4.4.30]$$

Here, "τ" denotes the entire active sites existing per unit area and "t" refers to time. θ_1, θ_2 and θ_3 represents the fractional steady state surface coverage values of the intermediate adsorbed species of Co_{ad}^{+}, Co_{ad}^{2+} and Co_{ad}^{3+} respectively whereas, $(1-\theta_1-\theta_2-\theta_3)$ denotes the empty sites. The surface coverage is assumed to be 1. As reported in literature, all the adsorption models lead to a fixed a time constant and in the proposed mechanism, Langmuir adsorption isotherm model was adopted.(Keddam, Mottos and Takenouti, 1981)

The steady state (denoted by subscript "ss"), mass balance of the adsorbed species, Co_{ad}^{+}, Co_{ad}^{2+} and Co_{ad}^{3+} for the proposed mechanism are given by the following expressions:

$$k_1(1-\theta_{1ss}-\theta_{2ss}-\theta_{3ss}) + k_{-2}\theta_2 = k_2\theta_{1ss} + k_{-1}\theta_{1ss} \quad [4.4.31]$$

$$k_2\theta_{1ss} + k_{-3}\theta_{3ss} = (k_3 + k_5 + k_{-2})\theta_{2ss} \quad [4.4.32]$$

$$k_3\theta_{2ss} = \left(k_4 + k_{-3}\right)\theta_{3ss} \qquad [4.4.33]$$

Simplifying in terms of θ_{1ss} , θ_{2ss} and θ_{3ss} (surface coverage steady state), equations (4.4.31-4.4.33) can be written as

$$\theta_{1ss} = \frac{k_1\left(k_3k_4 + k_4k_5 + k_4k_{-2} + k_5k_{-3} + k_{-2}k_{-3}\right)}{D} \qquad [4.4.34]$$

$$\theta_{2ss} = \frac{k_1k_2\left(k_4 + k_{-3}\right)}{D} \qquad [4.4.35]$$

$$\theta_{3ss} = \frac{k_1k_2k_3}{D} \qquad [4.4.36]$$

Here,

$$D = k_4\left(k_1 + k_{-1}\right)\left(k_3 + k_5 + k_{-2}\right) + k_1k_2\left(k_3 + k_4\right) + k_2k_{-3}\left(k_1 + k_5\right) + k_2k_4\left(k_3 + k_5\right) + \left(k_1 + k_{-1}\right)\left(k_5k_{-3} + k_{-2}k_{-3}\right)$$

The current density (J) at steady state conditions is given by

$$J_{ss} = nF\left[3(k_4\theta_{3ss} + k_5\theta_{2ss})\right] \qquad [4.4.37]$$

To determine the faradic impedance, the current density is differentiated by voltage which is presented in the following equation

$$\frac{dJ}{dV} = (Z_{F,m/s})^{-1} = nF\left[\begin{array}{l}\frac{dk_1}{dV}(1-\theta_{1ss}-\theta_{2ss}-\theta_{3ss}) + k_1\left(-\frac{d\theta_1}{dV}-\frac{d\theta_2}{dV}-\frac{d\theta_3}{dV}\right) - \frac{dk_{-1}}{dV}\theta_{1ss} - k_{-1}\frac{d\theta_1}{dV} + \frac{dk_2}{dV}\theta_{1ss} \\ +k_2\frac{d\theta_1}{dV} - \frac{dk_{-2}}{dV}\theta_{2ss} - k_{-2}\frac{d\theta_2}{dV} + \frac{dk_3}{dV}\theta_{2ss} + k_3\frac{d\theta_2}{dV} - \frac{dk_{-3}}{dV}\theta_{3ss} - k_{-3}\frac{d\theta_3}{dV} + \frac{dk_5}{dV}\theta_{2ss} + k_5\frac{d\theta_2}{dV}\end{array}\right]$$

Rearranging it, the faradic impedance in terms of charge transfer resistance can be written as

$$(Z_{F,m/s})^{-1} = R_t^{-1} - nF\left[\frac{d\theta_1}{dV}\left(k_1 + k_{-1} - k_2\right) + \frac{d\theta_2}{dV}\left(k_1 + k_{-2} - k_3 - k_5\right) + \frac{d\theta_3}{dV}\left(k_1 + k_{-3}\right)\right] \qquad [4.4.38]$$

Here,

$$R_t^{-1} = nF\left[k_1 b_1\left(1-\theta_{1ss}-\theta_{2ss}-\theta_{3ss}\right)-k_{-1}b_{-1}\theta_{1ss}+k_2 b_2\theta_{1ss}-k_{-2}b_{-2}\theta_{2ss}+k_3 b_3\theta_{2ss}-k_{-3}b_{-3}\theta_{3ss}+k_5 b_5\theta_{2ss}\right]$$

[4.4.39]

Applying Taylor's approximation, $\frac{\mathrm{d}\theta_1}{\mathrm{d}V}$, $\frac{\mathrm{d}\theta_2}{\mathrm{d}V}$ and $\frac{\mathrm{d}\theta_3}{\mathrm{d}V}$ are determined by expanding the mass balance equation (unsteady state). It is to be mentioned that in order to maintain linearity the terms of higher order are neglected.

$$\frac{d\theta_1}{dV} = \frac{AK\left(F_1 J_1 - GK\right)+BIF_1 J_1 - BIGK + BJ_1\left(KH - F_1 I\right)}{D_1 K\left(KH - F_1 I\right)+KE\left(AK+BI\right)} \quad [4.4.40]$$

$$\frac{d\theta_2}{dV} = \frac{KE\left(\frac{d\theta_1}{dV}\right)-F_1 J_1 + GK}{KH - F_1 I} \quad [4.4.41]$$

$$\frac{d\theta_3}{dV} = \frac{IKE\left(\frac{d\theta_1}{dV}\right)-IF_1 J_1 + IGK - J_1\left(KH - F_1 I\right)}{K\left(KH - F_1 I\right)} \quad [4.4.42]$$

Here,

$$n = 1 \quad [4.4.43]$$

$$A = k_1 - k_{-2} \quad [4.4.44]$$

$$B = k_1 \quad [4.4.45]$$

$$C = k_1 b_1 - \left(k_1 b_1 + k_2 b_2 + k_{-1} b_{-1}\right)\theta_{1ss} - \left(k_1 b_1 - k_{-2} b_{-2}\right)\theta_{2ss} - k_1 b_1 \theta_{3ss} \quad [4.4.46]$$

$$D_1 = k_1 + k_2 + k_{-1} + j\omega\tau \quad [4.4.47]$$

$$E = k_2 \quad [4.4.48]$$

$$F_1 = k_{-3} \quad [4.4.49]$$

$$G = k_2 b_2 \theta_{1ss} - \left(k_3 b_3 + k_5 b_5 + k_{-2} b_{-2}\right)\theta_{2ss} + k_{-3} b_{-3} \theta_{3ss} \quad [4.4.50]$$

$$H = k_3 + k_5 + k_{-2} + j\omega\tau \quad [4.4.51]$$

$$I = k_3 \quad [4.4.52]$$

$$J_1 = \left(k_4 b_4 + k_{-3} b_{-3}\right)\theta_{3ss} - k_3 b_3 \theta_{2ss} \quad [4.4.53]$$

$$K = k_4 + k_{-3} + j\omega\tau \quad [4.4.54]$$

Thus, the total impedance (Z_t) of the system is specified by

$$Z_{total} = R_{sol} + \frac{1}{\left(Z_{F,m/s}\right)^{-1} + (j\omega)^{n_i} Y_0} \quad [4.4.55]$$

Here, R_{sol} stands for solution resistance; Y_0 and n_i corresponds to parameter and exponent of constant phase element (CPE) respectively.

Table 4.4. 3 Best fit RMA parameters obtained from simulation of the proposed Co dissolution in (a) 0.1wt.% H_2O_2 (b) 0.1wt.% H_2O_2 + 0.02 M oxalic acid at pH 9.

Parameters	0.1 wt.% H_2O_2	0.1 wt.% H_2O_2 + oxalic acid	units
F	96500	96500	C
R_{sol}	19	19	Ω cm^2
k_{10}	1.0E-10	5.0E-09	mol s^{-1} cm^{-2}
b_1	32	6.7	V^{-1}
k_{-10}	1.0E-02	5.0E-10	mol s^{-1} cm^{-2}
b_{-1}	-17.7	-9.9	V^{-1}
k_{20}	9.9E-03	1.0E-02	mol s^{-1} cm^{-2}
b_2	1.1	2.8	V^{-1}
k_{-20}	1.0E-12	1.0E-12	mol s^{-1} cm^{-2}
b_{-2}	0	-14	V^{-1}
k_{30}	9.0E-10	1.0E-09	mol s^{-1} cm^{-2}
b_3	8.5	4.2	V^{-1}
k_{-30}	2.0E-06	1.0E-12	mol s^{-1} cm^{-2}
b_{-3}	-6.4	-7.9	V^{-1}
k_{40}	3.0E-09	1.0E-08	mol s^{-1} cm^{-2}
b_4	0	0	V^{-1}
k_{50}	2.0E-10	1.0E-08	mol s^{-1} cm^{-2}
b_5	8.9	7.1	V^{-1}
T	1.8E-03	1.0E-02	mol cm^{-2}

The RMA parameters are illustrated in Table 4.4.3 are obtained by sequential quadratic programming (SQP). The optimization was performed is MATLAB platform with the objective of getting a minimum residue which is given in the following equation

$$Residue = \sum \left[\left(Z_{Re_{experimental}} - Z_{Re_{bestfit}} \right)^2 + \left(Z_{Im_{experimental}} - Z_{Im_{bestfit}} \right)^2 \right] \quad [4.4.56]$$

The detailed derivation process of obtaining impedance equations for given mechanism are presented in literature. (Keddam, Mottos and Takenouti, 1981; Bojinov, 1996)

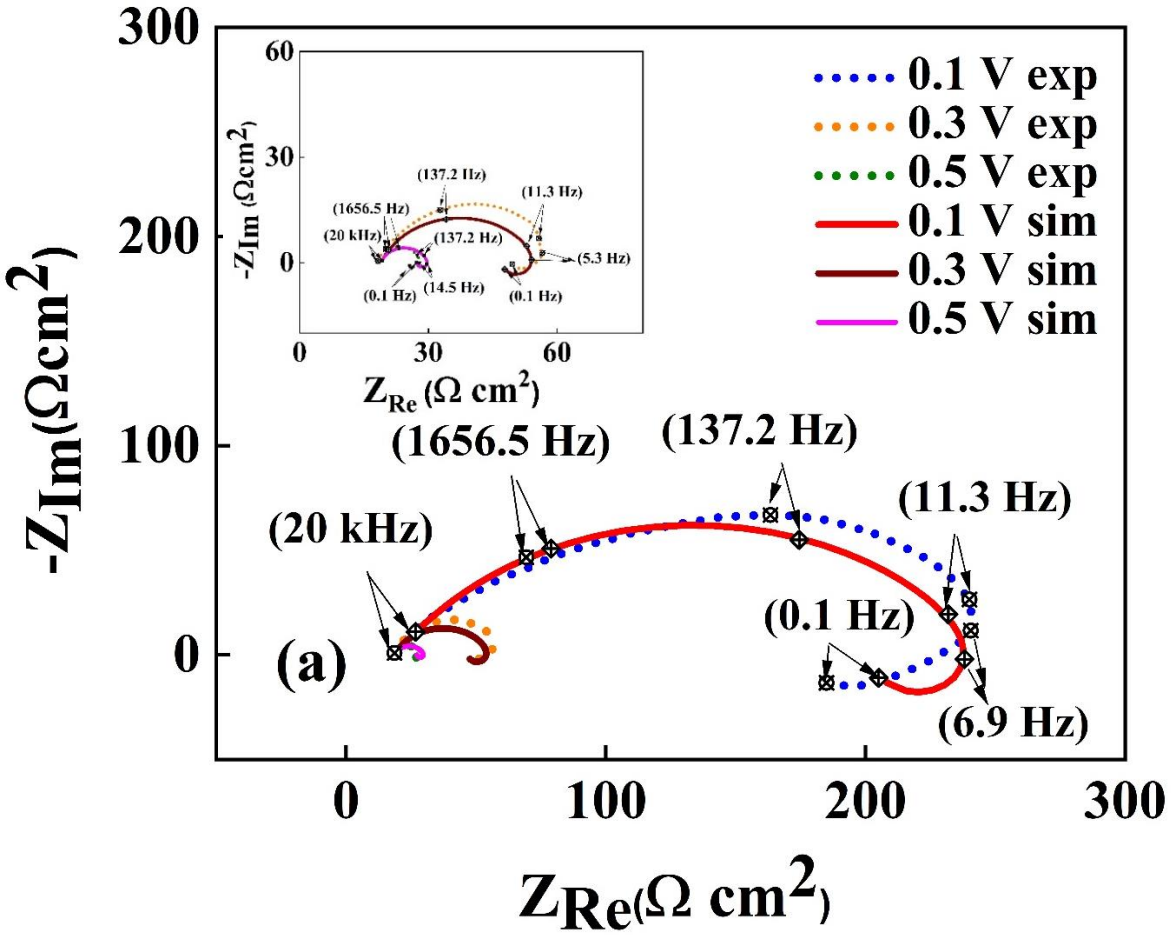

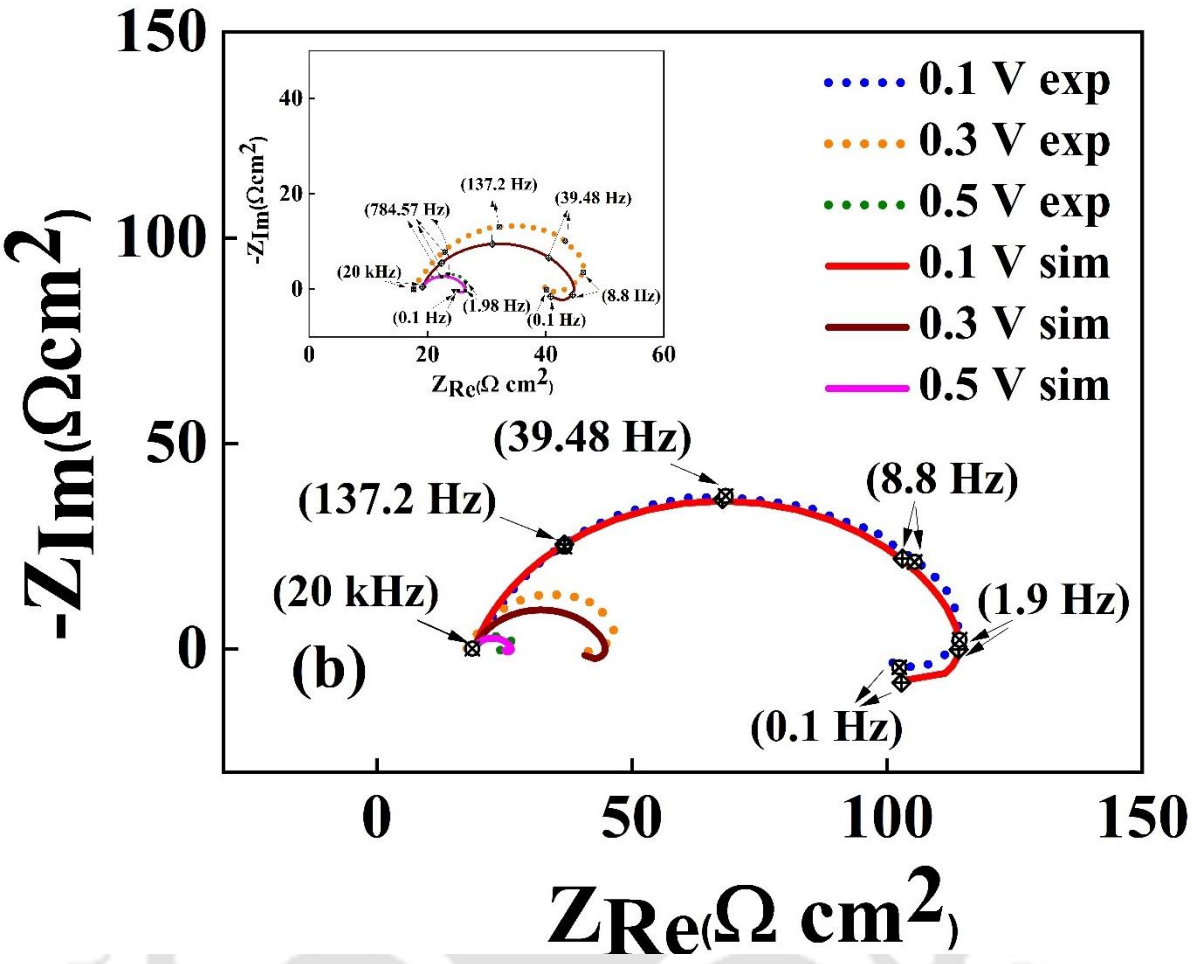

Figure 4.4. 7 Experimental and best fit simulated RMA impedance plots in (a) 1wt. % H_2O_2 (b) 1wt. % H_2O_2 + 0.02M oxalic acid system (pH 9) at different DC potential applied over OCP.

The simulated impedance data from the equation (4.4.55) are displayed in Figure 4.4.7a and 4.4.7b along with experimental data. It is seen that the modelled data fits quite well with the experimental data. Especially, the impedance patterns and the qualitative trends observed in both impedance and polarization experiments (i.e. the rate at which current density increases in polarization measurements for both the systems, the decrease in impedance w.r.t overpotential for both the systems and the lower impedance with the addition of complexing agent at any given overpotential) are well captured by the suggested mechanism. The optimized

RMA parameter at which minimum residue obtained are displayed in Table 4.4.3. The CPE parameter values obtained in EEC modelling are utilized in RMA simulation.

The fractional surface coverage of the various intermediate adsorbates is estimated from the RMA parameters. As expected, the surface coverage of Co_{ad}^{+} is negligible due to the higher k_2 values compared to k_1 values for both the system. Co_{ad}^{+} are generally unstable in nature and hence thermodynamically not favored. This attributes to the reason behind unavailability of Co^{+} products during XPS analysis.

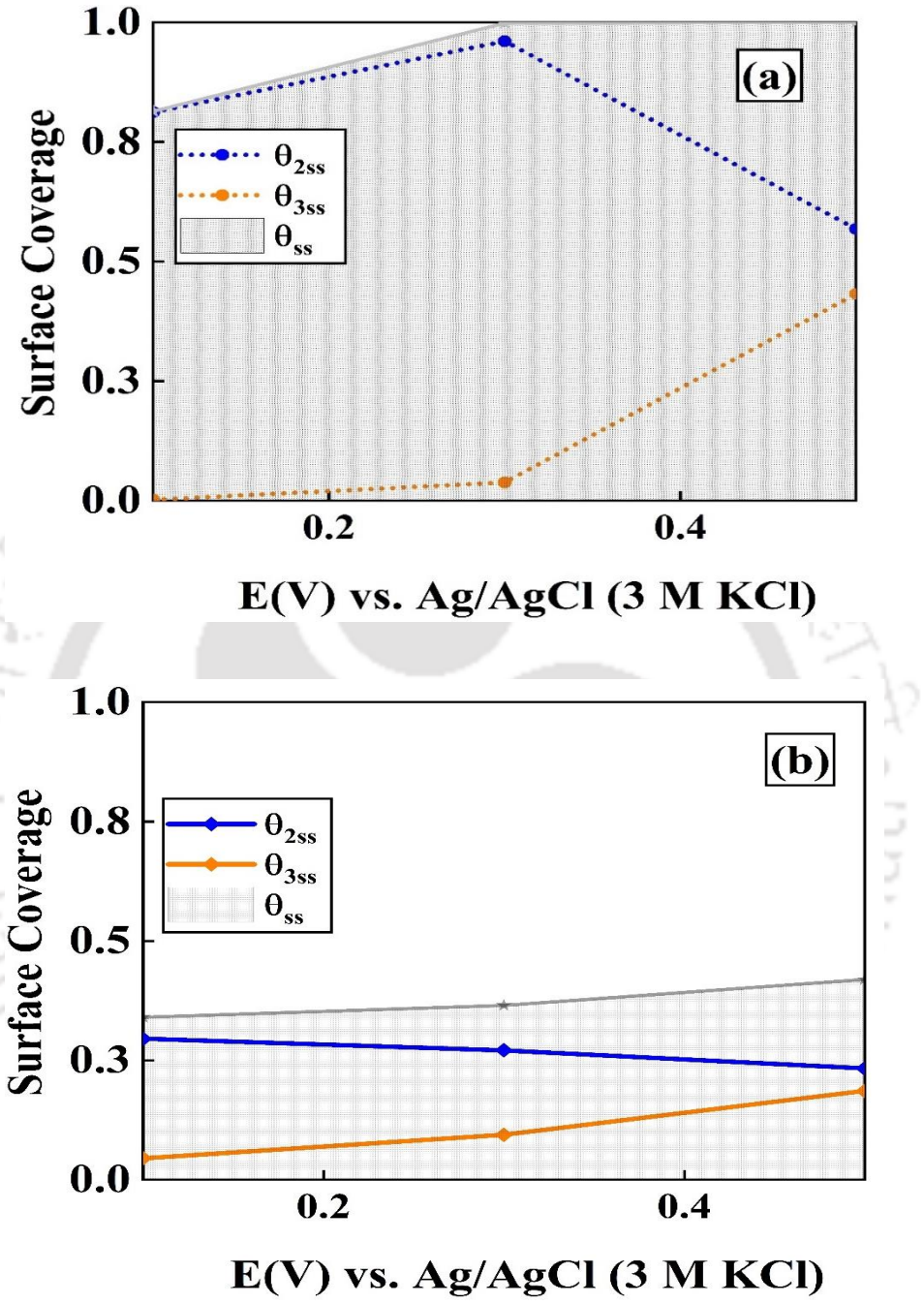

Figure 4.4. 8 Surface coverage of Co adsorbed species (a) 1wt. % H_2O_2 and (b) 1wt.% H_2O_2 + 0.02M oxalic acid system (pH 9) for the proposed mechanism.

The variation of Co_{ad}^{2+} and Co_{ad}^{3+} w.r.t. overpotential is shown in Figure 4.4.8. It is evident from this figure that the surface coverage of Co in H_2O_2 solution is significantly higher compared to that one observed in H_2O_2+oxalic acid solution at all overpotentials. Especially in H_2O_2 solution, the surface coverage approaches to one with the increase in overpotential. Being a strong oxidizer, H_2O_2 oxidizes the Co metal to Co^{2+} and Co^{3+}. However, the dissolution rate of these species is lower in the absence of complexing agent and hence it starts occupying the metal surface. But, in the presence of a complexing agent and oxidizer, simultaneous occurrence of oxidation and complexation processes (The oxalate ion ($C_2O_4^{2-}$) reacts with the Co_{ad}^{2+} and Co_{ad}^{3+} species to form highly soluble Co-oxalate complexes) leads to lower surface coverage (0.35 and 0.42 at overpotentials of 0.1 V and 0.5 V respectively) and eventually higher dissolution rate. Besides, at all over potential, the θ_{2ss} is higher than θ_{3ss} for both the systems. However, at higher overpotential, the tendency of Co^{2+} to get converted into Co^{3+} gets higher as evident from Figure 4.4.8.

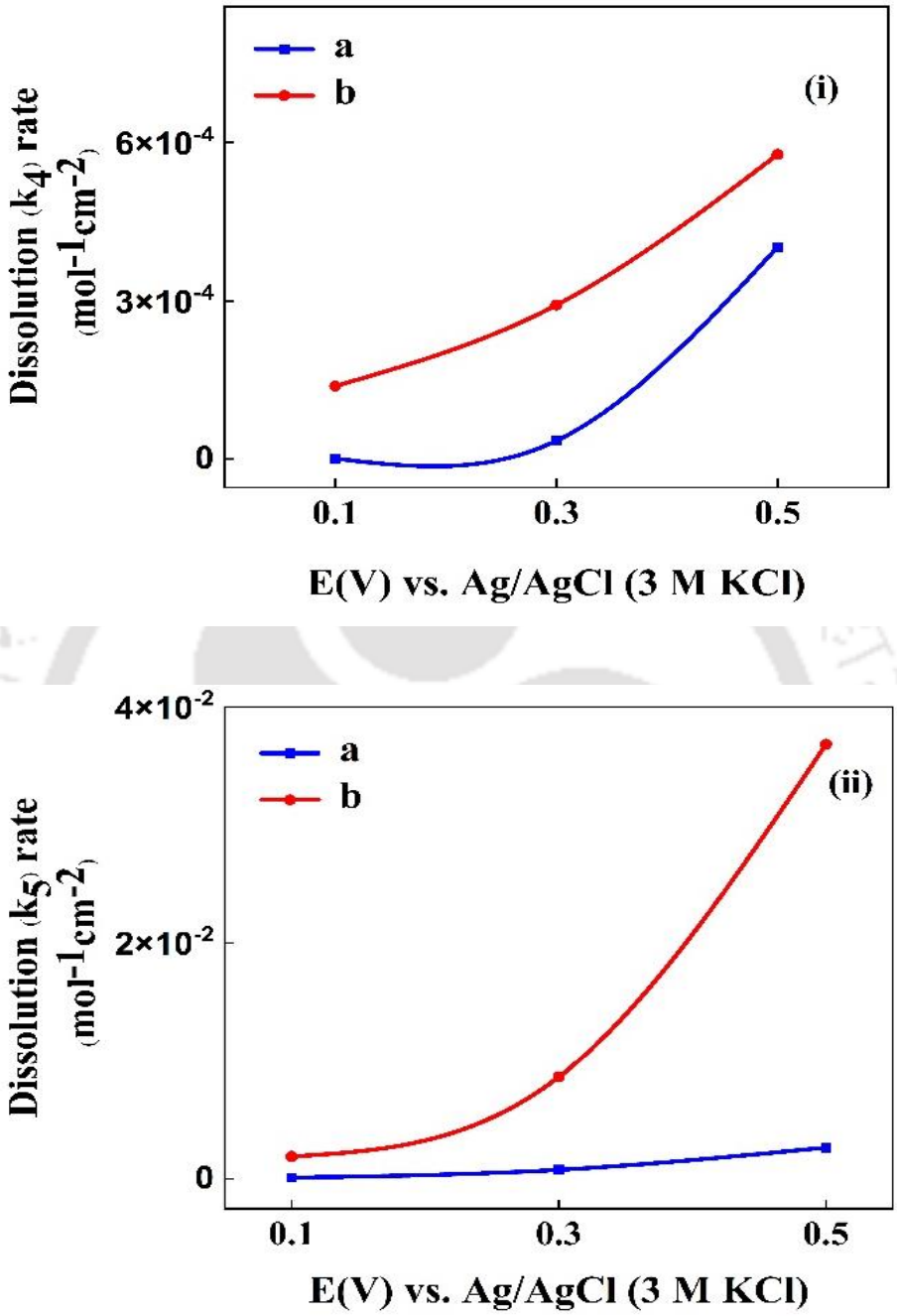

Figure 4.4. 9 Dissolution rate via (i) chemical steps and (ii) electrochemical steps in (a) 1wt. % H_2O_2 and (b) 1wt.% H_2O_2 + 0.02M oxalic acid system (pH 9).

On the addition of oxalic acid to the system, an enhanced dissolution via both k_4 and k_5 is observed. However, the effect is more prominent via k_5 pathway. This is likely due to the presence of higher Co^{2+} on the surface for both the systems at any given overpotentials. Unlike in k_4 dissolution step, the difference in dissolution rate via k_5 step between the two solutions of interest significantly changes with overpotential as clearly observed from Figure 4.4.9b. Hence, the observed change in current densities w.r.t DC potential in the polarization curve (Figure 4.4.10) is prominently due to the effect of dissolution via the electrochemical step (k5).

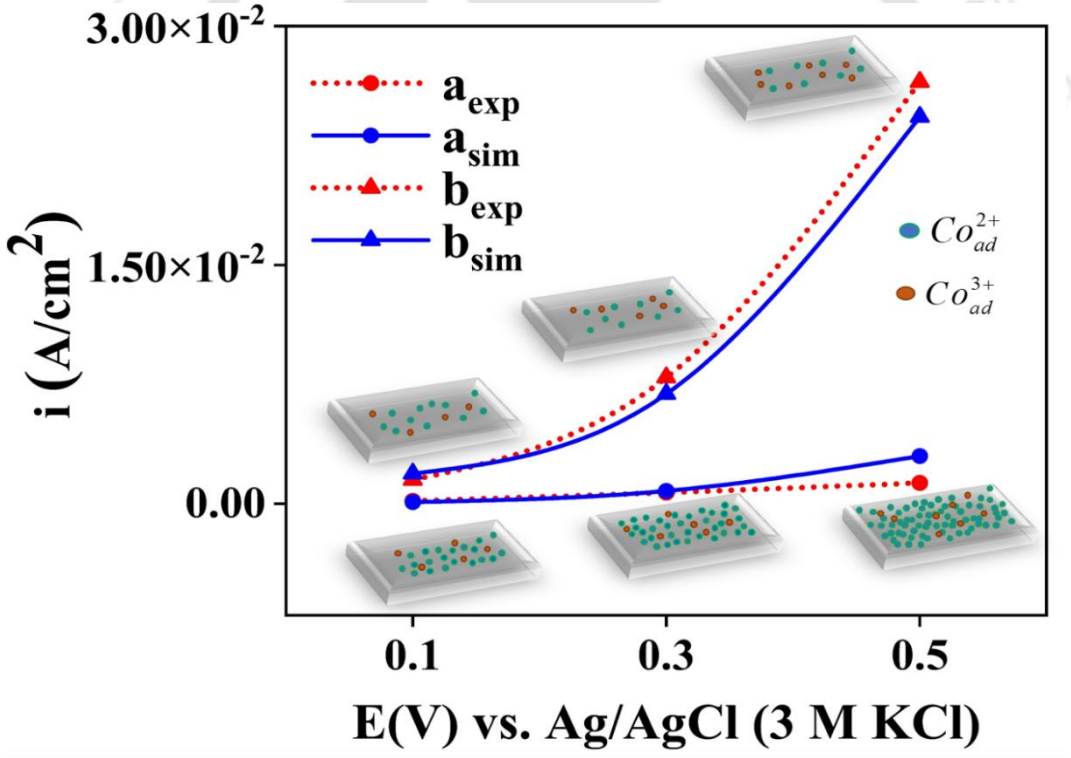

Figure 4.4. 10 Anodic current density simulated vs experimental (a) 1wt. % H_2O_2 (b) 1wt. % H_2O_2 + 0.02M oxalic acid system (pH 9) at different DC potential applied over OCP. Schematics of the metal surface covered with different species at different overpotential are also displayed herewith.

The current density values obtained from the suggested model are comparable with the anodic polarization curve and the same is displayed in Figure 4.4.10. This confirms that the suggested mechanism satisfactorily fits well (polarization, eis data) for both the systems. This suggested mechanism properly illustrates the kinetics of Co dissolution on the addition of oxalic acid as complexing agent to H_2O_2 system. The mechanism is schematically explained in Figure 4.4.11.

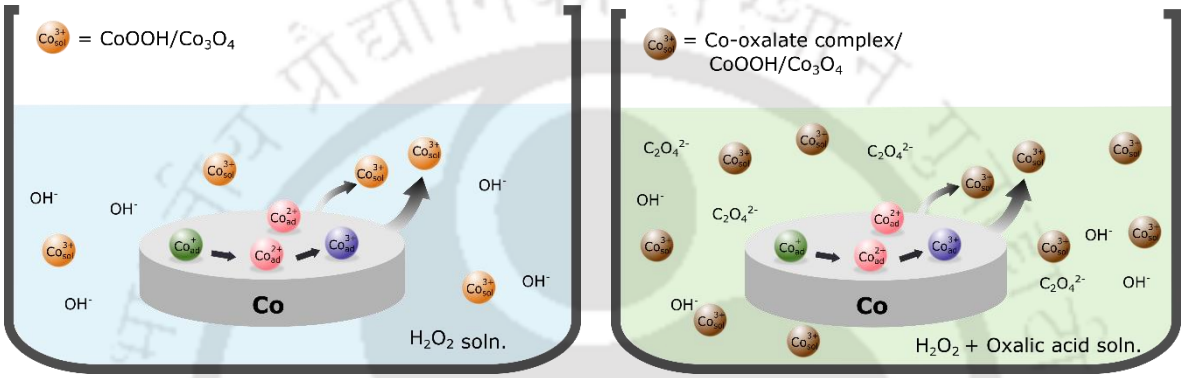

(a) (b)

Figure 4.4. 11 Schematics of Co treated in 0.1wt.% H_2O_2 and 0.1wt.% H_2O_2 + 0.02 M oxalic acid at pH 9

4.4.4 Conclusion

The anodic dissolution of Cobalt in alkaline solutions containing H_2O_2 as oxidizer with and without oxalic acid as complexing agent is investigated in this study. The anodic polarization curves reveal that slope of DC current vs DC potential is significantly higher for H_2O_2+oxalic acid compared to that of H_2O_2 system. This signifies that oxalic acid enhances the dissolution of Co by forming complexes. XPS results confirms the presence of Co-oxalate complexes along with oxides (Co_3O_4/CoOOH) on treating Co in H_2O_2+oxalic acid. Both the systems exhibit same EIS patterns of comprising of 2 loops: capacitance loop arising from higher frequency and inductance loop arising from lower frequency. A multi-step mechanism

comprising of 3 adsorbed species with 2 dissolution paths is suggested for both the systems. It is observed that dissolution is mainly favored by the electrochemical step with Co^{2+} covering the more surface area. An enhanced dissolution is observed at higher over potentials due to the increase in oxidation of Co^{2+} to Co^{3+} .The proposed mechanism satisfactorily explains the anodic polarization and impedance data.

CHAPTER 5

5. SUMMARY, CONCLUSION AND FUTURE SCOPE

5.1 Summary of the study done

With the reduction of microelectronic devices to lower nodes, fabricating the precise structures has become an unavoidable task. To overcome such challenges and attain a planar surface for further level metallization, Chemical Mechanical Planarization was opted.

In order to complete a circuit, the active and passive elements are connected with interconnect Cu. However, a major challenge Cu faces is that it has poor adhesion to the dielectric materials, i.e. it is highly mobile and liable to diffuse into dielectric material. This deteriorates the device performance. Thus, to resolve these issues, a barrier is introduced between the Cu and the dielectric. Ta/TaN is one such metal that has been used as a barrier material to prevent the diffusion of Cu into the dielectric material.

However, with the shrinkage of the technology node to 10 nm and below, maintaining the diffusion barrier property and the desired thickness at the same time has become a major challenge. Therefore, various other barrier metals were studied in order to substitute this existing one. Recently as per study, Co(Nishizawa, Nojo and Isobe, 2010b; Peethala *et al.*, 2012) and Ru(Peethala, Roy and Babu, 2011a; Yadav, Jitendra C. Bisen, *et al.*, 2017) are considered as two of the most potency metals to act as barrier metal because of its many properties such as lower resistivity, good stability, better adhesion properties with Cu. After the deposition of interconnect Cu and barrier metal, the structures demand for a planar topography for the following level metallization, for which CMP is opted. CMP being a 2-step process, the initial step involved is removal of bulk Cu whereas the second step involved is removal of the surplus Cu along with barrier metal without excessive thinning. This calls for

the requirement of a CMP slurry that would give a Cu/barrier metal removal rate selectivity of ~1:1.

Although many types of slurry have been proposed for Cu CMP most of them were tilted towards higher selectivity between Cu and Ta. Slurry formulation for Co/Cu and Co/Cu is almost negligible. In addition to that, the very limited slurry developed till date for polishing Cu and Ru, Cu and Co possess various issues such as galvanic corrosion, selectivity etc.

Hence, in this context, a solution for Ru/Cu CMP (can also be employed for bulk removal of advanced Ru interconnects) was proposed by introducing potassium iodate (KIO_3) as the oxidizer along with silica abrasives and 1,2,3 Benzotriazole (BTA) as corrosion inhibitor for practicable wet operations such as etching and CMP and reduced oxidation. The amount of abrasives silica employed in the proposed slurry is relatively low (concentration reduced by 60 %), thereby reducing the possibility of any post-CMP issues.

The few slurry formulations proposed for Co / Cu system in literature, were oriented either towards selectivity or towards reducing galvanic corrosion. Studies referring to obtain desired selectivity of ~1:1 for Co/Cu along with reduced galvanic corrosion and high polish rate: static etch ratio are limited in the literature. Hence, silica-based polishing slurries to attain Co/Cu RR selectivity ratio of 1:1 (with good removal rates and lower etch rates) and reduced corrosion potential gap of a Co-Cu galvanic couple were formulated and reported in the study.

It is to be noted that the kinetics and mechanistic reaction pathway of Co in carbonate/bicarbonate, glycine etc. are investigated and reported in literature, however, the Co anodic dissolution mechanism in H_2O_2 (oxidizer) solution (solution of interest) is yet to be studied. Reaction mechanistic analysis of Co in H_2O_2 solution in the presence of a complexing agent (oxalic acid) is also not reported in any literature to the best of our knowledge. Therefore, the work presented here focuses on comparing the physio-chemical characteristics of Co metal upon exposure to only H_2O_2 solution and to H_2O_2—oxalic acid solution. Various

electrochemical experiments such as anodic polarization, electrochemical impedance spectroscopy (EIS) were performed to understand the anodic dissolution behavior. Also, both electrical equivalent circuit (EEC) and reaction mechanism analysis (RMA) were performed on EIS data to retrieve the kinetics of Co anodic dissolution.

The first objective of the study is to formulate a slurry that would give a desired Ru-Cu removal rate selectivity of 1:1 with good removal rate. Hence, the effects of different components: KIO_3 as oxidizer, silica as abrasives and BTA as inhibitor on removal rate of Ru-Cu were investigated which are illustrated in Figure 4.1.2(a), Figure 4.1.4 and Figure 4.1.5. The dissolution nature of the Ru and Cu in the proposed oxidizer, KIO_3 were also studied (Figure 4.1.3) and were found to be endothermic in nature. Also, it was seen that the dissolution followed an associative mechanism thereby forming activated complexes in the presence of KIO_3. This explains the reason behind lower etch rates observed in the presence of oxidizer KIO_3 as seen in Figure 4.1.2(b). The TGA analysis (Figure 4.1.6 and Figure 4.1.10a) were done to study the interaction of different additives and correlate its effect on the removal rates obtained. Polarization studies were performed to understand the inhibiting property of BTA (Figure 4.1.8). A reaction pathway was schematically presented to explain the inhibition property of BTA in the form of adsorbed BTA complex of the metal surface (Figure 4.1.7). The effect of process parameters on RR was examined and it was seen that the proposed slurry follows a non-Prestonian behavior (Figure 4.1.11). The different abrasives (Figure 4.1.10b) and inhibitors (Figure 4.1.9) were studied, however slurry comprising of fumed silica (2 wt. %), KIO_3 (0.2 M) and BTA (5 mM) gave a desired Cu-Ru selectivity of ~1:1.03, making it apt for effective polishing of barrier metal and interconnect.

As second part of the objective, slurry that would give a desired removal selectivity for Co-Cu was formulated. The effect of NaOCl as oxidizer and BTA as inhibitor on Co and Cu dissolution and RR were investigated, the results were displayed in Figure 4.2.1, Figure 4.2.2,

Figure 4.2.4 and Figure 4.2.5. The higher RR observed at acidic region attributed to direct dissolution of the metal whereas lower RR obtained at the alkaline region is due to the formation of passive layer on the metal surface. The formation of passive layer for Co in the form of Co $(OH)_2$ was confirmed by XRD analysis (Figure 4.2.9). It was seen that the addition of fumed silica enhanced the RRs of the metals (Figure 4.2.3). A desired Co-Cu RR selectivity of ~1:1.006 was achieved on using 2 wt. % silica, 0.5 wt.% NaOCl and 5mM BTA slurry at pH 9 (Figure 4.2.4). The tailored slurry gave a RR of ~ 99.1 nm min−1 for Cu and ~ 99.7 nm min−1 for Co respectively. In addition to that, using the tailored slurry, no significant impact of process parameters on selectivity was observed (Figure 4.2.6 and Figure 4.2.7). Based on the findings, the chemical reactions occurring on the Co metal surface were postulated.

Cu being more noble in nature as compared to Co, in a Cu-Co couple, Cu acts as anode whereas Co acts as cathode. The high potential difference obtained in DI water at pH 9 confirms the occurrence of galvanic corrosion (Figure 4.3.2). Galvanic corrosion being a major concern in the semiconductor industry, in the third objective of the study a slurry is formulated that would reduce the galvanic corrosion and give a desired Co-Cu RR selectivity. Addition of 0.1 wt.% H_2O_2 as oxidizer to DI water significantly reduced the potential gap from ~279 mV to ~49 mV (Figure 4.3.4). However, using only H_2O_2 also with silica abrasives gave lower RRs with a RR selectivity of ~0.38 (Figure 4.3.7b). Hence, to enhance the removal rates, complexing agent oxalic acid was added to the solution. The carboxyl group of oxalic acid forms easily soluble complexes with the oxides on the metal surface thereby increasing the RRs of the metal coupons (Figure 4.3.7b). Addition of 0.02 M of oxalic acid to 0.1 wt.% H_2O_2 gave RRs selectivity (Figure 4.3.7b) and potential gap (Figure 4.3.9b) of ~1.95 and 60 mV respectively. To reduce the potential gap and galvanic current, 5ppm imidazole as corrosion inhibitor was added to the system. The use of imidazole along with 1 wt.% fumed silica + 0.1 wt.% H_2O_2 + 0.02 M oxalic acid desired selectivity of ~1.05:1 (Figure 4.3.7b). Also, the potential gap was

reduced to 12 mV, thus, making the slurry apt to be used in semiconductor industry. (Figure 4.3.9c) It was seen that although imidazole suppresses the anodic current for both the metals, its effect is more pronounced for Co. Formation of the metal compounds and complexes along with inhibition effect by imidazole in the presence of H_2O_2, oxalic and imidazole respectively were confirmed using FTIR analysis (Figure 4.3.5) and UV spectroscopy (Figure 4.3.6).

The fourth part of the objective is a comparative reaction mechanistic analysis of Co anodic dissolution with and without the presence of 0.02 M oxalic acid along with 0.1 wt.% H_2O_2 at pH 9. Hence, anodic polarization and EIS measurements were performed which illustrated in Figure 4.4.1 and Figure 4.4.5. It was seen that Co anodic dissolution rate is higher in H_2O_2 +oxalic acid system as compared to H_2O_2 system. Similar two looped impedance curves (higher frequency capacitance loop - charge transfer resistance and electrical double layer; lower frequency loop -faradic and non-faradic reactions processes occurring between the interface of the metal and the bulk solution) were observed for both the system. Based on the impedance curve trend, a combination of circuit elements was modelled and simulated at different overpotentials (Figure 4.4.6). The EEC parameters (Table 4.4.2) obtained justifies the findings quantitatively. To get a detailed understanding of the dissolution pathway, a multi-step mechanism for both the systems was proposed. Three intermediate adsorbates species Co_{ad}^{+}, Co_{ad}^{2+} and Co_{ad}^{3+} and two dissolution paths (chemical and electrochemical step) were considered for the proposed mechanism. Reaction mechanism analysis (RMA) approach was employed to analyze the kinetics of Co anodic dissolution. Based on the best fit RMA parameters (Table 4.4.3) it was confirmed that oxalic acid enhances dissolution of Co in the form of Co^{3+} ions. Surface coverage studies (Figure 4.4.8) and k_4 and k_5 values (Figure 4.4.9) confirm that dissolution is mainly favored by the electrochemical step (k_5) with Co^{2+} covering the more surface area on the metal surface. The simulated data fits well with the experimental anodic polarization data and EIS data, confirming that the mechanism proposed explains properly both

the system (Figure 4.4.7 and Figure 4.4.10). Surface morphologies studies were done using FESEM (Figure 4.4.2) and contact angle analysis (Figure 4.4.3) and the compounds formed were confirmed using XPS analysis (Figure 4.4.4). The corrosion observed is general corrosion.

5.2 Conclusion

The major conclusions that can be extracted from the thesis are:

- Solution comprising of fumed silica (2 wt. %), KIO_3 (0.2 M) and BTA (5 mM) gives a selectivity of Ru-Cu selectivity of ~1.03:1 and is appropriate for effective polishing of barrier metal and interconnect. The dissolution of the metals is endothermic in nature. Temperature and pH play an important role in RR. The system defies Prestonians equation.
- NaOCl (0.5 wt. %), fumed silica (2 wt. %), and BTA (5 mM) gives a Co-Cu a selectivity of ~1:1.006 at pH 9 with high RR and low SER. The process parameters do not have any significant impact on selectivity. Dissolution is low in the alkaline region due to formation of stable passive layer on the metal surfaces. However, the passivation and the removal process are quite dynamic is nature.
- Addition of oxalic acid (complexing agent) increased the RR of Co and Cu to a great extent by forming Co-oxalate and Cu-oxalate complexes. Corrosion potential difference (Cu_{Ecorr} - Co_{Ecorr}) was reduced to 12mV by using 0.1 wt.% H_2O_2 + 0.02M oxalic acid + 5ppm imidazole solution at pH 9. The proposed slurry also gave a Co/Cu selectivity ratio of 1.05:1 thus making it apt to be used for Co-Cu polishing in semiconductor industry.

- The multi-step mechanism with three intermediate adsorbates and two dissolution paths (chemical and electrochemical step) is suggested to explain the anodic dissolution behavior of Co in H_2O_2 solution both with and without oxalic acid:

$$Co \underset{k_{-1}}{\overset{k_1}{\rightleftarrows}} Co_{ad}^{+} \underset{k_{-2}}{\overset{k_2}{\rightleftarrows}} Co_{ad}^{2+} \underset{k_{-3}}{\overset{k_3}{\rightleftarrows}} Co_{ad}^{3+} \xrightarrow{k_4} Co_{sol}^{3+}$$

$$Co_{ad}^{2+} \xrightarrow{k_5} Co_{sol}^{3+}$$

- Oxalic enhances the dissolution of Co in the form of Co^{3+} ions. Dissolution is mainly favored by the electrochemical step with Co^{2+} covering the more surface area. An enhanced dissolution is observed at higher over potentials due to the increase in oxidation of Co^{2+} to Co^{3+}.

5.3 Future Scope

The findings of the thesis are summarized above and based on that future scope is proposed as follows:

- To understand adsorption of inhibitor elaborately.
- Detailed study about dissolution mechanism and adsorption mechanism at molecular level using molecular dynamics simulation and quantum chemical calculation.
- With the intensification in number of CMP steps associated with scaling down of device, generates new types of defects. This demands the need of effective new cleaning methods and development of novel post-CMP cleaning chemistries using non-conventional solutions at escalation.

THIS PAGE IS LEFT BLANK INTENTIONALLY

6. REFERENCES

Ã, K.M. *et al.* (2009) 'Galvanic Corrosion Control in Chemical Mechanical Polishing of Cu Interconnects with Ruthenium Barrier Metal Film', *Japanese Journal of Applied Physics*, 48, pp. 1–4. doi:10.1143/JJAP.48.04C022.

Abdel-Moemin, A.R. (2014) 'Oxalate Content of Egyptian Grown Fruits and Vegetables and Daily Common Herbs', *Journal of Food Research*, 3(3), p. 66. doi:10.5539/jfr.v3n3p66.

Abu-Zeid, M.E., Yousef, Y.A. and Kordia, H.A. (1992) 'Photoacoustic studies of interaction of O2 with Cu2O thin films', *Applied Physics Letters*, 61(8), pp. 907–909. doi:10.1063/1.107724.

Abu-Zied, B.M. *et al.* (2015) 'Effect of microwave power on the thermal genesis of Co 3 O 4 nanoparticles from cobalt oxalate micro-rods', *Applied Surface Science*, 351, pp. 600–609. doi:10.1016/j.apsusc.2015.05.151.

Agarwal, P., Orazem, M.E. and Garcia-Rubio, L.H. (1992) 'Measurement models for electrochemical impedance spectroscopy: I. Demonstration of applicability', *Journal of the Electrochemical Society*, 139(7), p. 1917.

Ahmad, Z. (2006) *Principles of corrosion engineering and corrosion control*. Elsevier.

Ahn, Y. *et al.* (2004) 'Chemical mechanical polishing by colloidal silica-based slurry for micro-scratch reduction', *Wear*, 257(7–8), pp. 785–789. doi:10.1016/j.wear.2004.03.020.

Aledresse, A. (2004) 'A study on the corrosion behavior of nanostructured electrodeposited cobalt', *Journal of Materials Science*, 9, pp. 1523–1526.

Aledresse, A. and Alfantazi, A. (2004) 'A study on the corrosion behavior of

nanostructured electrodeposited cobalt', *Journal of Materials Science*, 39(4), pp. 1523–1526. doi:10.1023/B:JMSC.0000013934.85378.40.

Allam, N.K., Nazeer, A.A. and Ashour, E.A. (2009) 'A review of the effects of benzotriazole on the corrosion of copper and copper alloys in clean and polluted environments', *Journal of Applied Electrochemistry*, 39(7), pp. 961–969.

Amanapu, H.P. *et al.* (2013) 'Role of Guanidine Carbonate and Crystal Orientation on Chemical Mechanical Polishing of Ruthenium Films', *ECS Journal of Solid State Science and Technology*, 2(11), pp. P445–P451. doi:10.1149/2.018311jss.

Arunagiri, T. N. *et al.* (2005) '5 Nm Ruthenium Thin Film As a Directly Plateable Copper Diffusion Barrier', *Applied Physics Letters*, 86(8), pp. 1–3. doi:10.1063/1.1867560.

Arunagiri, Tiruchirapalli N *et al.* (2005) 'Interfacial Diffusion Studies of Cu/(5 nm Ru)/Si Structures', *Journal of The Electrochemical Society*, 152(11), p. G808. doi:10.1149/1.2039939.

Atanasova-Stamova, S.Y., Georgieva, S.F. and Georgieva, M.B. (2018) 'Reaction strategies for synthesis of imidazole derivatives: a review', *Scripta Scientifica Pharmaceutica*, 5(2), p. 7. doi:10.14748/ssp.v5i2.5483.

Awwad, A.M. and Albiss, B. (2015) 'Biosynthesis of colloidal copper hydroxide nanowires using Pistachio leaf extract', (January). doi:10.5185/amlett.2015.5630.

Badawy, W.A., Al-Kharafi, F.M. and Al-Ajmi, J.R. (2000) 'Electrochemical behaviour of cobalt in aqueous solutions of di € erent pH', *Journal of Applied Electrochemistry*, 30, pp. 693–704.

Badawy, W.A., Al-Kharafi, F M and Al-Ajmi, J.R. (2000) 'Electrochemical behaviour of cobalt in aqueous solutions of different pH', *Journal of Applied Electrochemistry*, 30, pp.

P693–P704.

Bajaj, R. *et al.* (2019) '(12) United States Patent'.

Baklanov, M., Ho, P.S. and Zschech, E. (2012) *Advanced interconnects for ULSI technology*. John Wiley & Sons.

bama, P.S., Kiruban, P.D. and dran, S.R. (2017) 'Self Assembling monolayers of nanofilms by oxalic acid', *International Journal of Applied Chemistry*, 4(3), pp. 8–12. doi:10.14445/23939133/ijac-v4i3p102.

Baranwal, P.K. and Prasanna Venkatesh, R. (2017) 'Investigation of carbon steel anodic dissolution in ammonium chloride solutions using electrochemical impedance spectroscopy', *Journal of Solid State Electrochemistry*, 21(5), pp. 1373–1384. doi:10.1007/s10008-016-3497-8.

Baranwal, P.K. and Rajaraman, P.V. (2019a) 'Electrochemical investigation on effect of sodium thiosulfate (Na 2 S 2 O 3) and ammonium chloride (NH 4 Cl) on carbon steel corrosion', *Journal of Materials Research and Technology*, 8(1), pp. 1366–1378. doi:10.1016/j.jmrt.2018.05.029.

Baranwal, P.K. and Rajaraman, P.V. (2019b) 'Kinetics of carbon steel dissolution in ammonium chloride solution containing sodium thiosulfate', *International Journal of Chemical Kinetics*, 51(7), pp. 497–510. doi:10.1002/kin.21272.

Barney, J.E., Argersinger, W.J. and Reynolds, C.A. (1951) 'A Study of Some Complex Chlorides and Oxalates by Solubility Measurements', *Journal of the American Chemical Society*, 73(8), pp. 3785–3788. doi:10.1021/ja01152a065.

Barsoukov, E. and Macdonald, J.R. (2005) 'Impedance Spectroscopy Theory, Experiment, and', *Applications, 2nd ed.(Hoboken, NJ: John Wiley &Sons, Inc., 2005)* [Preprint].

Behl, W.K. and Toni, J.E. (1971) 'Anodic oxidation of cobalt in potassium hydroxide electrolytes', *Journal of Electroanalytical Chemistry and Interfacial Electrochemistry*, 31(1), pp. 63–75.

Bernhard, T., Pfandzelter, R. and Winter, H. (2003) 'Growth and structure of Mn and CoMn on Cu (001) studied by ion scattering', *Surface science*, 543(1–3), pp. 36–46.

Beyer, K.D. (1999) 'A" dirty" risk', *Innovative Leader*, 8, p. 407.

Bian, Y.-F. *et al.* (2020) 'Electrolyte composition and galvanic corrosion for ruthenium/copper electrochemical mechanical polishing', *Rare Metals*, 39(11), pp. 1300–1306. doi:10.1007/s12598-014-0286-3.

Biesinger, M.C. *et al.* (2011) 'Resolving surface chemical states in XPS analysis of first row transition metals, oxides and hydroxides: Cr, Mn, Fe, Co and Ni', *Applied Surface Science*, 257(7), pp. 2717–2730. doi:10.1016/j.apsusc.2010.10.051.

Bilouk, S. *et al.* (2009a) 'Electrochemical behavior of copper and cobalt in post-etch cleaning solutions Microelectronic Engineering Electrochemical behavior of copper and cobalt in post-etch cleaning solutions', *Microelectronic Engineering*, 86(10), pp. 2038–2044. doi:10.1016/j.mee.2009.01.035.

Bilouk, S. *et al.* (2009b) 'Microelectronic Engineering Electrochemical behavior of copper and cobalt in post-etch cleaning solutions', *Microelectronic Engineering*, 86(10), pp. 2038–2044. doi:10.1016/j.mee.2009.01.035.

Bojinov, M. (1996) 'A model of the anodic oxidation of metals in concentrated solutions: second-order dynamics at the anodic film| solution interface', *Journal of Electroanalytical Chemistry*, 405(1–2), pp. 15–22.

Boukamp, B.A. (1993) 'Practical application of the Kramers-Kronig transformation on

impedance measurements in solid state electrochemistry', *Solid State Ionics*, 62(1–2), pp. 131–141. doi:10.1016/0167-2738(93)90261-Z.

Boyd, G.E. and Larson, Q. V. (1969) 'Chemistry of Iodine-128 and Iodine-130 Recoils in Neutron-Irradiated Crystalline Potassium Iodate and Potassium Periodate', *Journal of the American Chemical Society*, 91(17), pp. 4639–4644. doi:10.1021/ja01045a006.

Brett, C.M.A., Brett, O. and Electrochemistry, A.M. (1993) 'Principles, methods and applications'.

Bui, S.H. *et al.* (2012) *Unusual spectroscopic and ligand binding properties of the cytochrome P450-flavodoxin fusion enzyme XplA*, *Journal of Biological Chemistry*. doi:10.1074/jbc.M111.319202.

Burstein, G.T. and Davies, D.H. (1980) 'The analysis of anodic films formed on cobalt in bicarbonate and borate electrolytes', *Corrosion Science*, 20(8–9), pp. 989–995. doi:10.1016/0010-938X(80)90079-7.

Calderón, J.A., Barcia, O.E. and Mattos, O.R. (2008) 'Reaction model for kinetic of cobalt dissolution in carbonate/bicarbonate media', *Corrosion Science*, 50(7), pp. 2101–2109. doi:10.1016/j.corsci.2008.04.013.

Cao, P., Gu, R. and Tian, Z. (2002) 'Electrochemical and Surface-Enhanced Raman', (6), pp. 7609–7615. doi:10.1021/la025570m.

Carpio, R., Farkas, J. and Jairath, R. (1995) 'Initial study on copper CMP slurry chemistries', 266(95), pp. 238–244.

Chen, Y. *et al.* (2018) *Post-CMP Cleaning. In Handbook of Silicon Wafer Cleaning Technology*, *Post-CMP Cleaning. In Handbook of Silicon Wafer Cleaning Technology*. William Andrew Publishing.

Chen, Y.H., Tsai, T.H. and Yen, S.C. (2010) 'Acetic acid and phosphoric acid adding to improve tantalum chemical mechanical polishing in hydrogen peroxide-based slurry', *Microelectronic Engineering*, 87(2), pp. 174–179. doi:10.1016/j.mee.2009.07.009.

Chen, Z. *et al.* (2017) 'Activity of pure and transition metal-modified CoOOH for the oxygen evolution reaction in an alkaline medium', *Journal of Materials Chemistry A*, 5(2), pp. 842–850. doi:10.1039/c6ta07482k.

Chenakin, S.P. and Kruse, N. (2021) 'Surface compositional changes upon heating cobalt oxalate dihydrate in vacuum', *Vacuum*, 187(January), p. 110090. doi:10.1016/j.vacuum.2021.110090.

Cheng, J. *et al.* (2014) 'Synergetic effect of potassium molybdate and benzotriazole on the CMP of ruthenium and copper in KIO 4 -based slurry', *Applied Surface Science*, 320, pp. 531–537. doi:10.1016/j.apsusc.2014.09.062.

Cheng, J. *et al.* (2015) 'Surface characteristics of ruthenium in periodate-based slurry during chemical mechanical polishing', *Applied Surface Science*, 351, pp. 401–409.

Cheng, J. *et al.* (2016) 'Effects of KIO4 concentration and pH values of the solution relevant for chemical mechanical polishing of ruthenium', *Microelectronic Engineering*, 151, pp. 30–37. doi:10.1016/j.mee.2015.12.003.

Cheng, J. (2017) *Research on Chemical Mechanical Polishing Mechanism of Novel Diffusion Barrier Ru for Cu Interconnect*. Springer.

Cheng, J. *et al.* (2018) 'Micro-galvanic corrosion of Cu/Ru couple in potassium periodate (KIO4) solution', *Corrosion Science*, 137(August 2016), pp. 184–193. doi:10.1016/j.corsci.2018.03.045.

Cheng, J., Wang, T. and Lu, X. (2017) 'Galvanic Corrosion Inhibitors for Cu / Ru Couple

during Chemical Mechanical Polishing of Ru Galvanic Corrosion Inhibitors for Cu / Ru Couple during Chemical Mechanical Polishing of Ru', (February), pp. 1–7. doi:10.1149/2.0181701jss.

Cheng, J., Wang, T. and Lu, X. (2020) 'Galvanic corrosion inhibitors for Cu/Ru couple during chemical mechanical polishing of Ru', *ECS Journal of Solid State Science and Technology*, 9(4), p. 049002. doi:10.1149/2162-8777/ab8f1a.

Cui, H., Park, J.H. and Park, J.G. (2013) 'Environmentally clean slurry using nano-TiO 2 - abrasive mixed with oxidizer H 2 O 2 for ruthenium-film chemical mechanical planarization', *Applied Surface Science*, 282, pp. 844–850. doi:10.1016/j.apsusc.2013.06.068.

Damayanti, M. *et al.* (2006) 'Effects of dissolved nitrogen in improving barrier properties of ruthenium', *Applied Physics Letters*, 88(4), pp. 1–3. doi:10.1063/1.2167610.

Damayanti, M *et al.* (2006) 'Ruthenium Barrier/Seed Layer for Cu/Low-κ Metallization', *Journal of The Electrochemical Society*, 153(6), p. J41. doi:10.1149/1.2188328.

Davies, D.H. and Burstein, G.T. (1980) 'The electrochemical behaviour of cobalt in bicarbonate and borate electrolytes', *Corrosion Science*, 20(8–9), pp. 973–987. doi:10.1016/0010-938X(80)90078-5.

DeNardis, D. *et al.* (2005) 'Impact of Gaseous Additives on Copper CMP in Neutral and Alkaline Solutions Using a CAP System', *Journal of The Electrochemical Society*, 152(11), p. G824. doi:10.1149/1.2042908.

Devamani, R Hepzi Pramila Alagar, M. (2017) 'Article Nano Biomed Eng Synthesis and Characterisation of Copper', (September 2013), pp. 1–6. doi:10.5101/nbe.v5i3.p116-120.

Dewi, N.O.M., Yulizar, Y. and Bagus Apriandanu, D.O. (2019) 'Green synthesis of Co3O4

nanoparticles using Euphorbia heterophylla L. leaves extract: Characterization and photocatalytic activity', *IOP Conference Series: Materials Science and Engineering*, 509(1). doi:10.1088/1757-899X/509/1/012105.

Ding, S.F. *et al.* (2010) 'Cu adhesion on tantalum and ruthenium surface: Density functional theory study', *Journal of Applied Physics*, 107(10). doi:10.1063/1.3369443.

Du, T. *et al.* (2004) 'Electrochemical characterization of copper chemical mechanical planarization in KIO 3 slurry', *Applied Surface Science*, 229(1–4), pp. 167–174. doi:10.1016/j.apsusc.2004.01.062.

Du, Y. *et al.* (2017) 'Effect of Guanidinium Ions on Ruthenium CMP in H_2O_2-Based Slurry', *ECS Journal of Solid State Science and Technology*, 6(8), pp. P521–P525. doi:10.1149/2.0131708jss.

Duan, B. *et al.* (2015) 'Effect of FA/O complexing agents and H2O2 on chemical mechanical polishing of ruthenium in weakly alkaline slurry', *Journal of Semiconductors*, 36(7). doi:10.1088/1674-4926/36/7/076002.

Edelstein, D. *et al.* (2002) 'A high performance liner for copper damascene interconnects', in *IEEE International Interconnect Technology Conference (IITC)*, pp. 9–11. doi:10.1109/iitc.2001.930001.

Ein-Eli, Y. *et al.* (2003) 'The Compatibility of Copper CMP Slurries with CMP Requirements', *Journal of The Electrochemical Society*, 150(9), p. C646. doi:10.1149/1.1600465.

Ein-eli, Y. and Starosvetsky, D. (2007) 'Review on copper chemical – mechanical polishing (CMP) and post-CMP cleaning in ultra large system integrated (ULSI)— An electrochemical perspective', 52, pp. 1825–1838. doi:10.1016/j.electacta.2006.07.039.

Ein-Eli, Y. and Starosvetsky, D. (2007) 'Review on copper chemical-mechanical polishing (CMP) and post-CMP cleaning in ultra large system integrated (ULSI)-An electrochemical perspective', *Electrochimica Acta*, 52(5), pp. 1825–1838. doi:10.1016/j.electacta.2006.07.039.

El-Naggar, M.M. (2000) 'Bis-triazole as a new corrosion inhibitor for copper in sulfate solution. A model for synergistic inhibition action', *Journal of Materials Science*, 35(24), pp. 6189–6195. doi:10.1023/A:1026725110344.

Faulkner, A.J.B.L.R. (2000) *ELECTROCHEMICAL METHODS Fundamentals and Applications*, *Annual Review of Materials Science*. doi:10.1146/annurev.matsci.30.1.117.

Felix, S., Chakkravarthy, R.B.P. and Grace, A.N. (2015) 'Microwave assisted synthesis of copper oxide and its application in electrochemical sensing', *IOP Conference Series: Materials Science and Engineering*, 73(1). doi:10.1088/1757-899X/73/1/012115.

Feng, C. *et al.* (2016) 'Investigation of aluminum gate CMP in a novel alkaline solution', *Journal of Semiconductors*, 37(1), p. 016002. doi:10.1088/1674-4926/37/1/016002.

Feng, H.-P. *et al.* (2008) 'Behavior of Copper Removal by CMP and Its Correlation to Deposit Structure and Impurity Content', *Journal of The Electrochemical Society*, 155(1), p. H21. doi:10.1149/1.2801394.

Feng, Y. *et al.* (2012) 'Controlled synthesis of highly active mesoporous Co 3O 4 polycrystals for low temperature CO oxidation', *Applied Catalysis B: Environmental*, 111–112, pp. 461–466. doi:10.1016/j.apcatb.2011.10.035.

Fu, L. *et al.* (2018) 'Effect of 1,2,4-triazole on galvanic corrosion between cobalt and copper in CMP based alkaline slurry', *Journal of Semiconductors*, 39(4), p. 46001. doi:10.1088/1674-4926/39/4/046001.

Gašparac, R., Martin, C.R. and Stupnišek-Lisac, E. (2000) 'In situ studies of imidazole and its derivatives as copper corrosion inhibitors. I. Activation energies and thermodynamics of adsorption', *Journal of the Electrochemical Society*, 147(2), p. 548.

Gayer, K.H. and Garrett, A.B. (1949) 'The Equilibria of Nickel Hydroxide, Ni(OH)2, in Solutions of Hydrochloric Acid and Sodium Hydroxide at 25°', *Journal of the American Chemical Society*, 71(9), pp. 2973–2975. doi:10.1021/ja01177a008.

Gerken, J.B. *et al.* (2011) 'Electrochemical water oxidation with cobalt-based electrocatalysts from pH 0-14: the thermodynamic basis for catalyst structure, stability, and activity.', *Journal of the American Chemical Society*, 133(36), pp. 14431–14442. doi:10.1021/ja205647m.

Gervasi, C.A. *et al.* (1991) 'A kinetic study of the electroreduction of anodically formed cobalt oxide layers', *Electrochimica acta*, 36(14), pp. 2147–2152.

Gervasi, C.A., Vilche, J.R. and Alvarez, P.E. (1996) 'A transition in the kinetics of electroreduction of anodically formed cobalt oxides. Influence of potentiostatic ageing', *Electrochimica acta*, 41(3), pp. 455–461.

Gorantla, V R K *et al.* (2005) 'Citric acid as a complexing agent in CMP of copper: Investigation of surface reactions using impedance spectroscopy', *Journal of the Electrochemical Society*, 152(5), p. G404.

Gorantla, Venkata R K *et al.* (2005) 'Oxalic acid as a complexing agent in CMP slurries for copper', *Electrochemical and Solid State Letters*, 8(5), p. G131.

Gregori, J. *et al.* (2006) 'Calculation of the rate constants of nickel electrodissolution in acid medium from EIS', *Journal of Solid State Electrochemistry*, 10(11), pp. 920–928.

Griffin, G.L. (1984) 'A Simple Phase Transition Model for Metal Passivation Kinetics',

Journal of The Electrochemical Society, 131(1), pp. 18–21. doi:10.1149/1.2115505.

Guan, H. *et al.* (2003) 'A novel method for preparing Co3O4 nanofibers by using electrospun PVA/cobalt acetate composite fibers as precursor', *Materials chemistry and Physics*, 82(3), pp. 1002–1006.

Gupta, A., Manivannan, R. and Noyel Victoria, S. (2019) 'Effect of potassium periodate oxidizer on germanium chemical mechanical planarization using fumed silica as abrasive', *ECS Journal of Solid State Science and Technology*, 8(5), pp. P3085–P3090. doi:10.1149/2.0151905jss.

Gutmann, R.J. *et al.* (1995) 'Chemical-mechanical polishing of copper with oxide and polymer interlevel dielectrics', *Thin Solid Films*, 270(1–2), pp. 596–600. doi:10.1016/0040-6090(95)06717-5.

Halloway, M. *et al.* (1992) 'Tantalum as a diffusion barrier between copper and silicon : Failure mechanism and effect of nitrogen additions mechanism and effect of nitrogen additions', *Journal of applied physics*, 71 (5433)(September 1991). doi:10.1063/1.350566.

Han, Z. (2016) 'Reticle Cleaning: Don't Go Gently…', *BACUS NEWS*, 32.

Hazarika, J., Gupta, A. and Rajaraman, P.V. (2022) 'Controlling Galvanic Corrosion with Oxalic Acid and Imidazole for Chemical Mechanical Planarization of Cobalt-Copper Interface', *ECS Journal of Solid State Science and Technology*, 11(5), p. 54007. doi:10.1149/2162-8777/ac6d72.

Hazarika, J., Patil, C.S. and Rajaraman, P.V. (2020) 'Formulation of slurry for chemical mechanical polishing of Cu substrates', *Materials Today: Proceedings*, 39, pp. 1781–1785. doi:10.1016/j.matpr.2020.07.545.

Hazarika, J. and Rajaraman, P.V. (2020) 'Formulation of Sodium Hypochlorite Based

Slurry for Copper-Cobalt Chemical Mechanical Planarization Process', *ECS Journal of Solid State Science and Technology*, 9(2), p. 024008. doi:10.1149/2162-8777/ab682a.

He, T. *et al.* (2005) 'Solubility-controlled synthesis of high-quality Co3O4 nanocrystals', *Chemistry of materials*, 17(15), pp. 4023–4030.

He, X. *et al.* (2014) 'Inhibition properties and adsorption behavior of imidazole and 2-phenyl-2-imidazoline on AA5052 in 1.0M HCl solution', *Corrosion Science*, 83(JUNE 2014), pp. 124–136. doi:10.1016/j.corsci.2014.02.004.

Hegde, S., Patri, U.B. and Babu, S. V. (2005) 'Chemical-mechanical polishing of copper using molybdenum dioxide slurry', *Journal of Materials Research*, 20(9), pp. 2553–2561. doi:10.1557/JMR.2005.0305.

Hong, Y. *et al.* (2005) 'Utility of dodecyl sulfate surfactants as dissolution inhibitors in chemical mechanical planarization of copper', *Journal of Materials Research*. 2005/12/01, 20(12), pp. 3413–3424. doi:DOI: 10.1557/jmr.2005.0419.

Hsien, Y.H. *et al.* (2012) 'Process development of high-k metal gate aluminum CMP at 28 nm technology node', *Microelectronic Engineering*, 92, pp. 19–23. doi:10.1016/j.mee.2011.04.013.

Hsu, H.K. *et al.* (2014) 'Optimized Copper Chemical Mechanical Polishing with CVD Co Barrier at 14nm Technology Node', in *International Conference on Planarization/CMP Technology*, pp. 63–65.

Hu, C.K. *et al.* (1995) 'Copper interconnection integration and reliability', *Thin Solid Films*, 262(1–2), pp. 84–92. doi:10.1016/0040-6090(94)05807-5.

Hu, L., Pan, G., Zhang, X., *et al.* (2019) 'Inhibition Effect of TT-LYK on Cu Corrosion and Galvanic Corrosion between Cu and Co during CMP in Alkaline Slurry', *ECS Journal*

of Solid State Science and Technology, 8(8), pp. P437–P447. doi:10.1149/2.0181908jss.

Hu, L., Pan, G., Li, C., *et al.* (2019) 'Potassium tartrate as a complexing agent for chemical mechanical polishing of Cu/Co/TaN barrier liner stack in H2O2 based alkaline slurries', *Materials Science in Semiconductor Processing*, 108(December 2019), p. 104883. doi:10.1016/j.mssp.2019.104883.

Hu, L., Pan, G., Xu, Y., *et al.* (2020a) ' The Effect of Hydroxyethylidene Diphosphonic Acid on the Chemical Mechanical Polishing of Cobalt in H 2 O 2 Based Alkaline Slurries ', *ECS Journal of Solid State Science and Technology*, 9(3), p. 034007. doi:10.1149/2162-8777/ab80b2.

Hu, L., Pan, G., Li, C., *et al.* (2020) 'Potassium tartrate as a complexing agent for chemical mechanical polishing of Cu/Co/TaN barrier liner stack in H2O2 based alkaline slurries', *Materials Science in Semiconductor Processing*, 108(December 2019), p. 104883. doi:10.1016/j.mssp.2019.104883.

Hu, L., Pan, G., Xu, Y., *et al.* (2020b) 'The Effect of Hydroxyethylidene Diphosphonic Acid on the Chemical Mechanical Polishing of Cobalt in H2O2 Based Alkaline Slurries', *ECS Journal of Solid State Science and Technology*, 9(3), p. 34007. doi:10.1149/2162-8777/ab80b2.

Hu, L. *et al.* (2021) 'Electrochimica Acta Experimental and density functional theory study of complexing agents on cobalt dissolution in alkaline solutions', *Electrochimica Acta*, 375, p. 137977. doi:10.1016/j.electacta.2021.137977.

Hussain, S.S., Al-nuzal, S.M.D. and Al-qazzaz, S.F. (2016) 'Preparation of copper oxalate and copper oxide nanoparticles and their antibacterial effect against P . aeruginosa and Methicillin Resistant S . aureus from burn and wound infections ... Preparation of copper oxalate and copper oxide nanoparticles and the', (January 2015).

Ichige, Y. *et al.* (2015) 'Three dimensional pH-potential diagram of cobalt slurry with corrosion rate', in *2015 International Conference on Planarization/CMP Technology (ICPT)*. IEEE, pp. 1–4.

Identification, P. and Identification, H. (2008) *Material Safety Data Sheet ZBLAN Material Safety Data Sheet*.

Idouhli, R. *et al.* (2019) 'Inhibitory effect of Senecio anteuphorbium as green corrosion inhibitor for S300 steel', *International Journal of Industrial Chemistry*, 10(2), pp. 133–143. doi:10.1007/s40090-019-0179-2.

Imanaka, T. (1980) 'COO-MoO,/Al,O, Catalysts', *Journal of Catalysis*, 460, pp. 448–460.

Ismail, K.M. and Badawy, W.A. (2000) 'Electrochemical and XPS investigations of cobalt in KOH solutions', *Journal of Applied Electrochemistry*, 30, pp. 1303–1311.

Jadhav, S. *et al.* (2011) 'Copper oxide nanoparticles: synthesis, characterization and their antibacterial activity', *Journal of Cluster Science*, 22(2), pp. 121–129.

Jagadale, A.D., Dubal, D.P. and Lokhande, C.D. (2012) 'Electrochemical behavior of potentiodynamically deposited cobalt oxyhydroxide (CoOOH) thin films for supercapacitor application', *Materials Research Bulletin*, 47(3), pp. 672–676. doi:10.1016/j.materresbull.2011.12.029.

Janjam, S. *et al.* (2008) 'Tartaric acid as a complexing agent for selective removal of tantalum and copper in CMP', *Electrochemical and Solid State Letters*, 11(12), p. H327.

Janjam, S. *et al.* (2009) 'Chemical mechanical planarization of TaN wafers using oxalic and tartaric acid based slurries', *Electrochemical and Solid State Letters*, 13(1), p. H1.

Jayaraman, T.R., Venkatesan, V.K. and Udupa, H.V.K. (1975) 'Cyclic voltammetric studies of electroless cobalt in NaOH', *Electrochimica Acta*, 20(3), pp. 209–213.

Jeong, Y.A. *et al.* (2019) 'Investigation of particle agglomeration with in-situ generation of oxygen bubble during the tungsten chemical mechanical polishing (CMP) process', *Microelectronic Engineering*, 218(September), p. 111133. doi:10.1016/j.mee.2019.111133.

Ji, J. *et al.* (2017) 'Role of Additive in Alkaline Slurries for Co CMP', *ECS Journal of Solid State Science and Technology*, 6(12), pp. P813–P818. doi:10.1149/2.0111712jss.

Jiang, L., He, Y., Li, Yuzhuo, *et al.* (2014) 'Effect of ionic strength on ruthenium CMP in H 2 O 2 -based slurries', *Applied Surface Science*, 317, pp. 332–337. doi:10.1016/j.apsusc.2014.08.063.

Jiang, L., He, Y., Li, Yan, *et al.* (2014a) 'Microelectronic Engineering Synergetic effect of H 2 O 2 and glycine on cobalt CMP in weakly alkaline slurry', *Microelectronic Engineering*, 122, pp. 82–86. doi:10.1016/j.mee.2014.02.002.

Jiang, L., He, Y., Li, Yan, *et al.* (2014b) 'Synergetic effect of H2O2 and glycine on cobalt CMP in weakly alkaline slurry', *Microelectronic Engineering*, 122, pp. 82–86.

Jillani, S. *et al.* (2018) 'Synthesis, characterization and biological studies of copper oxide nanostructures', *Materials Research Express*, 5(4). doi:10.1088/2053-1591/aab864.

Jindal, A. and Babu, S. V (2004) 'Effect of pH on CMP of Copper and Tantalum', *Journal of The Electrochemical Society*, 151(10), p. G709. doi:10.1149/1.1792871.

Johnson, C.A., Wei, S. and Roy, D. (2018) 'An Alkaline Slurry Design for Co-Cu CMP Systems Evaluated in the Tribo-Electrochemical Approach', *ECS Journal of Solid State Science and Technology*, 7(2), pp. P38–P49. doi:10.1149/2.0091802jss.

Josell, D. *et al.* (2003) 'Seedless Superfill: Copper Electrodeposition in Trenches with Ruthenium Barriers', *Electrochemical and Solid-State Letters*, 6(10), p. C143.

doi:10.1149/1.1605271.

Kadam, Y., Yerramilli, U. and Bahadur, A. (2009) 'Solubilization of poorly water-soluble drug carbamezapine in Pluronic® micelles: Effect of molecular characteristics, temperature and added salt on the solubilizing capacity', *Colloids and Surfaces B: Biointerfaces*, 72(1), pp. 141–147. doi:10.1016/j.colsurfb.2009.03.027.

Kaufman, V.B., C. Kistler, R. and Wang, S. (2000) 'CHEMICAL MECHANICAL POLISHING SLURRY USEFUL FOR COPPERITANTALUM SUBSTRATE'. United States Patent. Available at: https://patentimages.storage.googleapis.com/3d/99/74/0826d1c6e4e086/US6063306.pdf.

Keddam, M., Mottos, O.R. and Takenouti, H. (1981) 'Reaction model for iron dissolution studied by electrode impedance: I. Experimental results and reaction model', *Journal of the Electrochemical Society*, 128(2), p. 257.

Khanna, A.J., Kakireddy, V.R., *et al.* (2020) 'High-Performance Pad Conditioning (HPPC) Arm for Augmenting CMP Performance', *ECS Journal of Solid State Science and Technology*, 9(6), p. 64012. doi:10.1149/2162-8777/aba9fd.

Khanna, A.J., Yamamura, M., *et al.* (2020) 'Investigation of the Impact of Pad Surface Texture from Different Pad Conditioners on the CMP Performance', *ECS Journal of Solid State Science and Technology*, 9(6), p. 64011. doi:10.1149/2162-8777/aba726.

Kim, I.-P. *et al.* (2003) 'Cu CMP Property by Addition of Corrosion Inhibitor and Complexing Agent', *The Korean Institute of Electrical and Electronic Material Engineers*, 07(a), pp. 343–346.

Kim, J. *et al.* (2022) 'Effects of aging time in hydrogen peroxide-glycine-based Cu CMP slurry', *Materials Science in Semiconductor Processing*, 140(November 2021), p. 106343.

doi:10.1016/j.mssp.2021.106343.

Ko, S.J. *et al.* (2021) 'Effect of imidazole as corrosion inhibitor on carbon steel weldment in district heating water', *Materials*, 14(16). doi:10.3390/ma14164416.

Kolodny, A. (2009) *Advance Nanoscale ULSI Interconnects : Fundamentals and applications*. Available at: https://download.e-bookshelf.de/download/0000/0029/59/L-G-0000002959-0002340701.pdf.

Kondo, S. *et al.* (2000) 'Slurry chemical corrosion and galvanic corrosion during copper chemical mechanical polishing', *Japanese Journal of Applied Physics, Part 1: Regular Papers and Short Notes and Review Papers*, 39(11), pp. 6216–6222. doi:10.1143/jjap.39.6216.

Krishnan, M., Nalaskowski, J.W. and Cook, L.M. (2010) 'Chemical mechanical planarization: slurry chemistry, materials, and mechanisms', *Chemical reviews*, 110(1), pp. 178–204.

Kuijer, T.J.M., Giling, L.J. and Bloem, J. (1974) 'Gas phase etching of silicon with HCl', *Journal of Crystal Growth*, 22(1), pp. 29–33.

Künzelmann, U. *et al.* (2012) 'Chemical-mechanical planarization of aluminium damascene structures', in *ICPT 2012 - International Conference on Planarization/CMP Technology, Proceedings*, pp. 371–376.

Kuo, Y. *et al.* (2004) 'Diffusion of Copper in Titanium Zirconium Nitride Thin Films', *Electrochemical and Solid-State Letters*, 7(3), pp. 35–37. doi:10.1149/1.1644355.

Kwon, O. *et al.* (2020) 'Study on effect of complexing agents on Co oxidation/dissolution for chemical-mechanical polishing and cleaning process', *Microelectronic Engineering*, 227(August 2019), p. 111308. doi:10.1016/j.mee.2020.111308.

Lee, S.W. *et al.* (2016) 'The effect of TAD based cleaning solution on post Cu CMP process', *Microelectronic Engineering*, 162, pp. 17–22.

Lee, W.-J. (2003) 'Inhibiting effects of imidazole on copper corrosion in 1 M HNO3 solution', *Materials Science and Engineering A*, A348(1–2), pp. P217–P226. doi:10.1016/S0921-5093(02)00734-7.

Lee, W.J. and Park, H.S. (2004) 'Development of novel process for Ru CMP using ceric ammonium nitrate (CAN)-containing nitric acid', *Applied Surface Science*, 228(1–4), pp. 410–417. doi:10.1016/j.apsusc.2004.01.060.

Li, X. *et al.* (2016) 'Effect of chelating agent on reducing galvanic corrosion between cobalt and copper in alkaline slurry', *ECS Journal of Solid State Science and Technology*, 5(9), p. P540.

Li, Y. (2007) *Microelectronic applications of chemical mechanical planarization*. John Wiley & Sons.

Li, Y. and Babu, S. V (2001) 'Chemical Mechanical Polishing of Copper and Tantalum in Potassium Iodate-Based Slurries', pp. 20–22. doi:10.1149/1.1342185.

Li, Y.D. *et al.* (1999) 'Preparation of pure nickel, cobalt, nickel±cobalt and nickel±copper alloys by hydrothermal reduction', *Journal of Materials Chemistry*, 4(10 ml), pp. 9–11.

Li, Yanxia *et al.* (2013) 'Molecularly imprinted fluorescent and colorimetric sensor based on TiO 2@Cu(OH)2 nanoparticle autocatalysis for protein recognition', *Journal of Materials Chemistry B*, 1(9), pp. 1256–1262. doi:10.1039/c2tb00398h.

Li, Z. *et al.* (2005) 'Nucleation and Adhesion of ALD Copper on Cobalt Adhesion Layers and Tungsten Nitride Diffusion Barriers', *Electrochemical and Solid-State Letters*, 8(7), p. G182. doi:10.1149/1.1924929.

Liu, F. *et al.* (2019) 'Effect of diethylenetriamine pentaacetate pentapotassium on chemical mechanical polishing of cobalt in H2O2 based slurry', *ECS Journal of Solid State Science and Technology*, 8(5), p. P3201.

Liu, S.G. *et al.* (2018) 'A fluorescence and colorimetric dual-mode assay of alkaline phosphatase activity: Via destroying oxidase-like CoOOH nanoflakes', *Journal of Materials Chemistry B*, 6(18), pp. 2843–2850. doi:10.1039/c7tb03275g.

Lowalekar, V.P. (2006) *Oxalic acid based chemical systems for electrochemical mechanical planarization of copper*. The University of Arizona. Available at: http://arizona.openrepository.com/arizona/handle/10150/193886.

Lu, H.-S., Zeng, X., *et al.* (2012) 'The effect of glycine and benzotriazole on corrosion and polishing properties of cobalt in acid slurry', *Journal of The Electrochemical Society*, 159(9), p. C383.

Lu, H.-S., Wang, J.-X., *et al.* (2012) 'The effect of H2O2 and 2-MT on the chemical mechanical polishing of cobalt adhesion layer in acid slurry', *Electrochemical and Solid State Letters*, 15(4), p. H97.

Luan, X. *et al.* (2016) 'A study on exploring the alkaline copper CMP slurry without inhibitors to achieve high planarization efficiency', *Microelectronic Engineering*, 160, pp. 5–11. doi:10.1016/j.mee.2016.02.044.

Luo, Q., Campbell, D.R. and Babu, S. V (1997) 'Chemical – mechanical polishing of copper in alkaline media', *Thin Solid Films 311*, 177–182.

Luo, Q., Mackay, R.A. and Babu, S. V. (1997) 'Copper Dissolution in Aqueous Ammonia-Containing Media during Chemical Mechanical Polishing', *Chemistry of Materials*, 9(10), pp. 2101–2106. doi:10.1021/cm970168s.

Ma, P. *et al.* (2009) 'Optimized Integrated Copper Gap-fill Approaches for 2x Flash Devices', in *2009 IEEE International Interconnect Technology Conference*. IEEE, pp. 38–40. doi:10.1109/IITC.2009.5090334.

Ma, T. *et al.* (2020) 'Corrosion control of copper wiring by barrier CMP slurry containing azole inhibitor: Combination of simulation and experiment', *Colloids and Surfaces A: Physicochemical and Engineering Aspects*, 599(March). doi:10.1016/j.colsurfa.2020.124872.

Macdonald, D.D. and Urquidi-Macdonald, M. (1985) 'Application of Kramers-Kronig Transforms in the Analysis of Electrochemical Systems: I . Polarization Resistance', *Journal of The Electrochemical Society*, 132(10), pp. 2316–2319. doi:10.1149/1.2113570.

Maddala, J. *et al.* (2010) 'Identification of reaction mechanism for anodic dissolution of metals using Electrochemical Impedance Spectroscopy', *Journal of Electroanalytical Chemistry*, 638(2), pp. 183–188. doi:10.1016/j.jelechem.2009.11.021.

Manivannan, R. and Ramanathan, S. (2009) 'Applied Surface Science The effect of hydrogen peroxide on polishing removal rate in CMP with various abrasives', *Applied Surface Science*, 255(6), pp. 3764–3768. doi:10.1016/j.apsusc.2008.10.040.

Massalski, T.B. and Okamoto, H. (1990) 'Binary phase alloy diagrams', *ASM, Metals Park, Ohio*, p. 1390.

Matsumoto, K. *et al.* (2009) 'Chemical Vapor Deposition of Mn and Mn Oxide and their Step Coverage and Diffusion Barrier Properties on Patterned Interconnect Structures', *Applied Physics Express*, 2, p. 36503. doi:10.1143/apex.2.036503.

Maugis, D. and Pollock, H.M. (1984) 'Surface forces, deformation and adherence at metal microcontacts', *Acta Metallurgica*, 32(9), pp. 1323–1334. doi:10.1016/0001-

6160(84)90078-6.

McAuley, A. and Nancollas, G.H. (1960) 'Complex formation in solutions of copper oxalate', *Transactions of the Faraday Society*, 56, pp. 1165–1171.

Meites, L. (1950) 'Polarographic Studies of Metal Complexes. II. The Copper (II) Citrates1', *Journal of the American Chemical Society*, 72(1), pp. 180–184.

Miller, A. and Granstrom, J. (2017) 'POLISHING SLURRY FOR COBALT REMOVAL'.

Min, K.-H. (1996) 'Comparative study of tantalum and tantalum nitrides (Ta2N and TaN) as a diffusion barrier for Cu metallization', *Journal of Vacuum Science & Technology B: Microelectronics and Nanometer Structures*, 14(5), p. 3263. doi:10.1116/1.588818.

Min, K.-H., Chun, C.C. and Kim Ki-Bum (1996) 'Comparative study of tantalum and tantalum nitrides (Ta2N and TaN) as a diffusion barrier for Cu metallization', *Journal of Vacuum Science & Technology B: Microelectronics and Nanometer Structures*, 14(5), p. 3263. doi:10.1116/1.588818.

Min, K. *et al.* (1996) 'Comparative study of tantalum and tantalum nitrides (Ta2N and TaN) as a diffusion barrier for Cu metallization Comparative study of tantalum and tantalum nitrides (Ta 2 N and TaN) as a diffusion barrier for Cu metallization *', *Journal of Vacuum Science & Technology*, 14, pp. 3263–3269. doi:10.1116/1.588818.

Minu Mary, C. *et al.* (2016) 'Growth and characterization of Sm3+ doped cerium oxalate single crystals', *Journal of Materials Research and Technology*, 5(3), pp. 268–274. doi:10.1016/j.jmrt.2016.01.001.

Muthuselvi, C., Arunkumar, A. and Rajaperumal, G. (2017) 'Growth and Characterization of Oxalic Acid Doped with Tryptophan Crystal for Antimicrobial Activity', (July 2016). Available at: www.pelagiaresearchlibrary.com.

Ng, D. *et al.* (2007) 'Oxidation and removal mechanisms during chemical-mechanical planarization', *Wear*, 263(7-12 SPEC. ISS.), pp. 1477–1483. doi:10.1016/j.wear.2006.11.023.

Nguyen, V.H. *et al.* (2001) 'Copper chemical mechanical polishing using a slurry-free technique', *Microelectronic Engineering*, 55(1–4), pp. 305–312. doi:10.1016/S0167-9317(00)00461-5.

Nishizawa, H., Nojo, H. and Isobe, A. (2010a) 'Fundamental Study of Chemical--Mechanical Polishing Slurry of Cobalt Barrier Metal for the Next-Generation Interconnect Process', pp. 4–6. doi:10.1143/JJAP.49.05FC03.

Nishizawa, H., Nojo, H. and Isobe, A. (2010b) 'Fundamental study of chemical-mechanical polishing slurry of cobalt barrier metal for the next-generation interconnect process', *Japanese Journal of Applied Physics*, 49(5 PART 3), pp. 4–6. doi:10.1143/JJAP.49.05FC03.

Niveditha, C. V. *et al.* (2018) 'Feather like highly active Co3O4 electrode for supercapacitor application: A potentiodynamic approach', *Materials Research Express*, 5(6). doi:10.1088/2053-1591/aac5a7.

Oh, M.H. *et al.* (2011) 'Polishing behaviors of ceria abrasives on silicon dioxide and silicon nitride CMP', *Powder Technology*, 206(3), pp. 239–245. doi:10.1016/j.powtec.2010.09.025.

Oliver, M.R. (2004) *Chemical-mechanical planarization of semiconductor materials*. Springer Science & Business Media.

Onwudiwe, D.C., Ravele, M.P. and Elemike, E.E. (2020) 'Eco-friendly synthesis, structural properties and morphology of cobalt hydroxide and cobalt oxide nanoparticles using extract

of Litchi chinensis', *Nano-Structures and Nano-Objects*, 23, p. 100470. doi:10.1016/j.nanoso.2020.100470.

Orazem, M.E. and Tribollet, B. (2008) 'Electrochemical impedance spectroscopy', *New Jersey*, pp. 383–389.

Oxide, R. *et al.* (2002) 'Effect of Organic Acids in Copper Chemical Mechanical Planarization Slurry on Slurry Stability and Particle Contamination on Copper Surfaces'. doi:10.1143/JJAP.41.1305.

Pachimatla, R. and Srinivasan, R. (2018) 'Non-Linear Electrochemical Impedance Spectroscopic Analysis of Instabilities in Electrochemical Systems', *ECS Transactions*, 85(13), pp. 1145–1153. doi:10.1149/08513.1145ecst.

Pandey, B.K. (2015) 'Synthesis and Characterization of Cobalt Oxalate Nanomaterial for Li-Ion Battery', (October). doi:10.1166/mat.2015.1267.

Pandija, S., Roy, D. and Babu, S. V. (2007) 'Chemical mechanical planarization of copper using abrasive-free solutions of oxalic acid and hydrogen peroxide', *Materials Chemistry and Physics*, 102(2–3), pp. 144–151. doi:10.1016/j.matchemphys.2006.11.015.

Park, J.-G., Paluvai, N.R. and Venkatesh, R.P. (2018) 'Metal Surface Chemical Composition and Morphology', in *Handbook of Silicon Wafer Cleaning Technology*. Elsevier, pp. 579–618.

Patil, D. *et al.* (2010) 'Highly sensitive and fast responding CO sensor based on Co3O4 nanorods', *Talanta*, 81(1–2), pp. 37–43. doi:10.1016/j.talanta.2009.11.034.

Patlolla, R.R. *et al.* (2018) 'CMP Development for Ru Liner Structures beyond 14nm', *ECS Journal of Solid State Science and Technology*, 7(8), pp. P397–P401. doi:10.1149/2.0181808jss.

Paul, E. *et al.* (2005) 'A Model of Copper CMP', *Journal of The Electrochemical Society*, 152(4), p. G322. doi:10.1149/1.1861175.

Paul, T. and Srinivasan, R. (2020) 'Mechanistic analysis of anodic dissolution of cobalt in alkaline glycine solution', *Journal of Solid State Electrochemistry*, 24(6), pp. 1291–1304. doi:10.1007/s10008-020-04613-2.

Peddeti, S. *et al.* (2011) 'Chemical Mechanical Polishing of Ge Using Colloidal Silica Particles and H2O2', *Electrochemical and Solid-State Letters*, 14(7), p. H254. doi:10.1149/1.3575166.

Peethala, B.C. (2011) *Chemical Mechanical Polishing of Ruthenium , Cobalt , and Black Diamond Films*. CLARKSON UNIVERSITY.

Peethala, B.C. *et al.* (2012) 'Cobalt Polishing with Reduced Galvanic Corrosion at Copper/Cobalt Interface Using Hydrogen Peroxide as an Oxidizer in Colloidal Silica-Based Slurries', *Journal of The Electrochemical Society*, 159(6), p. H582. doi:10.1149/2.073206jes.

Peethala, B.C. and Babu, S. V (2011) 'Ruthenium Polishing Using Potassium Periodate as the Oxidizer and Silica Abrasives', pp. 271–276. doi:10.1149/1.3528942.

Peethala, B.C., Roy, D. and Babu, S. V (2011a) 'Controlling the Galvanic Corrosion of Copper during Chemical Mechanical Planarization of Ruthenium Barrier Films', *Electrochemical and Solid-State Letters* , 14(7), pp. H306–H310. doi:10.1149/1.3589308.

Peethala, B.C., Roy, D. and Babu, S. V (2011b) 'Controlling the Galvanic Corrosion of Copper during Chemical Mechanical Planarization of Ruthenium Barrier Films', *Electrochemical and Solid-State Letters*, 14(7), pp. 306–310. doi:10.1149/1.3589308.

Poddar, M.K. *et al.* (2021) 'Tungsten passivation layer (WO3) formation mechanisms

during chemical mechanical planarization in the presence of oxidizers', *Applied Surface Science*, 537(September 2020), p. 147862. doi:10.1016/j.apsusc.2020.147862.

Popuri, R, Sagi, K. V, Alety, S.R., Peethala, B.C., Amanapu, H., Patlolla, R., *et al.* (2017) 'Citric Acid as a Complexing Agent in Chemical Mechanical Polishing Slurries for Cobalt Films for Interconnect Applications', 6(9), pp. 594–602. doi:10.1149/2.0111709jss.

Popuri, R, Sagi, K. V, Alety, S.R., Peethala, B.C., Amanapu, H. and Patlolla, R. (2017) 'Citric Acid as a Complexing Agent in Chemical Mechanical Polishing Slurries for Cobalt Films for Interconnect Applications Citric Acid as a Complexing Agent in Chemical Mechanical Polishing Slurries for Cobalt Films for Interconnect Applications', *ECS Journal of Solid State Science and Technology*, 6(January), p. P594. doi:10.1149/2.0111709jss.

Popuri, R. *et al.* (2017) 'Potassium Oleate as a Dissolution and Corrosion Inhibitor during Chemical Mechanical Planarization of Chemical Vapor Deposited Co Films for Interconnect Applications', *ECS Journal of Solid State Science and Technology*, 6(12), pp. P845–P852. doi:10.1149/2.0251712jss.

Pourbaix, M. (1974) *Atlas of electrochemical equilibria in aqueous solution, NACE International*.

Pourbaix, M., Zhang, H. and Pourbaix, A. (1997) 'Presentation of an Atlas of chemical and electrochemical equilibria in the presence of a gaseous phase', *Materials Science Forum*, 251–254, pp. 143–148. doi:10.4028/www.scientific.net/msf.251-254.143.

Prasad, Y.N. and Ramanathan, S. (2007) 'Chemical mechanical planarization of copper in alkaline slurry with uric acid as inhibitor', *Electrochimica Acta*, 52, pp. 6353–6358. doi:10.1016/j.electacta.2007.04.044.

Prasanna Venkatesh, R. and Ramanathan, S. (2010) 'Electrochemical characterization of Cu dissolution and chemical mechanical polishing in ammonium hydroxide–hydrogen peroxide based slurries', *Journal of Applied Electrochemistry*, 40(4), pp. 767–776. doi:10.1007/s10800-009-0055-4.

Qi, D. (2018) 'Chapter 7 - Chemical Separation Method', in Qi, D.B.T.-H. of R.E. (ed.). Elsevier, pp. 671–741. doi:https://doi.org/10.1016/B978-0-12-813920-2.00007-6.

Qin, K., Moudgil, B. and Park, C.W. (2004) 'A chemical mechanical polishing model incorporating both the chemical and mechanical effects', *Thin Solid Films*, 446(2), pp. 277–286. doi:10.1016/j.tsf.2003.09.060.

Qu, X. *et al.* (2004) 'Effects of preannealing on the diffusion barrier properties for ultrathin W – Si – N thin film', *Thin Solid Films*, 463, pp. 67–71. doi:10.1016/j.tsf.2004.05.023.

Raj, A.D. *et al.* (2012) 'Gas Sensing Behavior of High Surface Area Co3O4 Micro / Nano Gas Sensing Behavior of High Surface Area Co 3 O 4 Micro / Nano Structures Synthesized by Simple Sonication Process', 2(August 2014). doi:10.1166/sl.2012.2574.

Rajkumar, T. and Ranga Rao, G. (2008) 'Synthesis and characterization of hybrid molecular material prepared by ionic liquid and silicotungstic acid', *Materials Chemistry and Physics*, 112(3), pp. 853–857. doi:10.1016/j.matchemphys.2008.06.046.

Ramakrishnan, S. *et al.* (2007) 'Comparison of dicarboxylic acids as complexing agents for abrasive-free chemical mechanical planarization of copper', *Microelectronic Engineering*, 84(1), pp. 80–86. doi:10.1016/j.mee.2006.08.011.

Ranaweera, C.K. *et al.* (2019) 'Ammonium Persulfate and Potassium Oleate Containing Silica Dispersions for Chemical Mechanical Polishing for Cobalt Interconnect Applications', *ECS Journal of Solid State Science and Technology*, 8(5), pp. P3001–P3008.

doi:10.1149/2.0021905jss.

Ranjith, P.M. *et al.* (2018) 'On the Anodic Dissolution of Tantalum and Niobium in Hydrofluoric Acid', *Journal of The Electrochemical Society*, 165(5), pp. C258–C269. doi:10.1149/2.0691805jes.

Real, S.G., Ribotta, S.B. and Arvia, A.J. (2008) 'The electrochemical dissolution of cobalt in carbonate-bicarbonate solutions from EIS and steady polarization data', *Corrosion Science*, 50(2), pp. 463–472. doi:10.1016/j.corsci.2007.07.001.

Recovery, E.O. *et al.* (2016) 'Synthesis and Characterization of Polyacrylamide Crosslinked Copolymer for Synthesis and Characterization of Polyacrylamide Crosslinked Copolymer for Enhanced Oil Recovery and Rock Wettability Alteration', (January 2015). doi:10.11648/j.ogce.20150304.11.

Reichardt, R. *et al.* (2021) 'USE OF A CHEMICAL MECHANICAL POLISHING (CMP) COMPOSITION FOR POLISHING OF COBALT COMPRISING SUBSTRATES'.

Rights, A.P. (2017) 'Contamination and galvanic corrosion in metal chemical- mechanical planarization'.

Roule, A. *et al.* (2007) 'Seed layer enhancement by electrochemical deposition: The copper seed solution for beyond 45 nm', *Microelectronic Engineering*, 84(11), pp. 2610–2614. doi:10.1016/j.mee.2007.06.014.

Ryu, H.-Y. *et al.* (2019) 'Selection and Optimization of Corrosion Inhibitors for Improved Cu CMP and Post-Cu CMP Cleaning', *ECS Journal of Solid State Science and Technology*, 8(5), pp. P3058–P3062. doi:10.1149/2.0101905jss.

Ryu, H.-Y. *et al.* (2020) 'Characterization of Different Cobalt Surfaces and Interactions with Benzotriazole for CMP Application', *ECS Journal of Solid State Science and*

Technology, 9(6), p. 64005. doi:10.1149/2162-8777/aba331.

Sagi, K. V. *et al.* (2016) 'Potassium Permanganate-Based Slurry to Reduce the Galvanic Corrosion of the Cu/Ru/TiN Barrier Liner Stack during CMP in the BEOL Interconnects', *ECS Journal of Solid State Science and Technology*, 5(5), pp. P256–P263. doi:10.1149/2.0141605jss.

Sagi, K. V. and Babu, S. V. (2016) 'Mitigation of corrosion challenges for barrier films at advanced nodes', in *China Semiconductor Technology International Conference 2016, CSTIC 2016*. IEEE, pp. 1–4. doi:10.1109/CSTIC.2016.7464038.

Sagi, K. V *et al.* (2016) 'Potassium Permanganate-Based Slurry to Reduce the Galvanic Corrosion of the Cu / Ru / TiN Barrier Liner Stack during CMP in the BEOL Interconnects Potassium Permanganate-Based Slurry to Reduce the Galvanic Corrosion of the Cu / Ru / TiN Barrier Liner Stac', (January). doi:10.1149/2.0141605jss.

Salavati-Niasari, M., Mir, N. and Davar, F. (2009) 'Synthesis and characterization of Co3O4 nanorods by thermal decomposition of cobalt oxalate', *Journal of Physics and Chemistry of Solids*, 70(5), pp. 847–852. doi:10.1016/j.jpcs.2009.04.006.

SASTRI, V.S. (1998) *Corrosion inhibitors: principles and applications*. Wiley.

Sato, N. (1990) 'An overview on the passivity of metals', *Corrosion Science*, 31(C), pp. 1–19. doi:10.1016/0010-938X(90)90086-K.

Sekhar, M.S. and Ramanathan, S. (2006) 'Characterization of copper chemical mechanical polishing (CMP) in nitric acid-hydrazine based slurry for microelectronic fabrication', *Thin Solid Films*, 504(1–2), pp. 227–230. doi:10.1016/j.tsf.2005.09.128.

Seo, S.-C. *et al.* (2011) 'Thermal Stability of Copper Contact Metallization Using Ru-Containing Liner', *Electrochemical and Solid-State Letters*, 14(5), p. H187.

doi:10.1149/1.3545963.

Shi, X. *et al.* (2019) 'CHEMICAL MECHANICAL PLANARIZATION (CMP) COMPOSITION AND METHODS THEREFORE FOR COPPER AND THROUGH SILICA VIA (TSV) APPLICATIONS ('.

Shi, X., Schlueter, J.A. and O'Neill, M.L. (2016) 'CHEMICAL MECHANICAL POLISHING (CMP) OF COLBALTCONTAINING SUBSTRATE'. united states.

Shibli, S.M.A. and Saji, V.S. (2005) 'Co-inhibition characteristics of sodium tungstate with potassium iodate on mild steel corrosion', *Corrosion Science*, 47(9), pp. 2213–2224. doi:10.1016/j.corsci.2004.09.012.

Shima, S., Fukunaga, A. and Tsujimura, M. (2007) 'Effects of Liner Metal and CMP Slurry Oxidizer on Copper Galvanic Corrosion', *ECS Transactions*, 11(6), pp. 285–295. doi:10.1149/1.2778386.

Shimizu, H., Sakoda, K. and Shimogaki, Y. (2013) 'CVD of cobalt-tungsten alloy film as a novel copper diffusion barrier', *Microelectronic Engineering*, 106, pp. 91–95. doi:10.1016/j.mee.2012.08.008.

Shukla, A., Selvam, N.V. and Ramachandran, M. (2022) 'Urea as a complexing agent for selective removal of Ta and Cu in sodium carbonate based alumina chemical-mechanical planarization slurry', *Journal of the Serbian Chemical Society*, 87(2), pp. 219–232. doi:10.2298/JSC201220049S.

Singh, J. *et al.* (2013) 'XPS, UV-Vis, FTIR, and EXAFS studies to investigate the binding mechanism of N719 dye onto oxalic acid treated TiO2 and its implication on photovoltaic properties', *Journal of Physical Chemistry C*, 117(41), pp. 21096–21104. doi:10.1021/jp4062994.

Sipaut, C.S. *et al.* (2005) 'ICCBPE / SOMChE 2005 Surface Modification of Fumed Nanosilica with Epoxy Molecule ICCBPE / SOMChE 2005', (December), pp. 946–950.

Starosvetsky, D. and Ein-Eli, Y. (2009) 'Electrochemical View of Copper Chemical-Mechanical Polishing (CMP) BT - Advanced Nanoscale ULSI Interconnects: Fundamentals and Applications', in Shacham-Diamand, Y. et al. (eds) *Advanced Nanoscale ULSI Interconnects: Fundamentals and Applications*. New York, NY: Springer New York, pp. 359–378. doi:10.1007/978-0-387-95868-2_24.

Stavreva, Z. *et al.* (1997) 'Characteristics in chemical-mechanical polishing of copper: Comparison of polishing pads', *Applied Surface Science*, 108(1), pp. 39–44. doi:10.1016/S0169-4332(96)00572-7.

Steigerwald, J.M. *et al.* (1995) 'Chemical processes in the chemical mechanical polishing of copper', *Materials Chemistry and Physics*, 41(3), pp. 217–228. doi:10.1016/0254-0584(95)01516-7.

Steigerwald, J.M., Murarka, S.P. and Gutmann, R.J. (2008) *Chemical mechanical planarization of microelectronic materials*. John Wiley & Sons.

Stupian, G.W. and Fleischauer, P.D. (1981) 'Corrosion Protection of Aluminum BY SOLUTION-DEPOSITED OXIDE FILMS', *Applications of Surface Science*, 9, pp. 250–265. doi:10.1201/9781420030297.ch31.

Stupnišek-Lisac, E., Gazivoda, A. and Madžarac, M. (2002) 'Evaluation of non-toxic corrosion inhibitors for copper in sulphuric acid', *Electrochimica Acta*, 47(26), pp. 4189–4194. doi:10.1016/S0013-4686(02)00436-X.

Sun, X. *et al.* (2021) 'Adsorption Mechanism of Potassium Oleate on Cobalt Surface Based on Cobalt Interconnection CMP: A Combined Experimental and DFT Investigation', *ECS*

Journal of Solid State Science and Technology, 10(2), p. 024003. doi:10.1149/2162-8777/abe1d8.

Sverdlov, V. (2011) 'Scaling, power consumption, and mobility enhancement techniques', in *Strain-Induced Effects in Advanced MOSFETs*. Springer, pp. 5–22.

Talukdar, A. and Rajaraman, P.V. (2020) 'Investigation of Acetic Acid Effect on Carbon Steel Corrosion in CO2-H2S Medium: Mechanistic Reaction Pathway and Kinetics', *ACS Omega*, 5(20), pp. 11378–11388. doi:10.1021/acsomega.0c00387.

Tamilmani, S. *et al.* (2002) 'Potential-pH diagrams of interest to chemical mechanical planarization of copper', *Journal of The Electrochemical Society*, 149(12), p. G638.

Tan, B. *et al.* (2022) '18 - Environmentally sustainable corrosion inhibitors used for electronics industry', in Hussain, C.M., Verma, C., and Aslam, J.B.T.-E.S.C.I. (eds). Elsevier, pp. 359–381. doi:https://doi.org/10.1016/B978-0-323-85405-4.00007-0.

Tanwar, K. (2014) 'BEOL INTEGRATION SCHEME FOR COPPER CMP TO PREVENT DENDRITE FORMATION'. United States: United States Patent.

Tian, Y. *et al.* (2022) ' Role of Potassium Tolyltriazole as an Inhibitor in H 2 O 2 -Based Slurry on Cu/Ru Patterned Wafer CMP ', *ECS Journal of Solid State Science and Technology*, 11(3), p. 034006. doi:10.1149/2162-8777/ac5eac.

Tsai, T.H., Wu, Y.F. and Yen, S.C. (2005) 'Glycolic acid in hydrogen peroxide-based slurry for enhancing copper chemical mechanical polishing', *Microelectronic Engineering*, 77(3–4), pp. 193–203. doi:10.1016/j.mee.2004.10.008.

Turk, M.C. *et al.* (2013) 'Investigation of Percarbonate Based Slurry Chemistry for Controlling Galvanic Corrosion during CMP of Ruthenium', *ECS Journal of Solid State Science and Technology*, 2(5). doi:10.1149/2.009305jss.

Turk, M.C. *et al.* (2015) 'Chemical and mechanical aspects of a Co-Cu planarization scheme based on an alkaline slurry formulation', *ECS Journal of Solid State Science and Technology*, 5(2), p. P88.

Venkatesh, R.P. *et al.* (2013) 'Characterization of TMAH based cleaning solution for post Cu-CMP application', *Microelectronic Engineering*, 102, pp. 74–80.

Venkatesh, R.P. and Ramanathan, S. (2010) 'Electrochemical impedance spectroscopic studies of copper dissolution in glycine – hydrogen peroxide solutions', pp. 2057–2064. doi:10.1007/s10008-010-1037-5.

Victoria, S.N. *et al.* (2010a) 'Potassium Bromate as an Oxidizing Agent in a Titania-Based Ru CMP Slurry', *Electrochemical and Solid-State Letters* , 13(11), pp. H385–H387. doi:10.1149/1.3481948.

Victoria, S.N. *et al.* (2010b) 'Potassium Bromate as an Oxidizing Agent in a Titania-Based Ru CMP Slurry', *Electrochemical and Solid-State Letters*, 13(11), pp. H385–H387. doi:10.1149/1.3481948.

Victoria, S.N. *et al.* (2012) 'Chemical Mechanical Planarization of Ruthenium with Oxone as Oxidizer', *Electrochemical and Solid-State Letters*, 15(3), p. H55. doi:10.1149/2.005203esl.

Wang, Chenwei *et al.* (2021) 'Effect of UV Radiation on Oxidation for Ru CMP', *ECS Journal of Solid State Science and Technology*, 10(3), p. 034007. doi:10.1149/2162-8777/abe97b.

Wang, L. *et al.* (2014a) 'Cobalt polishing slurries for 10 nm and beyond', *Proceedings of International Conference on Planarization/CMP Technology 2014*, pp. 233–233. doi:10.1109/ICPT.2014.7017287.

Wang, L. *et al.* (2014b) 'Cobalt polishing slurries for 10 nm and beyond', in *International Conference on Planarization/CMP Technology*. IEEE, p. P233. doi:10.1109/icpt.2014.7017287.

Wang, M.T. *et al.* (1997) 'Effects of corrosion environments on the surface finishing of copper chemical mechanical polishing', *Thin Solid Films*, 308–309(1–4), pp. 518–522. doi:10.1016/S0040-6090(97)00500-2.

Wang, Q. *et al.* (2018) 'Controlling the Removal Rate Selectivity of Ruthenium to Copper during CMP by Using Guanidine Carbonate and 1, 2, 4-Triazole', *ECS Journal of Solid State Science and Technology*, 7(10), pp. P567–P574. doi:10.1149/2.0151810jss.

Wang, Q. *et al.* (2020) 'Effect of arginine-based cleaning solution on BTA residue removal after Cu-CMP', *Colloids and Surfaces A: Physicochemical and Engineering Aspects*, 586(November 2019), p. 124286. doi:10.1016/j.colsurfa.2019.124286.

Wang, Y.L. *et al.* (1998) 'Material characteristics and chemical-mechanical polishing of aluminum alloy thin films', *Thin Solid Films*, 332(1–2), pp. 397–403. doi:10.1016/S0040-6090(98)01200-0.

Wang, Zhi *et al.* (2019) 'Effect of Cystine in Alkaline CMP Slurry on Controlling the Galvanic Corrosion at Al-Co Interface', *ECS Journal of Solid State Science and Technology*, 8(10), pp. P580–P590. doi:10.1149/2.0071910jss.

Wang, Ziyan *et al.* (2019) 'Role of Ammonium Ions in Colloidal Silica Slurries for Ru CMP', *ECS Journal of Solid State Science and Technology*, 8(4), pp. P285–P292. doi:10.1149/2.0171904jss.

Wei, W. *et al.* (2007a) 'Study of copper diffusion through a ruthenium thin film by photoemission electron microscopy', *Applied Physics Letters*, 90(11).

doi:10.1063/1.2712832.

Wei, W. *et al.* (2007b) 'Study of copper diffusion through a ruthenium thin film by photoemission electron microscopy', *Applied Physics Letters*, 90(11), pp. 88–91. doi:10.1063/1.2712832.

Wu, C. *et al.* (2017) 'Cobalt CMP development for 7nm logic device', *ECS Transactions*, 77(5), p. 93.

Wu, Y.-F. and Tsai, T.-H. (2007) 'Effect of organic acids on copper chemical mechanical polishing', *Microelectronic Engineering*, 84(12), pp. 2790–2798.

Xie, X. *et al.* (2010) 'Synthesis of nanorod-shaped cobalt hydroxycarbonate and oxide with the mediation of ethylene glycol', *The Journal of Physical Chemistry C*, 114(5), pp. 2116–2123.

Xu, A. *et al.* (2021) 'Effect of Diethanolamine as Corrosion Inhibitor for the Chemical Mechanical Polishing of Cobalt in H2O2 Based Slurry', *ECS Journal of Solid State Science and Technology*, 10(4), p. 43006. doi:10.1149/2162-8777/abf49c.

Xu, R. and Zeng, H.C. (2003) 'Dimensional control of cobalt-hydroxide-carbonate nanorods and their thermal conversion to one-dimensional arrays of Co3O4 nanoparticles', *The Journal of Physical Chemistry B*, 107(46), pp. 12643–12649.

Yadav, K., Bisen, Jitendra C, *et al.* (2017) 'Microelectronic Engineering Sodium hypochlorite as an oxidizing agent in silica based ruthenium chemical mechanical planarization slurry', *Microelectronic Engineering*, 180, pp. 96–100. doi:10.1016/j.mee.2017.06.006.

Yadav, K., Bisen, Jitendra C., *et al.* (2017) 'Sodium hypochlorite as an oxidizing agent in silica based ruthenium chemical mechanical planarization slurry', *Microelectronic*

Engineering, 180, pp. 96–100. doi:10.1016/j.mee.2017.06.006.

Yan, Q. *et al.* (2012) 'Shape-controlled fabrication of the porous Co 3O 4 nanoflower clusters for efficient catalytic oxidation of gaseous toluene', *Journal of Hazardous Materials*, 209–210, pp. 385–391. doi:10.1016/j.jhazmat.2012.01.039.

Yang, G. *et al.* (2019) 'Integrated electrochemical analysis of polyvinyl pyrrolidone (PVP) as the inhibitor for copper chemical mechanical planarization (Cu-CMP)', *Journal of Alloys and Compounds*, 770, pp. 175–182. doi:10.1016/j.jallcom.2018.08.101.

Yang, S. *et al.* (2019) 'A study of cobalt galvanic and pitting corrosion with combination of BTA and PMP', *ECS Journal of Solid State Science and Technology*, 8(8), p. P416.

Yang, X., Zhang, B. and Yang, Z. (2022) 'Study of novel chelator and 1, 2, 4-triazole on cobalt corrosion and Co/Cu surface finishing in barrier CMP', *Materials Chemistry and Physics*, 278(October 2021), p. 125630. doi:10.1016/j.matchemphys.2021.125630.

Yano, H. *et al.* (2001) 'High-performance CMP Slurry with Inorganic/Resin Abrasive for Al/Low k Damascene', in *MRS Proceedings*. 2011/03/18. Cambridge University Press, p. M2.4. doi:DOI: 10.1557/PROC-671-M2.4.

Yao, C. *et al.* (2018) 'Effect of 1 , 2 , 4-triazole on galvanic corrosion between cobalt and copper in CMP based alkaline slurry', *Journal of Semiconductors*, 39(4), pp. 046001 (1–6). doi:10.1088/1674-4926/39/4/046001.

Yin, D., Yang, L., Ma, T., *et al.* (2020) 'Synergistic effect of composite complex agent on BTA removal in post CMP cleaning of copper interconnection', *Materials Chemistry and Physics*, p. 123230.

Yin, D., Yang, L., Niu, X., *et al.* (2020) 'Theoretical and electrochemical analysis on inhibition effect of benzotriazole and 1, 2, 4-triazole on cobalt surface', *Colloids and*

Surfaces A: Physicochemical and Engineering Aspects, 591, p. 124516.

Zantye, P.B., Kumar, A. and Sikder, A.K. (2004) 'Chemical mechanical planarization for microelectronics applications', *Materials Science and Engineering: R: Reports*, 45(3–6), pp. 89–220.

Zeng, X., Wang, J.-X., *et al.* (2012) ' Improved Removal Selectivity of Ruthenium and Copper by Glycine in Potassium Periodate (KIO 4)-Based Slurry ', *Journal of The Electrochemical Society*, 159(11), pp. C525–C529. doi:10.1149/2.055211jes.

Zeng, X., Wang, J., *et al.* (2012) 'Improved Removal Selectivity of Ruthenium and Copper by Glycine in Potassium Periodate (KIO 4) -Based Slurry', 159(11), pp. 525–529. doi:10.1149/2.055211jes.

Zhang, F. *et al.* (2012) 'Facile growth of mesoporous Co 3O 4 nanowire arrays on Ni foam for high performance electrochemical capacitors', *Journal of Power Sources*, 203(January 2018), pp. 250–256. doi:10.1016/j.jpowsour.2011.12.001.

Zhang, J. *et al.* (2016) 'Investigation on Chemical Mechanical Planarization Performance of the Replacement Metal Gate Aluminum Polishing Slurry', *ECS Journal of Solid State Science and Technology*, 5(7), pp. P446–P450. doi:10.1149/2.0291607jss.

Zhang, L., Wang, T. and Lu, X. (2020) 'Potassium persulfate as an oxidizer in chemical mechanical polishing slurries relevant for copper interconnects with cobalt barrier layers', *Journal of Materials Science*, 55(21), pp. 8992–9002. doi:10.1007/s10853-020-04579-6.

Zhang, W. *et al.* (2017) 'Role of 1, 2, 4-triazole in Co/Cu removal rate selectivity and galvanic corrosion during barrier CMP', *ECS Journal of Solid State Science and Technology*, 6(12), p. P786.

Zhang, Y. *et al.* (2022) 'Surface corrosion inhibition mechanism of sarcosine as a green

novel inhibitor on a novel barrier layer material of cobalt in copper film CMP for GLSI', *Materials Science in Semiconductor Processing*, 140(October 2021), p. 106402. doi:10.1016/j.mssp.2021.106402.

Zhao, D. and Lu, X. (2013) 'Chemical mechanical polishing: Theory and experiment', *Friction*, 1(4), pp. 306–326. doi:10.1007/s40544-013-0035-x.

Zhong, M. *et al.* (2014) 'Role of 1, 2, 4-triazole as a passivating agent for cobalt during post-chemical mechanical planarization cleaning', *Journal of The Electrochemical Society*, 161, p. C138.

Zuo, J. *et al.* (no date) 'EFFECT OF COMPLEXING AGENT IN SLURRY ON CMP PROPERTY FOR BARRIER MATERIAL COBALT', pp. 10–12.

THIS PAGE IS LEFT BLANK INTENTIONALLY

RESEARCH OUTPUT FROM THE THESIS

PUBLICATIONS

International Journals

- **Jenasree Hazarika**, R. Prasanna Venkatesh *"Formulation of Sodium Hypochlorite Based Slurry for Copper- Cobalt Chemical Mechanical Planarization Process",* ECS Journal of Solid-State Science and Technology 9(2), 024008 (2020). *Available at: https://doi.org/10.1149/2162-8777/ab682a*

- **Jenasree Hazarika***, Apeksha Gupta*, R. Prasanna Venkatesh *"Controlling Galvanic Corrosion with Oxalic acid and Imidazole for Chemical Mechanical Planarization of Cobalt-Copper Interface",* ECS Journal of Solid-State Science and Technology, 11, 054007, 2022. *Available at: https://doi.org/10.1149/2162-8777/ac6d72*

- **Jenasree Hazarika**, Anusuya Talukdar, R. Prasanna Venkatesh *"Anodic dissolution of Cobalt in hydrogen peroxide solutions with and without complexing agent: Kinetic analysis by electrochemical impedance spectroscopy,''* Journal of Solid State Electrochemistry, 2023. *Available at: https://doi.org/ 10.1007/s10008-023-05379-z*

- **Jenasree Hazarika***, Apeksha Gupta*, R. Prasanna Venkatesh *"A Review on Post-Chemical Mechanical Planarization Cleaning Technology",* ECS Journal of Solid-State Science and Technology, 2023. *(Provisionally accepted)*

- **Jenasree Hazarika**, Anusuya Talukdar, R. Prasanna Venkatesh *"Investigation of Polishing Characteristics of Interconnect (Cu) – Barrier metal (Ru) in Potassium Iodate-based Slurry,"* (under review)

Conference Proceeding /Presentation

- **Jenasree Hazarika**, Chetana Sudhakar Patil, R. Prasanna Venkatesh *"Formulation of slurry for chemical mechanical polishing of Cu substrates", 2nd* International Conference on Recent trends in Metallurgy, Materials Science and Manufacturing, December (27-28), Tiruchirappalli, India. Materials Today: Proceedings, 39, 1781-1785, 20221